University of Alberta

Sensorimotor mechanisms for the neural control of movement

By

Yoichiro Aoyagi ©

A thesis submitted to the Faculty of Graduate Studies and Research in partial fulfillment of the requirements for the degree of Doctor of Philosophy

Centre for Neuroscience

Edmonton, Alberta
Fall 2002

National Library
of Canada

Acquisitions and
Bibliographic Services

395 Wellington Street
Ottawa ON K1A 0N4
Canada

Bibliothèque nationale
du Canada

Acquisitions et
services bibliographiques

395, rue Wellington
Ottawa ON K1A 0N4
Canada

Your file Votre référence

Our file Notre référence

The author has granted a non-exclusive licence allowing the National Library of Canada to reproduce, loan, distribute or sell copies of this thesis in microform, paper or electronic formats.

The author retains ownership of the copyright in this thesis. Neither the thesis nor substantial extracts from it may be printed or otherwise reproduced without the author's permission.

L'auteur a accordé une licence non exclusive permettant à la Bibliothèque nationale du Canada de reproduire, prêter, distribuer ou vendre des copies de cette thèse sous la forme de microfiche/film, de reproduction sur papier ou sur format électronique.

L'auteur conserve la propriété du droit d'auteur qui protège cette thèse. Ni la thèse ni des extraits substantiels de celle-ci ne doivent être imprimés ou autrement reproduits sans son autorisation.

0-612-81159-X

Canada

University of Alberta

Library Release Form

Name of Author: Yoichiro Aoyagi

Title of Thesis: *Sensorimotor mechanisms for the neural control of movement*

Degree: Doctor of Philosophy

Year this Degree Granted: 2002

Permission is hereby granted to the University of Alberta Library to reproduce single copies of this thesis and to lend or sell such copies for private, scholarly or scientific research purposes only.

The author reserves all other publication and other rights in association with the copyright in the thesis, and except as herein before provided, neither the thesis nor any substantial portion thereof may be printed or otherwise reproduced in any material form whatever without the author's prior written permission.

Y. Aoyagi

Yoichiro Aoyagi
University Centre for Neuroscience
513 Heritage Medical Research Building
University of Alberta
Edmonton, AB
T6G 2S2

5/24/02
Date

University of Alberta

Faculty of Graduate Studies and Research

The undersigned certify that they have read, and recommended to the Faculty of Graduate Studies and Research for acceptance, a thesis "*Sensorimotor mechanisms for the neural control of movement*" submitted by Yoichiro Aoyagi in partial fulfillment of the requirements for the degree of Doctor of Philosophy.

Supervisor:

RBStein

Dr. Richard Stein, PhD.

Chair:

Teresa Krukoff

Dr. Teresa Krukoff, PhD.

Comittee Members:

Dr. Arthur Prochazka, PhD.

Dr. Ming Chan, MD.

Dr. Paul Zehr, PhD.

External Examiner:

Dr. Andrew Schwartz, PhD.

Date:

April 4th, 2002

ABSTRACT

Functional motion and control of limbs paralyzed after spinal cord injury or stroke can be restored by using electrodes implanted within the body. Unfortunately, not many motor prostheses have been established as standard devices for restoring functional limb movement. Direct stimulation of the neuromuscular junction is most commonly used. However, nerve trunk, spinal cord and spinal roots are other feasible control sites. From the viewpoint of understanding neural mechanisms toward more graceful control of limb movement, this thesis focused on the general role played by the spinal cord, the biomechanics of multiarticulated limb, and sensorimotor regulation by first order sensory neurons.

Muscle, nerve and spinal cord stimulation generated selective movements in all directions. Ventral and dorsal roots only elicited extension and flexion responses respectively. Muscle stimulation produced the most smoothly graded recruitment curves, but required an order of magnitude more current. The evidence for the existence of 4 or 5 clear 'primitives', originally suggested using frogs, was not verified in the mammalian spinal cord. However, a noteworthy finding was that the intermediate gray matter contains some rostrocaudal and ventrodorsal localization (but not complete modules) that would produce coordinated synergies. Movement elicited by simultaneous stimulation of multiple sites did not follow the linear summation of the vectors produced by stimulating individual sites, but tended to converge to an equilibrium point, suggesting that musculoskeletal properties play an important role in determining the trajectory. These principles should allow a more rational choice of stimulation site to restore particular functions in paralyzed human subjects.

A high-density, intrafascicular microelectrode array implanted in the sciatic nerve permitted more selective stimulation with more graded recruitment of individual muscles in chronic cats than was achieved by conventional cuff electrodes. The microelectrode arrays simultaneously recorded from over 100 sensory neurons in dorsal root ganglia in anesthetized cats. The activity of many neurons was correlated with the position of the foot and the activity in a population of neurons can be used to predict this position accurately. These methods may be useful for developing advanced prosthetic devices in which sensory information is used in a feedback control system.

ACKNOWLEDGEMENTS

There are many people who made this thesis possible. First, I thank my supervisor, Dr. Richard B. Stein for his continuous support, guidance, and encouragement during my doctoral training. I would like to thank the members of my supervisory and examining committees – Drs. Ming Chan, Arthur Prochazka, Paul Zehr and Andy Schwartz – for useful and constructive interactions.

I would like to thank to my colleagues and ex-colleagues in the lab for their friendship and scientific interactions: Doug Weber, Sean Maw, Su Ling Chong, Aiko Kido, Naofumi Tanaka, Ksenija Jovanovic, and Jianguo Cheng. A special thanks goes to the Rehabilitation Neuroscience Group members: Robert Rolf, Kelly James, Fay Strohschein, and Al Denington for their technical abilities without which I could not have completed the experiments. I would also like to thank the administrative staff of the University Centre for Neuroscience and Rehabilitation Neuroscience Group: Carol Ann, Brenda, and Toni (retired).

There are people with whom I have collaborated over the years and I am thankful for their significant scientific contribution to this thesis: Drs. Richard Normann, Almut Branner, and Shy Shoham in the Department of Bioengineering in University of Utah and Dr. Keir Pearson in the University Centre for Neuroscience in University of Alberta.

I thank the Canadian Institute of Health Research (CIHR) as well as the Faculty of Graduate Studies and Research for their financial support during my PhD.

A very special thanks goes to my family for their understanding and support of my scientific quest throughout my academic career: my wife Nori, my son Amon, my mother Kimie, and my father Yukio.

TABLE OF CONTENTS

CHAPTER 1:
GENERAL INTRODUCTION

CLASSICS IN MOVEMENT SCIENCE 2
PRESENT STATUS OF THE MOTOR CONTROL RESEARCH 3
MOTOR CONTROL RESEARCH IN REHABILITATION MEDICINE 3
REHABILITATIVE STRATEGY TO RESTORE MOTOR FUNCTION: FUNCTIONAL ELECTRICAL STIMULATION (FES) 4
  Open versus closed loop control 5
  Neuromuscular properties after central motor paralysis 6
  Multi-segmental nature of the skeletal systems 7
  Dynamic versus inverse dynamic strategy 7
SPINAL CORD ORGANIZATION FOR MOTOR OUTPUT 8
  Force field primitives 8
  Central pattern generators (CPG) 9
THESIS OBJECTIVES 10
REFERENCES 12

CHAPTER 2:
CAPABILITIES OF A PENETRATING MICROELECTRODE ARRAY FOR RECORDING SINGLE UNITS IN DORSAL ROOT GANGLIA OF THE CAT

INTRODUCTION 18
METHODS 20
  Microelectrode Array 20
  Animal Preparation and Electrode Implantation 21
  Classification of Afferents 21
  Conduction Velocity 22
  Decerebrate Walking 22
  Data Acquisition and Analysis 23
RESULTS 26
  Recording Statistics 26
  Classification of Afferents 26
  Localization of afferent neurons within the DRG 27
  Signal Amplitude and Impedance 30
  Frequency analysis and recording during passive movement 32
  Conduction Velocity 32
  Decerebrate Walking 34
DISCUSSION 36
  Recording capabilities of the penetrating microelectrode array 37
  Amplitude, impedance and distance 38
  Somatotopic organization 38
  Potentials for sensorimotor control research and clinical application 39
REFERENCES 41

CHAPTER 3:
CODING OF LIMB POSITION BY SENSORY NEURONS STUDIED WITH A

MULTIELECTRODE ARRAY

- INTRODUCTION 44
- RESULTS AND DISCUSSION 44
  - *Sensory encoding* 47
  - *Sensory decoding* 50
  - *Coordinate systems for sensory coding* 52
  - *Decoding and neural prostheses* 53
- METHODS 53
- REFERENCES 55

CHAPTER 4:
LONG-TERM STIMULATION AND RECORDING WITH A PENETRATING MICROELECTRODE ARRAY IN CAT SCIATIC NERVE

- INTRODUCTION 57
- METHODS 59
  - *Electrode Array* 59
  - *Surgical Procedure* 61
  - *Experimental procedure* 63
  - *Behavioral Tests* 63
  - *Stimulation* 63
  - *Recording* 63
  - *Histology* 64
- RESULTS 65
  - *General Observation* 65
  - *Stimulation* 68
  - *Recording* 74
  - *Histology and General Observation after Explanation* 75
- DISCUSSION 79
- REFERENCES 82

CHAPTER 5:
COMPARING MOVEMENTS ELICITED BY ELECTRICAL STIMULATION OF MUSCLE, NERVE, SPINAL CORD AND SPINAL ROOTS IN ANESTHETIZED AND DECEREBRATE CATS

- INTRODUCTION 86
- METHODS 87
  - *Animal preparation* 87
  - *Nerves* 88
  - *Muscles* 88
  - *Spinal cord* 90
  - *Motion analysis* 90
  - *Experimental protocol* 91
  - *Data acquisition* 92
- RESULTS 92
  - *Trajectories elicited by stimulating muscles, nerves, spinal cord and roots* 94

- *Maximal movements* 98
- *Recruitment curves* 100
- *Consistency of trajectory between animals* 102
- *EMG* 105

DISCUSSION 107
- *Selectivity* 107
- *Stimulus intensity, recruitment properties and movement distance* 109
- *Perspectives on clinical application to restore functional movements* 110

REFERENCES 113

CHAPTER 6:
THE ROLE OF NEUROMUSCULAR PROPERTIES IN DETERMINING THE END-POINT OF A MOVEMENT

INTRODUCTION 117

METHODS 118
- *Stimulation and recording* 118
- *Data acquisition and analysis* 119

RESULTS 122
- *Actual versus predicted vectors* 122
- *Equilibrium point* 125

DISCUSSION 136
- *Intrinsic peripheral properties contributing toa preferred direction and an equilibrium point* 137
- *Relation to spinal organization* 139
- *Control of the limb at a higher level* 140

REFERENCES 142

CHAPTER 7:
MOVEMENTS GENERATED BY INTRASPINAL MICROSTIMULATION IN THE INTERMEDIATE GRAY MATTER OF THE ANESTHETIZED, DECEREBRATE AND SPINAL CAT

INTRODUCTION 145

METHODS 147
- *General overview* 147
- *Surgical procedure and electrode implantation* 148
- *Experimental protocol and data acquisition* 150

RESULTS 154
- *Contribution of peripheral elements to movement construction* 154
- *Characterization of the role of intermediate neuronal elements in movement construction* 157
- *Effect of descending input on spinal elements of movement construction* 160
- *Summary of evoked responses under conditions of intact and interrupted descending drive* 165

DISCUSSION 167

REFERENCES 169

CHAPTER 8:
DIFFERENTIAL DISTRIBUTION OF THE INTERNEURONS IN THE NEURAL NETWORKS FOR WALKING IN THE MUDPUPPY (*Necturus Maculatus*) SPINAL CORD

INTRODUCTION 172
METHODS 173
  Recording cells 174
  Stimulation of the ventral roots 174
  Analysis 175
RESULTS 178
  Phasic classification of the cells 178
  Longitudinal distribution of the recorded cells in the spinal cord 183
  Connectivity of the rhythmic cells 184
DISCUSSION 186
REFERENCES 190

CHAPTER 9:
GENERAL DISCUSSION

SPINAL CORD ORGANIZATION FOR MOTOR OUTPUT 194
FES TO RESTORE MOTOR FUNCTION 196
  Stimulation of selective muscle groups 197
  Closed loop control 198
  Problems associated with rhythmic movement such as locomotion 198
  Concluding remarks: the future 199
REFERENCES 201

LIST OF TABLES

Chapter 3:

Table 3. Average correlation coefficients between firing rates of 64 neurons and position plus other variables in three coordinate systems 48

Chapter 4:

Table 4-1. Summary of the animals' walking behavior on the treadmill after surgery.... 68
Table 4-2. Proportion of hypomyelinated axons and axons undergoing axonal degenerations after electrical stimulation of the sciatic nerves 78

Chapter 5:

Table 5. Mean ± S.D. of direction of movement before and after decerebration.......... 98

LIST OF FIGURES

Chapter 2:

Figure 2-1. Scanning electron micrograph of the Utah Electrode Array 20
Figure 2-2. Single-unit identification on an individual electrode channel 24
Figure 2-3. Analysis of cyclic responses. 25
Figure 2-4. Histogram of identified units 28
Figure 2-5. An example of a recording map from L6 DRG. 29
Figure 2-6. Histogram of the amplitudes of sensory action potentials and the impedance of electrodes. 31
Figure 2-7. Simultaneous recording from L6 and L7 DRGs during ankle flexion and extension 33
Figure 2-8. Spike-triggered averaged records obtained from a muscle afferent fiber. 35
Figure 2-9. Sensory units and EMGs recorded during decerebrate walking. 36
Figure 2-10. pattern of EMG and sensory activity from Figure 2-9 averaged over the step cycle 37

Chapter 3:

Figure 3-1. Motion of the foot (a) and surface plots of the firing rate of cutaneous (b) and muscle (c) afferents. 45
Figure 3-2. The neural responses of 87 neurons varied with random movements of the cat's hind limb 46
Figure 3-3. Encoding of kinematic values in single sensory neurons 49
Figure 3-4. Time course of the actual and predicted position of the foot in polar coordinates 51

Chapter 4:

Figure 4-1. Picture of the Utah Slanted Electrode Array (USEA) 60
Figure 4-2. Three of the four different containment systems used in the study 62
Figure 4-3. Light microscopic pictures of cat sciatic nerve cross sections. 66
Figure 4-4. Photograph of cat sciatic nerve implant with 'oval' custom containment system 67
Figure 4-5. Cross-section of the cat hindlimb just above the ankle joint. 70
Figure 4-6. Functional stimulation maps of the USEA implanted in sciatic nerve and monitored at different times after implantation. 72
Figure 4-7. Summary of the stimulation data between three different kinds of implants by connector fixation techniques and containment systems used 73
Figure 4-8. Average electrode impedance over time for two different animals. 74
Figure 4-9. Sensory nerve fiber recordings. 76
Figure 4-10. Light microscopic picture of a cross section of cat sciatic nerve. 77
Figure 4-11. Light microscopic picture of cross sections of nerve fibers. 77
Figure 4-12. Comparison of nerve morphology in a control (A & B) versus an implanted nerve 79

Chapter 5:

Figure 5-1. A schematic view of the hamstring branch of the sciatic nerve and bipolar, epineural electrodes 89

Figure 5-2. **a.** A schematic view of the experimental setup. **b.** Sagittal trajectory of the hindlimb generated during stimulation of posterior biceps femoris 93
Figure 5-3. Typical results of movement vectors by stimulating muscle, nerve, ventral root, dorsal root, and spinal cord 95
Figure 5-4. Comparison of maximal directional change 97
Figure 5-5. Examples of movement vectors from nerve stimulation in one animal 99
Figure 5-6. Comparison of stimulation threshold current (**a**) and normalized displacement (**b**) for stimulation of muscles, nerves, spinal cord and roots .. 101
Figure 5-7. Extreme positions from maximal stimulation of muscles and nerves 103
Figure 5-8. Comparison of the coefficient of variation between maximal movements induced by stimulating nerves and muscles in different animals. 104
Figure 5-9. Comparison of latency, jitter and coefficient of variation of EMG amplitude 106

Chapter 6:

Figure 6-1. **a.** The sagittal trajectory of the hindlimb generated during simultaneous stimulation of posterior biceps femoris and lateral gastrocnemius. **b.** Corresponding changes of horizontal and vertical components of the trajectory shown in **a**. 121
Figure 6-2. **a.** An example of actual vectors obtained by nerve stimulation **b.** Polar graphs of predicted vectors obtained in **a** 123
Figure 6-3. **a.** The actual distance moved increased with an increase in the number of sites stimulated. **b.** The absolute distance between actual and predicted end-points 125
Figure 6-4. Predicted versus actual distances 126
Figure 6-5. Histograms of absolute angle differences between the actual and the corresponding predicted vectors 128
Figure 6-6. Examples of individual vectors at front, neutral and back positions 130
Figure 6-7. **a.** Equilibrium point index of individual vectors **b.** Actual and predicted Equilibrium point index 131
Figure 6-8. Examples of vectors elicited by intramuscular stimulation of muscles at back, neutral and front positions 132
Figure 6-9. Actual and predicted equilibrium point index as a function of the number of stimulated sites 133
Figure 6-10. Actual and predicted equilibrium point index as a function of the number of joints involved 134
Figure 6-11. Equilibrium point index when combine stimulation of two sites was delivered to antagonistic and non-antagonistic muscles 135

Chapter 7:

Figure 7-1. Force-displacement curve characterizing the uniformity of the sagittal stiffness 149
Figure 7-2. End-point movement vectors generated by intramuscular stimulation 155
Figure 7-3. End-point movement vectors evoked by epineural stimulation of nerves 156
Figure 7-4. Locations of intraspinal microwire tips 158
Figure 7-5. End-point movement vectors evoked by intraspinal microstimulation under anesthesia 159

Figure 7-6. End-point movement vectors evoked by intraspinal microstimulation under conditions of anesthesia, decerebration and spinalization 162
Figure 7-7. Example of changes in movement between experimental states 164
Figure 7-8. Summary of changes in direction of end-point movement vectors between experimental states 166

Chapter 8:

Figure 8-1. Extracellular recording of an interneuron at 1 mm caudal to the C2 dorsal root, together with the rectified flexor and extensor EMG 176
Figure 8-2. Longitudinal distribution of cells recorded in the C2 and C3 segments 179
Figure 8-3. Comparison of rhythmic and non-rhythmic cells in terms of location (**a**), firing rate (**b**), modulation (**c**), and variance accounted for (**d**) 180
Figure 8-4. Classification of cells and their distribution along the spinal cord 182
Figure 8-5. **a.** Rhythmic discharges on top of membrane voltage undulations
b. Inactivation of the spikes by depolarizing current injection 183
Figure 8-6. Spike-triggered, short latency excitation of the extensor muscle 185

CHAPTER 1

GENERAL INTRODUCTION

Activities of daily life such as reaching and walking are motor functions that most people take for granted. These natural motions require an exquisite control system and coordinated actuators that consist of multi-joint skeletal muscles. Imagine, for example, an act as simple as hammering a nail: while the hand grasps the hammer, a number of muscle acting across the wrist, elbow, and shoulder work together in an overlapping sequence to propel and land the hammer on the head of the nail. In essence, the coordinated limb movement is accomplished through the control signals generated in the brain. The descending commands activate motoneuron pools that innervate muscles. These control commands are modulated by proprioceptive information arising from afferent signals. We do not usually appreciate the complexity of human limb movement control and the elegance with which it is performed until an injury to the brain or the spinal cord disrupts the neural circuitry responsible for motor action and sensation. Unfortunately, the incidence rates of spinal cord injury and stroke are about 12,000 and 600,000 every year in the U.S (Thurman et al. 1994; Johnson et al. 1997). Many of the survivors will continue to have major impairments such as tetraplegia, paraplegia, or hemiplegia.

In this General Introduction, I will briefly touch the beginning of movement science, and then will discuss the current status of motor control research and where movement research will go in the future from the standpoint of rehabilitation. Next, I will overview two issues that are deeply related to this thesis: (1) rehabilitative strategies to restore functional limb movement, primarily focusing on functional electrical stimulation (FES), (2) functional organization of the interneuronal area of the spinal cord, the stimulation of which may be a feasible new strategy to restore functional limb movement. Finally, I will mention the general purpose of this dissertation and also touch on the specific purpose of each chapter (Chapter 2-8).

CLASSICS IN MOVEMENT SCIENCE

It was not until the 17th-century that movement was thought to be governed by the brain. People believed that movement was governed by the 'soul', a spiritual entity separate from and above the brain. Redi postulated in 1666 that electricity was generated from muscle, a fact not demonstrated until late 18th-century by Luigi Galvani using frogs (cf. (Piccolino 1997)). The first radical step was taken by de la Mettrie (1748). He thought that an animating principle in the brain coordinated real motor action. The term 'reflex' was first defined by Georgiy Prochaska in 1784 as a behavior in response to an excitation, mediated by separate motor and sensory nerves. In 1855, Spencer proposed that all motor acts were simply chains of elemental reflexes.

In the late 19th-century, the very need for the term 'voluntary' was gradually questioned. Around 1870, Eduard Hitzig and Gustav Fritsch found that electrical stimulation of brain areas in a dog caused body movements. Hughlings Jackson (1884) suggested based on his observations of his wife's epileptic seizures that a different section of the brain controlled the movement of a different part of the body, and that movements ranged from most automatic (evolutionarily primitive) to least automatic (most advanced).

The 20th-century was undoubtedly the most productive and rapidly progressing period for neural and movement science when innumerable experiments were conducted. Graham Brown (1911) found that the brainstem and spinal cord were capable of generating basic rhythmical activity even without sensory input (half center theory) (Brown 1911). This ability is now termed a 'central pattern generator (CPG)' and is explained in terms of activation of ion channels and receptors (Grillner and Matsushima 1991). About the same time, Charles Sherrington established that sensory receptors provide feedback via reflexes and voluntary reactions for the control of movements such as posture and locomotion (Sherrington 1910, 1906). The 'motor unit' was defined as the anatomical unit of muscle function by Liddell and Sherrington in 1925. In 1936, acetylcholine was demonstrated to be the transmitter released at neuromuscular junction by the stimulation of motor nerves (Dale et al. 1936). Wilder Penfield, a pioneering brain surgeon, mapped the human motor cortex using mild electric current in the 1940s. It was in the middle of the 20th century that the complex nature of the electric signaling mechanism in nerve cells emerged clearly. Hodgkin, Huxley and Katz showed, using the squid giant axon, that the action potential occurs with a rapid increase of Na+ permeability through opening of the voltage sensitive Na channels (Hodgkin and Huxley 1939) and subsequent increase of K+ permeability (Hodgkin et al. 1952). Many other great scientists, such as Bernstein, Denny-Brown, Hill, Woodworth, Von Helmholtz worked in areas that are now associated with biomechanics, neurophysiology of movements, and motor control (Latash and Zatsiorsky 2001).

PRESENT STATUS OF THE MOTOR CONTROL RESEARCH

A better understanding of sensorimotor control has been possible with progress in electronic technology. For example, non-invasive brain imaging techniques such as functional magnetic resonance imaging (fMRI) has led to new insights into the functioning of the motor system. Impressive technological advances have increased the spatial and temporal resolution of functional imaging. In the area of electroneurophysiology, the intracellular recording technique has allowed researchers to study cellular physiology. In recent years, multi-unit recording techniques have allowed the study of multiple representations and parallel processing of sensory and motor information. With these technological developments, modern motor control research has developed extensively. Motor learning and adaptation, computational neuroscience, and functional motor recovery are a few examples of related approaches.

Despite the major discoveries made in the 20th-century, there are a number of unresolved issues, controversial theories, and emerging new topics in motor control and its related areas that motor control researchers including neurophysiologists, biomechanists, biomedical engineers and physiatrists should tackle. One field in which an understanding of what is a normal movement is crucial for the development of therapeutic strategy is rehabilitation medicine.

MOTOR CONTROL RESEARCH IN REHABILITATION MEDICINE

Frank Krusen, recognized as the father of physical medicine and rehabilitation, described rehabilitation as follows (Krusen et al. 1971). Rehabilitation involves treatment and training for the patient to the end that he may attain his maximal potential for normal living physically, psychologically, socially, and vocationally. To improve motor function of patients with motor impairments is one major area of clinical practice in physical medicine and rehabilitation. Thus, rehabilitation medicine is tightly linked with motor function and requires a much better understanding of basic and applied motor control. Development and optimization of its therapeutic approaches largely depends on a deep understanding of the mechanisms in healthy as well as disabled individuals.

REHABILITATIVE STRATEGY TO RESTORE MOTOR FUNCTION: FUNCTIONAL ELECTRICAL STIMULATION (FES)

Neurological and functional recovery after the incidence of spinal cord injury, stroke and other central motor disorders is typically limited. Comprehensive medical treatment with an intensive rehabilitation program promotes the central nervous system (CNS) regeneration to a limited extent. The degree and period of the recovery depend on the injured location, size of the lesion, and age etc. It is generally agreed that 90 % of the CNS recovery occurs by the end of three months following the onset, and the spontaneous recovery is extremely limited after the first year (Ditunno et al. 1997). Minimizing the damage to the CNS and maximizing the recovery is a continuing goal in rehabilitation medicine. Although advances have been made in the field of CNS regeneration, a cure for spinal cord injury or stroke does not yet exist (Behar et al. 2000; Girardi et al. 2000).

The spinal cord below the lesion, as well as the muscles and nerves, remain essentially intact in many individuals, though reflex transmission and the tonic state of interneuronal networks may be abnormal (Sherrington 1906). Thus, stimulating the surviving neurons below the lesion is another approach to restore motor function. Since the introduction of the first FES system in 1961 (Liberson et al. 1961), intramuscular, epimysial or nerve cuff electrodes have been used to activate muscle either experimentally or clinically. Although limited clinical applications of FES have been relatively successful (Kralj et al. 1988; Peckham and Creasey 1992; Dai et al. 1996; Prochazka et al. 1997), the restoration of limb movements remains an elusive goal.

What limits the wider usage of clinical FES? Clearly, a number of issues need to be addressed. First of all, the physiological system that we are trying to control has many complex features, many of which are far from completely understood and characterized. Thus, apart from current technological issues on neural prostheses, the countless normal physiological events that continuously occur with even the simplest motor task are clearly still far more complex than what can be currently accomplished by FES. In addition to incomplete knowledge of the normal physiological system, little is known about neuromuscular-skeletal related pathological changes occurring after central motor paralysis. These musculoskeletal changes would complicate motor control strategies associated with the biomechanics of the multi-segmental nature of musculoskeletal systems.

Another problem is control and command issue. Since it is practically impossible to electrically stimulate all muscles of the extremities, the question arises as to which muscles should be stimulated and what individual muscle stimulation profiles should be applied in order to restore functional movement. In conventional clinical applications of the FES, decisions regarding the choice of muscles, and adjustments of the stimulation parameters (timing and magnitude) have been typically made on a trial and error basis without using any feedback signals (open-loop control). However, such empirical adjustments of the stimulation profiles are likely to be restricted by the limited patience of paralyzed individuals. Finally, though not the main focus of this thesis, the performance gains in technological advancements in electronics, communication, and control have been relatively modest since their initial development. Stimulation hardware containing an external stimulator and percutaneous electrodes caused infrequent but serious problems such as wire breakage and skin infection. In the following subsections, these specific issues will be discussed in more detail.

Open versus closed loop control

Although many current FES systems use the input signals in an open loop control system configuration, these systems often lead to robotic, jerky movements. Closed loop control has obvious advantages (Solomonow et al. 1986; Lan et al. 1991; Hoffer et al. 1996; Stein et al. 1992a; Yoshida and Horch 1996). Closed loop automatic control systems have been primarily investigated using joint angle, force, or electromyographic (EMG) signals. Based on the measured signals, the controller determines the stimulation pattern that is required to achieve a specific movement task. However, artificial sensors are more or less primitive, unreliable, and inflexible when compared with natural sensors (Prochazka 1993). Perhaps a more fascinating alternative is to use the natural sensors which are already present within the body. During natural volitional control of muscles, natural sensors such as muscle spindles and Golgi tendon organs relay muscle length and tendon force information from the extremity through the PNS to the CNS. Previous work has been done using cuff electrodes implanted in the peripheral nerves (Hoffer et al. 1996; Yoshida and Horch 1996). However, the signal to noise ratio was relatively low and smaller nerves could be damaged over the course of a long-term implantation.

Neuromuscular properties after central motor paralysis

Disuse-related changes (muscular atrophy, bone loss, connective tissue reorganization, muscle contracture, calcification of the joint) will appear not long after the onset of paralysis, though they are partly preventable (Belanger et al. 2000). These changes should certainly affect viscoelastic properties and inertia in the musculoskeletal system. Unfortunately, so far, very few studies have compared the inertia and other biomechanical parameters during movement between normal and disabled subjects. Indeed, Stein et al. showed that the inertia of the lower leg was reduced significantly in disabled subjects (Stein et al. 1996). Furthermore, pathological spinal reflex activities cause spasticity, rigidity or flaccidity. More importantly, most type I (slow, aerobic) fibers are transformed into type II (fast, anaerobic) fibers with disuse and paralysis (Grimby et al. 1976). These pathological conditions change muscle contractile properties significantly. Normally, type I and II muscle fibers are recruited selectively by the CNS in order to perform different voluntary motor tasks, but such selectivity is far from accomplished in the transformed paralyzed muscles by electrical stimulation. The recruitment of motor units becomes disrupted or even reversed and the resulting synchronous activation of large, fatigable type II fibers leads to rapid muscle fatigue (Prochazka 1993; Levy et al. 1990; Peckham et al. 1976; Kralj et al. 1980; Stein et al. 1992b). Upon contraction of type II fibers, muscle contraction and relaxation speed increases, and the muscle becomes unable to generate prolonged contractions. A feasible strategy being explored to circumvent this problem would be intraspinal microstimulation, which provides a more normal order of recruiting motor units and may induce more graded movement (Mushahwar and Horch 2000). Anyhow, changes associated with motor paralysis that significantly affect limb biomechanics must always be kept in mind by researchers involved with biomechanics in disabled subjects.

Multi-segmental nature of the skeletal systems

Musculoskeletal geometry, nonlinear dynamic response properties of muscle, joint properties, segmental coupling, and reflex interactions have all caused problems for many of the FES control systems that have been tested. The multi-joint nature of the skeletal systems complicates the process of controlling posture and movement. Some of the complexity arises because dynamic coupling occurs in multilinked segments, and biarticular muscles may produce different actions across the joints they span. Biarticular muscles may enhance interjoint coordination and provide some mechanical coupling effects between joints. The effect of mechanical coupling can be advantageous in FES-induced movement since it is very unlikely in natural movement that each compartment of biarticular muscles is activated in total isolation. Thus, typical activities in daily life utilize coordinated movement by the activity of biarticular muscles.

Conversely, the 'nonselective' function of biarticular muscle may be a drawback in generating selective single joint movement. However, contrary to the common view of biarticular function, recent evidence suggests that movements can be generated quite effectively at one joint in such biarticular, but compartmentalised muscles (Herrmann and Flanders 1998).

Dynamic versus inverse dynamic strategy

One of the central questions in motor control is how the CNS may form the motor commands that guide the limbs. Several models of how motor commands are generated have been proposed. One proposal is that an internal model is constructed to map the desired state at each point along the trajectory into motor commands (so called 'inverse dynamic model') (Kawato et al. 1987). An alternative proposal is that the CNS specifies spatial parameters and relies on the spring-like properties of muscles plus reflex loops to move the limb (so called 'direct dynamic model') (Feldman 1966a; Hogan 1984; Bizzi et al. 1984). Kawato suggested that internal models are probably located not only in the cerebellum but also in all brain regions endowed with synaptic plasticity (Kawato 1999). The inverse dynamic theory, although very fascinating, requires a complex computation process mainly in cerebellum, cerebral cortex and basal ganglia that are not fully available in individuals with their ascending tracts injured. Thus, the inverse dynamic model is not a feasible control system in complete spinal cord injury, unless the inverse dynamics are calculated externally.

The direct dynamic strategy should be more important for limb control using FES especially for reaching and posture control. Bizzi et al. (Bizzi et al. 1982) suggested a hypothesis that the movement to an equilibrium point is determined by an interaction of agonist and antagonist muscles' force-length properties at a joint. This hypothesis is attractive because it suggests the possibility that the trajectory of movement is simply determined by the inherent stiffness and inertial properties of the limb and muscles around a joint. Because of the system dynamics, the actual positions will not follow exactly the desired trajectory unless the stiffness is high (in inverse model, the limb can be controlled with low stiffness) (Wolpert and Ghahramani 2000). However, this issue does not necessarily limit the usefulness of the dynamic model in FES because generating finely graded movement with low stiffness would be difficult anyway under peripheral FES due to the reversal of recruiting motor units (Levy et al. 1990). In this sense a realistic goal would be the control of reaching movement and posture control where relatively high muscle stiffness may be required.

SPINAL CORD ORGANIZATION FOR MOTOR OUTPUT

Force field primitives

In modern neuroscience it seems a common view that specific behaviors arise from localized regions of the brain. While the motor cortex was first mapped early in the 20th century, the spinal cord organization was not systematically mapped until ten years ago. Experimental data and modeling in frogs suggest that there is a limited number of force directions that can be specified (Bizzi et al. 1991; Giszter et al. 1993; Saltiel et al. 1998; d'Avella and Bizzi 1998; Bizzi et al. 2000). Activation of a discrete spinal interneuronal area often led to forces that converge to a point. Bizzi and his colleagues also suggested that the simultaneous stimulation of two sites of 'force-field primitives' leads to the vectorial summation of the end-point forces generated by each site separately (Mussa-Ivaldi et al. 1994). This idea could lead to the view that the spinal circuitry is modular, the output of each module driving the limb into a particular posture. This approach has been used to argue for the concept that movement is guided using an equilibrium point method (see (Bizzi et al. 2000; Bizzi et al. 1992)). If this idea is true, the control of movements through spinal stimulation might be simpler than the control through intramuscular stimulation. Stimulation of a combination of spinal modules might provide a way to produce coordinated functional movements.

However, evidence against the idea of force-field primitives has been also reported recently (cf. (Aoyagi et al. 2000a; Tresch and Kiehn 2000; Loeb 2001; Gomi and Kawato 1996)). Thus, the existence of the 'primitives' remains controversial. If they exist, to what extent are force-field primitives a consequence of the anatomical and biomechanical organization of the limb and its muscles or a consequence of special spinal circuits?

Central pattern generators (CPG)

It is known that spinal motor systems are capable of generating rhythmic motor behaviors, even when isolated from the rest of the nervous system. Neuronal network responsible for producing coordinated spatio-temporal patterns of rhythmic behavior is call as CPG (for review (Grillner et al. 1991; Pearson 1993; McClellan 1996)). The first demonstration that spinal networks can generate the details of the rhythmic locomotor output resulted from Graham Brown's experiments (Brown 1911) using acute and decerebrate cats. He proposed the half-center model to explain alternating activation of flexor and extensor muscles during locomotion. Each half-center was thought to activate either flexor or extensor muscles while the connection between the half-centers was thought to be mutually inhibitory to ensure that when one center is active the center is inactive. Further comprehensive evidence for central origin of locomotion was obtained from the newt (Szekely et al. 1969) and cat (Grillner and Zangger 1979) where the isolated parts of brachial or caudal spinal cord, respectively, can also generate rhythmic motor output even in the absence of the afferent input. These works not only confirmed but also refined and expanded Brown's initial observations providing a framework for a new concept of multiple unit burst generators (Grillner 1985). Unlike half-centers, each unit burst generator can generate rhythmic output on its own and be combined with other unit burst generators thereby participating in the production of different behaviors. This concept, together with the descriptions of many interneuronal pathways within the spinal cord and their elaborate interactions (Baldissera et al. 1977; Jankowska 1992, 2001), further indicates that the spinal cord cannot be viewed as a simple relay of supraspinal motor commands to the periphery. Indeed, rhythmic motor behaviors are generated through localized and distributed networks in the spinal cord. Evidence in support of this idea has come from several experiments (Rossignol 1996; Stein 1997; Cheng et al. 1998; Kiehn and Kjaerulff 1998; Beato and Nistri 1999). Despite the variety of preparations (cat, rat, turtle, mudpuppy) and methods (in vitro, in vivo) used to address this idea, however, spinal interneurons associated with half-centers or multiple unit burst generators have not yet been completely identified for walking. Clearly, a systematic mapping of rhythmically active interneurons is needed to clarify the exact rostrocaudal and transverse location of the CPG network controlling walking movements.

THESIS OBJECTIVES

As implied above, the following chapters are all associated with sensorimotor control of normal as well as artificial movement. A major goal of my research has been and will perhaps be toward a better understanding of basic sensorimotor control that should consequently be applied to motor rehabilitation especially for restoring functional movement. Thus, this dissertation has two objectives: (1) to pursue the sensorimotor control principles underlying natural and artificial movement and (2) to test the new potential for FES.

In Chapters 2-4, a novel intrafascicular microelectrode array, the Utah Electrode Array (UEA) was used in dorsal root ganglion (DRG) and peripheral nerve of the cat for recording and stimulation. The UEA, containing up to 100 electrodes, was originally developed for use in cerebral cortex (Schmidt et al. 1993; Nordhausen et al. 1996). We successfully recorded stable, phase dependent multiple sensory units during passive movement and decerebrate walking (Chapter 2). In Chapter 3, we describe a mathematical structure for the coding occurring in sensory neurons (encoding). Furthermore, we demonstrate that the position of the limb in space can be predicted from the impulses in a population of neurons (decoding). These methods may be useful for developing advanced prosthetic devices in which sensory information is used to control stimulation in FES. In Chapter 4, the UEA was chronically implanted in the cat's sciatic nerve to investigate the biocompatibility of the UEA and its ability for selectively stimulating muscle in the long-term.

Chapter 5 compares biomechanical and neurophysiological characteristics of stimulation at five sites: muscle, nerve, ventral and dorsal roots, and spinal cord in anaesthetized and decerebrate cat. Not only conventionally used sites (muscle and nerve) but also spinal cord and roots turned out to be theoretically possible to reproduce wide range of movements in paralyzed individuals. In Chapter 6, we tested musculoskeletal biomechanical properties during stimulation of up to 6 sites in muscles, nerves and the spinal cord. These stimuli elicited flexion and extension of the hip, knee and ankle in the anesthetized and decerebrate cat. We demonstrate that the equilibrium-point hypothesis is strongly rooted in the biomechanics of musculoskeletal systems and in particular in their spring-like properties as originally implied by Feldman and Bizzi (Bizzi et al. 1982; Feldman 1966b).

In Chapters 7 and 8, we tested the output properties of the spinal cord (functional localization) using different preparations: an electrically stimulated *in vivo* preparation (cat; Chapter 7) and a pharmacologically activated *in vitro* walking preparation (mudpuppy; Chapter 8). The results suggested that the interneuronal area of the spinal cord contains some functional localization (but not complete modules) that will produce coordinated synergies, but also that biomechanical actions of the limb muscles set limits on movements that can be generated through central commands.

Two other papers (Aoyagi et al. 2000b; Aoyagi et al. submitted) were produced during my graduate period with Dr. Ming Chan, but have not been included here because their focus was distinct from the other work on motor control.

REFERENCES:

1. Thurman DJ, Burnett CL, Jeppson L, Beaudoin DE and Sniezek JE. Surveillance of spinal cord injuries in Utah, USA. *Paraplegia* 32: 665-669., 1994.

2. Johnson RL, Gabella BA, Gerhart KA, McCray J, Menconi JC and Whiteneck GG. Evaluating sources of traumatic spinal cord injury surveillance data in Colorado. *Am J Epidemiol* 146: 266-272., 1997.

3. Piccolino M. Luigi Galvani and animal electricity: two centuries after the foundation of electrophysiology. *Trends Neurosci* 20: 443-448., 1997.

4. Brown TG. The intrinsic factors in the act of progression in the mammal. *Proc Lon B Biol Sci* 84: 308-319, 1911.

5. Grillner S and Matsushima T. The neural network underlying locomotion in lamprey--synaptic and cellular mechanisms. *Neuron* 7: 1-15, 1991.

6. Sherrington CS. Flexion-reflex of the limb, crossed extension reflex and reflex stepping and standing. *J Physiol (Lond)* 40: 28-121, 1910.

7. Sherrington CS. *The integrative action of the nervous system*. New Haven: Yale University Press, 1906.

8. Dale HH, Feldberg W and Vogt M. Release of acetylcholine at voluntary motor nerve endings. *J Physiol* 86: 353-380, 1936.

9. Hodgkin A and Huxley AF. Action potentials recorded from inside a nerve fibre. *Nature* 144: 710-711, 1939.

10. Hodgkin A, Huxley AF and Katz B. Measurement of current-voltage relations in the membrane of the giant axon of Likigo. *J Physiol (Lond)* 116: 424-448, 1952.

11. Latash ML and Zatsiorsky VM. *Classics in movement science*. Champaign, IL: Human Kinetics, 2001.

12. Krusen FH, Kottke FJ, Ellwood PM and American Rehabilitation Foundation. *Handbook of physical medicine and rehabilitation*: Saunders, 1971.

13. Behar O, Mizuno K, Neumann S and Woolf CJ. Putting the spinal cord together again. *Neuron* 26: 291-293, 2000.

14. Girardi FP, Khan SN, Cammisa FP, Jr. and Blanck TJ. Advances and strategies for spinal cord regeneration. *Orthop Clin North Am* 31: 465-472, 2000.

15. Liberson WT, Holmquest HJ, Scott D and Dow M. Functional electrotherapy:

stimulation of the peroneal nerve synchronized with the swing phase of the gait of hemiplegic patients. *Arch Phys Med Rehabil* 42: 101-105, 1961.

16. Kralj A, Bajd T and Turk R. Enhancement of gait restoration in spinal injured patients by functional electrical stimulation. *Clin Orthop*: 34-43, 1988.

17. Peckham PH and Creasey GH. Neural prostheses: clinical applications of functional electrical stimulation in spinal cord injury. *Paraplegia* 30: 96-101, 1992.

18. Dai R, Stein RB, Andrews BJ, James KB and Wieler M. Application of tilt sensors in functional electrical stimulation. *IEEE Trans Rehabil Eng* 4: 63-72, 1996.

19. Prochazka A, Gauthier M, Wieler M and Kenwell Z. The bionic glove: an electrical stimulator garment that provides controlled grasp and hand opening in quadriplegia. *Arch Phys Med Rehabil* 78: 608-614, 1997.

20. Solomonow M, Baratta R, Shoji H and D'Ambrosia RD. The myoelectric signal of electrically stimulated muscle during recruitment: an inherent feedback parameter for a closed-loop control scheme. *IEEE Trans Biomed Eng* 33: 735-745, 1986.

21. Lan N, Crago PE and Chizeck HJ. Control of end-point forces of a multijoint limb by functional neuromuscular stimulation. *IEEE Trans Biomed Eng* 38: 953-965., 1991.

22. Hoffer JA, Stein RB, Haugland MK, Sinkjaer T, Durfee WK, Schwartz AB, Loeb GE and Kantor C. Neural signals for command control and feedback in functional neuromuscular stimulation: a review. *J Rehabil Res Dev* 33: 145-157., 1996.

23. Stein RB, Peckham PH and Popovic D. *Neural prostheses: replacing motor function after disease or disability*. New York: Oxford University Press, 1992a.

24. Yoshida K and Horch K. Closed-loop control of ankle position using muscle afferent feedback with functional neuromuscular stimulation. *IEEE Trans Biomed Eng* 43: 167-176, 1996.

25. Prochazka A. Comparison of Natural and artificial control of movement. *IEEE Trans Rehabil Eng* 1: 7-17, 1993.

26. Chapin JK and Moxon KA. *Neural Prostheses for Restoration of Sensory and Motor Function*. Boca Raton: CRC Press, 2000.

27. Belanger M, Stein RB, Wheeler GD, Gordon T and Leduc B. Electrical stimulation: can it increase muscle strength and reverse osteopenia in spinal cord injured individuals? *Arch Phys Med Rehabil* 81: 1090-1098., 2000.

28. Stein RB, Zehr EP, Lebiedowska MK, Popovic DB, Scheiner A and Chizeck HJ. Estimating mechanical parameters of leg segments in individuals with and without physical disabilities. *IEEE Trans Rehabil Eng* 4: 201-211, 1996.

29. Grimby G, Broberg C, Krotkiewska I and Krotkiewski M. Muscle fiber composition in patients with traumatic cord lesion. *Scand J Rehabil Med* 8: 37-42, 1976.

30. Levy M, Mizrahi J and Susak Z. Recruitment, force and fatigue characteristics of quadriceps muscles of paraplegics isometrically activated by surface functional electrical stimulation. *J Biomed Eng* 12: 150-156., 1990.

31. Peckham PH, Mortimer JT and Marsolais EB. Alteration in the force and fatigability of skeletal muscle in quadriplegic humans following exercise induced by chronic electrical stimulation. *Clin Orthop*: 326-333, 1976.

32. Kralj A, Bajd T and Turk R. Electrical stimulation providing functional use of paraplegic patient muscles. *Med Prog Technol* 7: 3-9, 1980.

33. Stein RB, Gordon T, Jefferson J, Sharfenberger A, Yang JF, de Zepetnek JT and Belanger M. Optimal stimulation of paralyzed muscle after human spinal cord injury. *J Appl Physiol* 72: 1393-1400, 1992b.

34. Mushahwar VK and Horch KW. Muscle recruitment through electrical stimulation of the lumbo-sacral spinal cord. *IEEE Trans Rehabil Eng* 8: 22-29, 2000.

35. Herrmann U and Flanders M. Directional tuning of single motor units. *J Neurosci* 18: 8402-8416, 1998.

36. Kawato M, Furukawa K and Suzuki R. A hierarchical neural-network model for control and learning of voluntary movement. *Biol Cybern* 57: 169-185, 1987.

37. Feldman AG. Functional tuning of the nervous system with control of movement or maintenance of a steady posture. III. Mechanographic analysis of the excution by man of the simplest motor task. *Biophysics* 11: 766-775, 1966a.

38. Hogan N. An organizing principle for a class of voluntary movements. *J Neurosci* 4: 2745-2754., 1984.

39. Bizzi E, Accornero N, Chapple W and Hogan N. Posture control and trajectory formation during arm movement. *J Neurosci* 4: 2738-2744., 1984.

40. Kawato M. Internal models for motor control and trajectory planning. *Curr Opin Neurobiol* 9: 718-727., 1999.

41. Bizzi E, Accornero N, Chapple W and Hogan N. Arm trajectory formation in monkeys. *Exp Brain Res* 46: 139-143, 1982.

42. Wolpert DM and Ghahramani Z. Computational principles of movement neuroscience. *Nat Neurosci* 3 Suppl: 1212-1217., 2000.

43. Bizzi E, Mussa-Ivaldi FA and Giszter S. Computations underlying the execution of movement: a biological perspective. *Science* 253: 287-291, 1991.

44. Giszter SF, Mussa-Ivaldi FA and Bizzi E. Convergent force fields organized in the frog's spinal cord. *J Neurosci* 13: 467-491, 1993.

45. Saltiel P, Tresch MC and Bizzi E. Spinal cord modular organization and rhythm generation: an NMDA iontophoretic study in the frog. *J Neurophysiol* 80: 2323-2339, 1998.

46. d'Avella A and Bizzi E. Low dimensionality of supraspinally induced force fields. *Proc Natl Acad Sci U S A* 95: 7711-7714, 1998.

47. Bizzi E, Tresch MC, Saltiel P and d'Avella A. New perspectives on spinal motor systems. *Nat Rev Neurosci* 1: 101-108., 2000.

48. Mussa-Ivaldi FA, Giszter SF and Bizzi E. Linear combinations of primitives in vertebrate motor control. *Proc Natl Acad Sci U S A* 91: 7534-7538, 1994.

49. Bizzi E, Hogan N, Mussa-Ivaldi FA and Giszter SF. Does the nervous system use equilibrium-point control to guide single and multiple joint movements? *Behavior and Brain Science* 15: 603-613, 1992.

50. Aoyagi Y, Mushahwar VK, Stein RB and Prochazka A. Are movement primitives determined by spinal cord circuitry or biomechanics? *Society for Neuroscience 30th Annual Meeting*, New Orleans, La. Society for Neuroscience, 2000a, p. 696.

51. Tresch MC and Kiehn O. Motor coordination without action potentials in the mammalian spinal cord. *Nat Neurosci* 3: 593-599., 2000.

52. Loeb GE. Learning from the spinal cord. *J Physiol* 533: 111-117., 2001.

53. Gomi H and Kawato. Equilibrium-point control hypothesis examined by measured arm stiffness during multijoint movement. *Science* 272: 117-120., 1996.

54. Grillner S, Wallen P, Brodin L and Lansner A. Neuronal network generating locomotor behavior in lamprey: circuitry, transmitters, membrane properties, and simulation. *Annu Rev Neurosci* 14: 169-199, 1991.

55. Pearson KG. Common principles of motor control in vertebrates and invertebrates. *Annu Rev Neurosci* 16: 265-297, 1993.

56. McClellan AD. Organization of spinal cord locomotor networks: Contributions from model systems. *Comments Theor. Biol.* 4: 63-91, 1996.

57. Szekely G, Czeh G and Voros G. The activity pattern of limb muscles in freely moving normal and deafferented newts. *Exp Brain Res* 9: 53-62, 1969.

58. Grillner S and Zangger P. On the central generation of locomotion in the low spinal cat. *Exp Brain Res* 34: 241-261, 1979.

59. Grillner S. Neurobiological bases of rhythmic motor acts in vertebrates. *Science* 228: 143-149, 1985.

60. Baldissera F, Hultborn H and Illert M. Integration in spinal neuronal systems. In: *Handbook of physiology : a critical, comprehensive presentation of physiological knowledge and concepts.* Washington: American Physiological Society ; [distributed by Williams & Wilkins Baltimore], 1977, p. 509-595.

61. Jankowska E. Interneuronal relay in spinal pathways from proprioceptors. *Prog Neurobiol* 38: 335-378, 1992.

62. Jankowska E. Spinal interneuronal systems: identification, multifunctional character and reconfigurations in mammals. *J Physiol* 533: 31-40., 2001.

63. Rossignol S. Neural control of stereotypic limb movements. In: *Handbook of physiology ; section 12.* New York: Published for the American Physiological Society by Oxford University Press, 1996, p. 173-216.

64. Stein PSG. *Neurons, networks, and motor behavior.* Cambridge, Mass.: MIT Press, 1997.

65. Cheng J, Stein RB, Jovanovic K, Yoshida K, Bennett DJ and Han Y. Identification, localization, and modulation of neural networks for walking in the mudpuppy (Necturus maculatus) spinal cord. *J Neurosci* 18: 4295-4304, 1998.

66. Kiehn O and Kjaerulff O. Distribution of central pattern generators for rhythmic motor outputs in the spinal cord of limbed vertebrates. *Ann N Y Acad Sci* 860: 110-129, 1998.

67. Beato M and Nistri A. Interaction between disinhibited bursting and fictive locomotor patterns in the rat isolated spinal cord. *J Neurophysiol* 82: 2029-2038., 1999.

68. Schmidt S, Horch K and Normann R. Biocompatibility of silicon-based electrode

arrays implanted in feline cortical tissue. *J Biomed Mater Res* 27: 1393-1399, 1993.

69. Nordhausen CT, Maynard EM and Normann RA. Single unit recording capabilities of a 100 microelectrode array. *Brain Res* 726: 129-140., 1996.

70. Feldman AG. Functional tuning of the nervous system with control of movement or maintenance of a steady posture. II. Controllable parameters of the muscle. *Biophysics* 11: 565-578, 1966b.

71. Aoyagi Y, Strohschein FJ and Ming Chan K. Use of the collision technique to improve the accuracy of motor unit number estimation. *Clin Neurophysiol* 111: 1315-1319, 2000b.

72. Aoyagi Y, Strohschein FJ, Pang M and Chan KM. Neural mechanisms of central fatigue during submaximal isometric contraction of the thumb in humans. *Brain*, submitted.

CHAPTER 2

CAPABILITIES OF A PENETRATING MICROELECTRODE ARRAY FOR RECORDING SINGLE UNITS IN DORSAL ROOT GANGLIA OF THE CAT*

INTRODUCTION

To execute motor commands accurately, the central nervous system requires information about peripheral variables such as muscle force, position, and velocity. Sensory receptors have long been known to provide such feedback via reflexes and voluntary reactions for the control of posture and locomotion. Cutaneous, muscle and articular receptors form the main elements of this natural feedback system that has been the focus of intensive study throughout the last century (Matthews. 1982). Research on sensorimotor control has revealed that the properties of the musculoskeletal and the sensory systems are complex and the state of these systems changes from moment to moment as a function of the motor task (Stein and Capaday. 1988). Large ensembles of sensory receptors mediate this feedback pathway, but they have yet to be studied simultaneously in behaving animals, or even in anesthetized preparations. Understanding sensorimotor control will require access to a large, diverse population of afferents with large and stable signal-to-noise ratios.

Normann and his colleagues have developed a novel microelectrode array (the Utah Electrode Array) (Figure 2-1) that provides unprecedented access to large numbers of neurons (Campbell et al. 1991). This penetrating microelectrode array contains as many as 100 electrodes, and was originally developed for use in the cerebral cortex (Nordhausen et al. 1996; Schmidt et al. 1993). Earlier work confirmed that the microelectrode array can be used successfully in animals to stimulate cortical tissue. It can also record single- and multi-unit neural activity in sensory and motor cortex (Maynard et al. 1999; Maynard et al. 1997; Normann et al. 1999; Rousche and Normann. 1998; Rousche and Normann. 1999).

---

* A version of this chapter will be submitted to *J Neurosci Methods* by the authors of Aoyagi. Y, Stein. RB, Branner. A, Pearson. KG, Normann, RA.

Recently, we implanted a variant (the Utah Slanted Electrode Array) into the sciatic nerve of the cat (Branner and Normann. 2000; Branner et al. 2001) and showed this electrode permitted more selective stimulation with more graded recruitment of individual muscles than was achieved by conventional cuff electrodes. This suggests that such a microelectrode array could be used for restoration of motor function in paralyzed people.

In addition to its potential for selective muscle stimulation, we now suggest that the microelectrode array can provide sensory information in a feedback-controlled neuroprosthesis to improve the controllability of functional movement (Hoffer et al. 1996; Stein et al. 1992; Yoshida and Horch. 1996). Although sensory units could be recorded from the peripheral nerve, their quality, quantity, and stability were not satisfactory; the amplitudes of the recorded sensory units ranged from 15 to 200μV and the percentage of electrodes that recorded sensory units was only 10- 20 %) (Branner and Normann. 2000; Branner et al. 2001). To circumvent this drawback, we considered another potential recording locus: the dorsal root ganglion (DRG) (Loeb et al. 1977). Each DRG receives and conveys impulses from a variety of receptors in peripheral nerve fibers and has the advantage of containing large somata (40–70 μm) (Willis and Coggeshall. 1991) that may allow the recording of large single units.

The aim of this project was therefore to test the capabilities of the penetrating microelectrode array in providing access to DRGs in acute anesthetized cats, and in decerebrate walking cats, by recording single- and multi-unit neural activity from L6 and L7 DRGs. We also wanted to determine some physiological and anatomical characteristics of the sensory afferents accessed by the microelectrode array. We found that the penetrating microelectrode array is capable of recording from somata in DRGs with more and larger, discriminable sensory unit action potentials than has been achieved by conventional recording techniques. Finally, because the microelectrode array is also capable of recording from a variety of afferent sensory neurons, we suggest that the microelectrode array could provide a useful sensory interface in basic sensorimotor studies and in eventual neuroprosthetic applications.

METHODS

Microelectrode Array

The Utah Electrode Array (Bionic Technologies, LLC., Salt Lake City, UT) was used in this study (Figure 2-1a). The manufacturing process has been described in detail elsewhere (Campbell et al. 1991; Jones et al. 1992), but its architecture will be briefly described. The electrodes are regularly spaced on 400 μm centers and project up to 1.5 mm out of the plane of a 0.2-mm thick silicon substrate. Each electrode is electrically isolated from the neighboring electrodes with a 'moat' of glass around its base, and electrical insulation of the conducting silicon microelectrodes is accomplished with polyimide or with silicon nitride. Each electrode is approximately 80 μm wide at its base and tapers to a sharpened tip. The tip of each electrode is coated with platinum; 25 μm diameter insulated lead wires are soldered to a connector that plugs into a data-acquisition system. The arrays used in this study contained 5x8, 5x10, and 10x10 arrays. The 5x8 arrays were led to a 40-pin "tulip" connector (see Figure 2-1b and (Branner et al. 2001)). The impedance of each electrode was measured with the electrode array implanted using a commercial impedance monitor (Ωmega-Tip Z, World Precision Instruments, Sarasota, FL).

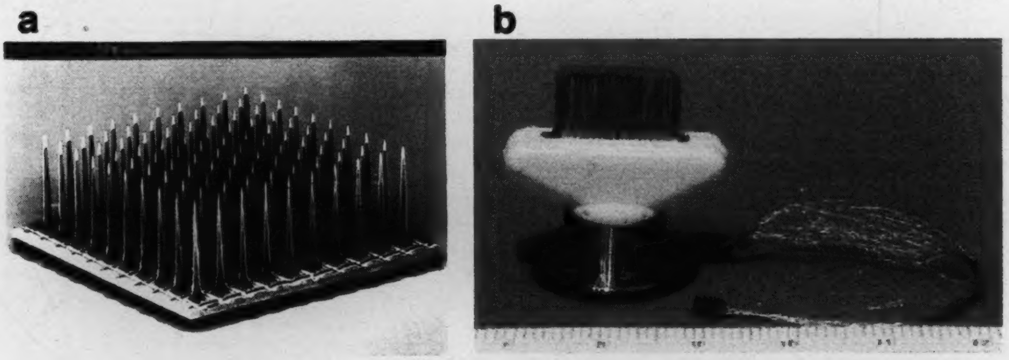

Figure 2-1. a. Scanning electron micrograph of the Utah Electrode Array. Note that the white part at the sharp tip of each electrode is deinsulated. **b.** Picture of a"tulip" connector with leads to the array. This is an example of 10x10 electrode array, although 5x8 arrays were used more commonly in this study to match the size of the dorsal root ganglion (DRG).

Animal Preparation and Electrode Implantation

Eleven cats were used in these experiments at the University of Utah and the University of Alberta. The local animal welfare committees approved all procedures. Depending on the approved protocols at the two universities anesthesia was either induced with Telazol (10 mg/kg) or with Halothane. The animals were maintained either with halothane or with sodium pentobarbital. Animals either breathed voluntarily or were mechanically ventilated as needed with 95% O_2 and 5% CO_2 while anesthetized with halothane. The electrocardiogram (ECG), expired CO_2, blood pressure, O_2 saturation, and core temperature were monitored throughout most experiments. The animals were placed on a heated water blanket that maintained body temperature close to 37°C. The animal's back was shaved and a skin incision was made lateral to the midline of the back. Paraspinal muscles overlying the transverse processes of L6, L7 and S1 vertebrae were removed on the right side. The right side of the lumbosacral cord was exposed by a L5-S2 hemi-laminectomy. The right transverse processes and the surrounding tissue were dissected to expose the DRGs. The dura remained intact.

In eight animals, L6 (n=6) and/or L7 (n=6) DRGs were used for the classification of afferents and recording statistics. The electrode array was positioned on the L6 and/or L7 DRGs and then inserted through the dura into the DRG with a pneumatic inserter that has been used successfully in cerebral cortex and peripheral nerve (Branner and Normann. 2000; Rousche and Normann. 1992). After implantation, a Pt/Ir reference wire was placed in the fluids surrounding the DRGs and the skin was closed.

Classification of Afferents

For identification, individual sensory action potentials were recorded from each electrode channel during various manual manipulations (Loeb et al. 1977; Loeb and Duysens. 1979; Matthews. 1972; Prochazka et al. 1976). Manual manipulations included the passive range of motion for hip, knee and ankle joints and tapping over a muscle belly or a tendon to identify muscle and articular receptors. Palpation (touch, pressure, pinch) was also used to identify cutaneous and subcutaneous receptors and gentle blowing to identify hair receptors. A Q-tip, forceps, or brush were used to activate skin receptors as the need arose. Some units were further identified by 'stretching' and 'vibration' (see section below for analysis procedures) delivered by a servocontrolled muscle mechanical stimulator with a built-in force transducer (Cambridge Technology, Inc., Series 300B, Cambridge, MA). In some experiments, triangular or sinusoidal displacements were applied to the skin over the plantar area of the right foot at various frequencies to simultaneously record from all available electrode channels.

Conduction Velocity

In one animal the conduction velocity of sensory neurons recorded by the microelectrode array implanted in L7 DRG was measured using the technique of spike-triggered averaging from a nerve cuff electrode (Hoffer et al. 1981; Stein et al. 1977). After the microelectrode array was implanted in the L7 DRG as described above, the right sciatic nerve was exposed. A silastic nerve cuff with tripolar recording electrodes was implanted around the sciatic nerve. After the compound action potentials had been examined to ensure that the nerve was in good condition, each sensory unit action potential was induced by limb manipulation. Each occurrence of an extracted spike using a threshold procedure (see *Data Acquisition and Data Analysis*) triggered the sweep of a signal averager (TDS3014, Tektronix Inc., Beaverton, OR). As sweeps accumulated (usually 50 -1000 times), a correlated neural potential was resolved at a fixed latency from the extracted spike at the DRG. At the termination of this acute experiment, the distance between the cuff electrodes and the microelectrode array was measured to calculate the conduction velocity.

Decerebrate Walking

Two animals were used for recording during walking-like movements under decerebration. The microelectrode arrays were implanted in L7 and S1 DRGs as described above. After each sensory unit was identified (see *Classification of Afferents*), the animal was placed over a treadmill with its head secured in a stereotaxic holder. Radiant heat was applied to maintain a temperature close to 37°C. Animals were decerebrated at a precollicular level and walking-like movements were induced after they recovered from anesthesia (Whelan. 1996). Decerebration was performed by removing the cerebral hemispheres and then transecting the brainstem at a 50° angle, rostral to the superior colliculi. The anesthetic was discontinued at this point. Within one hour, animals produced spontaneous periods of walking. Electromyographic (EMG) recordings were made from vastus lateralis (VL), sartorius (ST), extensor digitorum longus (EDL), and medial gastrocnemius (MG) of the right leg during walking. The EMGs were recorded using a pair of stainless steel wires (Cooner Wire, AS632) implanted into the bellies of the muscles. The wires were Teflon-coated except for a 5mm deinsulated region. The wires of a recording pair were separated by a distance of about 5mm within the muscle. In order to reconfirm possible muscle afferents, appropriate tendons were transected, connected to a muscle mechanical stimulator and activated individually using standard ramp, vibration and twitch tests (Matthews. 1972) at the termination of the experiment.

Data Acquisition and Analysis

The electrode array was connected to either a 16- or 100-channel amplifier (bandwidth from 250-7500 Hz). The gain of the amplifier was either 5,000 or 25,000 and each electrode was sampled at 30 kHz. A Pentium III class PC simultaneously saved the responses from the 16 or 100 electrodes via a 16-channel Neural Signal Amplifier / WinAcq System (Bionic Technologies, LLC, Salt Lake City, UT) or a 100-channel Neural Signal Acquisition Systems (Bionic Technologies, LLC) (Guillory and Normann. 1999).

To extract the activity of a unit from a multi-unit recording, individual sensory action potentials were first extracted from the records of neural activity using a threshold procedure. These action potential waveforms were aligned on the threshold crossing and then passed to a neural spike classification program (Bionic Technologies, LLC) (see Figure 2-2a). Multiple units could often be extracted on a single electrode if they had sufficiently large signal-to-noise ratios. Figure 2-2b shows an example of single-units identified using a principle component analysis (PCA) under Matlab (Math Works, Inc., Natick, MA), where the first two principle components have been plotted against one another. Principle component analysis is a frequently used statistical method that distinguishes different shapes by their position along orthogonal axes (Johnson and Wichern. 1988). In this example, the three spikes fall into three readily distinguishable clusters.

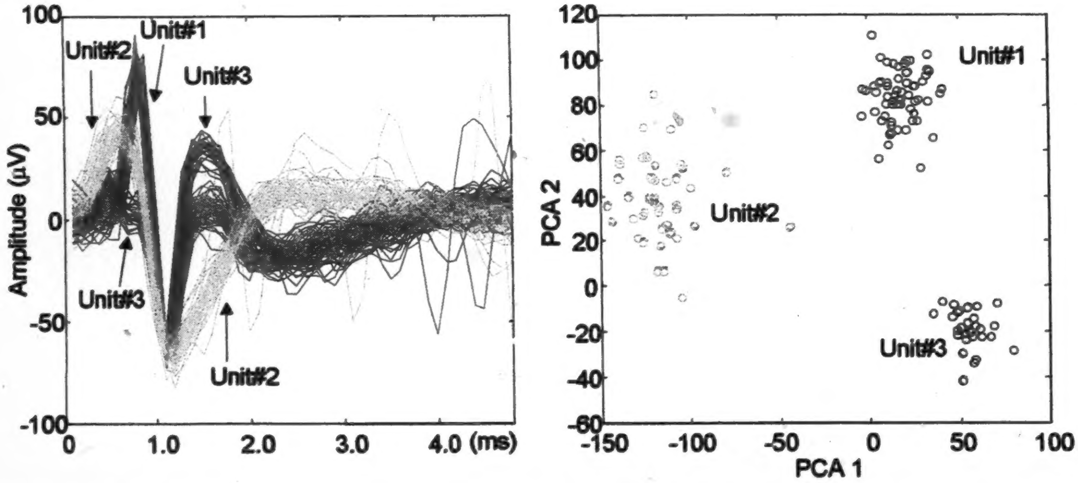

Figure 2-2. Single-unit identification on an individual electrode channel. Three units were identified from an electrode implanted in L7 DRG: Units#1 and #2 were muscle receptors responding to hip extension and knee extension respectively. Unit#3 was a cutaneous receptor responding to light touch on the medial surface of the foot. During a passive, manual movement of the hip and knee, the three units were recorded (10 s duration). Later, they were classified into three groups using a principle components analysis (PCA). Note that a few action potentials occurred soon after a triggered unit, and these would not be classified.

Triangular, sinusoidal or ramp movements were applied to the skin over a muscle belly or a tendon at frequencies between 0.5 and 300 Hz using a mechanical actuator (Cambridge Instruments Series 300B, Cambridge MA). For analysis the sync pulses from the mechanical stimulator were used to produce a cycle histogram with a Matlab program for each unit as shown in Figure 2-3. The y-axis was converted to impulses per second by dividing the number of spikes in each time bin by the number of cycles averaged and the bin width. The bin width was adjusted automatically to be 1% of the cycle time. The neural data were fitted by a curve of the form

1) $y_n = a_n + b_n \sin\theta + c_n \cos\theta$

The mean rate of firing was a_n. The magnitude M_n and phase φ_n of the modulations were given by:

2) $M_n = \sqrt{(b_n^2 + c_n^2)}$; $\varphi_n = \tan^{-1}(b_n/c_n)$

A similar analysis was done for the length changes applied, resulting in M_l and φ_l. The gain or sensitivity of the receptor and the phase advance were defined by:

3) gain = M_n/M_l; phase = $\varphi_l - \varphi_n$

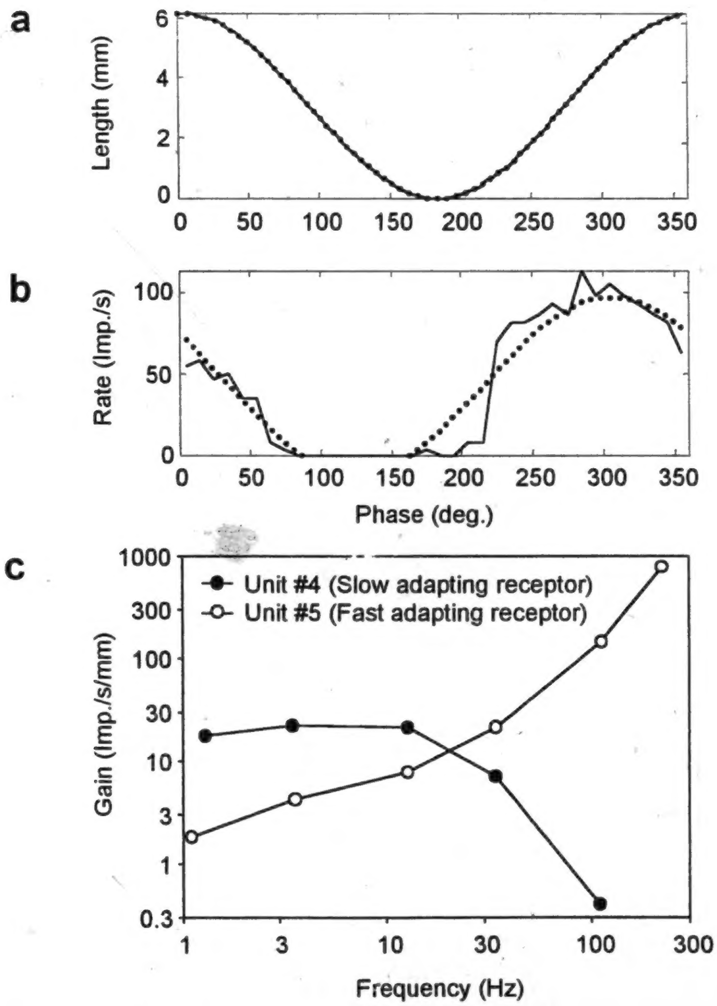

Figure 2-3. Analysis of cyclic responses. **a.** Sinusoidal movements were applied over the skin near a cutaneous receptor at 1.3 Hz for 10 s. **b.** The solid line represents the average firing rate elicited by the sinusoidal movements (see Methods). The phase advance and the mean rate were calculated as 58° and 42.7 imp./s respectively in this example. The gain was calculated as 17.5 imp./s/mm. **c.** The gains of two cutaneous receptors at various frequencies were displayed in a log-log plot.

RESULTS

Recording Statistics

The arrays used to determine the statistics of the recorded units were rectangular with 5x8 (n=5), 5x10 (n=6), and 10x10 (n=1) electrodes. Out of a total of 600 electrodes used in the anesthetized cats, 587 electrodes were regarded as 'potentially active electrodes' (13 electrodes were used as reference or ground). Out of the 587 potentially active electrodes, 247 electrodes (42%) recorded at least one sensory unit using various manipulations. Some electrodes picked up two or more units. Figure 2-2 shows an example of multi-unit neural activity recorded from L7 DRG. In this electrode channel, three units (two muscle receptors and a cutaneous receptor) were identified using manipulation. The three units in Figure 2-2a were simultaneously recorded during a 10 s manipulation. Thus, the 247 individual electrodes picked up from 1 to 5 sensory neurons (mean=1.51) and detected a total of 373 sensory units by manual manipulations.

Classification of Afferents

The identified units were classified into muscle receptors, deep receptors, cutaneous receptors (Brown and Koerber. 1978) and articular receptors (Grigg and Greenspan. 1977). Muscle receptors can be subclassified into Ia, II afferents and Golgi tendon organs. However, in the experiment under anesthesia, we did not stimulate all the muscle nerves. Also, we did not isolate the tendons to hold the muscles isometrically or apply ramp stretches. We therefore treated the muscle receptors as a single group. Deep receptors included receptors responding to strong pressure applied through the skin, but not responding to passive joint displacement, light touch or manipulation of the skin between the fingers. This last group was classed as cutaneous receptors. Hair receptors were included in the category of cutaneous receptor. Receptors firing only at near the physiological extreme of joint angle were classified as articular receptors, but they were sometimes difficult to distinguish from Golgi tendon organs in the intact, anesthetized animal. From a total of 373 identified units (168 from L6 and 205 from L7), approximately half (200, 53.6%) were muscle receptors (Figure 2-4a), 100 (26.8%) were cutaneous receptors, 41 (11.0%) were deep pressure receptors, and 15 (4.0%) were articular receptors. 17 (4.6%) units fired spontaneously and did not respond to any specific manipulations that were applied.

We classified muscle receptors according to the joint(s) whose manipulation elicited responses. Some of the muscle receptors in biarticular muscles responded to movement of two joints. Of 100 muscle receptors with somata in the L6 DRG, 76 responded to movement of a single joint and 24 responded to movements of two joints. Similarly, of 100 muscle receptors with somata in the L7 DRG, 65 responded to movement of one joint and 35 responded to movement of two joints. L6 units responded mainly to hip and knee extension, flexion, and ankle extension, whereas L7 responded mainly to toe and ankle extension and flexion (Figure 2-4b). The L6 and L7 cutaneous and pressure receptors had distinct, but overlapping innervation. L6 units responded to skin areas that included those anterior to the medial surface of the knee, lower leg, ankle and foot. Most L7 units were localized to areas around the toes and were seen sparsely on heel and sole. These results are consistent with a previous report (Brown and Koerber. 1978).

Localization of afferent neurons within the DRG

The dermatomal organization within the DRG has been a long-standing question (see Discussion). The microelectrode array allowed us to construct anatomical maps, as shown for the L6 DRG in Figure 2-5. Each square represents one electrode in a 5x10 array implanted along the longitudinal axis of the DRG. Five rows typically covered most of the width of the ganglion so the rows represent the proximal (lateral) to the distal (medial) edges of the ganglion. For electrodes that recorded two or more units, the square was divided into parts corresponding to the number of obtained units (Figure 2-5). Muscle, cutaneous, deep, articular and unclassified receptors were expressed by 'M', 'C', 'D', 'A', and 'U'. All types of receptors could be obtained from any row and more than two types of afferents were often obtained from one electrode, suggesting that the cells were scattered through the DRG without any clustering according to cell type.

In addition, one electrode often picked up muscle afferents from reciprocal muscle groups. Thus, no obvious topographical organization of muscle groups was detected, although some clustering of cutaneous afferents was observed within the DRG. For example, the most laterally implanted electrodes in Figure 2-5 recorded cutaneous afferents originating from

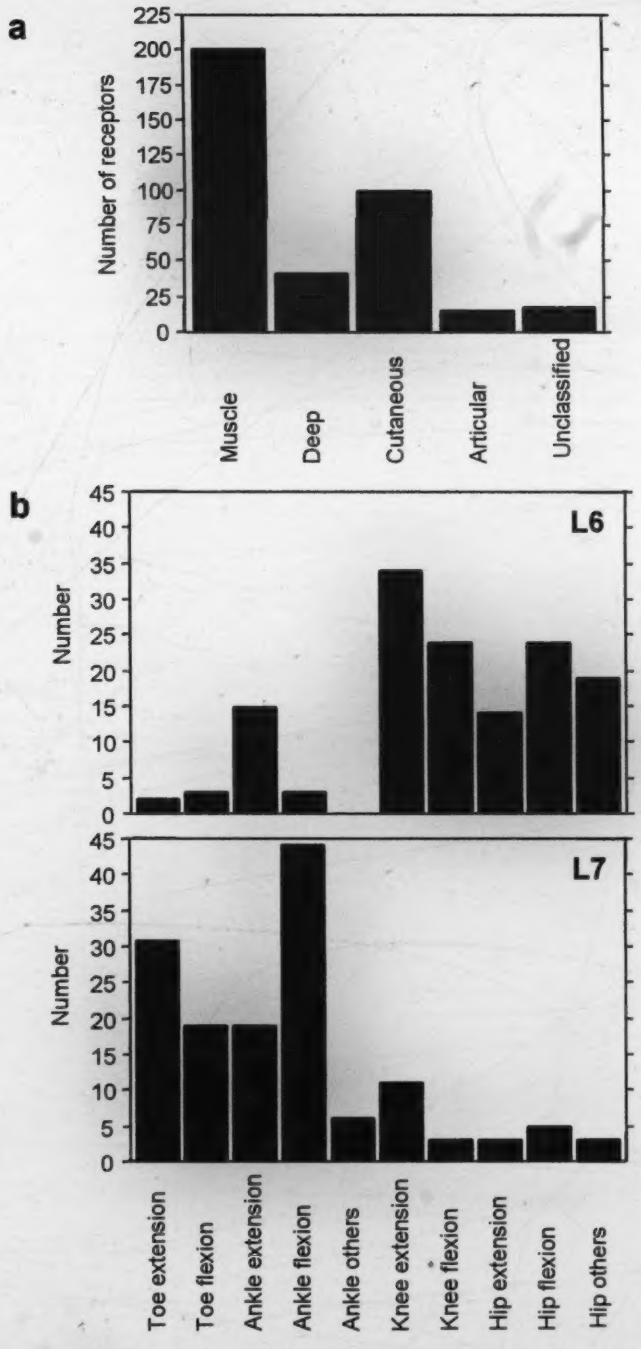

Figure 2-4. a. Histogram of 373 identified units from L6 (168 units) and L7 DRGs (20 units). Muscle, deep, cutaneous, and articular receptors were 200 (53.6%), 41 (11.0%), 10 (26.8%), 15 (4.0%) respectively. 17 (4.6%) units were unclassified (see also text). **b.** L6 unit responded mainly to displacement of hip and knee joints and ankle extension. L7 responde mainly to displacement of toe and ankle joints. 'Others' included abduction, adduction inversion, eversion, external and internal rotation of the various joints.

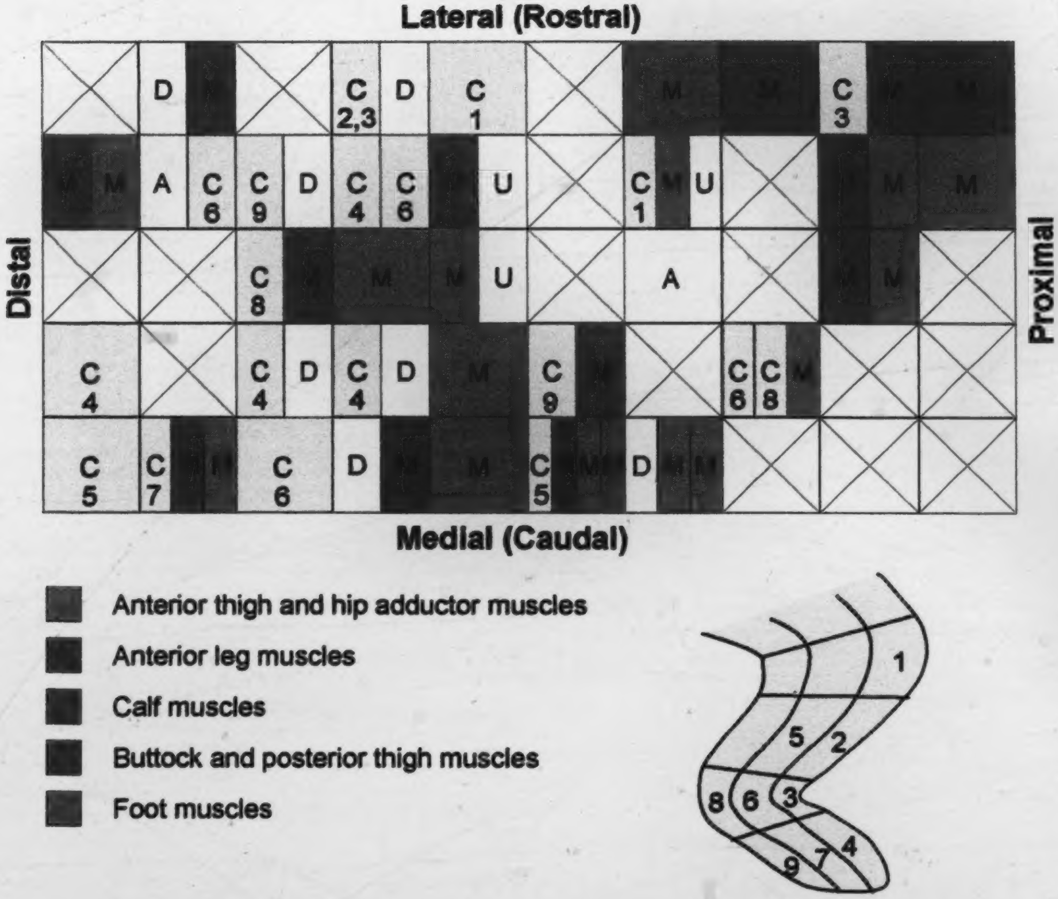
Lateral (Rostral)
Medial (Caudal)
Distal
Proximal
Anterior thigh and hip adductor muscles
Anterior leg muscles
Calf muscles
Buttock and posterior thigh muscles
Foot muscles
1
2
3
4
5
6
7
8
9

Figure 2-5. An example of a recording map from L6 DRG. Each square represents one electrode in a 5x10 array. For electrodes where more than two units were obtained, the square was divided according to the number of recorded units. Muscle, cutaneous, deep, articular and unclassified receptors were expressed by 'M', 'C', 'D', 'A', and 'U'. Different muscles were represented by different colors, while different areas of skin were numbered as shown in the diagram of the leg.

the anterior surface of the knee and lower leg, which corresponds to the border with the L5 dermatome (Brown and Koerber. 1978). Medially located electrodes tended to record cutaneous afferents originating from the lateral and plantar surfaces of the foot and ankle. The ratio of cutaneous receptors from the anterior knee and lower leg areas (1, 2, and 3 in Figure 2-5) in individual lines was: 100% (4/4), 20% (1/5), 0% (0/1), 0% (0/6), 0% (0/4) (chi-square test for independence, $p<0.01$). Some tendency for clustering of cutaneous afferents according to dermatome was generally seen in the other DRGs. However, cutaneous afferents showed considerable overlap and intermingling, so the distinction was not always clear from one row to the next.

Signal Amplitude and Impedance

Figure 2-6a shows a histogram of the recorded amplitudes from 8 anesthetized cats. The amplitudes of single units obtained during manual manipulations ranged between 15 μV and 1750μV (mean ± S.D. = 132 ± 147μV, median = 95μV) (Figure 2-6a). Impedance was measured for 387 implanted electrodes. Electrodes that did or did not record some sensory activity are shown respectively by dotted and clear areas as a function of electrode impedance (Figure 2-6b). Electrodes with impedances more than 800 kΩ recorded with lower probability (mean=14.5%) whereas those with impedances less than 800 kΩ recorded neural activities with a mean probability of 50.5%. Electrodes with impedances between 30 kΩ and 200 kΩ had the highest percentage (56-57%). Sensory units with larger amplitudes were mostly observed in electrodes with less than 800 kΩ (Figure 2-6c).

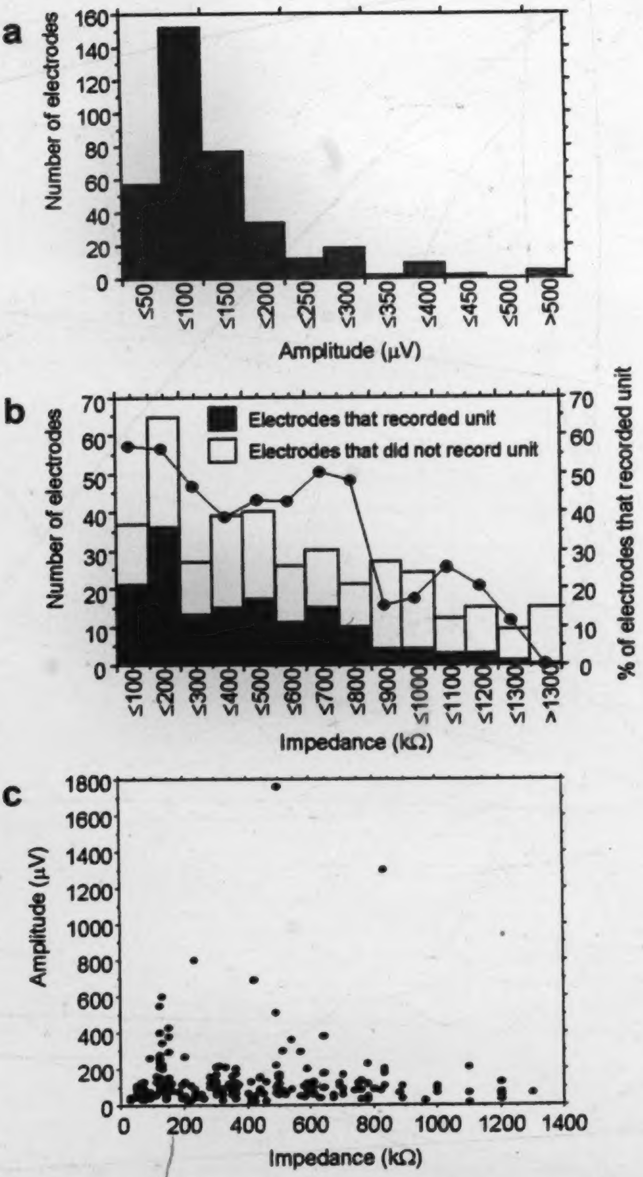

Figure 2-6. a. Histogram of the amplitudes of sensory action potentials recorded from individual electrode channels during manual manipulations. Sensory action potentials with large amplitudes (>500 μV) were occasionally observed. **b.** Histogram of the impedance of electrodes. 154 (shown by dotted area) out of 387 electrodes recorded sensory units. 233 electrodes did not (shown by clear area). The percentage of electrodes in each range that recorded neural activity was plotted by the line graph. Electrodes with less than 800 kΩ had a tendency to record units with a probability as high as 50%, whereas those with more than 800 kΩ recorded units with a probability of less than 25%. **c.** Relationship between amplitude and impedance. Large amplitude sensory units were mostly observed in electrodes with less than 800 kΩ.

Frequency analysis and recording during passive movement

We were interested in the extent to which sensory receptors could be analyzed in intact preparations. Therefore, triangular or sinusoidal movements were applied at various frequencies in some animals using an actuator. Figure 2-3 shows the averaged response of a cutaneous afferent (Figure 2-3b) to a 1.3 Hz indentation of the skin (Figure 2-3a). The gain could be calculated (see Methods) over a range of different frequencies (Figure 2-3c). This is helpful to distinguish rapidly adapting units such as Pacinian corpuscles (Bell et al. 1994) that continue to increase their gain up to 300 Hz, from slowly adapting receptors such as Merkel discs that respond best below 10 Hz (Munger and Ide. 1988). However, a detailed quantitative analysis of receptor types is beyond the scope of this paper.

We were more interested to analyze the sensory neural activity from many electrodes simultaneously. Figure 2-7 demonstrates a recording during application of triangular movements with an amplitude of 2.4 cm at 1.1 Hz to a plantar area (4.3 cm from the heel) to generate cyclic ankle flexion and extension. Many of the 52 units recorded were recruited at 1.1 Hz, as shown in Figure 2-7. Electrodes #1-50 were implanted in L6 DRG and #51-100 in L7. As expected, muscle receptors in quadriceps and hamstrings (e.g. 19.0, 20.0, 45.0, 49.1) were not very well modulated by the ankle movement, while those in tibialis anterior and triceps surae were (e.g. 77.0 78.0, 87.0, 89.1, 96.1, 96.2, 97.1, 99.0). Many other receptor types can be seen. Two ankle articular receptors (48.0 and 56.2) tended to fire one or two spikes at specific angles of the joint. Hair receptors (66.0 and 66.1) fired rather sparsely, but were somewhat modulated, probably with a touch of the force transducer to the hair. Some ‘unidentified’ units were activated by the mechanical stimulus that we had not noted during previous manual manipulations.

Conduction Velocity

Figure 2-8a shows an example of unitary potentials obtained from spike-triggered, averaged records. The sensory unit action potential in the top trace was recorded from a muscle afferent fiber by a microelectrode in the L7 DRG. The lower trace presents the corresponding spike-triggered, averaged potential obtained from the sciatic cuff electrode. The negative peak to negative peak latency between the two potentials was 1.9ms. Since the distance between the cuff electrodes and the microelectrode array was 10.9cm, the

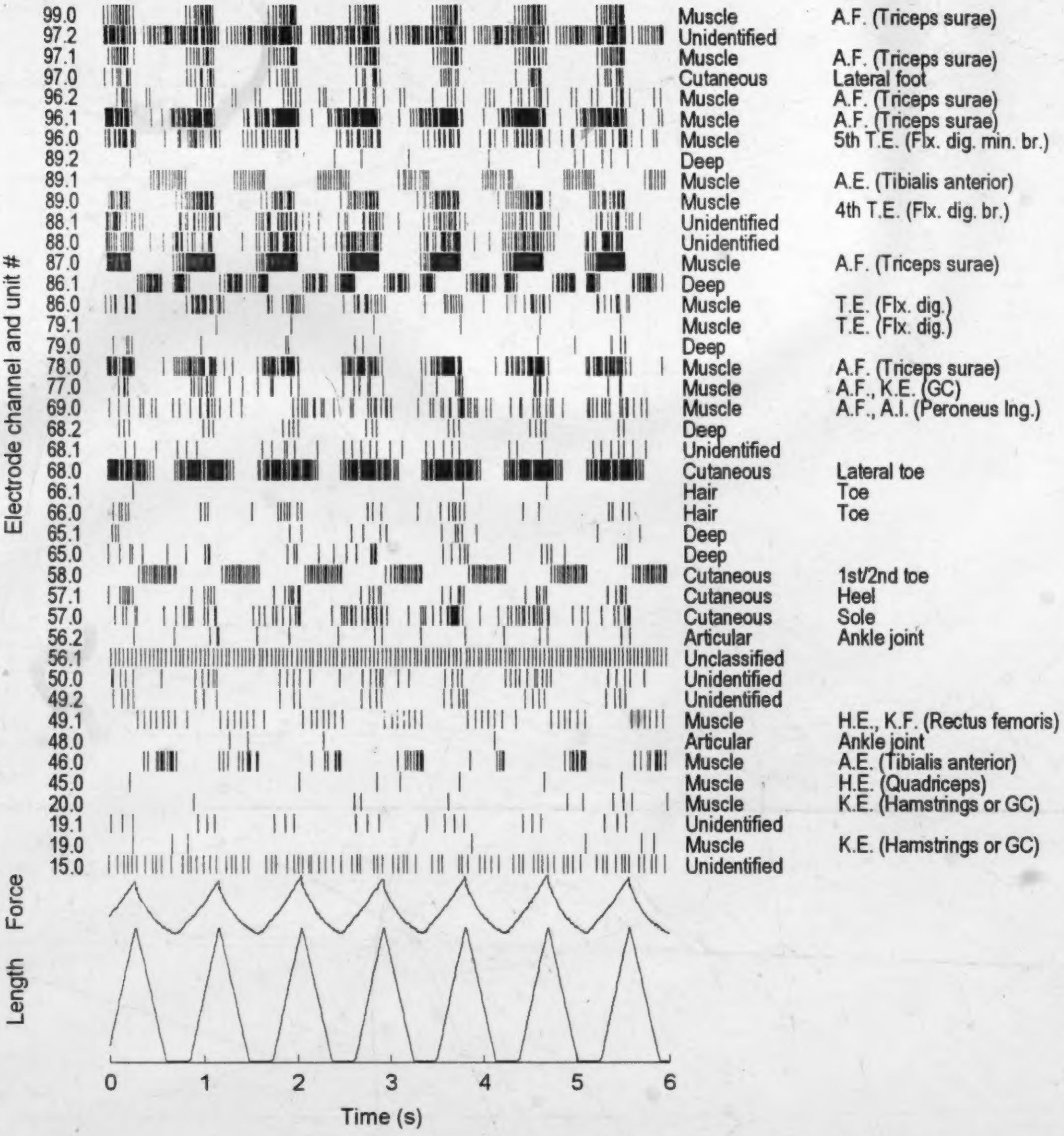

Figure 2-7. Simultaneous recording from L6 and L7 DRGs during ankle flexion and extension generated by a servo-controlled actuator with a mechanical force transducer. Triangular movements were applied to the plantar surface (4.3 cm from the heel) at 1.1 Hz with an amplitude of 2.4 cm. Modulated activity from 42 sensory units are shown. The sensory modalities that evoked the activity are listed. For muscle receptors the movement(s) that evoked a response (e.g. ankle flexion, AF) are given together with muscles (e.g., triceps surae) in which the receptor may have been. Unfortunately, in this example the length recording saturated at the most negative values. Abbreviations: A.;ankle, K.;knee; H.;hip, E.;extension, F.;flexion, I.;inversion, flx.;flexor, dig.;digiti, min.;minimi, br.;brevis, lng.;longus, GC; gastrocnemius, SM;semimembraneous, ST;semitendinosus.

conduction velocity was calculated as 57 m/s.

In this study on conduction velocity 33 sensory units were detected in one 5x10 array. Spike-triggered averaged records that had clear potentials were obtained from the cuff electrode for 24 units (73%). No clear, spike-triggered average was seen for the other 9 units (27%). Figure 2-8b shows the relationship between sensory fiber conduction velocity and the peak-to-peak amplitude recorded by a microelectrode in L7 DRG. Conduction velocity ranged from 35 to 92 m/s. No clear correlation was found between the conduction velocity and the amplitude (Pearson's correlation coefficient, r=0.08).

Decerebrate Walking

The results up to this point were obtained in deeply anesthetized animals. In two experiments cats were decerebrated (see Methods) and walking on a treadmill was induced to determine the effects of EMG or other movement-related interference. Figure 2-9 demonstrates the simultaneous multiple firing of some units in the L7 DRG and normalized EMGs during decerebrate walking. We were able to isolate action potentials of as many as 15 sensory units from 20 - 25 available electrodes during a step cycle with very little noise or contamination of EMG signals. Figure 2-10 shows the pattern of EMG and sensory activity from Figure 2-9 averaged over the step cycle. The cycle time was 1.32 ± 0.03 s. The beginning of the flexion (swing) phase is 0 and the end of the extensor (stance) phase is 100%. Note the distinct patterns of EMG activity and of sensory afferents. Both the TA and the EDL spindles (c) reached their peaks late in the stance phase, when these muscles are stretched, but the TA (o) also had a substantial burst in the swing phase, presumably as a result of fusimotor activity. Two FHL spindles (d) fired mainly in the stance phase, but the activity began to rise already in the swing phase, presumably because the fusimotor activity

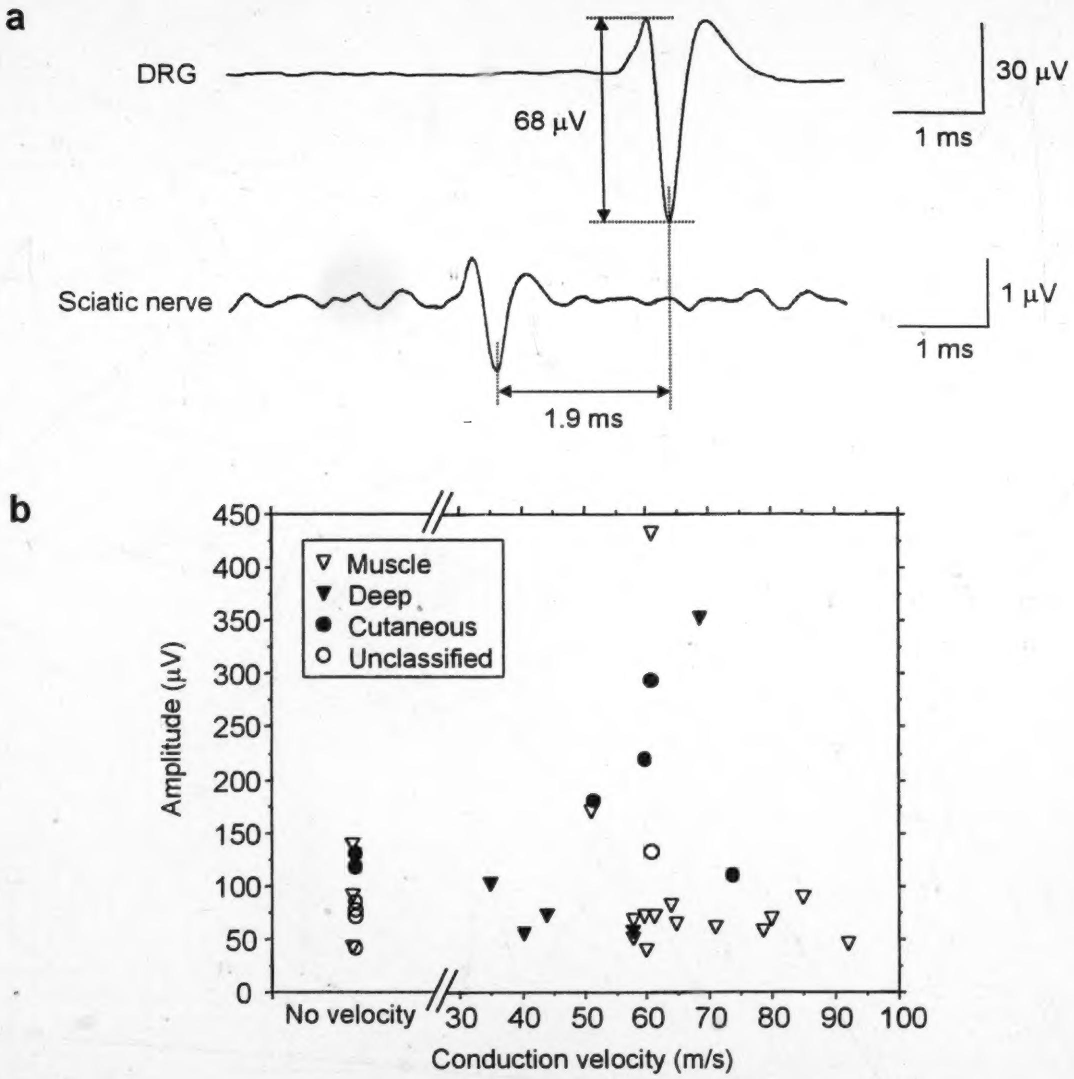

Figure 2-8 a. Spike-triggered averaged records obtained from a muscle afferent fiber. Uppe trace was recorded at L7 DRG using a penetrating microelectrode array. The peak to peak amplitude of the potential was 68 µV. Lower trace represents the spike-triggered, averaged potential recorded using cuff electrode implanted around the sciatic nerve. The negative peak to negative peak latency between the two potentials was 1.9ms. **b.** Relation between sensory fiber conduction velocity and peak-to-peak amplitude of action potentials recorded at the L7 DRG.

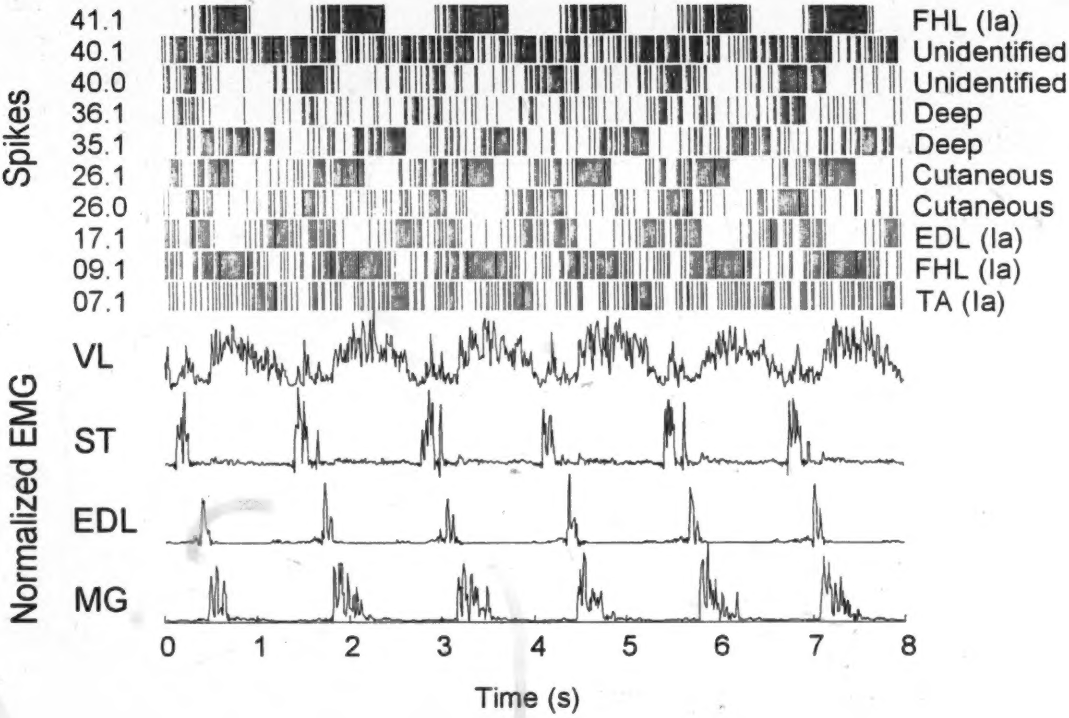

Figure 2-9. Sensory units and EMGs recorded during decerebrate walking. Abbreviations: VL;vastus lateralis, ST;sartorius, EDL;extensor digitorum longus, MG; medial gastrocnemius, FHL; flexor digitorum longus, TA;tibialis anterior

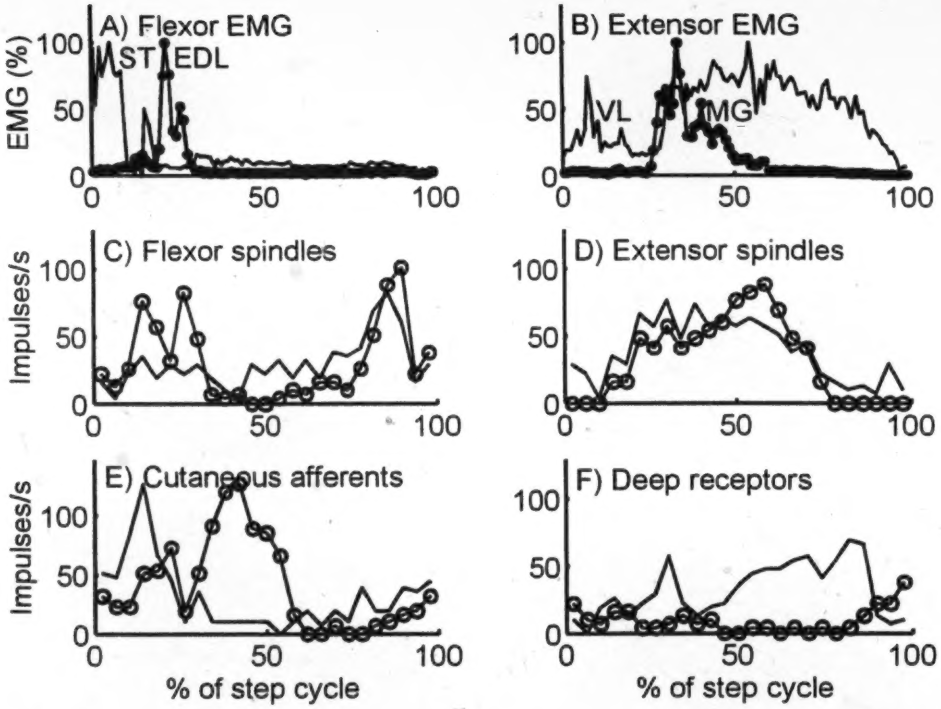

Figure 2-10. **a**) The ST EMG was used to average and normalize the step cycle. EDL fired later in the swing phase in this animal. **b**) MG mainly fired early in the stance phase, whereas VL fired throughout the stance phase and had a second smaller burst during swing. **c**) and **d**) show ankle flexor and extensor primary muscle spindle afferents, whereas **e**) and **f**) show the firing patterns of cutaneous and deep receptors. Each had a distinct pattern of firing during the step cycle.

began to rise before the α–motoneurons began to fire (Murphy et al. 1984). Two cutaneous afferents (e) fired mainly in the swing (-) and the stance (o) phases. Similarly, two deep receptors (f) fired in the stance phase (-) and the transition from stance to swing (o). These distinct patterns of activity provide several markers that might be useful in controlling walking naturally or with electrical stimulation (see Discussion).

DISCUSSION

This paper describes the first attempt to record sensory activity from the DRG using penetrating microelectrode arrays. We recorded and classified nearly 400 single sensory units from less than 600 implanted electrodes (0.64 units/electrode). This high yield occurred despite the fact that we re-used some arrays in more than one experiment. Nonetheless, we studied up to 100 units in a single experiment and more than 50 units simultaneously to a single movement (Figure 2-7). Although we did not derive new concepts from this first study, we were able to confirm a number of ideas and to describe a recording platform that should enable more detailed, future studies. The unrivalled access to sensory information supports our two longer-term goals, namely to provide a better understanding of the parallel processing of sensory information during multi-joint movements and to use this information to provide sensory feedback to a neural prosthesis. The application of this information to a neural prosthesis will require long-term, chronic recordings and this remains a topic for future work.

Recording capabilities of the penetrating microelectrode array

Much better signal quality was obtained from the DRG than from the peripheral nerve or spinal root recordings (Mannard et al., 1974; Kovacs et al., 1994; Loeb and Peck, 1996; Yoshida and Horch, 1996; Branner and Normann, 2000), and it was comparable to reports of the best DRG extracellular recordings made with conventional electrodes (Loeb et al. 1977; Loeb and Duysens. 1979; Prochazka et al. 1979). Average sensory action potentials recorded here had a mean amplitude of 132 μV and amplitudes of more than 500 μV were occasionally observed. No amplitudes exceeded 500 μV in the Figures shown in the cited references (Branner and Normann. 2000; Kovacs et al. 1994; Loeb et al. 1977; Loeb and Duysens. 1979; Loeb and Peck. 1996; Mannard et al. 1974; Prochazka et al. 1979; Yoshida and Horch. 1996).

The electrode impedances ranged from 30 kΩ to 1500 kΩ. Typically, the impedances of Utah electrode arrays are between 70 and 300 kΩ. However, some microelectrodes had tips that became damaged (broken) by the implantation procedure by hitting the bone underlying the DRGs. Also, we re-used partially damaged electrodes in some experiments. Despite this, half the electrodes with impedances less than 800 kΩ recorded neural activity from the DRGs. This is a high rate compared to peripheral nerve recording using the same electrode array (Branner and Normann. 2000). The better results are presumably a consequence of the larger size and much larger currents that are generated by somata that is not surrounded by myelin sheaths.

Amplitude, impedance and distance

The diameters of DRG somata are known to be linearly related to their peripheral axonal conduction velocity (Cameron et al. 1986; Yoshida and Matsuda. 1979). In this study, there was no significant difference in amplitude between muscle, deep, cutaneous, articular, and 'unclassified' receptors. We also found no relationship between the conduction velocity and the amplitude recorded by a microelectrode array. These results suggest that the distance from the recording site to the soma is the dominant factor in determining the amplitude.

Sensory fibers conduction velocities obtained by a penetrating microelectrode array (35 to 92 m/s, Figure 2-8) were similar to previous results using conventional electrodes (Hoffer et al. 1981; Stein et al. 1977), suggesting that sensory fibers whose potentials were successfully extracted by a sciatic cuff electrode using spike-triggered averaging (24/33, 73%) were group I and II fibers. For 9 fibers no conduction velocity could be extracted by spike-triggered averaging. Interestingly, 4 of the 9 units fired spontaneously and were not modulated by any manipulation that we tried. These units might be nociceptors (Cameron et al. 1986), thermal (Iggo. 1969), or other high threshold slow afferents with free endings that have smaller, slower conduction fibers (group III, IV). The much smaller action potentials from group III and IV fibers can not be extracted by spike-triggered averaging on the whole sciatic nerve (Hoffer et al. 1981). These other modalities should be studied further in the future.

Somatotopic organization

Some authors have suggested that somatotopy exists within the DRG, but others have disputed this point (cf. (Baron et al. 1988; Burton and McFarlane. 1973; McLachlan and Janig. 1983)). Our electrophysiological results support some somatotopy of cutaneous afferents in the DRG. For example, cutaneous afferents originating from the anterior knee, which corresponds to the border with the L5 dermatome (Brown and Koerber. 1978), were mostly obtained from rostrally (laterally) implanted electrodes in the L6 array (Figure 2-5). Cutaneous afferents whose dermatome was very close to the L7 dermatome (mainly toes, sole and heel) tended to be found mostly from caudally (medially) located row(s) of the array. These results suggest that the cells in each ganglion may be arranged in a weak, somatotopically-ordered sequence (Burton and McFarlane. 1973; McLachlan and Janig.

1983).

Potentials for sensorimotor control research and clinical application

Normann and his colleagues have been successful in chronically implanting Utah electrode arrays into cerebral cortex (Maynard et al. 1999; Normann et al. 1999; Rousche and Normann. 1998; Rousche and Normann. 1999). The next step will be to test the middle- and long-term stability for recording from a stable population of neurons in the DRG. The basic principles of motor control would best be determined by studying freely moving animals during natural motor tasks. Understanding parallel processing of somatosensory information in behaving animals would also provide useful information for neural modeling and robotic control.

If sensory action potentials can be reliably identified on chronically implanted electrodes, the spikes may be used as natural sensors to trigger and stimulate muscle activity. To use the microelectrode array in a feedback-controlled neuroprosthesis, effective sensory cues would be needed such as transitional signals from one phase of gait to another during movement. Figure 2-9 and 2-10 clearly demonstrate that there is a wealth of sensory information that is modulated at different points in the step cycle in a way that could be used to trigger the necessary motor sequences for locomotion. Thus, the microelectrode array, if successfully implanted on a chronic basis, could provide an attractive sensory element in a rehabilitative motor control system for people with spinal cord injury.

REFERENCES:

1. Baron R, Janig W, and Kollmann W. Sympathetic and afferent somata projecting in hindlimb nerves and the anatomical organization of the lumbar sympathetic nervous system of the rat. *J Comp Neurol* 275: 460-468., 1988.

2. Bell J, Bolanowski S, and Holmes MH. The structure and function of Pacinian corpuscles: a review. *Prog Neurobiol* 42: 79-128., 1994.

3. Branner A, and Normann RA. A multielectrode array for intrafascicular recording and stimulation in sciatic nerve of cats. *Brain Res Bull* 51: 293-306, 2000.

4. Branner A, Stein RB, and Normann RA. Selective stimulation of cat sciatic nerve using an array of varying-length microelectrodes. *J Neurophysiol* 85: 1585-1594, 2001.

5. Brown PB, and Koerber HR. Cat hindlimb tactile dermatomes determined with single-unit recordings. *J Neurophysiol* 41: 260-267., 1978.

6. Burton H, and McFarlane JJ. The organization of the seventh lumbar spinal ganglion of the cat. *J Comp Neurol* 149: 215-232., 1973.

7. Cameron AA, Leah JD, and Snow PJ. The electrophysiological and morphological characteristics of feline dorsal root ganglion cells. *Brain Res* 362: 1-6., 1986.

8. Campbell PK, Jones KE, Huber RJ, Horch KW, and Normann RA. A silicon-based, three-dimensional neural interface: manufacturing processes for an intracortical electrode array. *IEEE Trans Biomed Eng* 38: 758-768, 1991.

9. Chapin JK, and Moxon KA. *Neural Prostheses for Restoration of Sensory and Motor Function*. Boca Raton: CRC Press, 2000.

10. Grigg P, and Greenspan BJ. Response of primate joint afferent neurons to mechanical stimulation of knee joint. *J Neurophysiol* 40: 1-8., 1977.

11. Guillory KS, and Normann RA. A 100-channel system for real time detection and storage of extracellular spike waveforms. *J Neurosci Methods* 91: 21-29, 1999.

12. Hoffer JA, Loeb GE, and Pratt CA. Single unit conduction velocities from averaged nerve cuff electrode records in freely moving cats. *J Neurosci Methods* 4: 211-225., 1981.

13. Hoffer JA, Stein RB, Haugland MK, Sinkjaer T, Durfee WK, Schwartz AB, Loeb GE, and Kantor C. Neural signals for command control and feedback in functional neuromuscular stimulation: a review. *J Rehabil Res Dev* 33: 145-157., 1996.

14. Iggo A. Cutaneous thermoreceptors in primates and sub-primates. *J Physiol* 200: 403-430., 1969.

15. Johnson RA, and Wichern DW. *Applied multivariate statistical analysis*. Englewood Cliffs, N.J.: Prentice Hall, 1988.

16. Jones KE, Campbell PK, and Normann RA. A glass/silicon composite intracortical electrode array. *Ann Biomed Eng* 20: 423-437, 1992.

17. Kovacs GT, Storment CW, Halks-Miller M, Belczynski CR, Jr., Della Santina CC, Lewis ER, and Maluf NI. Silicon-substrate microelectrode arrays for parallel recording of neural activity in peripheral and cranial nerves. *IEEE Trans Biomed Eng* 41: 567-577, 1994.

18. Loeb GE, Bak MJ, and Duysens J. Long-term unit recording from somatosensory neurons in the spinal ganglia of the freely walking cat. *Science* 197: 1192-1194, 1977.

19. Loeb GE, and Duysens J. Activity patterns in individual hindlimb primary and secondary muscle spindle afferents during normal movements in unrestrained cats. *J Neurophysiol* 42: 420-440., 1979.

20. Loeb GE, and Peck RA. Cuff electrodes for chronic stimulation and recording of peripheral nerve activity. *J Neurosci Methods* 64: 95-103., 1996.

21. Mannard A, Stein RB, and Charles D. Regeneration electrode units: implants for recording from single peripheral nerve fibers in freely moving animals. *Science* 183: 547-549., 1974.

22. Matthews PBC. *Mammalian muscle receptors and their central actions*. London: Edward Arnold, 1972.

23. Matthews PBC. Where does Sherrington's "muscular sense" originate? Muscles, joints, corollary discharges? *Annu Rev Neurosci* 5: 189-218, 1982.

24. Maynard EM, Nordhausen CT, and Normann RA. The Utah Intracortical Electrode Array: a recording structure for potential brain-computer interfaces. *Electroencephalogr Clin Neurophysiol* 102: 228-239, 1997.

25. Maynard EM, Hatsopoulos NG, Ojakangas CL, Acuna BD, Sanes JN, Normann RA, and Donoghue JP. Neuronal interactions improve cortical population coding of movement direction. *J Neurosci* 19: 8083-8093., 1999.

26. McLachlan EM, and Janig W. The cell bodies of origin of sympathetic and sensory axons in some skin and muscle nerves of the cat hindlimb. *J Comp Neurol* 214: 115-130., 1983.

27. Munger BL, and Ide C. The structure and function of cutaneous sensory receptors. *Arch Histol Cytol* 51: 1-34., 1988.

28. Murphy PR, Stein RB, and Taylor J. Phasic and tonic modulation of impulse rates in gamma-motoneurons during locomotion in premammillary cats. *J Neurophysiol* 52: 228-243, 1984.

29. Nordhausen CT, Maynard EM, and Normann RA. Single unit recording capabilities of a 100 microelectrode array. *Brain Res* 726: 129-140., 1996.

30. Normann RA, Maynard EM, Rousche PJ, and Warren DJ. A neural interface for a cortical vision prosthesis. *Vision Res* 39: 2577-2587, 1999.

31. Prochazka A, Westerman RA, and Ziccone SP. Discharges of single hindlimb afferents in the freely moving cat. *J Neurophysiol* 39: 1090-1104., 1976.

32. Prochazka A, Stephens JA, and Wand P. Muscle spindle discharge in normal and obstructed movements. *J Physiol (Lond)* 287: 57-66., 1979.

33. Rousche PJ, and Normann RA. A method for pneumatically inserting an array of penetrating electrodes into cortical tissue. *Ann Biomed Eng* 20: 413-422, 1992.

34. Rousche PJ, and Normann RA. Chronic recording capability of the Utah Intracortical Electrode Array in cat sensory cortex. *J Neurosci Methods* 82: 1-15, 1998.

35. Rousche PJ, and Normann RA. Chronic intracortical microstimulation (ICMS) of cat sensory cortex using the Utah Intracortical Electrode Array. *IEEE Trans Rehabil Eng* 7: 56-68, 1999.

36. Schmidt S, Horch K, and Normann R. Biocompatibility of silicon-based electrode arrays implanted in feline cortical tissue. *J Biomed Mater Res* 27: 1393-1399, 1993.

37. Stein RB, Nichols TR, Jhamandas J, Davis L, and Charles D. Stable long-term recordings from cat peripheral nerves. *Brain Res* 128: 21-38., 1977.

38. Stein RB, and Capaday C. The modulation of human reflexes during functional motor tasks. *Trends Neurosci* 11: 328-332., 1988.

39. Stein RB, Peckham PH, and Popovic D. *Neural prostheses: replacing motor function after disease or disability*. New York: Oxford University Press, 1992.

40. Whelan PJ. Control of locomotion in the decerebrate cat. *Prog Neurobiol* 49: 481-515., 1996.

41. Willis WD, and Coggeshall RE. Dorsal root ganglion cells and their process. In: *Sensory mechanisms of the spinal cord* (2nd ed.). New York: Plenum Press, 1991, p. 47-78.

42. Yoshida K, and Horch K. Closed-loop control of ankle position using muscle afferent feedback with functional neuromuscular stimulation. *IEEE Trans Biomed Eng* 43: 167-176, 1996.

43. Yoshida S, and Matsuda Y. Studies on sensory neurons of the mouse with intracellular-recording and horseradish peroxidase-injection techniques. *J Neurophysiol* 42: 1134-1145., 1979.

CHAPTER 3

CODING OF LIMB POSITION BY SENSORY NEURONS STUDIED WITH A MULTIELECTRODE ARRAY[*]

INTRODUCTION

Somatosensory neurons continuously signal detailed information about skin and muscle properties (Kandel et al. 2000). How does the nervous system extract more global information such as the position of the hand or foot with respect to the body? No single cells convey this information, and techniques to study large populations of cells have been limited (Georgopoulos et al. 1992; Prochazka and Gorassini. 1998). We report here simultaneous recordings from over 100 sensory neurons in the dorsal root ganglia (DRG) of cats using arrays of implanted microelectrodes. We studied this question by first considering how limb movements are represented in the firing patterns of individual sensory neurons (the *sensory encoding* process), and then by modeling how the firing activity of the population of sensory neurons could be used to provide estimates of foot position (the *decoding* process). As few as 3 selected neurons provided good estimates of foot position ($r \geq 0.8$). These methods may also be useful for developing advanced prosthetic devices in which sensory information is used in a feedback control system for restoring motion to paralyzed limbs.

RESULTS AND DISCUSSION

Multi-channel recordings were made from sensory neurons in the lumbar DRG of anesthetized cats during passive motion of the hind limb (see Methods). Figure 3-1 shows the pseudo-random path of the foot, as the leg was moved during one 45 s trial (dotted line) over most of its passive range of motion in the sagittal plane (>15 cm forward, backward and upward; <2 cm in the medio-lateral direction). The Figure 3-2 shows stick figures of the cat's limb, together with the simultaneously recorded responses of 87 neurons. These neurons were selected from 128 discriminated neurons using the criterion that the firing rate be linearly correlated to combinations of kinematic parameters (e.g., positions, velocities) with a coefficient greater than 0.5.

---

[*] A version of this chapter will be submitted to *Nature Neurosci* by the authors of Stein. RB, Aoyagi. Y., Weber. DJ, McDonnall. D, Branner. A, Shoham. S, Normann, RA. Contribution to paper: participated in all experiments and contributed to data analysis and editing of manuscript.

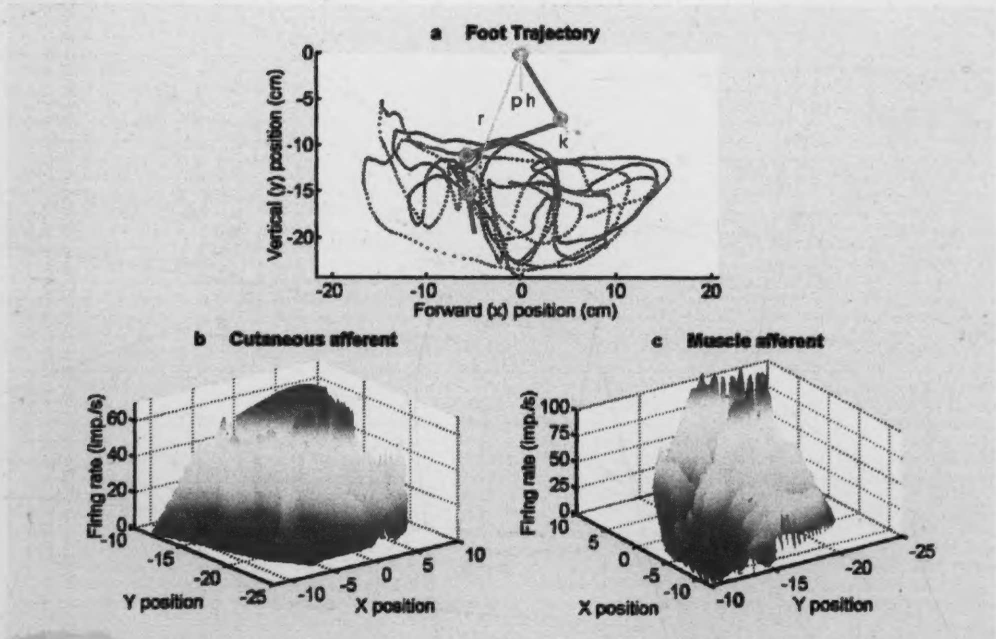

Figure 3-1. Motion of the foot (**a**) and surface plots of the firing rate of cutaneous (**b**) and muscle (**c**) afferents. Movement sensors (o) were placed near selected joints. The random movement of the foot is shown as a dotted line. The position of the foot can be represented in terms of the forward (*x*) and vertical (*y*) positions with respect to the hip (rectangular coordinates), in polar coordinates as the distance (*r*) and the angle (*p*) of the foot with respect to the hip or in angular coordinates (see Methods).

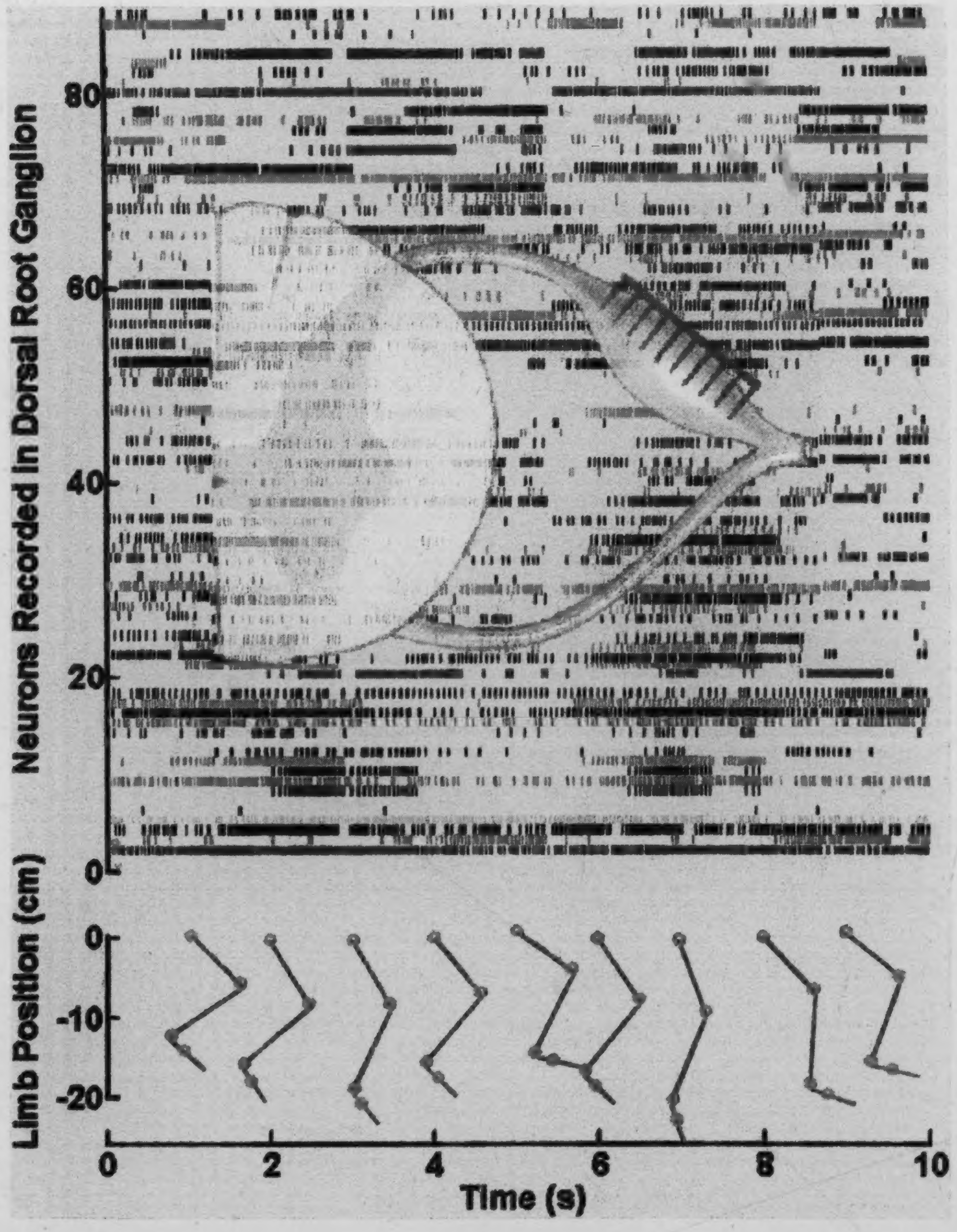

Figure 3-2. The neural responses of 87 neurons varied with random movements of the cat's hind limb. Each tick mark represents a single action potential and each row corresponds to a different neuron in the dorsal root ganglion (DRG). A schematic diagram of the electrode array in the DRG is superimposed. Stick figures indicate the limb position in 1s intervals.

Sensory encoding. Even though a cutaneous receptor responds exquisitely to pressure on a small skin area, its activity will also be related to large limb movements that stretch the skin. Similarly, a muscle receptor responds best to movement of one or two joints, as well as to movements of the whole limb that produce rotations about these joints. These relationships can be studied systematically in groups of simultaneously recorded neurons. Figure 3-1b shows the firing rate, as a function of foot position, of a cutaneous neuron with a receptive field on the front of the knee. When the foot was raised, for example from 20 to 15 cm below the hip, its firing rate increased, because the skin around the knee was stretched. Similarly, it fired faster when the foot was moved forward. Figure 3-1c shows the firing rate of a muscle spindle afferent in a hamstring muscle that responded to knee extension and hip flexion. These movements were correlated with downward and forward movements of the limb.

The neuronal firing rate can be described as a function of limb position in at least three different coordinate systems: 1) rectangular (x, y) coordinates, 2) polar coordinates (as the distance r of the foot from the hip and the angle p with respect to the vertical) or 3) in terms of the angles of the ankle, knee and hip. To determine which coordinate system provided the best description, the firing rate of each neuron was modeled as a weighted, linear sum of position variables in each coordinate system. For example, in rectangular coordinates, the firing rate $f(t)$ of each neuron was fitted (least mean squares method) to an equation of the form $f(t) = a_0 + a_1x(t) + a_2y(t)$. To include the effects of limb velocity, we added the terms $a_3dx(t)/dt + a_4dy(t)/dt$.

These linear models allowed us to predict the firing rate of each neuron from the position of the limb and joint angles. The linear correlation coefficient was then calculated between the measured and predicted firing rates and average values are presented in the table. The correlation was not significantly different when polar or joint angle coordinates were used for the prediction, but the correlation was significantly lower when rectangular coordinates were used. The lack of a significant difference between polar and angular coordinates is interesting, since the polar coordinates relate to the overall position of the foot with respect to the hip and are not explicitly signaled by any one cell. As mentioned above, the angles are more directly related, particularly for muscle receptors. Furthermore, there are three angles and only two polar variables; an extra fitted parameter might be expected to improve the fit (Bosco et al. 2000).

	Rectangular		Polar	Angles
Position	0.40	<	0.46	0.49
+ velocity	0.51	<	0.57	0.59
+ acceleration	0.52	<	0.57	0.60
+ nonlinearity	0.58	<	0.64	0.65
+ filtering	0.63	<	0.68	0.70

Table 3. Average correlation coefficients between firing rates of 64 neurons and position plus other variables in three coordinate systems. The < between adjacent columns indicates a significant difference ($p<0.05$) based on a Students t-test. Each added step (+) in the modeling process, except for acceleration, also increases the correlation significantly ($p<0.05$). The standard errors of all values are about 0.02.

The variations in firing rate at a given position (as shown in Figure 3-1b, c) would be expected if a neuron also responded to derivatives of position, such as velocity and acceleration. Adding velocity terms increased the correlation coefficients significantly in all coordinate systems, but acceleration (and higher derivatives) did not (see the table). The actual firing rates of two neurons are plotted against the predicted rates (Figure 3-3a, b), using positions and velocities in polar coordinates. Although there is a linear portion, the firing rate saturates at lower and upper limits, because the actual firing rate cannot become negative and is limited to a maximum rate. A cubic polynomial captures the curvature of the observed firing rate, as was also found for cortical cells (Shoham. 2001).

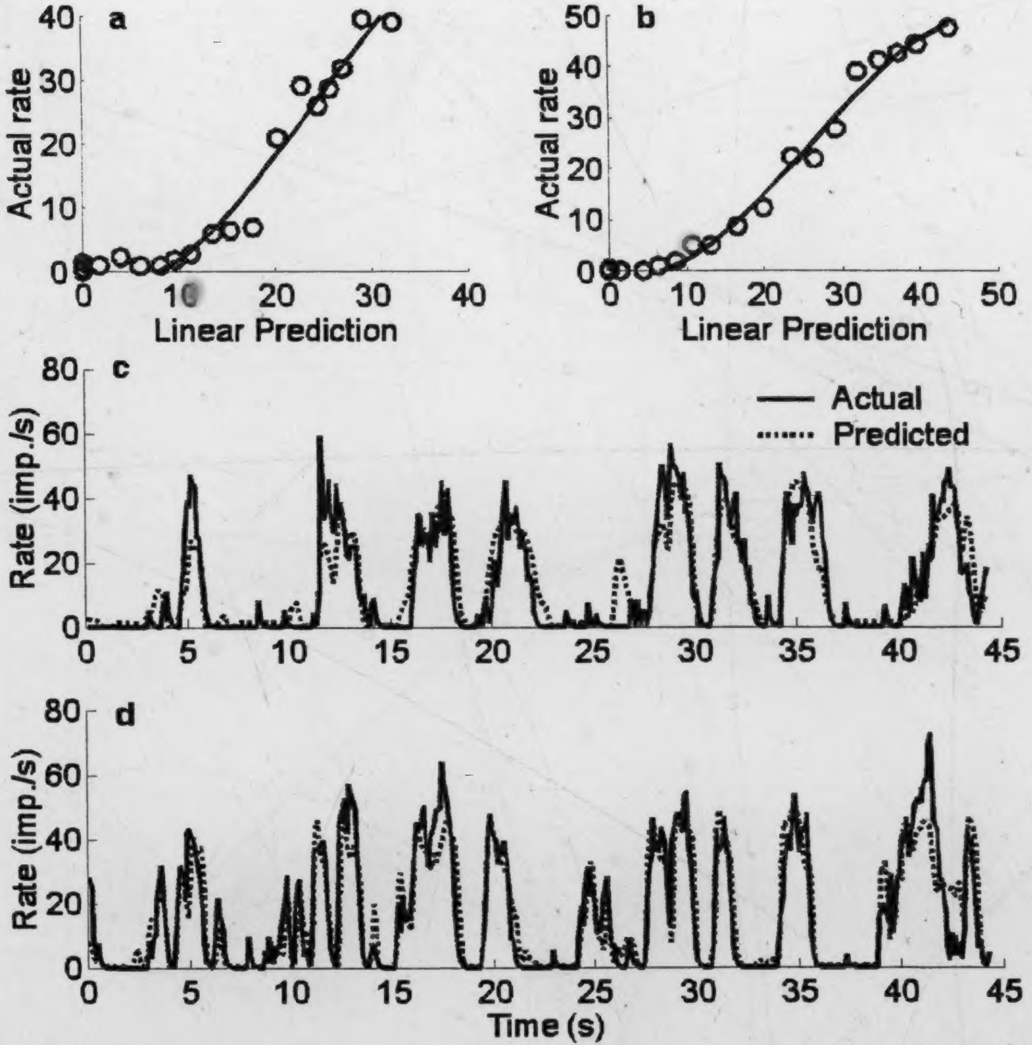

Figure 3-3. Encoding of kinematic values in single sensory neurons. The actual firing rate (impulses/s) of two representative neurons increases nonlinearly with the firing rate predicted as a linear combination of kinematic values (**a**, **b**). A cubic (3rd order) polynomial fit is superposed (solid lines). Predicted (dotted) and actual (solid) firing rates are shown for the same two units (**c**, **d**).

Incorporating the curvature as a nonlinear element in the encoding model for each neuron (Figure 3-3c, d) improved the correlation significantly for the population of cells in all coordinate systems (Table). However, some of the variance was still not accounted for, in part because of the short time intervals analyzed. In 0.1 s, a neuron may fire 1 or 2 impulses at a given position and velocity, depending on when it last fired an impulse. Filtering both the firing rates and the kinematic data with a first-order, low-pass filter (time constant = 0.2 s) reduced the consequences of this variation. The table shows correlations of 0.7 on average for the filtered results in angular coordinates, compared to less than 0.5 for the original linear model using only angular positions. Figure 3-3c and d show the close agreement between predicted and actual firing rates for the neurons of Figure 3-3a and 3b, after inclusion of the nonlinearity and filtering.

Sensory decoding. Several methods have been developed to decode limb kinematics from the firing patterns of a population of neurons (Bialek et al. 1991; Brown et al. 1998; Warland et al. 1997). We predicted foot position from the firing rates using linear and nonlinear estimation techniques (Salinas and Abbott. 1994; Stein et al. 1979) (see Methods). Firing rates and position data from the first half of a 45 s trial were used to identify the coefficients of the model. Data from the second half of the trial were used to test the model's ability to predict the foot position. Figure 3-4a and b demonstrate the model's ability to predict the actual movements in polar coordinates from the firing rates of 80 neurons. The predictions are nearly perfect for the training set (correlations of 0.99), as expected, since these data were used to develop the model. The predictions were also quite good for the test set (correlations of 0.88 and 0.96).

Figure 3-4c shows the effects of including different numbers of neurons in the prediction. For this analysis, 1-15 neurons were selected with the highest encoding correlation coefficients. Foot position was predicted from the neural activity in each group (optimum). Using the 3 best neurons, position was predicted with a correlation coefficient of 0.8, and predictions from the best 14 neurons yielded a correlation of 0.9. In addition, 100 groups of 1-15 neurons were sampled at random from the population of 80 neurons. For each sample size, the mean and S.D. of the correlation coefficients were

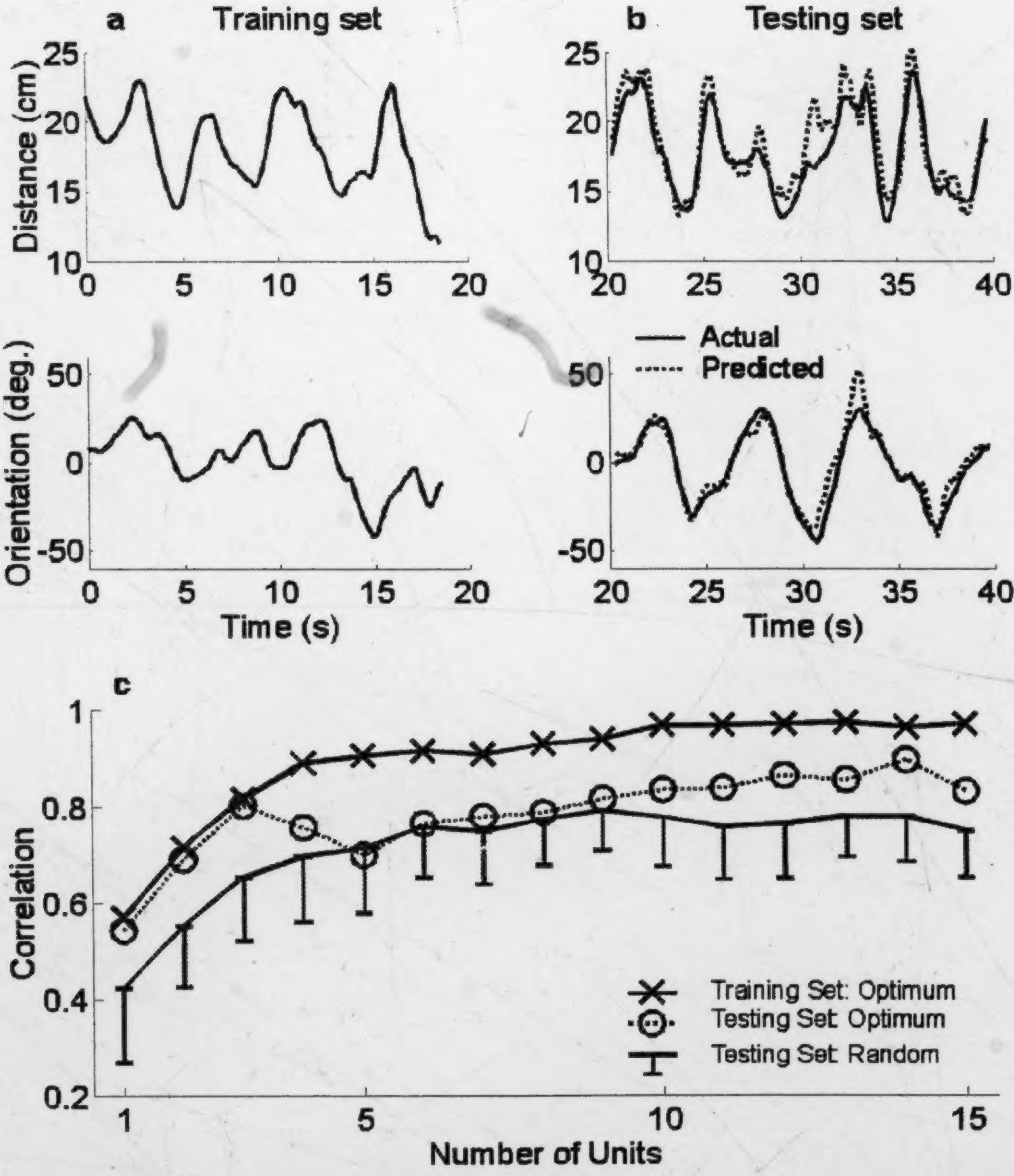

Figure 3-4. Time course of the actual (solid line) and predicted (dotted line) position of the foot in polar coordinates. The trial was divided into a *training* set to develop the model (**a**) and a *testing* set (**b**) to check its generalization to other data. The fit continued to improve as more neurons were added to the training set (**c**), but the fit to the test set improved more slowly. Neurons were selected in order of their correlation in the training set to the kinematic variables (from the best to the least correlated; optimum) or randomly sampled from the entire population.

calculated. When sampling neurons randomly, many more were required to obtain accurate predictions.

The encoding and decoding results will now be discussed separately in relation to the way the nervous system encodes information about limb position and how this information may be used to guide electrical stimulation for moving paralyzed limbs.

Coordinate systems for sensory coding. Work over the last 20 years has suggested that the motor cortex plans movements in terms of distances and directions, essentially a polar coordinate system (Georgopoulos et al. 1982; Nicolelis. 2001; Schwartz. 1994). Bosco and Poppele (Bosco and Poppele. 2001) recorded from relay neurons in the dorsal spino-cerebellar tract and found that the discharge of most cells at this level could already be well described in terms of movements of the end point (the foot), rather than of single joints. They suggested that the convergence of information from a number of sensory receptors could combine to represent this global information. By recording simultaneously from a large population of sensory receptors for the first time, we could compare the encoding of foot position in different coordinate systems. Predictions of firing rates were significantly better using a coordinate system based on joint angles than rectangular coordinates, but were not significantly different using polar or angular coordinates.

Thus, even at the level of sensory neurons the responses can be well described in terms of the endpoint (the cat's foot) in polar coordinates which agrees closely with Bosco and Poppele's results. The information is clearly present in the activity of sensory neurons and could be enhanced by appropriate synaptic connections onto dorsal spino-cerebellar tract cells. We obtained better results using a nonlinear model, as has been found in other neurobiological systems (Chander and Chichilnisky. 2001; Kearney and Hunter. 1990; Shoham. 2001), since firing rates saturate at upper and lower limits. However, quite good results could be obtained with linear models as well (Table 3). Active movements add more complexity, since the contraction of α and γ motoneurons will modify the firing of muscle receptors such as Golgi tendon organs and muscle spindles (Prochazka. 1989) and may stretch the skin in different ways than the passive movements studied here. We are extending these experiments to situations where the cat moves the limb actively to see what differences emerge.

Decoding and neural prostheses. The microelectrode arrays enabled recordings from a sufficiently large number of sensory neurons to reconstruct leg position accurately using linear and nonlinear methods (Figure 3-4). If recordings can be extended from the acute state described here to chronically implanted, behaving animals, then these techniques may prove useful in providing feedback to control stimulation of human muscles in paralyzed limbs after a spinal cord injury or stroke.

METHODS

The results shown here are from two animals, which were implanted at the University of Alberta, as approved by the local animal welfare committee in accordance with the Declaration of Helsinki. The animals were anesthetized with sodium pentobarbitol and a wide laminectomy was performed to expose the L6 and L7 DRG. The arrays were implanted in the L6 and the L7 DRG by insertion through the dura mater with a pneumatic inserter (Rousche and Normann 1992). The animals were suspended from a spinal frame and each recording channel was studied individually to identify the receptive fields of the sensory neurons it recorded. Then, a variety of movements were applied manually via a foot holder to minimize direct contact to the skin.

The microelectrode recordings in each cat were made with two 5x10 arrays of microelectrodes (Jones et al. 1992) (Bionic Technologies LLC, Salt Lake City UT). Each silicon-based electrode was 1.5 mm long and was separated from its neighbors by 0.4 mm. Electrode arrays were connected to a 100-channel amplifier (NSAS, Bionic Technologies, LLC). The gain of each amplifier was 5000 (bandpass filtered at 250-7500 Hz) and each electrode was sampled at 30 kHz. Thresholds were set and a Pentium computer recorded a period around the times of crossing the threshold. To isolate the activity of a single unit from a multiunit recording, the data were analyzed using the principle components of the waveforms. Principle component analysis is a frequently used statistical method that distinguishes different waveforms by their position along orthogonal basis vectors. All analysis was performed using custom software written in Matlab (MathWorks, Inc., Natick MA).

Limb positions were recorded with motion-tracking sensors (6-D Research, Skill Technologies Inc., Phoenix AZ, USA) placed at the hip, just above the knee and the ankle and on the foot near the metatarsal-phalangeal, as shown in Figure 3-1a. To avoid skin slippage or displacement during movement, sensors were rigidly fixed to the femur and tibia by surgical sutures through holes drilled in the bones. The distance of each sensor from its neighboring joints was measured in order to calculate the position of the joints in space. Joint angles were defined as the forward flexion of the hip (*h*, with respect to the vertical), the flexion of the knee (*k*, with respect to a straight knee) and the dorsiflexion of the ankle from a right angle (see Figure 3-1).

In the decoding model for predicting foot position, we first linearized the firing rates based on the coefficients of the cubic polynomial identified during the encoding stage (Figure 3-3). Then, we calculated the best linear prediction of foot position (least mean squares method) for the foot in rectangular or polar coordinates. In the calculations, the firing rates at time t and 2 previous times ($t-\tau$ and $t-2\tau$, τ=0.1 s) were used to predict the foot position at time t.

REFERENCES:

1. Bialek W, Rieke F, de Ruyter van Steveninck RR, and Warland D. Reading a neural code. *Science* 252: 1854-1857., 1991.

2. Bosco G, Poppele RE, and Eian J. Reference frames for spinal proprioception: limb endpoint based or joint-level based? *J Neurophysiol* 83: 2931-2945, 2000.

3. Bosco G, and Poppele RE. Proprioception from a spinocerebellar perspective. *Physiol Rev* 81: 539-568., 2001.

4. Brown EN, Frank LM, Tang D, Quirk MC, and Wilson MA. A statistical paradigm for neural spike train decoding applied to position prediction from ensemble firing patterns of rat hippocampal place cells. *J Neurosci* 18: 7411-7425., 1998.

5. Chander D, and Chichilnisky EJ. Adaptation to temporal contrast in primate and salamander retina. *J Neurosci* 21: 9904-9916., 2001.

6. Georgopoulos AP, Kalaska JF, Caminiti R, and Massey JT. On the relations between the direction of two-dimensional arm movements and cell discharge in primate motor cortex. *J Neurosci* 2: 1527-1537., 1982.

7. Georgopoulos AP, Ashe J, Smyrnis N, and Taira M. The motor cortex and the coding of force. *Science* 256: 1692-1695., 1992.

8. Jones KE, Campbell PK, and Normann RA. A glass/silicon composite intracortical electrode array. *Ann Biomed Eng* 20: 423-437, 1992.

9. Kandel ER, Schwartz JH, and Jessell TM. *Principles of neural science*. Stamford, Conn.: Appleton & Lange, 2000.

10. Kearney RE, and Hunter IW. System identification of human joint dynamics. *Crit Rev Biomed Eng* 18: 55-87, 1990.

11. Nicolelis MA. Actions from thoughts. *Nature* 409: 403-407., 2001.

12. Prochazka A. Sensorimotor gain control: a basic strategy of motor systems? *Prog Neurobiol* 33: 281-307, 1989.

13. Prochazka A, and Gorassini M. Ensemble firing of muscle afferents recorded during normal locomotion in cats. *J Physiol (Lond)* 507: 293-304, 1998.

14. Rousche PJ, and Normann RA. A method for pneumatically inserting an array of penetrating electrodes into cortical tissue. *Ann Biomed Eng* 20: 413-422, 1992.

15. Salinas E, and Abbott LF. Vector reconstruction from firing rates. *J Comput Neurosci* 1: 89-107., 1994.

16. Schwartz AB. Direct cortical representation of drawing. *Science* 265: 540-542., 1994.

17. Shoham S. *Advances Towards an Implantable Motor Cortical Interface* (Ph. D. Thesis). Salt Lake City, UT: University of Utah, 2001.

18. Stein RB, Andreassen S, and Oguztoreli MN. Mathematical analysis of optimal multichannel filtering for nerve signals. *Biol Cybern* 32: 19-24., 1979.

19. Warland DK, Reinagel P, and Meister M. Decoding visual information from a population of retinal ganglion cells. *J Neurophysiol* 78: 2336-2350., 1997.

CHAPTER 4

LONG-TERM STIMULATION AND RECORDING WITH A PENETRATING MICROELECTRODE ARRAY IN CAT SCIATIC NERVE*

INTRODUCTION

In spinal cord injury, ascending and descending nerve fibers are transected or crushed and as a result, the spinal cord is permanently damaged. Since only limited success has been achieved in regenerating the severed neuronal connections (Bunge. 2001; Jones et al. 2001), neuroprosthetic devices based on the activation of muscles distal to the injury (functional electrical stimulation (FES)) have been investigated for many years as an alternative method to restore motor function in paralyzed limbs. Apart from muscle stimulation, a neuroprosthetic device based on FES should also employ sensory feedback information to monitor the movement produced; this would be especially useful while generating complex movements. Several different devices have been studied as possible neural interfaces to the spinal cord (Grill. 2000; Mushahwar et al. 2000; Prochazka and Mushahwar. 2000; Woodford et al. 1996), peripheral nerve fibers (Bowman and Erickson. 1985; Branner et al. 2001; Choi et al. 2001; Crampon et al. 1999; Grill and Mortimer. 1998; Kovacs et al. 1994; Meier et al. 1995; Rodriguez et al. 2000; Rozman and Trlep. 1992; Slot et al. 1997; Smit et al. 1999; Strange and Hoffer. 1999; Sweeney et al. 1995; Tarver et al. 1992; Tyler and Durand. 1997; Veltink et al. 1989; Veraart et al. 1993; Walter et al. 1997; Yoshida and Horch. 1993; Yoshida and Horch. 1996), and the motor end plates of the muscles directly (Cameron et al. 1998; Loeb et al. 1991; Ziaie et al. 1997). Because peripheral nerves contain both sensory and motor fibers, electrodes implanted there may stimulate motor fibers as well as record signals from skin and muscle sensory fibers and the use of a peripheral nerve interface as a motor neuroprosthesis will be discussed here.

---

* A version of this chapter has been submitted *to IEEE Trans Neural Syst Rehabil Eng* by the authors of Branner A, Stein RB, Fernandez E, Aoyagi Y, Normann RA. Contribution to paper: participated in 50% (mainly electrophysiological part) of experiments and contributed to data analysis and editing of manuscript.

Desirable features of peripheral nerve interfaces are low required stimulation currents, and selectivity and stability of stimulation and recording. These properties depend on the proximity of the exposed electrode surface to the target nerve fibers. In addition, the epineurium and the perineurium of the nerve electrically shield the nerve fibers from their surroundings. Hence it is difficult to achieve good stimulation and recording selectivity with electrodes placed around the nerve on the outside of these two neural compartments. It has been shown that the stimulation selectivity and/or recording capability can be greatly enhanced by placing the electrodes within the fascicles of the nerve (Branner et al. 2001; Smit et al. 1999; Yoshida and Horch. 1993; Yoshida and Horch. 1996).

In this study, multiple electrodes were chronically placed in different fascicles of the sciatic nerve of cats. The microelectrode array used, the Utah Electrode Array (UEA), has a grid of up to 10 by 10 electrodes at 400 μm spacing and was originally developed for recording and stimulation of cortical nervous tissue (Nordhausen et al. 1996; Rousche and Normann. 1999). This planar structure was later modified to a three-dimensional electrode arrangement, the Utah Slanted Electrode Array (USEA), to be better suited for use in peripheral nerve. In previous acute experiments, the UEA and the USEA were safely implanted into peripheral nerve (Branner and Normann. 2000; Branner et al. 2001). Different muscle groups were stimulated in a highly selective fashion employing low stimulation currents, and information was recorded from sensory fibers of the skin and muscles. However, this device has not been used chronically to date for either stimulation or recording in peripheral nerve.

There are several issues associated with the chronic implantation of a microelectrode array such as the USEA. There is substantial relative motion between the nerve and its surrounding muscles. This motion can exert forces on the electrode array and eventually could extract it from the nerve. In addition, the nerve might be damaged if the electrodes are unable to move with the nerve. Therefore, some kind of containment system may be required to keep the electrodes within the nerve but yet not restrict nerve movement. Lead management and connector requirements offer additional challenges; lead wires can produce tethering forces on the array, resulting in damage to the nerve or breakage of the wires themselves. The connector system has to be able to accommodate as many electrodes in as little space as possible and should be mounted securely to the animal, close to the implant site. These issues were addressed in this study and a variety of containment systems were evaluated.

Electrical interference from surrounding muscles can be a problem in recording sensory information from peripheral nerves in an awake and freely moving animal. Ideally, the signal contamination can be eliminated by electrically shielding the electrodes and the nerve from its surroundings. Another possibility is to filter this noise out in either the analog or digital domain.

In this paper, we have focused our attention on the long-term stimulation and recording properties of the USEA. We found that threshold currents to evoke a twitch in distal musculature initially increased but tended to be constant after the first month. Muscle groups stimulated by individual electrodes changed little over the life of the implant. Recording of sensory activity, however, was not stable over time. Both the cats' behavior and the histology did not reveal any substantial nerve damage.

METHODS

Electrode Array

In this study, different sizes of the Utah Slanted Electrode Array (USEA) were used depending on the size of the nerve (Figure 4-1A). The size ranged from arrays containing 7 by 10 to 10 by 10 electrodes, which corresponds to a size from 2.8 by 4 mm to 4 by 4 mm; the length of the electrodes varied between 0.5 and 1.5 mm along the longer axis with 0.1 mm length difference between neighboring electrodes along this axis. The manufacturing and wiring process of the array was described in detail elsewhere (Branner et al. 2001; Nordhausen et al. 1996). Each array was wired to 36-pins of each of two 40-conductor edge connector mounted in a titanium base (Figure 4-1B) (Bionic Technologies, L.L.C., Salt Lake City, UT). The other four pins served as ground and reference electrodes.

The impedances of the electrodes were measured on a periodic basis after implantation using a WPI impedance meter (Omega-Tip Z, World Precision Instruments, Sarasota, FL); they generally varied between 100 and 350 kOhm at the time of implantation.

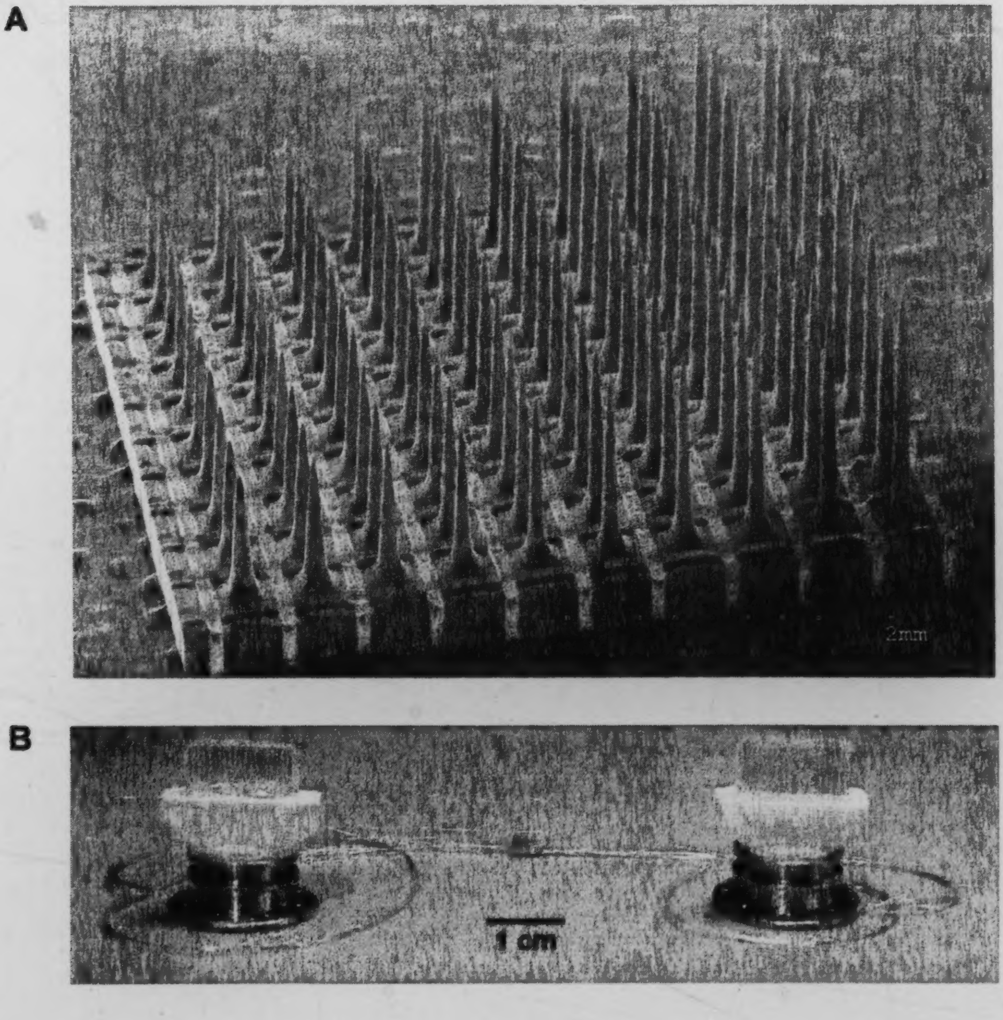

Figure 4-1. A) Scanning electron micrograph of the Utah Slanted Electrode Array (USEA). B) Picture of the array, the lead wires and the connector system. Each connector is wired to 36 electrodes and 2 reference electrodes. The titanium pedestal of the connector itself is used as ground.

Surgical procedure

Thirteen cats were studied of which 6 received non-functioning implants (11 implants; either bilateral or two arrays in the same nerve) where walking behavior and histology were studied and the electrode arrays did not have lead wires connected to them. The surgery in these animals was essentially the same as described below except for the implantation of the connectors. All experiments were performed under sterile conditions according to the National Institutes of Health guidelines for the use of animals.

Anesthesia was induced with Telazol (10 mg/kg) and maintained with halothane (0.8-1.5%) during the surgery. Electrocardiogram, blood pressure, expired CO_2, oxygen saturation and rectal temperature were continuously monitored. After the right leg and the lower back were shaved, a 5-6 cm long incision was made from the hip to the knee and the biceps femoris and vastus lateralis muscles were separated to gain access to the sciatic nerve. The array was positioned on the nerve and the wires on both sides of the array were sutured to the epineurium of the nerve. Then, the array was inserted into the nerve using a pneumatically actuated impulse inserter (Rousche and Normann. 1992) (Bionic Technologies, L.L.C., Salt Lake City, UT).

We put a containment system around the nerve and the array to improve the stability of the array in the nerve and to facilitate gliding of surrounding muscles over the structure without exerting major shear forces on the array. Figure 4-2 shows 3 of the 4 different containment systems used: a) a Gore-Tex® sheet sutured around the nerve, b) spiral cuffs (Axon Engineering Inc., Garfield Heights, OH), and c) custom cuffs made out of silicone in a dip process. The 4th containment system (not shown) consisted of Kwik-Cast® (World Precision Instruments, Inc., Sarasota, Florida), a two component silicone elastomer. The two-component elastomer was applied on the nerve and allowed to flow around the nerve at the implant site. The Gore-Tex® sheet was about 3 cm by 1.5 cm in size and had a thickness of 0.1 mm. It was wrapped around the nerve and the implanted array and sutured on the side. The commercially available spiral cuffs had an inner diameter of 2.7 or 3.5 mm depending on the size of the nerve. They were 1.5 cm long and fully wrapped around the nerve and array twice. The spiral cuffs were sutured to the nerve with a fine suture proximally to prevent the cuff from sliding away from the implant site.

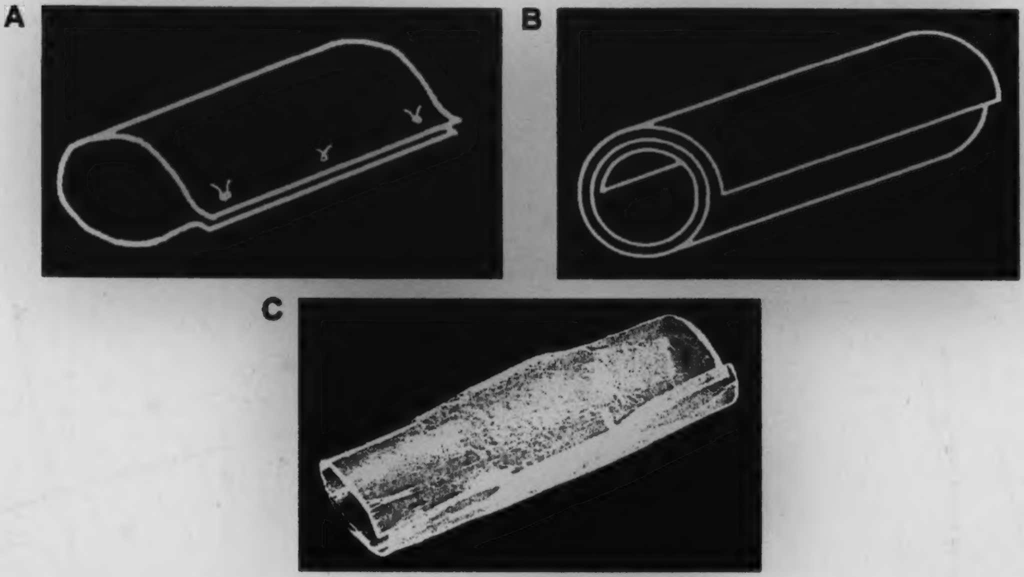

Figure 4-2. Three of the four different containment systems used in the study: A) a sheet of GoreTex® wrapped around the nerve, B) a self-sizing spiral cuff, and C) a silicone custom cuff (here oval shaped).

To produce the custom made cuffs, a Teflon rod was modified to have the shape of the nerve with the array implanted in it. This replica was then chemically cleaned and dipped in medical-grade silicone (MED-1037, NuSil) multiple times until the desired thickness of up to 0.5 mm was reached. The resulting cuff was then cut to a length of about 15 mm and cut open on one side. There were two versions of custom cuffs; the early ones used a circular diameter model of the nerve whereas later ones were more realistically oval shaped. After implantation of the array, the containment system being studied was put around the nerve with the array, a Pt/Ir reference wire (20IR2T, Medwire) was placed inside and the containment system was closed using polypropylene sutures.

For functional implants, an additional incision was made on the animals' back orthogonal to the vertebral column and spanning the two iliac crests. Both connectors were routed under the skin from the incision on the leg to the one on the back. The iliac crests and the L7 spinal process were partially exposed. In the first experiments, holes were drilled through all three bones and either silk sutures or stainless steel sutures were used to secure the connectors. In the more recent experiments, a stainless steel suture was put through the spinal process but each connector was attached to the iliac crest using two bone screws. Finally, the skin was closed at the implantation site and around the two connectors on the back.

Experimental procedures

After implantation, the animals were tested about once every 1 to 4 weeks and light Telazol anesthesia was applied when necessary. Three different kinds of tests were performed: behavioral tests of the animal's walking ability, measurement of the stimulation threshold of each electrode and recording of sensory activity.

Behavioral tests

The cats' ability to walk on a treadmill was monitored once a week for the first month and less frequently later. We categorized the extent of walking impairment into four different classes: 1: no visible discomfort or walking deficit, 2: some discomfort but no walking deficit, 3: unable to put weight on ankle and discomfort, and 4: no use of the leg. This scale was used as a measure of nerve damage after implantation.

Stimulation

For stimulation, biphasic, cathodic, constant-current stimuli with 200 μs per phase and a 100 μs interphase interval were delivered using a computer-controlled WPI Linear Stimulus Isolator (A395, World Precision Instruments, Sarasota, FL). To determine the stimulation threshold on each electrode, the stimulation was started at the expected threshold level, increased in 5 μA steps until a muscle twitch could be detected and then decreased in 1 μA steps until threshold was reached. The twitch and the type of muscle groups activated was detected using visual inspection and palpation around the ankle joint, foot and toes as described in more detail in the results section. While the stimulated muscle could sometimes be clearly identified, often only the direction of movement and location of muscles could be identified, rather than specific muscle groups.

Recording

Sensory activity was recorded using a 100-channel amplifier and data-acquisition system (Bionic Technologies, L.L.C., Salt Lake City, UT). Recording was either under Telazol anesthesia to avoid EMG contamination or in alert animals resting or walking on a treadmill. With the animal under anesthesia, sensory activity was evoked by mechanical stimulation. We determined the amplitude of the activity and the movement that evoked it and compared responses at different recording sessions.

Histology

At the end of the study, the animals were deeply anesthetized and transcardially perfused with 4% paraformaldehyde in 0.1 M phosphate buffer (pH 7.4) at room temperature. After perfusion the sciatic nerves and surrounding tissues were removed and kept overnight in the same fixative at 4°C before being rinsed in phosphate buffer. The nerves were then cut into two pieces at the midpoint of the implant. The proximal portion was washed in distilled water, dehydrated in graded concentrations of ethanol and embedded in paraffin. Light microscopy observations were performed on 5 µm serial sections stained with either haematoxylin and eosin (H&E) or TriChrome methods to reveal the position of the electrodes, the thickness of the connective tissue around the electrode shafts and signs of axonal degeneration. Distal portions of the nerves were postfixed for 1 hour in 2% OsO_4, dehydrated in graded concentrations of ethanol and embedded in Epon 812. Serial 0.5 µm semithin sections were stained with toluidine blue and examined with a Leica DMB Microscope.

Morphometrical evaluation was performed in 8 to 10 microscopic fields for each nerve with the help of a 6100 Apple Power Macintosh computer; each field spanning approximately 200 by 200 µm, and representing approximately 15-20% of the cross-sectional area of the nerve. The image fields were digitized using a high-resolution Olympus DP-11 digital camera and analyzed using the computer-assisted image analysis program (NIH Image, developed and maintained by the National Institutes of Health, Bethesda, MD) and a modified version of a software designed to study axonal morphometry (Fernandez et al. 1991). Because it was difficult to automatically select the boundary between the nerve fibers and the surrounding background for small axons and thinly-myelinated fibers using standard image analysis techniques, each digitized image was analyzed using a semi-automatic method. The axonal contour and the external contour of the myelin sheath (fiber contour) were manually traced on enlarged images. A set of custom macros allowed the calculation of the length of a line, the cross-sectional area, and the lengths of the major and minor axes of the best fitting ellipse. Fiber diameters and axonal diameters were deduced from the fiber and axonal perimeters assuming a cylindrical shape of axons. These basic data were used to derive the form factor, g-ratio and myelin sheath thickness (Fernandez et al. 1991). Axonal counts were performed using the Cavalieri 3.0 macros (Glen MacDonald, Virginia Merril Bloedel Hearing Research Center, University of Washington).

RESULTS

General observations

The four different kinds of containment systems tested were Kwik-Cast®, a simple Gore-Tex® sheet wrapped around the nerve, self-sizing spiral cuffs, and custom-built silicone cuffs that were molded to the shape of the array in the nerve. Kwik-Cast® was only used in one animal; it was difficult to apply around the nerve in a uniform fashion and it seemed to partially interpose between the array and the nerve. Because the Gore-Tex® used in two animals was relatively loose around the nerve and because of its flexible nature, connective tissue growth inside as well as outside of the cuff was extensive and, as will be seen later, stimulation thresholds and recordings were not stable over long periods of time.

Self-sizing cuffs work better in terms of keeping the array in the nerve but since the inner diameter of the cuff was defined by the diameter of the nerve and the array at the implantation site, there were big pockets for connective tissue growth proximally and distally within the cuff and the cuff could easily slide along the nerve and away from the implantation site. We tried to prevent this by suturing the cuff to the nerve proximally. However that limited the self-sizing capabilities of the cuff. In addition, the inner end of the cuff easily got caught under the base of the array, which did sometimes partially pull the array out of the nerve (Figure 4-3A).

The last containment system used was the custom-made silicone cuff. The round cuffs left too much room for connective tissue to grow between the array and the nerve and the connective tissue layer reached a thickness of 0.5 to 1.5 mm (Figure 4-3B & C) and was sometimes highly vascularized. Especially the later version of this cuff could easily be placed around the nerve; it did not leave much room for connective tissue growth and could not slide along the nerve if it fit well to the nerve (Figure 4-4).

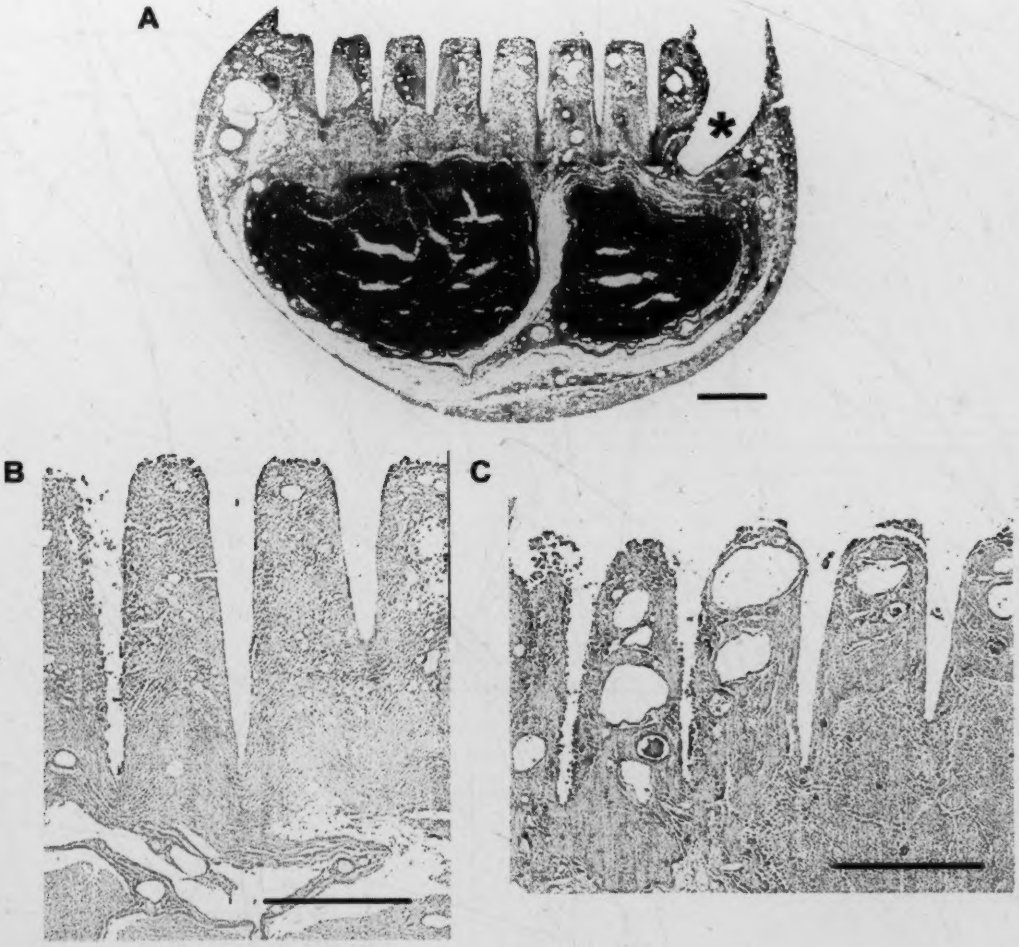

Figure 4-3. Light microscopic pictures of cat sciatic nerve cross sections. The tissue thickness was 1 µm. The bars are 0.5 mm long. A) A spiral cuff was used as a containment system. This particular row of electrodes does not reach the fascicles. The cuff seems to have pulled the array out of the nerve ('*' region where the spiral cuff penetrated the nerve. B and C) 'Round' silicone custom cuffs were used. The connective tissue could reach a thickness of 1.5 mm and be heavily vascularized.

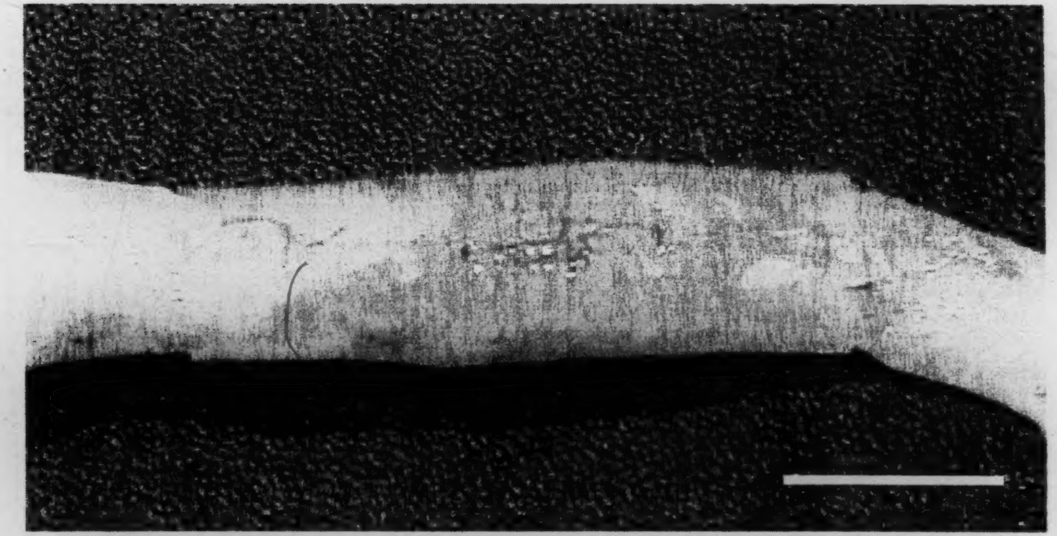

Figure 4-4. Photograph of cat sciatic nerve implant with 'oval' custom containment system. The bar is 5 mm long.

In summary, all different containment systems contained some connective tissue after a few weeks and all electrode arrays stayed within the nerve cuff but the electrodes themselves did not necessarily remain in the nerve and its fascicles. This macroscopic and histological evaluation of the implant systems gave an indication of the extent of the tissue response as a result of array implantation and the success of the containment system to hold the array in position.

Behavioral tests were conducted to analyze gross nerve damage that might be manifest in walking impairment after implantation. Each cat's ability to walk on a treadmill was monitored 1-2 times a week and placed in one of four categories (see Methods). Two cats showed significant walking impairment for up to a month after surgery (Table 4-1). One had two electrode arrays implanted in the same nerve and the other developed a strong inflammatory response in the leg; the reason for this is unknown. The other cats showed little or no walking deficit on the treadmill and any deficit disappeared within 2-3 weeks after implantation. These results were independent of the containment system used.

Table 4-1. Summary of the animals’ walking behavior on the treadmill after surgery. The ‘*’ indicates that two arrays were implanted and the ‘-‘ means that no measurements were taken (see Methods for classification of walking deficit).

Implant	Week after surgery									Duration (weeks)
	1	2	3	4	5	6	7	8	>9	
GoreTex	-	-	-	-	1	1	1	1	1	10
GoreTex	2	2	1	1	1	-	-	-	-	14
KwikCast/Round*	1	2	3	3	2	2	1	1	1	11
Round	2	3	3	2	1	1	1	1	1	17
Round	1	1	1	1	1	1	1	1	1	18
Round	1	1	1	1	1	1	1	1	1	14
Round/Spiral*	2	1	2	2	2	2	2	2	2	9
Round	1	2	1	1	1	1	1	1	1	24
Spiral	1	1	1	1						5
Spiral	1	1	1	1	1	1	1	1	1	16
Oval	1	1	1	1	1	1				7
Oval	1	1	1	1	1	1	1	1	1	31
Oval	1	1	1	1	1	1	1	1	1	10
Oval	1	1	1	1	1	1	1	1	1	26
Oval	1	1	1	1	1	1	1	1	1	20
Oval	1	1	1	1	1	1	1	1	1	24

Stimulation

In functioning implants, we analyzed which muscle groups could be stimulated, what currents were required to evoke a muscle twitch and what sensory information could be recorded for each electrode. The animals were subdivided into three different groups based on the techniques used to fix the connector on the back and the cuffs used around the sciatic nerve. For part of this analysis: 1) the connectors were sutured into the skin and heavy silk sutures were put through holes in the spinal process and the iliac crest and a GoreTex® sheet was put around the nerve (2 animals), 2) the same connector fixation as the first group but the oval shaped custom silicone cuff was put around the nerve (2 animals), and 3) the connectors were rigidly attached to the iliac crest with bone screws and the oval shaped custom silicone cuff was put around the nerve (3 animals). Because the connectors were not secured to bone in the first four animals, lead wires frequently broke and one animal even removed both connectors after 2 1/2 months. Connector problems this severe only occurred in one animal where the connectors were rigidly fixed to the iliac crest. The reason for this failure after 4 months is not known.

The muscles that were excited through stimulation of sciatic nerve were organized in three different groups based on the location of the muscle tendons around the ankle (groups 1, 2, and 3) (Figure 4-5). Within these groups muscles were further subdivided by the movement produced (ankle dorsiflexion (ADF), ankle plantarflexion (APF), toe extension (TE), toe flexion (TF), and foot extension (FE)). We used both criteria, direction of movement and tendon location, to establish which muscle was stimulated; however, in awake animals location of the tendon was easier to determine. In Figure 4-5 and in the following stimulation maps (Figure 4-6), groups are indicated by different shades of gray and the corresponding number; the letter abbreviations specify a subsection of a group organized by the movement produced. If a movement could not be assigned to one group alone, the two groups involved were noted by both numbers and an intermediate shade of gray.

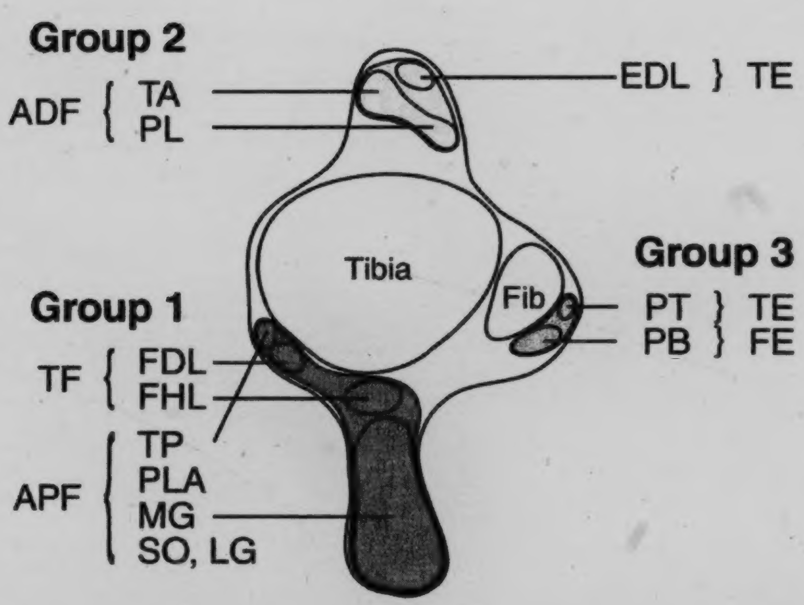
Group 2
ADF
TA
PL
EDL } TE
Tibia
Group 3
Fib
PT } TE
PB } FE
Group 1
TF
FDL
FHL
APF
TP
PLA
MG
SO, LG

Figure 4-5. Cross-section of the cat hindlimb just above the ankle joint. Muscle groups and their tendons (seen in figure) are divided into three groups based on their location (shades of gray) and further subdivided by the kind of movement produced (abbreviation). The following muscle groups are listed: Extensor and flexor digitorum longus (EDL, FDL), flexor hallucis longus (FHL), lateral and medial gastrocnemius (LG, MG), peroneus brevis, longus and tertius (PB, PL, PT), plantaris (PLA), soleus (SO), tibialis anterior and posterior (TA, TP). Movement categories: ankle dorsiflexion (ADF), ankle plantarflexion (APF), foot extension (FE), toe extension (TE) and toe flexion (TF).

As was already seen in a previous publication (Branner et al. 2001), maps showing the target muscles and stimulation threshold can be generated for each measurement day. Each row in the stimulation maps indicated a row of equal-length electrodes. The data for the shortest and most proximal electrodes are shown at the top of the graph. These stimulation maps were compared at different times to analyze potential movement or changes of the electrodes with respect to the nerve fibers. In most cases, axons targeting similar muscle groups had the tendency to run together in the nerve (Figure 4-6A), potentially in the same fascicle. The motor nerve fibers were divided into two major groups of fascicles (a line was drawn between them in Figure 4-6): a) the fascicles of the tibial nerve fibers (APF and TF; muscle group 1 in Fig.4-5) and b) the fascicles of the common peroneal nerve fibers (mainly ADF, TE and FE; muscle groups 2 and 3). Each group might contain more than one fascicle but the classification scheme used did not allow us to make that distinction.

For the majority of animals, the most substantial changes took place during the first 1 to 3 weeks after implantation likely due to nerve damage and/or degeneration and other tissue responses such as connective tissue growth. Thus, there was poor stability in terms of what muscles could be stimulated and especially what currents were required for threshold stimulation in some animals (not shown here). The location of the electrodes within the nerve stabilized after 3-6 weeks mainly due to completion of connective tissue growth that holds the array in place. The maps were very stable and did not show a clear trend of electrode movement. If the electrodes had slowly moved out of the nerve due to connective tissue between the array base and the nerve, shorter electrodes would have failed first and the longer electrodes would have stimulated the same muscles as the shorter ones did earlier but in general this was not seen. On the contrary, long electrodes within presumed fascicles often failed and stimulation of the shortest electrodes could still evoke muscle twitches (Figure 4-6A). Stimulation thresholds for these short electrodes were also not exceptionally high indicating that the electrode tips were still located in close proximity to motor fibers (Figure 4-6B).

In agreement with previous experiments, stimulation thresholds at the edge or between presumed fascicles had a tendency to be higher than within fiber groups producing similar motor activity. The stimulation thresholds on average went up by a factor of 2.5

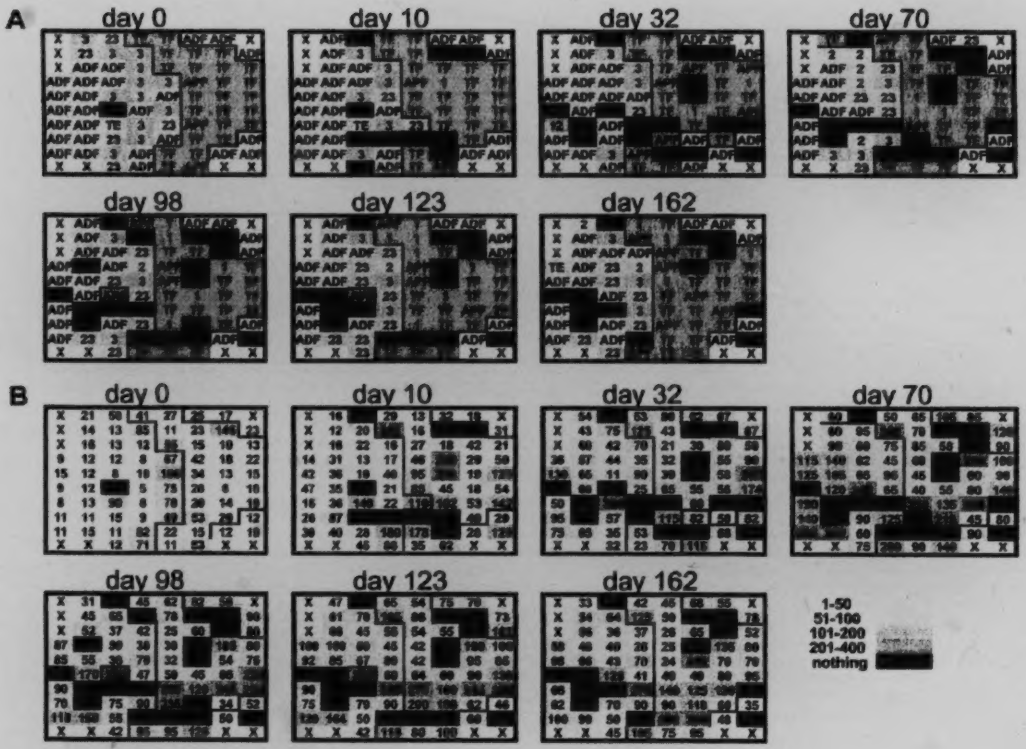

Figure 4-6. Functional stimulation maps of the USEA implanted in sciatic nerve and monitored at different times after implantation. The presumed boundaries between fascicles are indicated by black lines. An X indicates electrodes that were not connected, a black square indicates electrodes that do not produce a movement. With each row, electrodes were longer and more distal. A) Map of muscles activated at threshold by each electrode of the USEA. B) Single biphasic pulse, twitch current thresholds for each electrode in A.

within the first month (Figure 4-7A) and once a preparation was stable, electrodes with high stimulation thresholds had a tendency to have higher threshold currents in subsequent measurement sessions, whereas electrodes with lower threshold currents were more stable. The electrodes with high stimulation currents in excess of 400 μA were neither measured nor plotted on these graphs. There was no significant difference between groups of animals implanted using different containment systems or connector fixation techniques.

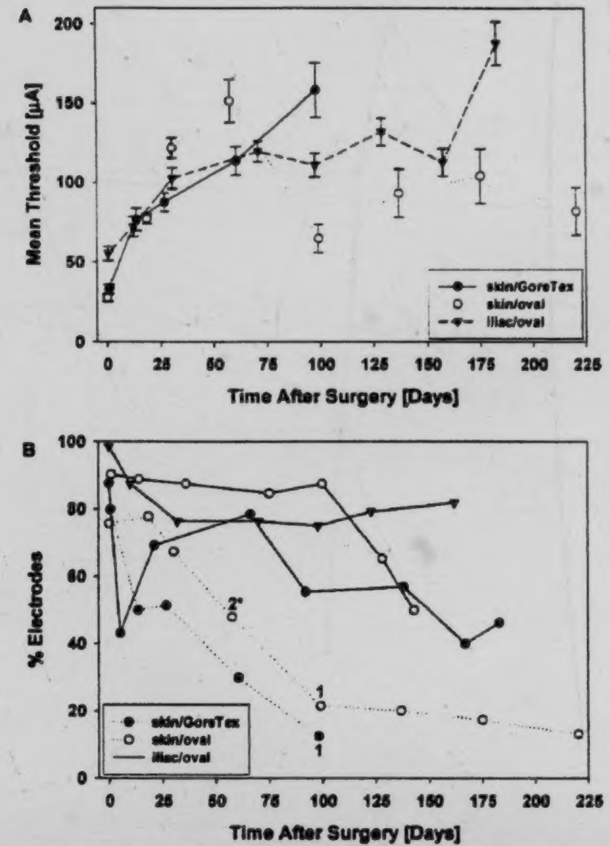

Figure 4-7. Summary of the stimulation data between three different kinds of implants by connector fixation techniques and containment systems used. A) Mean stimulation threshold (± standard error of mean) and B) average percentage of electrodes that can produce a muscle twitch over time. (Numbers describe the number of animals from that point on, the '*' means that one connector failed (with up to 36 electrodes in each connector))

The stimulation threshold data in Figure 4-7A were summarized for three different groups depending on the surgical procedure used; Figure 4-7B still used the same grouping but the data for each animal was shown for the most recent implants (iliac/oval). Not counting electrodes lost due to wire breakage or connector loss, we were still able to stimulate motor fibers using low stimulation currents (mostly under 100 µA) in 50% of the electrodes after 7 months in our longest running animal. We never lost all electrodes in any of the animals and in our best animal, 82% of all electrodes (59 electrodes) were still able to evoke motor responses after 162 days with 70% (49 electrodes) evoking the original movement (Figure 4-6 and 4-7B). Although one connector attached to the iliac crest did fail after about 4 months, there still is a significant difference in the number of electrodes lost over time between animals with different connector fixation techniques. The results of one implant (solid circle and line) were fairly variable and slowly degraded over time and visual inspection of the array after explantation showed that many electrodes were broken at the tip.

Recording

Recording using the electrodes in the array was not as successful as stimulation and data was only taken from the first five implants. On average 8% of the electrodes could record single unit activity during the first few days after implantation. Individual single units could sometimes be recorded for several weeks but in general the recording stability was poor in these experiments. Recording of neural activity was usually not possible for more than a month after implantation.

The electrodes' impedance can be influenced by chemical or physical changes of the recording surface. We observed a rapid drop of the electrodes' impedances within the first couple of weeks after implantation (Figure 4-8) but we did not do an in-depth analysis of the surface of the electrodes' tips after the array was removed from the tissue.

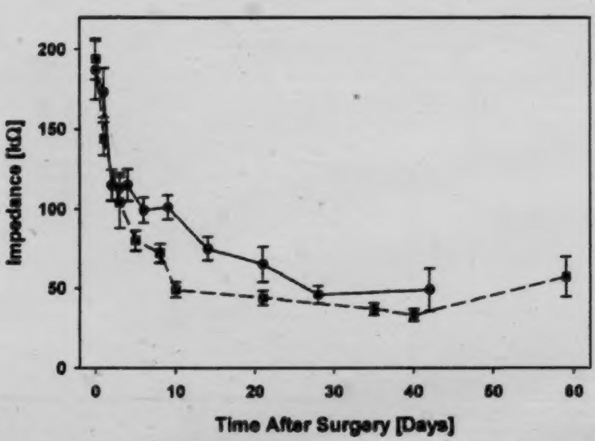

Figure4-8. Average electrode impedance over time for two different animals (with standard error of mean).

While nervous and muscle activity around the sciatic nerve are not an issue for stimulation, recordings can be seriously influenced if the electrodes and the reference electrode are not well shielded from this activity. In most cases, we attempted to place the reference electrode within the containment system surrounding the electrode array but they frequently did not stay there. While some single units could be recorded in anesthetized animals (Figure 4-9A), EMG activity and other noise contamination were so large when the animals were freely moving on the treadmill that the signal was not easily detectable (Figure 4-9B). However, Figure 4-9C, the close-up view of a small section of Figure 4-9B, illustrates that the neuronal spikes have a higher frequency content than the noise contamination. Filtering the signals using a 5th order highpass Butterworth filter with a cut-off frequency of 1 kHz caused a change in the waveform shape but the timing of the spikes did not change (Figure 4-9A,D). Most signal contamination could be removed using appropriate filtering and single units could be revealed (Figure 4-9E,F) that were previously very difficult to detect (Figure 4-9B,C). The 16-channel recording system also allowed selecting one of the electrodes in the array as reference, which in some cases reduced the amplitude of noise substantially.

Histology and general observations after explanation

At the time of sacrifice, a visual inspection and histological analysis were performed on all implanted functioning implants. There was little movement between the array, the containment system and the nerve in all cases but connective tissue around the containment system and the condition of the electrode arrays varied. Later experiments showed considerably less tissue response than earlier implants possibly due to the use of the custom cast containment system. Some electrode arrays had a lot of broken electrodes while others were still pristine; this most likely was influenced by the quality of implantation. Surprisingly, even electrodes with broken tips sometimes had good stimulation properties. The typical thickness of the connective tissue between the array and the nerve was 436.7 ± 62.3 μm (Mean ± Standard Error) whereas its thickness around the electrode shafts was only 30.4 ± 3.8 μm (Mean ± Standard Error). This means that some of the shorter electrodes did not reach inside the fascicles after a few months. In general, however, the electrodes were still located inside the nerve and its fascicles (Figure 4-10).

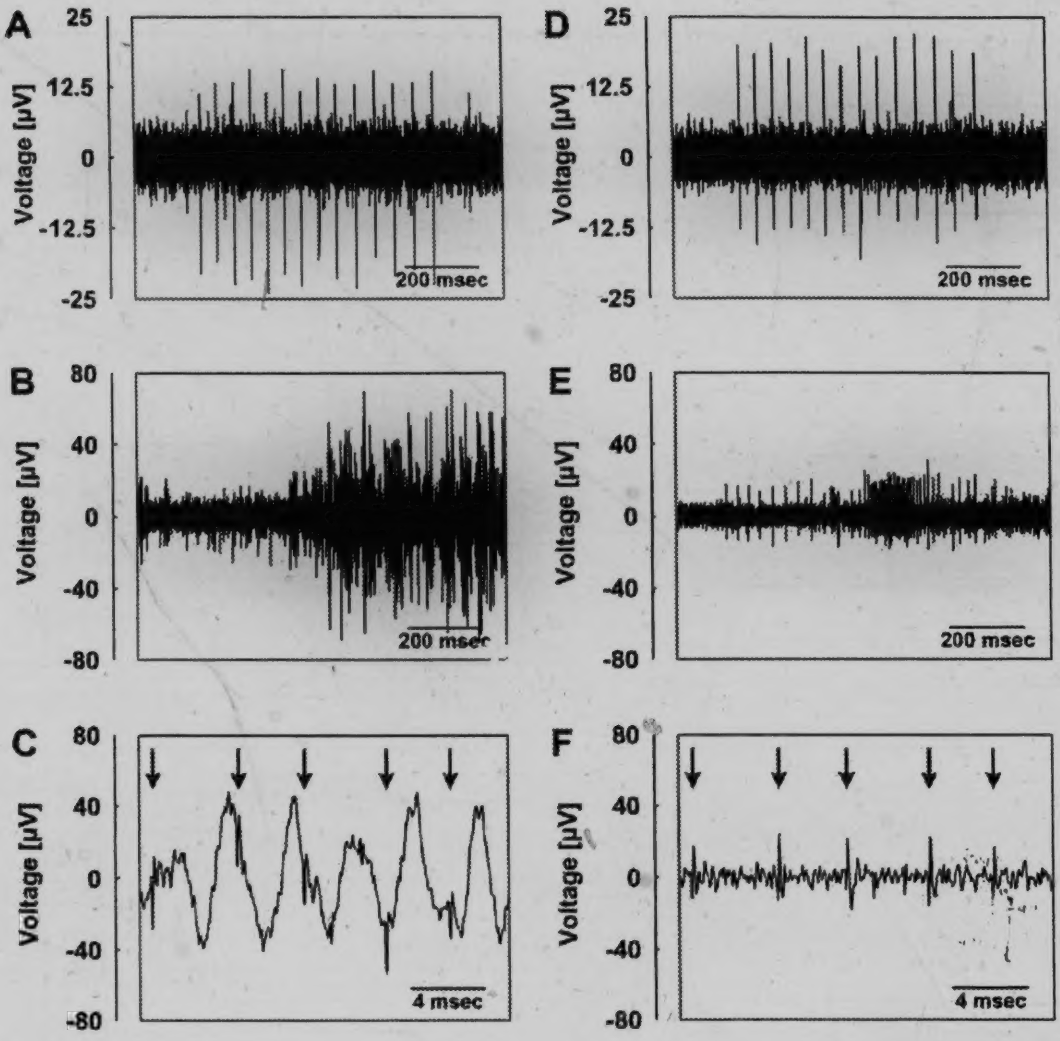

Figure 4-9. Sensory nerve fiber recordings taken from the same electrode in one animal during a measurement session ten days after implantation. A-C) Unprocessed recordings from the same electrode. Animal was A) anesthetized and B) walking on a treadmill. C) Close-up view of part of the recording in B). D-F) Same recordings as A-C filtered using a 5th order Butterworth highpass filter (at 1 kHz). The arrows indicate spiking events.

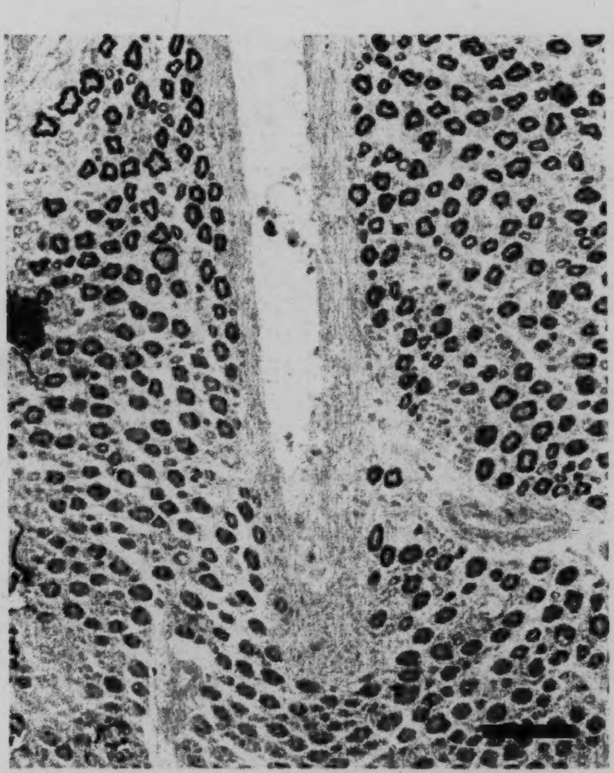

Figure 4-10. Light microscopic picture of a cross section of cat sciatic nerve. Many viable neurons can be seen in close opposition with an electrode. The bar is 40 μm long.

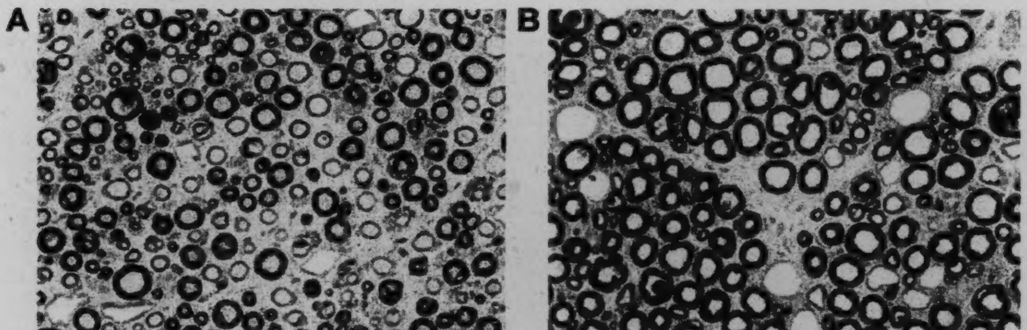

Figure 4-11. Light microscopic picture of cross sections of nerve fibers A) close to stimulated and B) far from stimulated electrodes. Regenerating fibers can be seen in the section close to stimulated electrodes. The bars are 20 μm long.

While there were signs of neuronal degeneration in some implants, oftentimes, viable neurons could be found around the electrode tips (Figure 4-11A).

Transverse semithin sections studied under light microscopy showed that the density and the estimated total number of myelinated fibers were similar in non-functioning implants and stimulated arrays (Table 4-2). Axonal degeneration, characterized by encroachment of axoplasm and myelin redundancy including collapse of the myelin into the axoplasm (Agnew and McCreery. 1990), was rarely observed beneath non-stimulated electrodes, although it was consistently seen in 5-10% of the fibers after chronic stimulation (Figure 4-11). The histogram distribution of axonal diameters and the scatter plots of the myelin area vs. axonal area are shown in Figure 4-12. There were an increasing number of thinly-myelinated axons (approximately 12% of the fibers) especially close to the electrode tracks in stimulated arrays which probably represent axons attempting to regenerate its distal segment after mechanical or electrical trauma.

Table 4-2. Proportion of hypomyelinated axons and axons undergoing axonal degenerations after electrical stimulation of the sciatic nerves.

	Density of myelinated Fibers (/mm^2)[1]	Percentage of Hypomyelinated fibers	Percentage of Degenerated Axons
Unfunctioning Arrays	7880 ± 693	3.46 %	0.52 %
Pulsed Arrays			
Close to electrode tracks	7875 ± 710	11.95 %	4.55 %
Far from electrode tracks	7548 ± 549	3.40 %	9.90 %

[1] Mean ± Standard Error

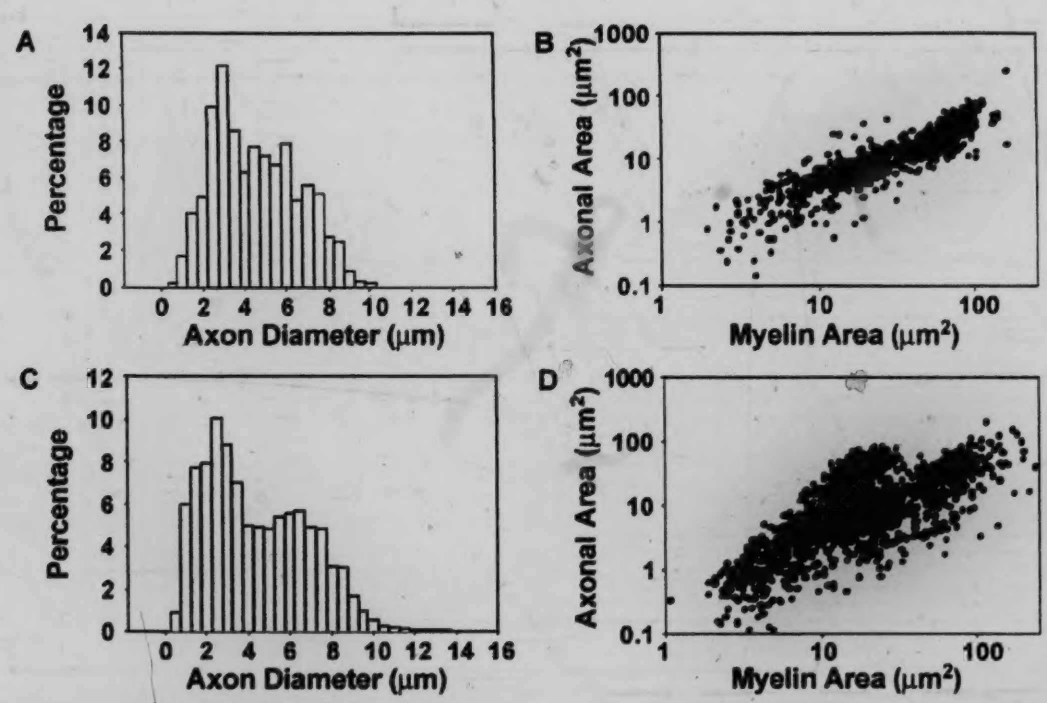

Figure 4-12. Comparison of nerve morphology in a control (A & B) versus an implanted nerve (C & D). **A** and **C.** Histogram distribution of axonal diameters. **B** and **D.** Scatter plots of myelin area vs. axonal area.

DISCUSSION

A general motor neuroprosthesis will use electrical stimulation to produce movement and sensory feedback signals to control the movement. For such a device to be useful, it has to be safe for the neural tissue and able to stimulate synergistic muscle groups selectively and consistently on a chronic basis. The feedback signal has to be easily analyzable and the kind of information that is encoded on each recording channel should be stable over time. The device should also be durable and have a long battery life. In the present study we tested the Utah Slanted Electrode Array (USEA) for its stimulation and recording properties over the time course of 4-7 months.

We demonstrated that the USEA can be implanted into peripheral nerve on a chronic basis and that selective stimulation of motor fibers can be performed over long periods of time. Improvements such as the fixation of the connectors on the iliac crest greatly helped to maintain the integrity of the lead wires from the connector to the array. We have shown that a containment system that surrounds the array and the nerve with a design that incorporates the shape of the array in the nerve reduced connective tissue growth around the electrodes and their surroundings.

After recovery from surgery, the animals did not react to the presence of the connectors on the iliac crest nor the array in the nerve; even when monitoring cables were plugged into the connectors and measurements were taken. Whereas stimulation thresholds did consistently increase within the first few weeks, they remained constant after the first month; only a few electrodes through which a muscle twitch could be evoked were lost after the first month. We believe that most axonal degeneration has taken place at this time but the damage to the nerve is not extensive enough to visibly affect the animal's movement or behavior. This was confirmed by the fact that the density of myelinated fibers was normal around the implanted electrodes with about 10% of the fibers regenerating. Because of the significant difference in the number of electrodes lost over time between animals with different connector fixation techniques and because electrodes do fail at random locations or by almost whole connectors, the loss of electrodes is most likely due to lead breakage or connector failure.

Smaller, lower aspect ratio and safer connectors will become available with improvements in micromaching techniques in the future and more flexible, permeable and/or potentially partially dissolvable containment systems can be implemented in the future to further improve the stability of the system. Even though there was variability in the stimulation response, changes were seldom drastic and there were generally multiple electrodes that could be used to evoke a particular muscle movement. In contrast to most techniques, this could potentially enable us not only to stimulate muscles selectively, but to do so in a fatigue resistant manner by interleaving stimulation between several electrodes as suggested by others (Yoshida and Horch. 1993) and provide us with backup electrodes if others should fail.

In terms of a neuroprosthetic application, the stimulation results shown here are encouraging, but the same is not true for recording of sensory activity. Neural recordings were either contaminated with noise such as EMG activity or could not be picked up at all after a few days. Three different things can influence the quality of recordings: a) the distance of the recording surface to the sensory fibers, b) the electrode impedance and c) the magnitude of the recorded noise in relation to the desired signal. The distance of the electrode tip to the recorded fibers is negatively influenced by the formation of connective tissue around the shaft of the electrodes; the greater the fibrotic buildup, the smaller the recorded signal will be. The increase in stimulation thresholds suggests that a formation of connective tissue or degeneration of nerve fibers around the electrode tips took place within the first month after implantation. In contrast to the connective tissue growth that would normally result in an electrode impedance increase (Stein et al. 1978), the electrode impedances dropped in the weeks after implantation. This suggests physical changes on the electrode surface that were not studied here however.

Some recorded signals could be recovered with digital filtering techniques but the gain was generally not satisfactory. Better electrical shielding of the nerve and coating the electrode shafts with an agent designed to minimize tissue reaction might improve results but recording sensory activity from a different location, such as the dorsal root ganglia, holds more promise. The cell bodies of sensory nerve fibers, which produce larger electrical activity, are located there and the site is better protected from sources of signal contamination such as large muscles. Acute experiments have shown that sensory signals can be recorded in the DRG with very high yields and with large signal-to-noise ratios (Aoyagi et al. 2001).

In summary, whereas many problems related to the electrode interface and its chronic implantation have yet to be solved, this study showed that the long-term implantation of a penetrating microelectrode array in peripheral nerve is possible with little permanent nerve damage and that this device is well suited for the stable and selective activation of several different muscle groups. Devices of this architecture may provide an effective neural interface for various motor neuroprosthetic applications.

REFERENCES:

1. Agnew WF, and McCreery DB. Considerations for safety with chronically implanted nerve electrodes. *Epilepsia* 31: S27-32., 1990.

2. Aoyagi Y, Stein RB, Branner A, and Normann RA. Single unit recording capabilities from dorsal root ganglia of using a microelectrode array. *Society for Neuroscience 31th Annual Meeting*, San Diego, Calif., 2001.

3. Bowman BR, and Erickson RC, 2nd. Acute and chronic implantation of coiled wire intraneural electrodes during cyclical electrical stimulation. *Ann Biomed Eng* 13: 75-93, 1985.

4. Branner A, and Normann RA. A multielectrode array for intrafascicular recording and stimulation in sciatic nerve of cats. *Brain Res Bull* 51: 293-306, 2000.

5. Branner A, Stein RB, and Normann RA. Selective stimulation of cat sciatic nerve using an array of varying-length microelectrodes. *J Neurophysiol* 85: 1585-1594, 2001.

6. Bunge MB. Bridging areas of injury in the spinal cord. *Neuroscientist* 7: 325-339., 2001.

7. Cameron T, Liinamaa TL, Loeb GE, and Richmond FJ. Long-term biocompatibility of a miniature stimulator implanted in feline hind limb muscles. *IEEE Trans Biomed Eng* 45: 1024-1035, 1998.

8. Choi AQ, Cavanaugh JK, and Durand DM. Selectivity of multiple-contact nerve cuff electrodes: a simulation analysis. *IEEE Trans Biomed Eng* 48: 165-172., 2001.

9. Crampon MA, Sawan M, Brailovski V, and Trochu F. New easy to install nerve cuff electrode using shape memory alloy armature. *Artif Organs* 23: 392-395, 1999.

10. Fernandez E, Cuenca N, and De Juan J. A useful programme in BASIC for axonal morphometry with introduction of new cytoskeletal parameters. *J Neurosci Methods* 39: 271-289., 1991.

11. Grill WM, and Mortimer JT. Stability of the input-output properties of chronically implanted multiple contact nerve cuff stimulating electrodes. *IEEE Trans Rehabil Eng* 6: 364-373., 1998.

12. Grill WM. Electrical activation of spinal neural circuits: application to motor-system neural prostheses. *neuromodulation* 3: 97-106, 2000.

13. Jones LL, Oudega M, Bunge MB, and Tuszynski MH. Neurotrophic factors, cellular bridges and gene therapy for spinal cord injury. *J Physiol* 533: 83-89., 2001.

14. Kovacs GT, Storment CW, Halks-Miller M, Belczynski CR, Jr., Della Santina CC, Lewis ER, and Maluf NI. Silicon-substrate microelectrode arrays for parallel recording of neural activity in peripheral and cranial nerves. *IEEE Trans Biomed Eng* 41: 567-577, 1994.

15. Loeb GE, Zamin CJ, Schulman JH, and Troyk PR. Injectable microstimulator for functional electrical stimulation. *Med Biol Eng Comput* 29: NS13-19., 1991.

16. Meier JH, Rutten WL, and Boom HB. Force recruitment during electrical nerve stimulation with multipolar intrafascicular electrodes. *Med Biol Eng Comput* 33: 409-417., 1995.

17. Mushahwar VK, Collins DF, and Prochazka A. Spinal cord microstimulation generates functional limb movements in chronically implanted cats. *Exp Neurol* 163: 422-429, 2000.

18. Nordhausen CT, Maynard EM, and Normann RA. Single unit recording capabilities of a 100 microelectrode array. *Brain Res* 726: 129-140., 1996.

19. Prochazka A, and Mushahwar VK. Voluntary muscle contractions can be boosted by spinal cord microstimulation. *J Physiol* 525: 6S, 2000.

20. Rodriguez FJ, Ceballos D, Schuttler M, Valero A, Valderrama E, Stieglitz T, and Navarro X. Polyimide cuff electrodes for peripheral nerve stimulation. *J Neurosci Methods* 98: 105-118., 2000.

21. Rousche PJ, and Normann RA. A method for pneumatically inserting an array of penetrating electrodes into cortical tissue. *Ann Biomed Eng* 20: 413-422, 1992.

22. Rousche PJ, and Normann RA. Chronic intracortical microstimulation (ICMS) of cat sensory cortex using the Utah Intracortical Electrode Array. *IEEE Trans Rehabil Eng* 7: 56-68, 1999.

23. Rozman J, and Trlep M. Multielectrode spiral cuff for selective stimulation of nerve fibres. *J Med Eng Technol* 16: 194-203., 1992.

24. Slot PJ, Selmar P, Rasmussen A, and Sinkjaer T. Effect of long-term implanted nerve cuff electrodes on the electrophysiological properties of human sensory nerves. *Artif Organs* 21: 207-209., 1997.

25. Smit JP, Rutten WL, and Boom HB. Endoneural selective stimulating using wire-microelectrode arrays. *IEEE Trans Rehabil Eng* 7: 399-412., 1999.

26. Stein RB, Charles D, Gordon T, Hoffer JA, and Jhamandas J. Impedance properties of metal electrodes for chronic recording from mammalian nerves. *IEEE Trans Biomed Eng* 25: 532-537., 1978.

27. Strange KD, and Hoffer JA. Restoration of use of paralyzed limb muscles using sensory nerve signals for state control of FES-assisted walking. *IEEE Trans Rehabil Eng* 7: 289-300., 1999.

28. Sweeney JD, Crawford NR, and Brandon TA. Neuromuscular stimulation selectivity of multiple-contact nerve cuff electrode arrays. *Med Biol Eng Comput* 33: 418-425., 1995.

29. Tarver WB, George RE, Maschino SE, Holder LK, and Wernicke JF. Clinical experience with a helical bipolar stimulating lead. *Pacing Clin Electrophysiol* 15: 1545-1556., 1992.

30. Tyler DJ, and Durand DM. A slowly penetrating interfascicular nerve electrode for selective activation of peripheral nerves. *IEEE Trans Rehabil Eng* 5: 51-61., 1997.

31. Veltink PH, van Alste JA, and Boom HB. Multielectrode intrafascicular and extraneural stimulation. *Med Biol Eng Comput* 27: 19-24., 1989.

32. Veraart C, Grill WM, and Mortimer JT. Selective control of muscle activation with a multipolar nerve cuff electrode. *IEEE Trans Biomed Eng* 40: 640-653., 1993.

33. Walter JS, Griffith P, Sweeney J, Scarpine V, Bidnar M, McLane J, and Robinson C. Multielectrode nerve cuff stimulation of the median nerve produces selective movements in a raccoon animal model. *J Spinal Cord Med* 20: 233-243., 1997.

34. Woodford BJ, Carter RR, McCreery D, Bullara LA, and Agnew WF. Histopathologic and physiologic effects of chronic implantation of microelectrodes in sacral spinal cord of the cat. *J Neuropathol Exp Neurol* 55: 982-991, 1996.

35. Yoshida K, and Horch K. Selective stimulation of peripheral nerve fibers using dual intrafascicular electrodes. *IEEE Trans Biomed Eng* 40: 492-494., 1993.

36. Yoshida K, and Horch K. Reduced fatigue in electrically stimulated muscle using dual channel intrafascicular electrodes with interleaved stimulation. *Ann Biomed Eng* 21: 709-714., 1993.

37. Yoshida K, and Horch K. Closed-loop control of ankle position using muscle afferent feedback with functional neuromuscular stimulation. *IEEE Trans Biomed Eng* 43: 167-176, 1996.

38. Ziaie B, Nardin MD, Coghlan AR, and Najafi K. A single-channel implantable microstimulator for functional neuromuscular stimulation. *IEEE Trans Biomed Eng* 44: 909-920., 1997.

CHAPTER 5

COMPARING MOVEMENTS ELICITED BY ELECTRICAL STIMULATION OF MUSCLE, NERVE, SPINAL CORD AND SPINAL ROOTS IN ANESTHETIZED AND DECEREBRATE CATS*

INTRODUCTION

Spontaneous neurological recovery after spinal cord injury or stroke occurs to some extent in the first months after the onset of the disorder, but is extremely limited after the first year (Ditunno et al. 1997). Minimizing the damage to the central nervous system and maximizing recovery is a continuing goal for research and treatment of these conditions. Although advances have been made in the field of central nervous system regeneration, a cure for spinal cord injury or stroke does not yet exist (Behar et al. 2000; Girardi et al. 2000). The spinal cord below the lesion, as well as the muscles and nerves, remain essentially intact in many individuals (Stein et al. 1992), though reflex transmission and the tonic state of interneuronal networks may be abnormal (Sherrington. 1906). Thus, stimulating the surviving neurons below the lesion is another approach to restore motor function (Liberson et al. 1961). If excitation of muscles or nerves can be suitably coordinated, functional movements such as walking and grasping can be generated (Kralj et al. 1988; Peckham and Creasey. 1992; Prochazka et al. 1997). Motor prostheses have been developed to restore functional movement and partially overcome the paralysis of spinal cord injury by electrical stimulation (Chapin and Moxon. 2000; Kralj and Bajd. 1989; Stein et al. 1992). Although some clinical applications of electrical stimulation have been successful (Dai et al. 1996; Kralj et al. 1988; Peckham and Creasey. 1992; Wieler et al. 1999), the electrical restoration of whole limb movements remains problematic (Field-Fote. 2000; Prochazka. 1993). More recently, stimuli have been applied to the spinal cord and ventral roots as other avenues for restoring functional movement by electrical stimulation (Mushahwar et al. 2000; Mushahwar and Horch. 1997; Rushton et al. 1997; Tai et al. 1999). One rationale for using spinal stimulation is the interesting suggestion that a spinal electrode may activate a group of muscles that form 'force-field primitives' (Bizzi et al. 2000; Giszter et al. 1993).

---

* A version of this chapter will be submitted to *IEEE Trans Neural Syst Rehabil Eng* by the authors of Aoyagi. Y, Mushahwar. VK, Stein. RB, Prochazka, A. Portions of this chapter have been published in *Proc 6th Ann. Conf. International Functional Electrical Stimulation Society (IFESS)*, pp. 120-122, 2001.

However, many unresolved questions remain about where and how to use electrical stimulation for restoring limb movement. To date, very few studies have compared results using different methods in the same subjects. In addition, many of the basic biomechanical and neurophysiological properties of movements produced by electrical stimulation are poorly understood. This study represents the first step in comparing these properties using electrical stimulation of muscles, nerves, ventral and dorsal roots, and the spinal cord in anesthetized and decerebrated cats. The results provide baseline information that can be tested further in chronically spinalized animals for eventual human application. Brief accounts of some of this material have appeared (Aoyagi et al. 2001; Aoyagi et al. 2000).

METHODS

Animal preparation

Ten adult cats were used in this study according to protocols approved by the University of Alberta animal care committee in accordance with the Declaration of Helsinki. Anesthesia was either induced by inhalation of halothane (5 cats that were decerebrated later in the experiment) or by use of sodium pentabarbital (the other 5 cats that remained under anesthesia until they were euthanized). For animals under halothane a tracheotomy was done and a tracheal tube was inserted and firmly tied to the trachea. The cats breathed spontaneously a mixture of 95% O_2 and 5% CO_2 mixed with halothane. The halothane-anesthetized cats also had the right jugular vein and right carotid artery cannulated. The left carotid artery was ligated. Arterial pressure was measured by connecting the carotid catheter to a pressure transducer. 10% dextran was given as necessary through a jugular vein cannula. Body temperature was monitored and maintained close to 37°C using heating pads and/or lamp. The animal's right leg and back were shaved.

Nerves

The following nerves were exposed in the right hindlimb: tibial nerve (TB), common peroneal nerve (CP), hamstring branches of the sciatic nerve supplying knee flexors (KF) and hip extensors (HE) (**Figure 5-1a**), and femoral nerve branches supplying hip flexors (HF) and knee extensors (KE) (**Figure 5-1b**). In the first two experiments, all nerves were implanted with cuff electrodes (Hoffer et al. 1996), but some fine nerves tended to block over the course of a long experiment. In later experiments, epineural electrodes were used for all but the CP and TB nerves and no blockage occurred. All data that could have been affected by nerve blockage were excluded from the analysis. After the nerves were cleared from surrounding tissue, cuff or epineural electrodes were implanted. Before implantation, each nerve was stimulated by a hook electrode in order to verify its innervation. The hamstring nerve, which separates from the sciatic nerve, has three main branches (**Figure 5-1a**) (Crouch. 1969; Hamm et al. 1985). Two branches innervate hip extensors: semimembranosus and anterior biceps femoris. One branch innervates knee flexors: posterior biceps femoris and semitendinosus. The femoral nerve typically had four main branches (**Figure 5-1b**); two innervated hip flexors: sartorius and rectus femoris, one innervated knee extensor branches of the quadriceps femoris and the remaining branch was the saphenous, a cutaneous nerve. The tibial and common peroneal nerves were exposed after an incision was made along the popliteal region and surrounding fatty tissue was removed. Those nerves innervate ankle plantarflexors and dorsiflexors respectively. Thus, six nerve electrodes were implanted. The skin was closed after each implant.

Muscles

To stimulate muscle, bipolar intramuscular electrodes were placed close to the motor points in seven right hindlimb muscles (lateral gastrocnemius (LG), tibialis anterior (TA), vastus lateralis (VL), semimembranosus anterior (SM), posterior biceps femoris (BF), sartorius (SA), and iliopsoas (IP)). Each electrode in a pair of intramuscular electrodes was prepared by passing a fine wire through a 21-gauge hypodermic needle. The electrodes were insulated except for 3-mm at the tip. Electromyograms (EMG) were also recorded with these electrodes.

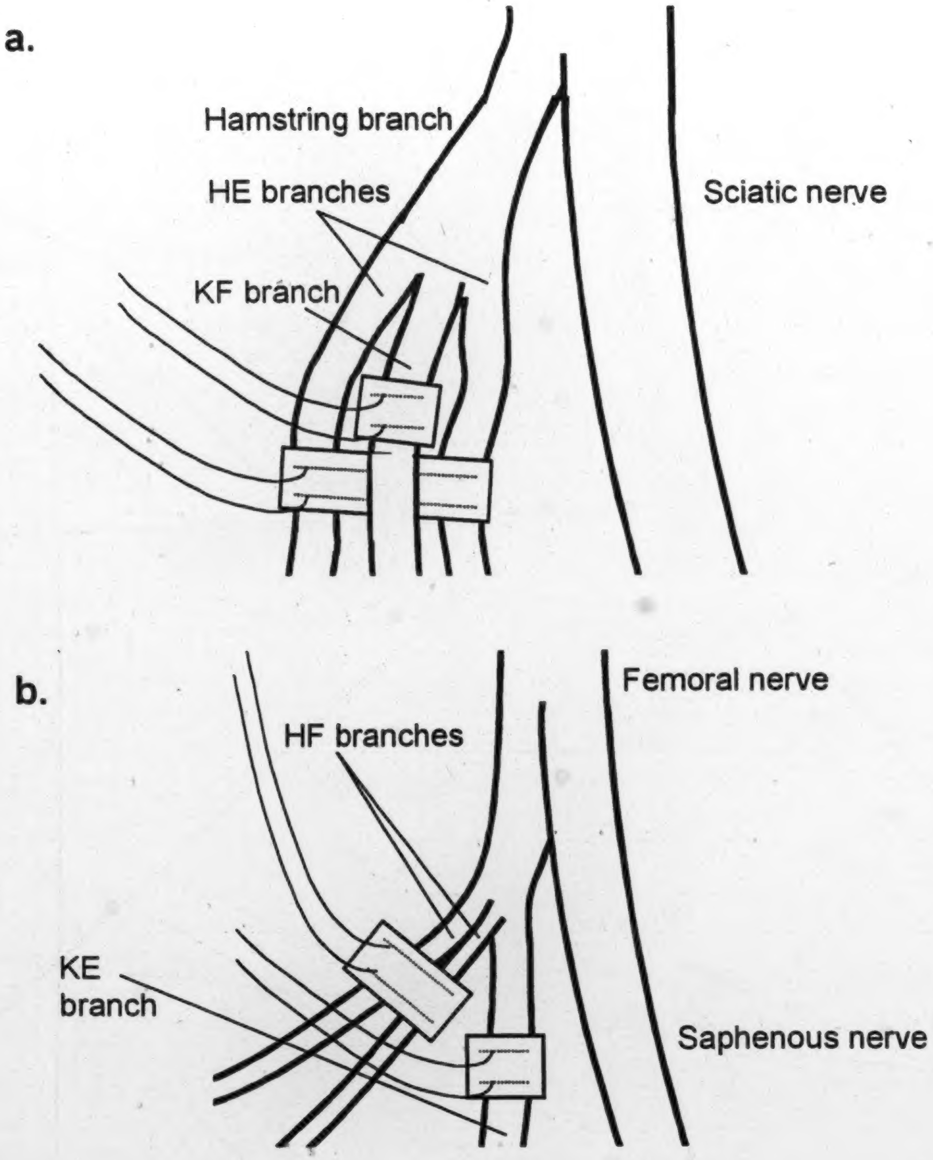
a.
Hamstring branch
HE branches
Sciatic nerve
KF branch
b.
Femoral nerve
HF branches
KE
branch
Saphenous nerve

Figure 5-1. a. A schematic view of the hamstring branch of the sciatic nerve and bipolar, epineural electrodes attached near the hip extensor (HE) and knee flexor (KF) branches. **b.** A schematic view of the femoral nerve and epineural electrodes attached over the surface of the hip flexor (HF) and knee extensor (KE) branches. After passing the dorsal iliopectineal arch, the femoral divides into four branches: two innervate hip flexors, one innervates knee extensors, and the remaining branch is the saphenous nerve.

Spinal cord

The spinal cord was exposed from L4 to S3 by a laminectomy. The cat was mounted in a conventional spinal frame. To stimulate the spinal cord, 10-19 microwire electrodes were inserted through minute holes made in the dura mater with a 30-gauge dental needle on the right side of the spinal cord (Mushahwar et al. 2000; Prochazka et al. 2001). The electrodes were 30-μm diameter, stainless-steel wires (California Fine Wire, Gover City, CA) with 30-70 μm exposed at the tip. They were inserted every 2-3 mm along the cord from L5 to S1, 1.5 – 2 mm from the midline and 1.5-3.0 mm deep, depending on the size of spinal cord at each level. The positions were generally verified histologically and most were located in intermediate gray matter locations thought to contain "movement primitives" (Chapin and Moxon. 2000; Giszter et al. 1993). Final placement was determined by stimulation through each electrode to ensure that a consistent, clear movement could be elicited.

Motion analysis

To monitor the movement of the joints three-dimensionally, motion tracking sensors (6D-Research™, Skill Technologies, Inc., Phoenix, AZ) were placed on the skin near (1) the hip joint, (2) the lateral epicondyle of the femur, (3) the lateral malleolus of the tibia, and (4) the lateral surface of the foot holder corresponding to the lateral metatarsophalangeal joint of the foot (**Figure 5-2a**). To avoid skin slippage or displacement during movement, sensors 2 and 3 were rigidly fixed to the femur and tibia by surgical suture through holes drilled in the respective bone. All instruments within 1 m from the sensors had no magnetic metals to avoid any electromagnetic interference with the signals recorded from the motion sensors. The right paw was fixed in a U-shaped foot holder. The foot holder was connected to one end of a 50cm rod that had a joystick-like fulcrum 40cm from the foot holder. The foot holder was designed to be able to move perpendicularly to the joystick to allow all sagittal movements. The other end of the rod was connected to a spring.

Prior to the experiment, the force to move the holder from the neutral position in the sagittal plane was measured. The mean change in force with distance in the forward, upward, backward and downward directions of the sagittal plane was 1.4 ± 0.1 N/cm (mean

± SD). None of the directions was statistically different from the others. Thus, the cat's right hindlimb was moving in a uniform stiffness field in the sagittal plane. The resting position of the limb was adjusted to approximate a normal standing posture.

Experimental protocol

The following measurements were made:

1. Passive range of motion of the right hindlimb in the sagittal plane was measured and recorded through the 6D-Research^{TM} system.
2. The muscles were stimulated individually and the kinematics were recorded through the 6D-Research^{TM} system. Bipolar stimulation was used and the stimulus consisted of trains of monophasic cathodic pulses at 50 pulses/sec (pulse of 1ms) lasting 0.8 sec. Each stimulus pulse had a duration of 300 μsec. The stimulation current needed to produce a threshold muscle movement was determined for each muscle using visual observation and was increased in steps up to several times threshold.
3. Nerves were stimulated individually in a bipolar manner through epineural or cuff electrodes over a similar range of intensities and the EMG and kinematics were recorded.
4. Intraspinal electrodes were also stimulated individually at a range of intensities up to several times threshold. Monopolar stimulation was used and the reference electrode [9-strand stainless steel Cooner wire (California Fine Wire, Gover City, CA)] was embedded within the back muscles. In order to prevent spinal cord damage or migration of electrode due to stimulation at high level intensity, we limited the maximal stimulus intensity to 500 μA.
5. In 5 animals, the right dorsal and ventral roots from L4 to S1 were exposed. Dorsal roots and ventral roots were sequentially cut peripherally and stimulated by hook electrodes at a range of intensities.
6. In some animals, to induce maximal movement in the forward, upward, backward and downward directions from muscle, nerve and spinal cord, various stimulus combinations were given. For example, to induce the maximal upward movement by nerve stimulation, a synergistic group of flexor nerves (CP, KF and HF) was stimulated together at a supramaximal level (see also **Figure 5-5a**). After decerebration at an intercollicular

level (n=5 cats) the anesthetic was discontinued and parts 2- 4 above were repeated for comparison after the animals came out of anesthesia (typically 1 hour after decerebration).

Data acquisition

Kinematic data recorded through the 6D-Research™ system were digitized at a rate of 30 samples per second. During stimulation, the trajectories of the four motion sensors in the sagittal plane were measured using the 6D-Research™ motion analysis software. Then, the direction and distance of the paw movement vector were calculated based on the trajectory produced by sensor 4 that was placed near the metatarsophalangeal joint. Calculations were done using custom-written programs in Matlab (Math Works, Inc., Natick, MA). The vectors shown in the polar plots of **Figure 5-2, 5-3, and 5-5** represent the movement of the paw from the rest position to the extreme position produced by stimulation.

RESULTS

The lengths of the thigh, shank, and foot were 9.4 ± 0.4, 10.9 ± 0.6, 9.8 ± 0.4 cm (mean ± S.D.). In the rest position of the hindlimb the hip was flexed by 30 ± 9°, the knee was flexed by 69 ± 9° and the ankle was plantarflexed by 19 ± 16° in a uniform stiffness field (see **METHODS** and **Figure 5-2a**). These values are similar to those found in a quiet standing animal (Macpherson. 1988).

As an example of the motion analysis, **Figure 5-2b** demonstrates the trajectory of the hip, knee, ankle and paw (near the lateral metatarsophalangeal joint) when BF was stimulated with 3 times threshold (T). The distance of the paw movement during stimulation was 6.4 cm from the rest to the extreme position. The direction was 143° with respect to the forward direction. In the same way, vectors induced by stimulation of muscles, nerves, spinal cord, ventral and dorsal roots were analyzed and plotted in polar coordinates. When the stimuli were repeated (not shown), the movements were very reproducible.

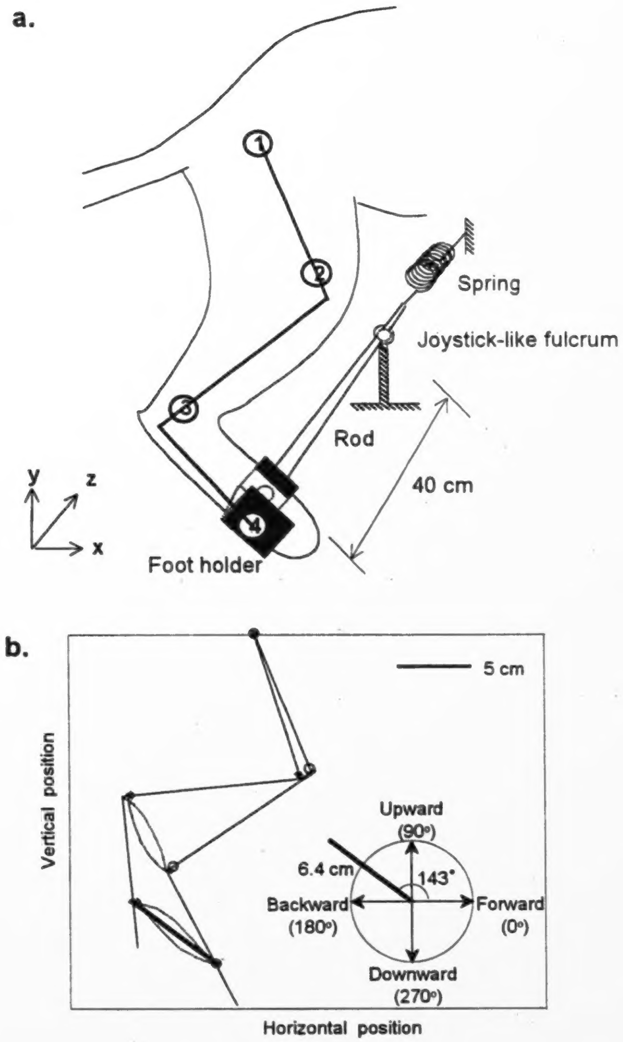
a.
1
2
3
4
Spring
Joystick-like fulcrum
Rod
40 cm
y
z
x
Foot holder
b.
5 cm
Vertical position
Upward
(90°)
143°
6.4 cm
Backward
(180°)
Forward
(0°)
Downward
(270°)
Horizontal position

Figure5-2. a. A schematic view of the experimental setup. The motion sensors were attached to the lateral surface of (1) the hip joint, (2) the lateral epicondyle of the femur, (3) the lateral malleolus of the tibia, and (4) the lateral metatarsophalangeal joint. The right paw was fixed in a foot holder. The foot holder was connected to an edge of a 50cm rod that had a joystick-like fulcrum 40cm from the foot holder. The other end of the rod was connected to a spring. **b.** Sagittal trajectory of the hindlimb generated during stimulation of posterior biceps femoris (BF) muscle. The stimulus threshold was 200μA. The figures illustrate the rest and extreme position when BF was stimulated by 1000μA. The O and * respectively represent the position of sensors 1 - 4 at rest and at the extreme position during stimulation. The dotted lines represent the real trajectory of the hindlimb joints during stimulation. The thick line represents the total vector (from rest to the extreme position) of the lateral metatarsal-phalangeal joint, which corresponds to sensor 4. Note that forward, upward, backward and downward directions correspond to 0°, 90°, 180° and 270° respectively.

Trajectories elicited by stimulating muscles, nerves, spinal cord and roots

Figure 5-3a-d show typical results elicited from one animal. Movement vectors (from rest to the maximal excursion) were generated by intramuscular electrodes (**Figure 5-3a**) and epineural electrodes (**Figure 5-3b**) with stimulus amplitudes ranging from 1.2 – 6T. Stimulation of individual muscles and nerves produced fairly distinct and reproducible preferred directions. Preferred directions for each muscle and nerve stimulation were always within 30° with stimulus levels from just above threshold to supramaximal. As expected, stimulation of the TB nerve and the LG muscle, which is innervated by TB, showed similar preferred directions. Also, CP and TA, KE and VL, HE and SM, KF and BF, HF, SA and IP showed almost identical preferred directions. The movements were also consistent between animals (**Table**).

Movement vectors from stimulating L4 – S1 ventral roots from the same animal after decerebration ranged between 149° - 360° under decerebration (**Figure 5-3c**), whereas the vectors from stimulating L4 – S1 dorsal roots ranged between 20° - 138° (**Figure 5-3d**). Interestingly, the vectors from ventral root stimulation mainly covered downward and backward directions and moved backwards in a clockwise direction as root stimulation moved from L4 to S1. The vectors from dorsal root stimulation mainly covered forward and upward directions and moved clockwise as root stimulation moved from S1 to L4. Thus, neither ventral nor dorsal root stimulation alone could cover the full range of movement directions, but the movements of the two were complementary and together covered all directions.

Figure 5-3e shows movement vectors produced by stimulating 19 intraspinal electrodes from another animal. The vectors covered all directions, but movements elicited through intraspinal electrodes often showed abrupt changes in direction with increasing stimulus amplitudes (**Figure 5-4**). In contrast, the preferred directions for stimulation of the muscles, nerves and roots were generally constant for stimulus levels from just above threshold to supramaximal (**Figure 5-4**). In this particular spinal stimulation, only 10 out of 19 sites showed relatively consistent direction (<30° change), 7 showed changes between 30 and 90° while 2 sites showed dramatic, directional changes (>90°) depending on the stimulus intensity.

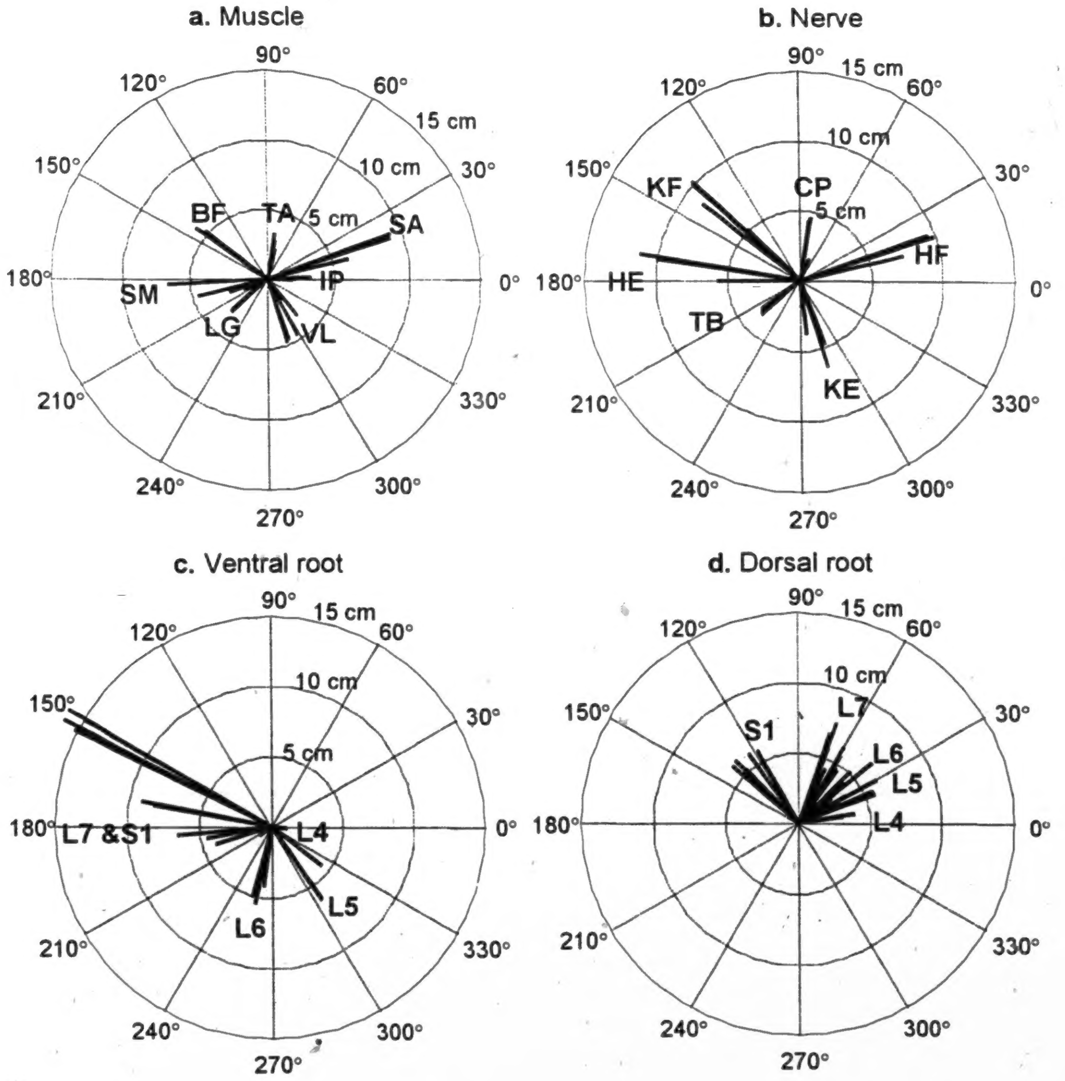

Figure 5-3. a and **b**. Muscles and nerves were stimulated with stimuli up to about 5 times threshold (T). Lines radiating from the center of the polar graphs represent the vectors from rest to extreme positions during stimulation. Both data were obtained from a halothane-anesthetized animal. The directions were quite consistent in all cases (see also **Table** and **Figure 5-7**). Abbreviations: lateral gastrocnemius (LG), tibialis anterior (TA), vastus lateralis (VL), semimembranosus anterior (SM), posterior biceps femoris (BF), sartorius (SA), and iliopsoas (IP), tibial (TB), common peroneal (CP), knee extensor (KE), hip extensor (HE), knee flexor (KF) and hip flexor (HF). **c** and **d**. Ventral and dorsal roots were stimulated at levels up to a few times threshold. Note that stimulating the ventral roots produced consistent movements at all stimulus levels (mainly down and forward). The direction rotated clockwise as more caudal roots were stimulated. In contrast, stimulating the dorsal roots produced movements up and forward, which rotated counterclockwise as more rostral roots were stimulated. All data were obtained from the same animal.

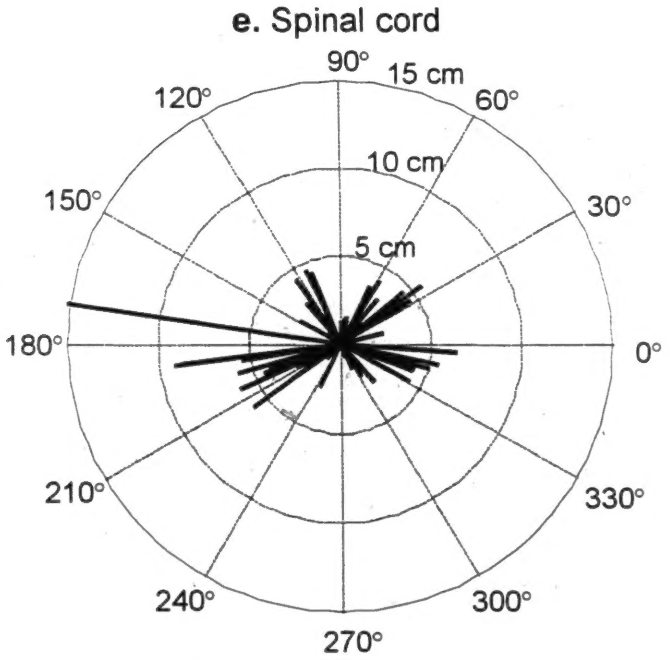

Figure 5-3e. All vectors produced by stimulation of 19 intraspinal electrodes with stimulation levels up to about 5T in an anesthetized animal. Those covered all directions including forward, upward, backward, and downward.

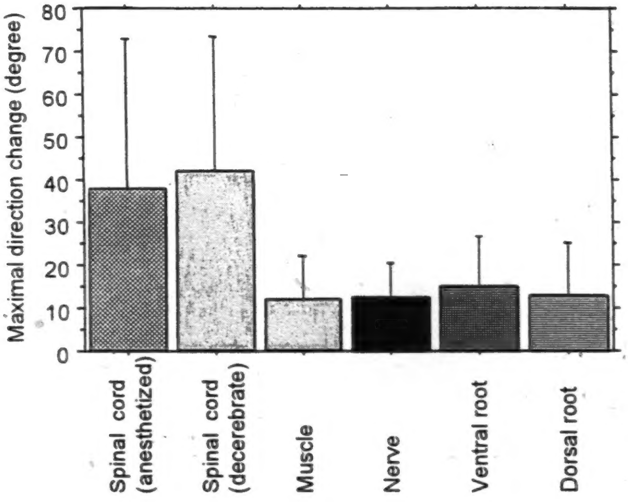

Figure 5-4. Comparison of maximal directional change according to the level of stimulus intensity in anesthetized animals. Directions generated by muscle, nerve, ventral and dorsal root stimulation were relatively constant from minimal to maximal stimulation (<20°) whereas directions generated through intraspinal electrodes in both anesthetized and decerebrate state often showed abrupt changes and were significantly larger than the other four types of stimulation ($p<0.01$). The data by muscle, nerve, and ventral root stimulation were elicited under anesthesia and the data by dorsal root stimulation was elicited in decerebrate.

The preferred directions remained relatively constant between anesthetized and decerebrate states in stimulation of muscle, nerve, ventral and dorsal root (**Table 5**). No statistically significant changes in direction were seen between two states except for LG, TA, CP, L5 and S1 ventral root. The state-dependence of spinal cord stimulation will be presented in a later paper.

Maximal movements

We compared the maximal paw movements in four different directions elicited by muscle, nerve and spinal stimulation (**Figure 5-5**). In order to produce maximal movements in the forward, upward, backward and downward directions, synergistic nerves

Muscle	**#**	**VL**	**IP**	**SA**	**SM**	**BF**	**LG****	**TA****
Anesthetized	10	290 ± 16	1 ± 13	12 ± 7	181 ± 11	140 ± 7	202 ± 12	80 ± 15
Decerebrate	5	285 ± 10	2 ± 8	12 ± 7	171 ± 9	141 ± 12	162 ± 22	60 ± 24
Nerve		**KE**		**HF**	**HE**	**KF**	**TB**	**CP***
Anesthetized	8	292 ± 18		20 ± 8	174 ± 9	139 ± 6	207 ± 17	80 ± 8
Decerebrate	4	298 ± 9		13 ± 9	180 ± 6	141 ± 12	210 ± 17	68 ± 17
Dorsal root		**L4**	**L5**	**L6**	**L7**	**S1**		
Anesthetized	5	14 ± 18	34 ± 35	50 ± 34	88 ± 34	141 ± 19		
Decerebrate	2	14 ± 8	29 ± 7	40 ± 13	58 ± 16	126 ± 15		
Ventral root		**L4**	**L5****	**L6**	**L7**	**S1****		
Anesthetized	5	356 ± 2	351 ± 9	251 ± 43	162 ± 9	167 ± 4		
Decerebrate	1	356 ± 3	314 ± 11	241 ± 20	160 ± 17	180 ± 15		

#; number of animals used, * $p < 0.05$, ** $p < 0.01$

Table 5. Mean ± S.D. of direction of movement before and after decerebration. Since the preferred directions were generally constant with stimulus levels producing from minimal up to maximal movement in stimulation of the muscles, nerves and roots, all data generated with all stimulus levels were included (typically 4-5 data were included for each site of each animal).

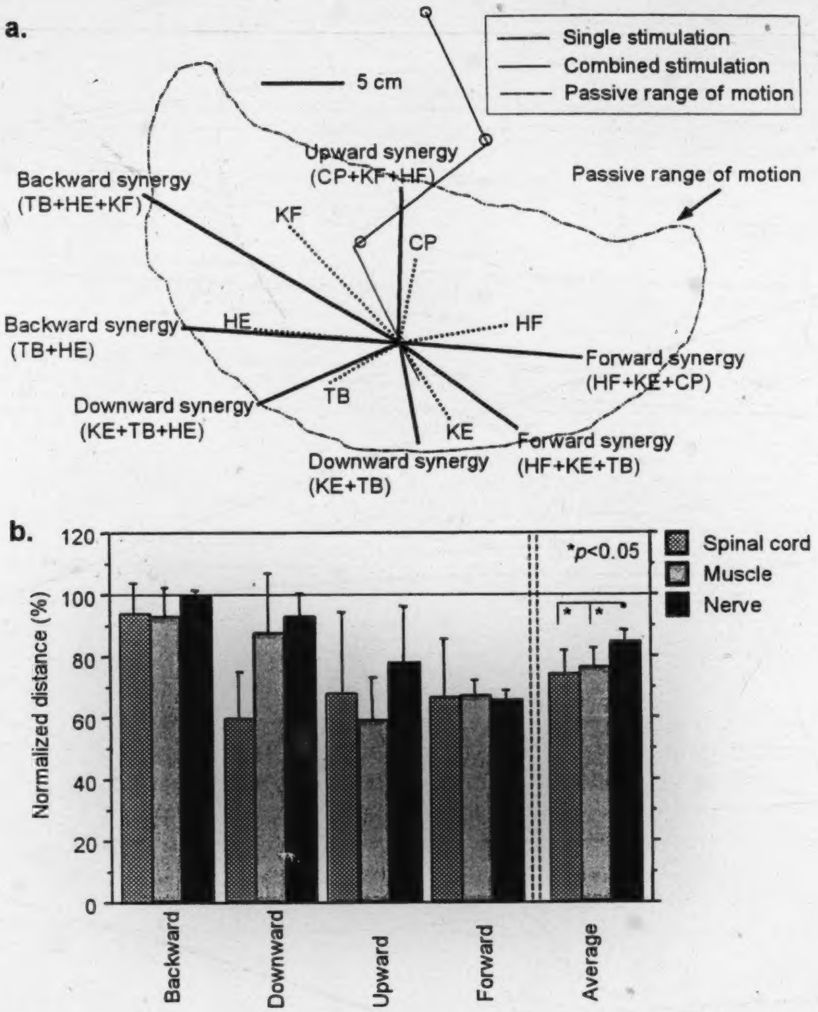

Figure 5-5. a. Examples of movement vectors from nerve stimulation in one animal. To induce maximal movements in the forward, upward, backward and downward directions, synergistic nerves were stimulated, as indicated. Movements generated by single and combined stimulation were expressed as dotted and straight lines respectively. Movement distances were normalized with respect to the passive range of motion of the paw (expressed as chain line). Thus, 100% means that the electrically-induced movement just reached the passive range of motion. The normalized distances were 68%, 96%, 100% and 93% for forward, upward, backward and downward directions respectively (average=89%). **b.** Comparison of distance in four different directions produced by muscle, nerve and spinal cord stimulation. Various combinations were used for muscle (n=5), nerve (n=5) and spinal cord (n=4) stimulation. On average, nerve stimulation produced longer distances than muscle and spinal cord stimulation ($p<0.05$). However, stimulation of muscle, nerve and spinal cord all generally produced at least 60% of the passive range of motion in all directions.

or muscles were stimulated simultaneously. **Figure 5-5a** shows seven combinations of stimulated nerves: HF+KE+CP and HF+KE+TB for forward movement, CP+KF+HF for upward movement, TB+HE and TB+HE+KF for backward movement, KE+TB and KE+TB+HE for downward movement. Similar combinations were used for muscle stimulation. Often, stimulation through a single intraspinal electrode was adequate to produce a whole synergy, so combinations were not required. Stimuli that produced directions in the ranges 0 ± 30°, 90 ± 30°, 180 ± 30°, and 270 ± 30° were used for analysis. We normalized the distance with respect to the passive range of movement of the cat's paw in the sagittal plane. Nerve stimulation produced longer distances than muscle and spinal stimulation ($p<0.05$), although all types of stimulation generally produced distances more than 60% of the passive range of movement (**Figure 5-5b**).

Recruitment curves

The threshold currents for stimulation were compared between muscle, nerve, spinal cord and spinal roots (**Figure 5-6a**). The threshold current for muscle stimulation was $470 \pm 275\ \mu A$, whereas those for stimulating nerve, spinal cord, and spinal roots were less than $100\ \mu A$ on average. Thus, muscle stimulation required over an order of magnitude higher currents to induce a minimal movement ($p<0.001$). The data for muscle, nerve, and ventral root stimulation were measured under anesthetized. The data for spinal cord stimulation differed significantly between under anesthetized and decerebrate, both data are shown. The data for dorsal root stimulation were measured in decerebrate in which the anesthetic was off.

Figure 5-6b shows normalized displacement for stimulation of muscles, nerves, spinal cord and roots at various stimulus intensity level (≤1.5T, 1.5-2.5, 2.5-3.5 ,and >3.5). Displacements induced by L4 ventral root stimulation were typically less than 1cm and were excluded from the analysis below. Analysis of variance (ANOVA) revealed that normalized displacements elicited by 5 different conditions were significantly different at the intensity levels of ≤1.5T, 1.5-2.5, and 2.5-3.5 ($p < 0.01$), where normalized displacements were generally larger for nerve, ventral roots and dorsal roots than for spinal cord and muscle (Fisher's protected least significant difference post hoc test). The muscle recruitment curves varied quite a lot, depending on whether the electrode was near the

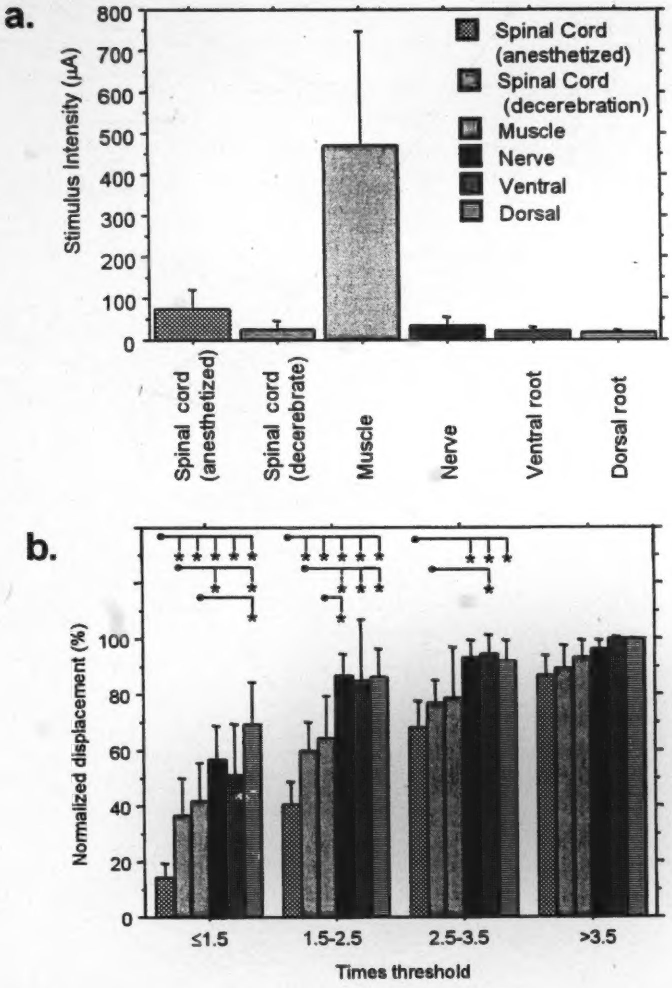

Figure 5-6. a. Comparison of stimulation threshold current between muscle, nerve, spinal cord and roots. Threshold current for muscle stimulation was an order of magnitude higher than nerve, spinal cord, and root stimulation (p<0.001). **b.** Normalized displacement for stimulation of muscles, nerves, spinal cord and roots at various stimulus intensity level (≤1.5T, 1.5-2.5, 2.5-3.5 ,and >3.5). Normalized displacements elicited by 5 different conditions were significantly different at the intensity levels of ≤1.5T, 1.5-2.5, and 2.5-3.5 (ANOVA, $p < 0.01$). * represents less than 5% error in the post hoc test using Fisher's protected least significant difference and error bar represents 95% confidential interval.

nerve entry zone or not. When it was near the nerve entry zone, the curve could be as steep as the nerve and root recruitment curve. In most of muscle stimulation, however, the recruitment curve was much slower than those for nerve and roots stimulation. The normalized displacement in spinal cord stimulation was among the lowest even in the decerebrate state in which anesthesia was off. In summary, the recruitment curve for spinal cord stimulation increased most gradually, but that for muscle was also quite gradual when stimulation was not applied directly to the entry zone into the muscle.

Consistency of trajectory between animals

We averaged all the maximally induced movements elicited by muscle and nerve stimulation to see the consistency of the trajectory between animals (**Figure 5-7**). Each oval represents an extreme position by maximal stimulation of muscle (gray) and nerve (white). The center of the oval represents the averaged angle and direction. The radius of the oval along the radiating line of the circle represents the S.D. of the distance, and the radius of the oval crossing the radiating line of the circle represents the S.D. of the angle. Muscle and nerve stimulation evoked reproducible, distinct movements. The angles were very close for muscle stimulation and stimulation of the nerve that innervated that muscle, although the nerve stimulation always produced longer trajectories. We compared the coefficient of variation for maximal movements evoked by stimulation of nerves and muscles (**Figure 5-8**). The coefficient of variation (%) of muscle-evoked maximal movement was significantly larger than the corresponding nerve-evoked maximal movement ($p<0.05$, paired t-test). Since the muscle electrodes were inserted into the muscle through the skin, it was difficult to place their tips at precisely defined locations with respect to the motor point of the muscle.

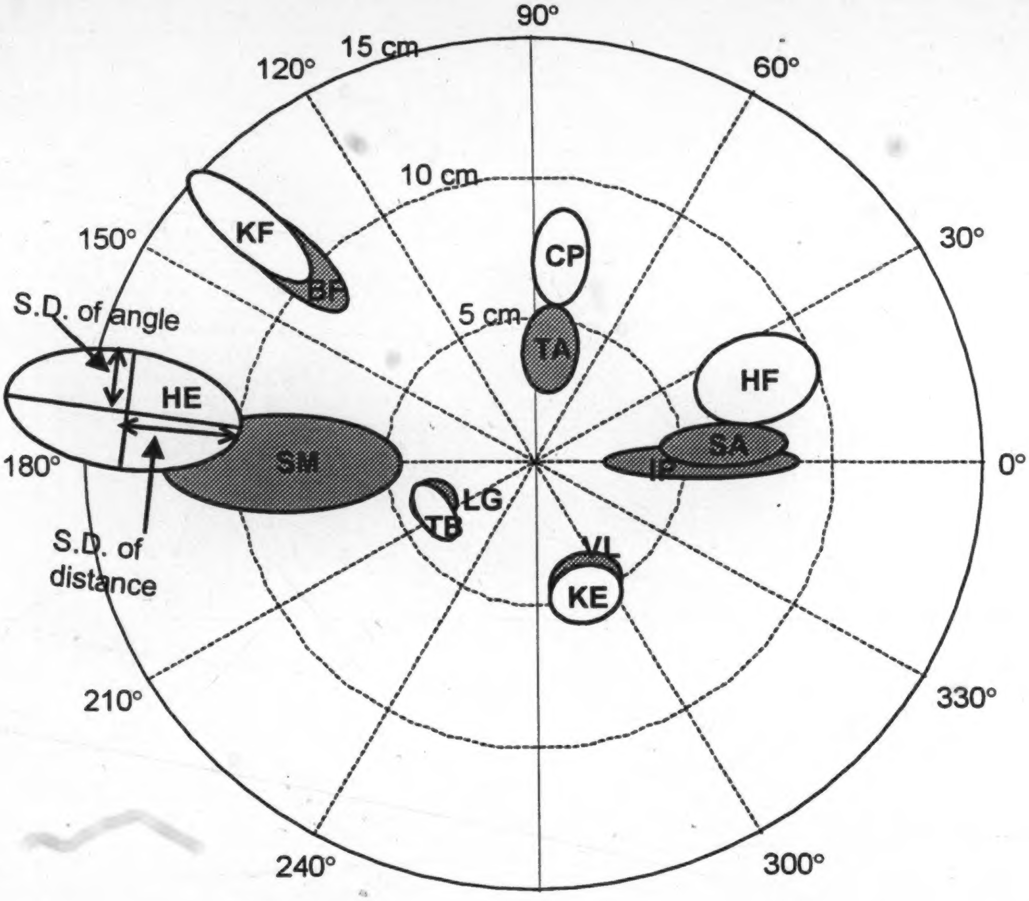

Figure 5-7. Extreme positions from maximal stimulation of muscles and nerves. Gray and white ovals respectively represent extreme positions by stimulating muscles and nerves. The centers of the oval represent the average values in different animals. The radius of the oval along the radiating line of the circle represents the S.D. of the distance and the radius of the oval crossing the radiating line of the circle represents the S.D. of the angle. For example, the average distance and angle from HE stimulation were 14.2 ± 4.4 cm and 173 ± 9°. Data for muscle and nerve extreme positions included 10 and 8 anesthetized animals, respectively.

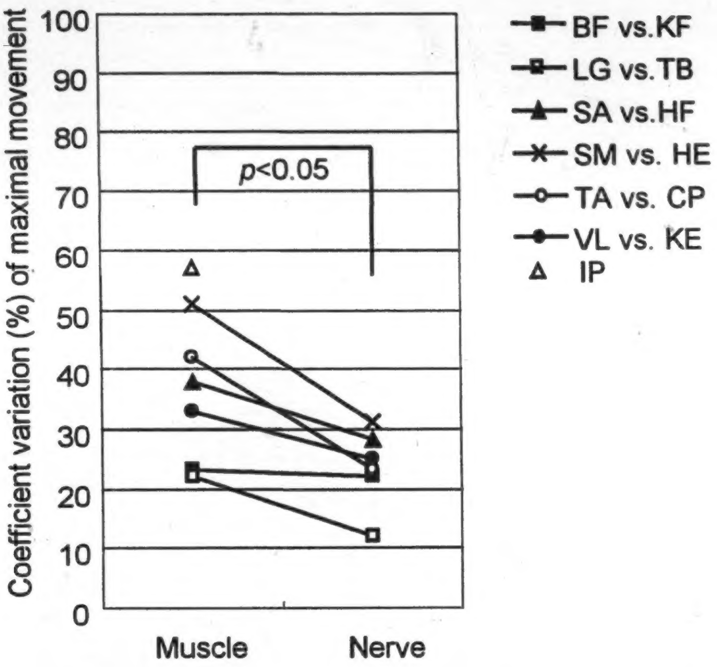

Figure 5-8. Comparison of the coefficient of variation (%) between maximal movements induced by stimulating nerves and muscles in different animals. The coefficient of variation of muscle-induced maximal movements was significantly larger than the corresponding nerve-induced maximal movements (paired t-test).

EMG

Figure 5-9 shows the relationship between latency, jitter, and coefficient of variation of the obtained EMG (TA in this case) during stimulation inducing near maximal movement. The data were plotted when TA was activated and the displacement was beyond half of its maximum. Latencies were measured at the start of the EMGs. Jitter and coefficient variation were calculated from the latency and amplitude of EMG obtained by the stimulus consisted of trains (0.8s) of monophasic cathodic pulses at 50 pulses. Not surprisingly, the latency, jitter, and coefficient variation were the lowest in the nerve stimulation (common peroneal nerve in this case) and the second lowest in the ventral root stimulation. The amplitude and waveform were more variable in dorsal root stimulation and the latency, jitter, and coefficient variation were larger. In spinal cord stimulation, the latency was very variable. This means that the stimuli in the intermediate region of the spinal cord occasionally spread directly to α–motoneurons. When interneuron were primarily stimulated (e.g.. latency > 4s), the jitter and coefficient variation were relatively large, suggesting that the recruitment of motoneurons were rather variable due to the extra synapses involved.

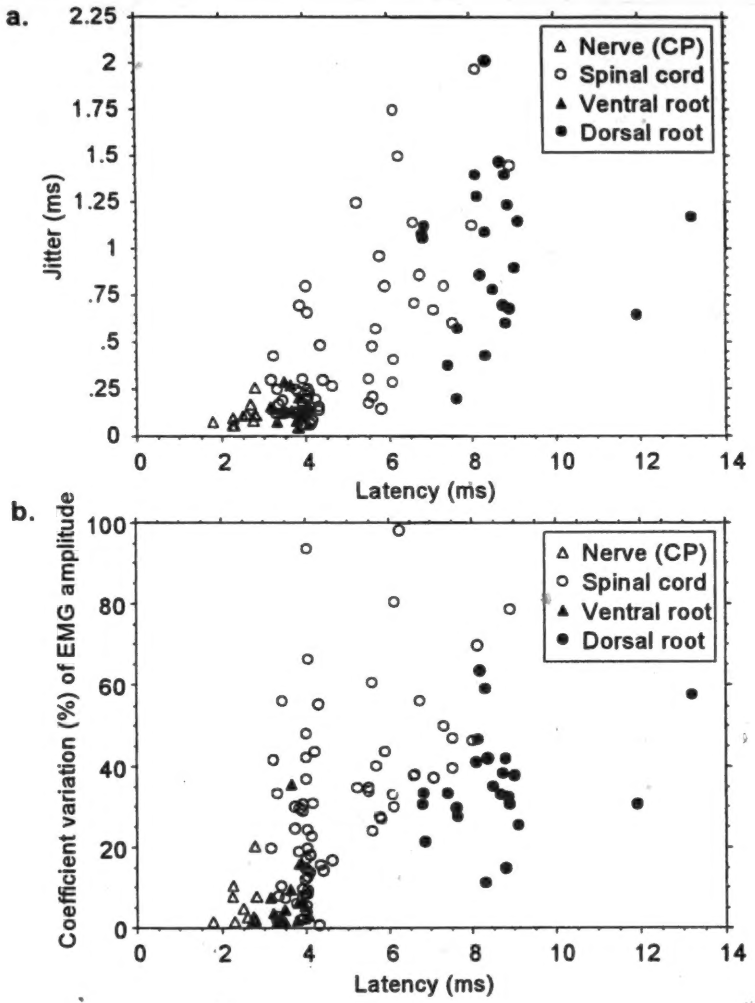

Figure 5-9. Comparison of latency, jitter and coefficient of variation (%) of EMG amplitude of TA between CP, intraspinal ventral and dorsal stimulation. TA was typically activated by L5-7 ventral and dorsal root stimulation. It was also occasionally activated by maximal or near maximal stimulation of S1 ventral root, L4 and S1 dorsal root. **a.** The order for latency was dorsal root > spinal cord > ventral root > nerve stimulation. For jitter, dorsal root > spinal cord > ventral root ~ nerve. For coefficient of variation, dorsal root ~ spinal cord > ventral root ~ nerve (Student t-test). **b.** The coefficient of variation (%) of EMG amplitude was the biggest by dorsal root stimulation and smallest by CP and ventral stimulation. The jitter and coefficient variation of EMG amplitude of intraspinal cord stimulation occasionally overlapped with those of ventral root stimulation, occasionally overlapped with those of dorsal root stimulation and were most likely intermediate between them. Plots of each latency of **a** and **b** are identical. The data from three anesthetized animals were plotted when TA was activated and the displacement was beyond the half of its maximum.

DISCUSSION

Our aim was to compare some biomechanical and neurophysiological characteristics of electrical stimulation through muscles, nerves, spinal cord, ventral and dorsal spinal roots in the anesthetized or decerebrate cat. We studied the selectivity of muscle activation, recruitment characteristics, maximal movements, movement directions, consistency of responses and required stimulus intensities.

Selectivity

Stimulating either nerve or muscle could evoke distinct, reproducible movements to 6 distinct directions, regardless of stimulus intensity level (**Figures 5-3** and **5-7**). Biceps femoris, a biarticular muscle, is well known to have separate nerve branches with different mechanical actions (Chanaud et al. 1991; Hamm et al. 1985; Sherrington. 1910). Thus, we could separately stimulate nerve branches to the hip extensors and knee flexors. In this experiment, we also found that the femoral nerve largely innervates hip flexors and knee extensors separately. For example, the biarticular muscle, rectus femoris is supplied by separate nerve branches that innervate hip flexor and knee extensor compartments separately. For the artificial control of limb movements through peripheral nerve stimulation, it is obviously desirable if motor nerves divide into branches that selectively control movement at one joint, as was seen here for the femoral and hamstring nerves, rather than activating uni- and biarticular muscle groups non-selectively.

Neither ventral nor dorsal root stimulation was able to induce movements in all directions (**Figure 5-3** and **Table**). A ventral root contains all the α–motoneurons from one spinal segment (Kahle et al. 1978). Since most lumbosacral segments contain both flexor and extensor α–motoneurons, it was initially surprising that ventral root stimulation was unable to induce flexor movements. However, the extensor (anti-gravity) muscles are generally stronger than the flexor muscles, so co-activation would result in a net downward (extensor) movement. The L4 spinal root primarily innervates hip flexor muscles and the L5 spinal root is composed of fibers of the femoral nerve that innervate hip flexor and knee extensor muscles (Romanes. 1951). At the resting position of the limb, L5 ventral root stimulation produced a movement that is directed between forward (hip flexor) and downward (knee extensor) (**Figure 5-3c**). The L6 spinal root is mainly composed of motoneurons innervating hip extensor, knee extensor and ankle flexor muscles (Romanes. 1951). The L7 spinal root is mainly composed of motoneurons innervating hip extensor, knee flexor and ankle flexor and extensor muscles (Romanes. 1951). The S1 spinal root is mainly composed of hamstring and tibial motoneurons (Romanes. 1951). Thus, broadly speaking the biomechanical results obtained by stimulating spinal roots are consistent with the anatomical distribution of α–motoneurons.

Stimulating the dorsal roots generated flexor movements. Sherrington made the classic observation that the flexor reflexes consist of hip, knee, and ankle flexion combined with extensor muscle relaxation. Flexor reflexes could be elicited by stimulating skin or mixed nerves in the decerebrate cat (Sherrington. 1910). Although skin stimulation and muscle stimulation can also produce crossed extension and stretch reflexes, the ipsilateral flexor component seemed to predominate with stimulation of whole dorsal roots. More interestingly, the movement vectors moved counterclockwise as root stimulation moved from L4 to S1 (**Figure 5-3d**). Forward movements generated by stimulating L4 and L5 dorsal roots were very similar to those generated by IP and SA stimulation, whose α–motoneurons are located primarily in the L4 and L5 segments (Romanes. 1951; Vanderhorst and Holstege. 1997). In addition to hip flexor movements, stimulation of the L4 and L5 roots also activated TA. As L6, L7 and S1 dorsal roots were stimulated, SA, TA and then BF were primarily activated. Since α–motoneurons of TA and BF are located primarily in the L6/L7 and L7/S1 segments respectively (Romanes. 1951; Vanderhorst and Holstege. 1997), stimulating each dorsal root appears to have excitatory synaptic connections mainly to flexor α–motoneurons at the same spinal segmental level. It may also have inhibitory synaptic actions on extensor α–motoneurons in the same spinal segmental level. Afferent information is conveyed to α–motoneurons in other spinal segments, but presumably with less strength and additional synaptic delays. Extensor muscles such as VL, LG and SM were also activated in accordance with the anatomical distribution of their α–motoneurons. However, the level of extensor muscle activation was significantly smaller than that for flexor muscles.

Spinal stimulation was able to induce movements in all directions in the anesthetized cat. However, vectors produced by the intraspinal electrodes showed large changes in direction with varying stimulus amplitudes, which was very different from stimulation of muscles, nerves and spinal roots. In this study we targeted intermediate areas that are thought to produce movement primitives (Giszter et al. 1993), so stimulation in the ventral horn may produce different results.

Stimulus intensity, recruitment properties and movement distance

As previously described (Branner et al. 2001; Popovic et al. 1991; Singh et al. 2000) using force transducers, thresholds for muscle stimulation were an order of magnitude higher than for nerve stimulation. Thresholds to elicit movement by spinal, ventral or dorsal root stimulation were also much lower than those for muscular stimulation ($p<0.001$) and were not significantly different from thresholds for nerve stimulation ($p>0.05$).

Muscle stimulation, compared to nerve stimulation, tends to produce a relatively gradual increase in the twitch contractile force of muscle as the stimulus intensity is increased (Gorman and Mortimer. 1983). Our results obtained from actual movements showed the same tendency, unless the electrodes were close to the nerve entry zone. The graded control of force and movement is needed to achieve precise artificial control of limb trajectories. The recruitment properties of muscle stimulation are influenced by two factors: electrode position and muscle volume. Electrodes placed close to the nerve entry point produced the greatest force but may also have the steepest recruitment (Cameron et al. 1998; Popovic et al. 1991). Recruitment curves tend to show sudden steps or increments that are attributable to the sequential activation of terminal nerve branches (Popovic et al. 1991). Therefore, the position of the stimulating point is a critical factor that determines the recruitment curve of muscle stimulation and the recruitment curves for muscle were more variable from experiment to experiment in spite of careful placement of electrodes by a skilled person.

Stimulation of nerves, ventral roots and dorsal roots produced the steepest recruitment curves. Interestingly, spinal stimulation showed the most gradual recruitment (for a detailed description and muscle recruitment with intraspinal stimulation see (Mushahwar and Horch. 2000)). In this study we primarily targeted intermediate areas of the spinal gray matter thought to include movement primitives (Giszter et al. 1993), but stimuli can spread up to 1 mm at the maximal stimulus intensities we used (Mushahwar and

Horch. 1997). Individual motoneuron pools are less than 1 mm in diameter (Chapin and Moxon. 2000; Mushahwar and Horch. 2000; Vanderhorst and Holstege. 1997). The chance of spreading to motoneuronal and interneuronal areas that may be dependent on the state of the animal probably explains the variability.

Nerve stimulation produced the longest distance of movement (**Figure 5-5**). It consistently produced more than 80% of the passive range of motion in the upward, backward and downward directions, but less than 70% in the forward direction. This is because the nerves to IP, one of the main muscles producing forward movement were not stimulated in these experiments. IP is innervated from the lumbar plexus in the cat (Crouch. 1969), whereas in human it is innervated by both the femoral nerve and lumbar plexus (Kahle et al. 1978). Muscle and spinal stimulation produced movements covering about 75% of the distance of the passive range of motion on average, indicating that not all the synergistic motor units were activated. Overall, since nerve, muscle and spinal stimulation produced distances >60% of the passive range of motion in all directions, these methods of stimulation have the potential to produce functional, whole limb movements using stimulation of appropriate synergies. This has also been shown previously in normal cats implanted with intramuscular and intraspinal microelectrodes (Mushahwar et al. 2000).

Perspectives on clinical application to restore functional movements

Muscle. Application of electrical simulation to persons with paraplegia has predominantly been used for the restoration of standing, walking, hand grasp, bladder and respiratory control (Kralj et al. 1988; Peckham and Creasey. 1992; Prochazka et al. 1997; Rushton. 1997). Intramuscular and surface stimulation, which are relatively non-invasive, are the most commonly used methods. Disadvantages of these approaches include the high currents required to stimulate the motor units and the technical difficulty in placing the electrodes on or very close to the nerve entry point, as our data indicate. These electrodes are then exposed to high mechanical stresses and motion, which can result in lead breakage and electrode migration (Prochazka. 1993; Somers. 1992). Moreover, the electrodes become encapsulated, elevating stimulus thresholds to higher levels and in some cases causing neuromuscular damage in the long run (Prochazka. 1993; Scheiner et al. 1990). To overcome these difficulties, recent work has shifted towards neural stimulation.

Nerve. Peripheral nerve stimulation also has some drawbacks. Large nerve trunks typically contain axons that innervate several different muscle groups, so selectivity can be a problem (Agnew and McCreery. 1990). However, we found that flexor and extensor muscles of the hip, knee and ankle joints can be activated selectively by electrodes placed close to selected nerve branches. The connecting wires were tunneled subcutaneously so that the electrodes are close to target muscle, which involves fairly extensive surgery, but the use of injectable microstimulators (Singh et al. 2000) may eliminate this problem. Nerve stimulation did produce the largest movements and they were relatively constant and reliable. In addition, the stimulus current required to activate nerve axons by stimulation with epineural or cuff electrodes is much lower than that required for intramuscular stimulation (**Figure 5-6a**), so electrode dissolution due to electrochemical reactions should be far slower. The main disadvantage of nerve stimulation demonstrated by our data is the relatively narrow range of stimulation intensity from threshold to maximal movements (i.e., steep recruitment, **Figure 5-6b**), which can also lead to variability in the outcome (Singh et al. 2000).

Spinal cord. When stimulation pulses were delivered through intraspinal electrodes, movements were activated with low stimulus intensity (**Figure 5-6**). Large jitter and coefficient variation suggested that identical motoneurons were not necessarily recruited with each stimulus through various interneuronal pathways (**Figure 5-9**). Thus, stimulation in the primitive area may reduce muscle fatigue compared to muscle and nerve stimulation (e.g. (Mushahwar and Horch. 2000)). The map of movement vectors demonstrated that there were regions within the spinal cord from which single muscles or synergistic muscle groups can be activated (Mushahwar et al. 2000). This is not surprising because individual α–motoneuronal pools exist as clusters along lumbo-sacral segments (Romanes. 1951; Sharrard. 1955; Vanderhorst and Holstege. 1997). However, movement recruitment curves generated by spinal stimulation were rather variable depending on the electrode location and the direction of movement could change dramatically. Presumably, these stimuli activated large numbers of interneurons, whose state may change, as well as activating neighboring motoneuron pools in the spinal cord. Overall, the data obtained in this study using cats did not necessarily correspond to data measuring isometric force by stimulating frog spinal cord in terms of 'primitives' (Giszter et al. 1993). This issue will be discussed in detail eleswhere. In the sense of clinical application, however, generating reproducible and selective movements may be a challenging problem for spinal stimulation targeting movement primitive locations. However, single chronically implanted microwires in the ventral horn can generate reproducible, synergistic movements of the whole limb sufficient for weight support or forward swing in the normal cat (Mushahwar et al. 2000). Intraspinal stimulation may therefore provide whole limb synergies from a small and contained implanted area.

Roots. Since ventral roots are composed of mixed nerve groups, selectivity is relatively poor compared to single nerve or muscle stimulation and mainly extensor movements are produced. Thus, stimulation of ventral roots clinically may not induce good functional cyclic movement such as walking, although it has been used to restore leg powered cycling for exercise (Donaldson et al. 1997; Rushton et al. 1997). Our results suggest that dorsal root stimulation, generating flexor movements through reflex pathways is not a good candidate to restore a full range of functional movements, though such movements can be useful for initiating swing. Furthermore, some improvement of motor function has been noted in paraplegic people with dorsal column stimulation (Davis and Emmonds. 1992). Dorsal root stimulation may cause pain or discomfort in individuals with incomplete spinal cord injury. Even with a complete spinal cord injury, stimulation of the dorsal roots may produce undesirable autonomic responses. However, dorsal roots may be a good location for recording sensory signals to control electrical stimulation (Loeb et al. 1977; Prochazka et al. 1979).

In conclusion, there is unlikely to be one best place to stimulate for all FES applications, but the results of the present study should help in deciding the best site for a given clinical application. The state-dependence of responses to spinal stimulation highlights the need for information from chronic studies to supplement the present acute data.

REFERENCES:

1. Agnew WF, and McCreery DB. *Neural prostheses. Fundamental Studies.* Englewood Cliffs, NJ: Prentice Hall, 1990.

2. Aoyagi Y, Stein RB, Mushahwar VK, and Prochazka A. Comparing stimulation of muscle, nerve, roots and cord: which is best for FES? *Alberta Motor Control XXVII Neurohike Meeting*, edited by Pearson KG and Hulliger M, Jasper, Alberta, Canada, 2000.

3. Aoyagi Y, Mushahwar V, Stein RB, and Prochazka A. Movement synergies elicited by intraspinal microstimulation compared to stimulation of muscles, nerves and roots in the cat. *6th Annual Conference of the International Functional Electrical Stimulation Society*, edited by Triolo RJ, Cleveland, Ohio. International Functional Electrical Stimulation Society, 2001, p. 120-122.

4. Behar O, Mizuno K, Neumann S, and Woolf CJ. Putting the spinal cord together again. *Neuron* 26: 291-293, 2000.

5. Bizzi E, Tresch MC, Saltiel P, and d'Avella A. New perspectives on spinal motor systems. *Nat Rev Neurosci* 1: 101-108., 2000.

6. Branner A, Stein RB, and Normann RA. Selective stimulation of cat sciatic nerve using an array of varying-length microelectrodes. *J Neurophysiol* 85: 1585-1594, 2001.

7. Cameron T, Richmond FJ, and Loeb GE. Effects of regional stimulation using a miniature stimulator implanted in feline posterior biceps femoris. *IEEE Trans Biomed Eng* 45: 1036-1043, 1998.

8. Chanaud CM, Pratt CA, and Loeb GE. Functionally complex muscles of the cat hindlimb. II. Mechanical and architectural heterogenity within the biceps femoris. *Exp Brain Res* 85: 257-270, 1991.

9. Chapin JK, and Moxon KA. *Neural Prostheses for Restoration of Sensory and Motor Function*. Boca Raton: CRC Press, 2000.

10. Crouch JE. *Text-atlas of cat anatomy*. Philadelphia: Lea & Febiger, 1969.

11. Dai R, Stein RB, Andrews BJ, James KB, and Wieler M. Application of tilt sensors in functional electrical stimulation. *IEEE Trans Rehabil Eng* 4: 63-72, 1996.

12. Davis R, and Emmonds SE. Spinal cord stimulation for multiple sclerosis: quantifiable benefits. *Stereotact Funct Neurosurg* 58: 52-58, 1992.

13. Ditunno JF, Jr., Graziani V, and Tessler A. Neurological assessment in spinal cord injury. *Adv Neurol* 72: 325-333, 1997.

14. Donaldson N, Rushton D, and Tromans T. Neuroprostheses for leg function after spinal-cord injury. *Lancet* 350: 711., 1997.

15. Field-Fote EC. Spinal cord control of movement: implications for locomotor rehabilitation following spinal cord injury. *Phys Ther* 80: 477-484, 2000.

16. Girardi FP, Khan SN, Cammisa FP, Jr., and Blanck TJ. Advances and strategies for spinal cord regeneration. *Orthop Clin North Am* 31: 465-472, 2000.

17. Giszter SF, Mussa-Ivaldi FA, and Bizzi E. Convergent force fields organized in the frog's spinal cord. *J Neurosci* 13: 467-491, 1993.

18. Gorman PH, and Mortimer JT. The effect of stimulus parameters on the recruitment characteristics of direct nerve stimulation. *IEEE Trans Biomed Eng* 30: 407-414, 1983.

19. Hamm TM, Koehler W, Stuart DG, and Vanden Noven S. Partitioning of monosynaptic Ia excitatory post-synaptic potentials in the motor nucleus of the cat semimembranosus muscle. *J Physiol (Lond)* 369: 379-398, 1985.

20. Hoffer JA, Stein RB, Haugland MK, Sinkjaer T, Durfee WK, Schwartz AB, Loeb GE, and Kantor C. Neural signals for command control and feedback in functional neuromuscular stimulation: a review. *J Rehabil Res Dev* 33: 145-157., 1996.

21. Kahle W, Leonhardt H, and Platzer W. *Color atlas and textbook of human anatomy*. Chicago: Thieme Publishers, 1978.

22. Kralj A, Bajd T, and Turk R. Enhancement of gait restoration in spinal injured patients by functional electrical stimulation. *Clin Orthop*: 34-43, 1988.

23. Kralj AR, and Bajd T. *Functional electrical stimulation: standing and walking after spinal cord injury*. Boca Raton, Fla.: CRC Press, 1989.

24. Liberson WT, Holmquest HJ, Scott D, and Dow M. Functional electrotherapy: stimulation of the peroneal nerve synchronized with the swing phase of the gait of hemiplegic patients. *Arch Phys Med Rehabil* 42: 101-105, 1961.

25. Loeb GE, Bak MJ, and Duysens J. Long-term unit recording from somatosensory neurons in the spinal ganglia of the freely walking cat. *Science* 197: 1192-1194, 1977.

26. Macpherson JM. Strategies that simplify the control of quadrupedal stance. I. Forces at the ground. *J Neurophysiol* 60: 204-217, 1988.

27. Mushahwar VK, and Horch KW. Proposed specifications for a lumbar spinal cord electrode array for control of lower extremities in paraplegia. *IEEE Trans Rehabil Eng* 5: 237-243, 1997.

28. Mushahwar VK, Collins DF, and Prochazka A. Spinal cord microstimulation generates functional limb movements in chronically implanted cats. *Exp Neurol* 163: 422-429, 2000.

29. Mushahwar VK, and Horch KW. Muscle recruitment through electrical stimulation of the lumbo-sacral spinal cord. *IEEE Trans Rehabil Eng* 8: 22-29, 2000.

30. Mushahwar VK, and Horch KW. Selective activation of muscle groups in the feline hindlimb through electrical microstimulation of the ventral lumbo-sacral spinal cord. *IEEE Trans Rehabil Eng* 8: 11-21, 2000.

31. Peckham PH, and Creasey GH. Neural prostheses: clinical applications of functional electrical stimulation in spinal cord injury. *Paraplegia* 30: 96-101, 1992.

32. Popovic D, Gordon T, Rafuse VF, and Prochazka A. Properties of implanted electrodes for functional electrical stimulation. *Ann Biomed Eng* 19: 303-316, 1991.

33. Prochazka A, Stephens JA, and Wand P. Muscle spindle discharge in normal and obstructed movements. *J Physiol (Lond)* 287: 57-66., 1979.

34. Prochazka A. Comparison of Natural and artificial control of movement. *IEEE Trans Rehabil Eng* 1: 7-17, 1993.

35. Prochazka A, Gauthier M, Wieler M, and Kenwell Z. The bionic glove: an electrical stimulator garment that provides controlled grasp and hand opening in quadriplegia. *Arch Phys Med Rehabil* 78: 608-614, 1997.

36. Prochazka A, Mushahwar VK, and McCreery DB. Neural prostheses. *J Physiol* 533: 99-109., 2001.

37. Romanes GJ. The motor cell columns of the lumbo-sacral spinal cord of the cat. *J Comp Neurol* 94: 313-363, 1951.

38. Rushton DN. *Neuroprostheses, Neuromodulators and Rehabilitation*. London: Brit Soc Rehab Med, 1997.

39. Rushton DN, Donaldson ND, Barr FM, Harper VJ, Perkins TA, Taylor PN, and Tromans AM. Lumbar root stimulation for restoring leg function: results in paraplegia. *Artif Organs* 21: 180-182, 1997.

40. Scheiner A, Mortimer JT, and Roessmann U. Imbalanced biphasic electrical stimulation: muscle tissue damage. *Ann Biomed Eng* 18: 407-425, 1990.

41. Sharrard WJW. The distribution of the permanent paralysis in the lower limb in poliomyelitis. A clinical and pathological study. *J Bone Joint Surg* 37B: 540-558, 1955.

42. Sherrington CS. *The integrative action of the nervous system*. New Haven: Yale University Press, 1906.

43. Sherrington CS. Flexion-reflex of the limb, crossed extension reflex and reflex stepping and standing. *J Physiol (Lond)* 40: 28-121, 1910.

44. Singh K, Richmond FJ, and Loeb GE. Recruitment properties of intramuscular and nerve-trunk stimulating electrodes. *IEEE Trans Rehabil Eng* 8: 276-285, 2000.

45. Somers MF. *Spinal cord injury: functional rehabilitation*. Norwalk, Conn.: Appleton & Lange, 1992.

46. Stein RB, Gordon T, Jefferson J, Sharfenberger A, Yang JF, de Zepetnek JT, and Belanger M. Optimal stimulation of paralyzed muscle after human spinal cord injury. *J Appl Physiol* 72: 1393-1400, 1992.

47. Stein RB, Peckham PH, and Popovic D. *Neural prostheses: replacing motor function after disease or disability*. New York: Oxford University Press, 1992.

48. Tai C, Booth AM, Robinson CJ, de Groat WC, and Roppolo JR. Isometric torque about the knee joint generated by microstimulation of the cat L6 spinal cord. *IEEE Trans Rehabil Eng* 7: 46-55, 1999.

49. Vanderhorst VG, and Holstege G. Organization of lumbosacral motoneuronal cell groups innervating hindlimb, pelvic floor, and axial muscles in the cat. *J Comp Neurol* 382: 46-76, 1997.

50. Wieler M, Stein RB, Ladouceur M, Whittaker M, Smith AW, Naaman S, Barbeau H, Bugaresti J, and Aimone E. Multicenter evaluation of electrical stimulation systems for walking. *Arch Phys Med Rehabil* 80: 495-500, 1999.

CHAPTER 6

THE ROLE OF NEUROMUSCULAR PROPERTIES IN DETERMINING THE END-POINT OF A MOVEMENT*

INTRODUCTION

Performing the same movement several times leads to different trajectories and end-points. This is true even in highly automated movements such as hammering by a blacksmith (Bernstein. 1935). Does this variability reflect that the number of control variables accessible for the central nervous system (CNS) is higher than the number of parameters that define the motor task, or does this variability have its basis in the number of joints and the number of muscles acting across these joints? Most frequently, researchers have tried to guess at the internal solution within the CNS by investigating the consequences of optimizing certain functions of performance related to movement kinematics and dynamics. One proposal was that an internal model is constructed to map the desired state at each point along the trajectory into motor commands (Kawato et al. 1987). An alternative proposal was that the CNS specifies spatial parameters and relies on the spring-like properties of muscles plus reflex loops to move the limb (Bizzi et al. 1984).

In the spinal cord, experimental data and modeling in frogs suggest that there are a limited number of force directions that can be specified. Activation of a discrete interneuronal zone often leads to forces that converge to a point (Bizzi et al. 1991; Bizzi et al. 2000; d'Avella and Bizzi. 1998; Giszter et al. 1993; Saltiel et al. 1998). They also suggested that the simultaneous stimulation of two sites of 'movement primitives' leads to the vectorial summation of the end-point forces generated by each site separately (Mussa-Ivaldi et al. 1994). This idea may represent a new perspective on how the forces induced by activation of movement primitives combine to produce complex motor behavior (Bizzi et al. 2000). However, evidence against movement primitives has also been reported (cf.

---

* A version of this chapter will be submitted to *IEEE Trans Neural Syst Rehabil Eng* by the authors of Aoyagi. Y, Mushahwar. VK, Stein. RB, Prochazka, A.

(Aoyagi et al. 2000; Loeb. 2001; Tresch and Kiehn. 2000)).

In addition controversy has arisen from studies of motor cortex about what is coded within individual neurons and populations (cf. (Georgopoulos. 1995; Loeb et al. 1996; Mussa-Ivaldi. 1988)). Proposals include the direction of movement, velocity, end-point of trajectory and pattern of muscle activity, joint torques, joint kinematics (Evarts. 1966; Fetz and Cheney. 1980; Georgopoulos et al. 1982; Kakei et al. 1999; Scott and Kalaska. 1995; Shen and Alexander. 1997).

Despite these continuing controversies, rather little has been discussed about how this CNS organization is linked to intrinsic neuromuscular and biomechanical properties. For example, which combinations of control parameters should be chosen to fit the requirement of a motor task? How do the responses sum to produce an end-point, when several muscles are activated? In this study, therefore, we addressed a basic biomechanical question: whether or not multi-joint movement consists of the simple vectorial summation of each single-joint movement? If not, what neuromuscular properties could contribute to determine the multi-joint movements? To answer this question, six individual single-joint movements (flexion and extension of hip, knee and ankle joints) were induced through peripheral electrical stimulation in anesthetized and decerebrate cats in a uniform stiffness field. The limb was allowed to move approximately in the saggital plane against a constant stiffness. Also, as many as six different hindlimb muscles or nerves were simultaneously stimulated to compare the actual versus predicted movements. Sites in the spinal cord were also stimulated by intraspinal microwires individually and simultaneously so that vectors produced by peripheral and spinal cord stimulation could be compared. Finally, for the purpose of investigating whether or not peripheral stimulation produces a convergent equilibrium point, we generated movements at different positions of the hindlimb.

METHODS

Six cats were used in this study. Anesthesia, animal preparation and experimental setup were described in Chapter 5 in detail and are not repeated here except for stimulation protocol which was different from Chapter 5.

Stimulation and recording

As shown in Chapter 5, stimulation of these six nerves evoked distinct, reproducible movements to six separate different directions, activating flexors and extensors of the hip, knee and ankle. In addition to individual stimulation, various kinds of synergistic and antagonistic movements were induced using simultaneous intramuscular, nerve and intraspinal stimulation with various combinations. In some animals, all possible combinations of simultaneous stimuli were systematically studied. For 6 different sites 2^6=64 combinations are possible. Six involve a single site and one involves no stimulation. The possible combinations of two or more sites are therefore 64 - 6 -1 = 57. The combinations involving 2,3, 4, 5 and 6 sites are 15, 20, 15, 6 and 1 respectively. The 57 combinations of simultaneous stimuli were given in random order. In order to obtain control values and calculate predicted vectors (see also *Data acquisition and analysis*), five sets of six individual single stimuli were interposed as follows: 6 individual, 14 combined, 6 individual, 14 combined, 6 individual, 14 combined, 6 individual, 15 combined and 6 individual stimulus trials. Overall, a total of 87 trials were delivered in sequence at intervals of at least 12 s.

In order to investigate whether elicited movements converge to an equilibrium point or not, a complete set of 87 muscle stimuli was delivered at three different positions of hindlimb in two animals. The joystick-like fulcrum and spring were moved backward and forward by several cm so that the paw was placed at forward and backward positions as well as the neutral position. Some animals were decerebrated at the intercollicular level, anesthetic was discontinued after decerebration, and the same stimulation protocol was performed.

Data acquisition and analysis

Kinematic data recorded through the 6D-Research™ system were digitized at a rate of 30 samples/s. Trajectory vectors and end-points were analyzed using custom-written programs in Matlab (Math Works, Inc., Natick, MA). The trajectory vector (distance, angle) was defined as a displacement from the rest to extreme position during stimulation. As an example of the motion analysis, **Figure 6-1a** demonstrates the trajectory of the hip, knee, ankle and paw (=metatarsophalangeal joint of the foot) when BF and LG were simultaneously stimulated. The hindlimb typically reached its extreme position within a few hundred ms. The corresponding changes in the horizontal and vertical positions are shown in **Figure 6-1b**. In this example, the distance of the paw's displacement was 17.7 cm from the rest to the extreme position. The direction was 153° with respect to the forward direction. When the stimuli were repeated (not shown), the trajectories were very reproducible.

A predicted vector was calculated by summing the corresponding individual vectors elicited by individual stimulation. **Figure 6-1c** compares the predicted vector with the actual vector shown in **Figure 6-1a**. The vectors of BF elicited in single stimulus sets just before (1st set) and after (2nd set) this BF + LG stimulation were (13.1cm, 147°) and (14.0cm, 145°) while those of LG were (3.0cm, 213°) and (3.5cm, 207°). The averages were used to calculate the predicted vector for combined stimulation by vector summation (15.3cm, 157°; **Figure 6-1c**). Since the corresponding actual vector was (17.7cm, 153°), the differences of the distance and angle between actual and predicted vectors were 2.4cm and 4°. The distance between actual and predicted extreme positions was also calculated (2.7cm in this example).

In order to examine how closely the movement end-points (=extreme positions) converge to an equilibrium point, end-points were elicited from front (f), neutral (n) and back (b) positions. The actual distances between the three end-points were then calculated and averaged. In other words, given that a triangle is formed by the three end-points, the individual sides (f-n, n-b and b-f) were measured and averaged. We defined this averaged value as 'equilibrium point index (EPI)'. If the three movements reach the same end-point, the EPI will be zero. Conversely, the EPI becomes bigger as the end-points converge less well. We also calculated the EPI of the predicted end-points. The calculation of end-points was done based on the supposition that rest positions are the same, since rest positions were very stable through a total of 87 stimuli (e.g. S.D. of the horizontal and vertical rest positions were both 0.3cm in the case of **Figure 6-2a**).

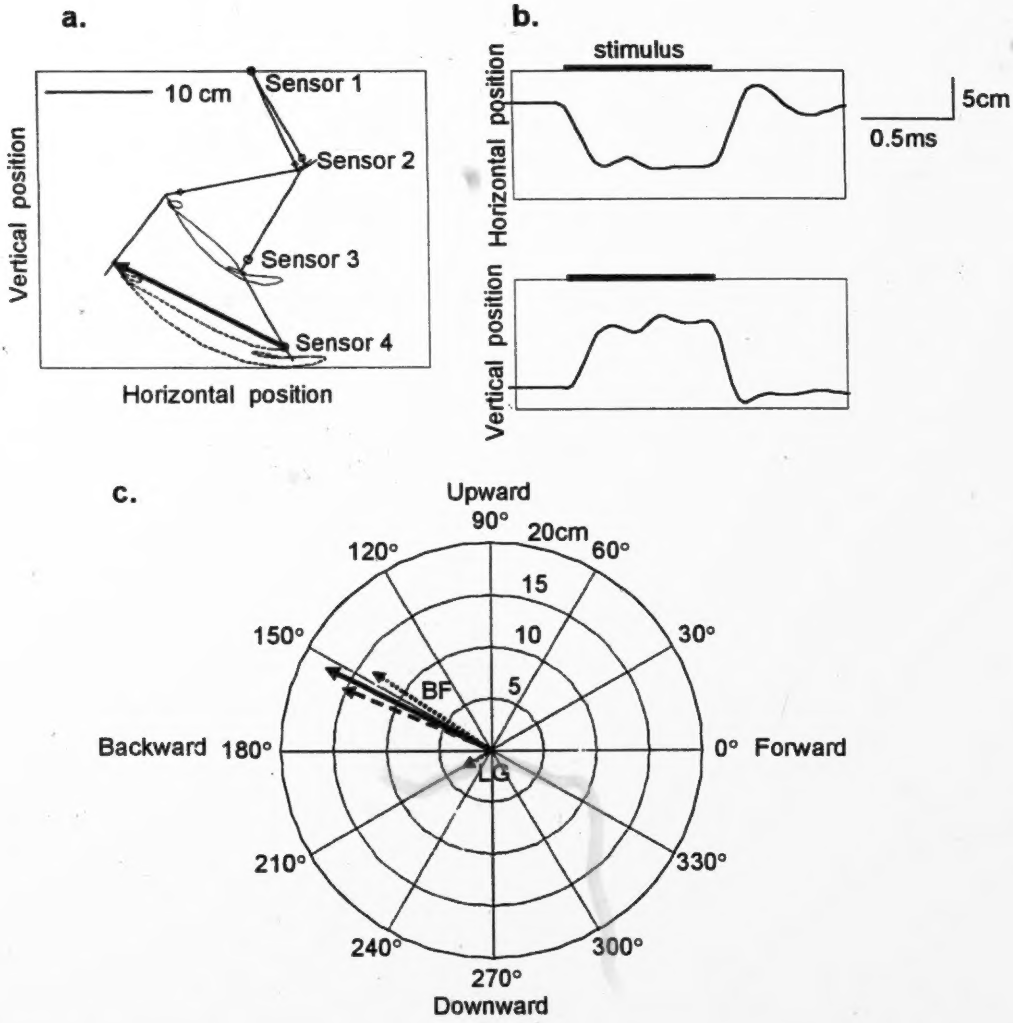

Figure 6-1. a. The sagittal trajectory of the hindlimb generated during simultaneous stimulation of posterior biceps femoris (BF) and lateral gastrocnemius (LG). The stick figures illustrate the rest and extreme position when BF and LG were stimulated. The $^{\circ}$ and * respectively represent the position of motion sensors at rest and at the extreme position during stimulation. The dotted lines represent the real trajectory of sensors during stimulation. The thick arrow represents the actual vector (from the rest to extreme position) of sensor 4. The distance was 17.7 cm and the angle was 153° with respect to the forward direction. **b.** Corresponding changes of horizontal and vertical components of the trajectory shown in **a**. As seen in this example, the hindlimb typically reached its extreme position in a few hundred ms, stayed there during the rest of the stimulation and returned to the rest position. **c.** Actual and predicted vectors. The vectors of BF and LG elicited in single stimulus sets just before and after this combined stimulation were averaged and calculated as (13.55cm, 146°) and (3.25cm, 210°) respectively (shown by the dotted line). Then, the predicted vector was determined by simple summation of individual control vectors and is shown by the dashed arrow. The solid arrow represents the actual vector. The differences of the distance and angle between actual and predicted vectors were 2.4cm and 4°. Note that forward, upward, backward and downward directions correspond to 0°, 90°, 180° and 270° respectively.

RESULTS

Actual versus predicted vectors

Figure 6-2a shows typical results of actual vectors obtained through a total of 87 nerve stimuli from an anesthetized animal. The dashed and solid lines represent 30 individual and 57 combinations of nerve stimuli respectively. As seen in **Figure 6-2a**, the vectors generally covered most of the area within the passive range of motion of the hindlimb, despite the resistance provided by the spring. Some actual vectors reached the edge of the passive range of motion of the hindlimb, particularly for backward movements. In comparison, the forward area was not fully covered. However, a major hip flexor, iliopsoas is supplied directly from the lumbar plexus in the cat (Crouch. 1969) and was not stimulated (see methods for a full list of muscle and nerves used). **Figure 6-2b** shows the polar graph for the corresponding predicted vectors. **Figure 6-2c** gives the difference of the corresponding actual and predicted end-points. The end-point 'x' represents the actual vector and the other end represents the end-point of the corresponding predicted vector. As seen in **Figure 6-2b** and **2c**, neither the actual nor the predicted vectors were uniformly distributed to all directions. Backward movements were overly represented. Note that each muscle group was activated at close to maximal levels, so the stronger muscles can overpower the weaker ones to some extent when both are stimulated together. The anti-gravity muscles that push backward and down are the ones that propel the animal forward and up during walking, and so are particularly strong. This predominance of backward vectors was seen in each experiment with all types of stimuli (intramuscular, nerve intraspinal).

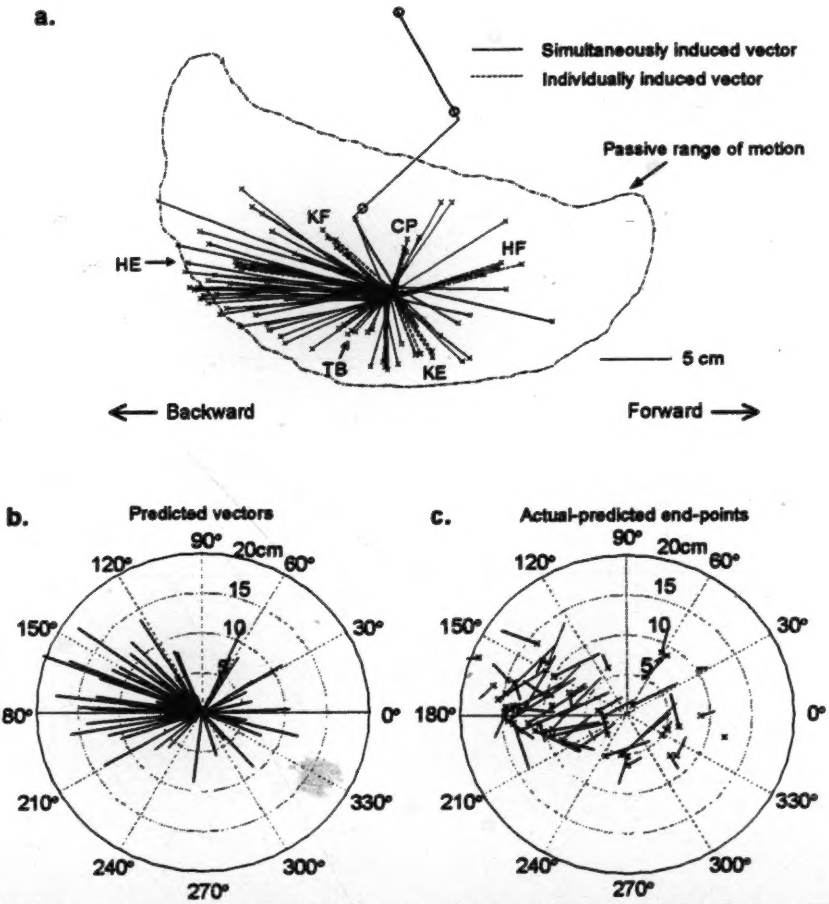

Figure 6-2. **a.** An example of actual vectors obtained by nerve stimulation. The dashed lines represent 30 vectors obtained by stimulation of six individual nerves: tibial nerve (TB), common peroneal nerve (CP), two hamstring branches of the sciatic nerve supplying knee flexors (KF) and hip extensors (HE), and two femoral nerve branches supplying knee extensors (KE) and hip flexors (HF). The solid lines represent vectors obtained by stimulation of 57 combinations of nerves. The chain line represents the passive range of motion of the paw. The 'x' represents the end-point (extreme position) for each stimulation. The actual vectors covered much of upward, backward and downward area within the passive rage of motion. The forward area was relatively less covered. However, a major hip flexor muscle, iliopsoas, is innervated by from the lumbar plexus and was not stimulated here. Note that vectors obtained by individual nerves were fairly constant without major fatigue. Note also that the rest positions were very stable throughout 87 periods of stimulation (the S.D.was 0.3cm for both the horizontal and vertical position). **b.** Polar graphs of predicted vectors obtained in **a.** Since the rest positions were extremely stable throughout the stimulation protocol, all the vectors were plotted from the origin of the coordinate axes. **c.** Difference of the end-points of the corresponding actual and predicted vectors. The 'x' represents the end-point of an actual vector and the other end represents the end-point of the corresponding predicted vector.

Figure 6-3a shows the actual distances for all 57 combined and 30 individual trials of nerve stimulation as a function of the number of sites stimulated (n=3 cats). One-factor analysis of variance (ANOVA) revealed that the actual distance increased significantly with the number of sites stimulated simultaneously ($p<0.01$). The absolute distance between the actual and the corresponding, predicted end-points (cf. **Figure 6-2c**) also increased significantly with the increase of the number of simultaneously stimulated sites ($p<0.01$) (**Figure 6-3b**). These characteristics were also commonly observed with intramuscular or intraspinal stimulation.

Figure 6-4a shows predicted versus actual distances for intramuscular, nerve and intraspinal stimulation. The data for all 57 combinations were plotted for both the anesthetized and decerebrate states, because the state did not affect the predicted versus actual distance curves. Regression equations are also shown. A common feature was that the regression curves had positive intercepts and positive linear coefficients. The curves for muscle and nerve had linear coefficients near one and a negative curvature, whereas the slope of the spinal cord was significantly less than one and the curvature was not significant with the number of data points available. These results suggest a more than linear summation for small amplitudes and a less than linear summation for large amplitudes. This is shown in another way in **Figure 6-4b**. Here points with a similar predicted distance have been grouped and the differences of the actual distance from the prediction are plotted as the ordinate. For all distances less than <3 cm the differences are positive (more than linear summation), whereas for all predictions above 11 cm the differences are negative (less than linear summation). In between, there is a clearly decreasing trend with the values being more negative for spinal cord stimulation (less good summation) than for nerve or muscle stimulation.

Figure 6-5 shows the differences between the actual and predicted angles of the corresponding vectors with intramuscular, nerve and intraspinal stimulus combinations. Average differences were 20.5 ± 24.9°, 22.9 ± 28.6° and 25.3 ± 32.6° respectively. 19.0%(54/284), 24.0%(41/171), and 27.2%(31/114) of actual vectors elicited by intramuscular, nerve and intraspinal stimulation differed by more than 30° in angle from the prediction.

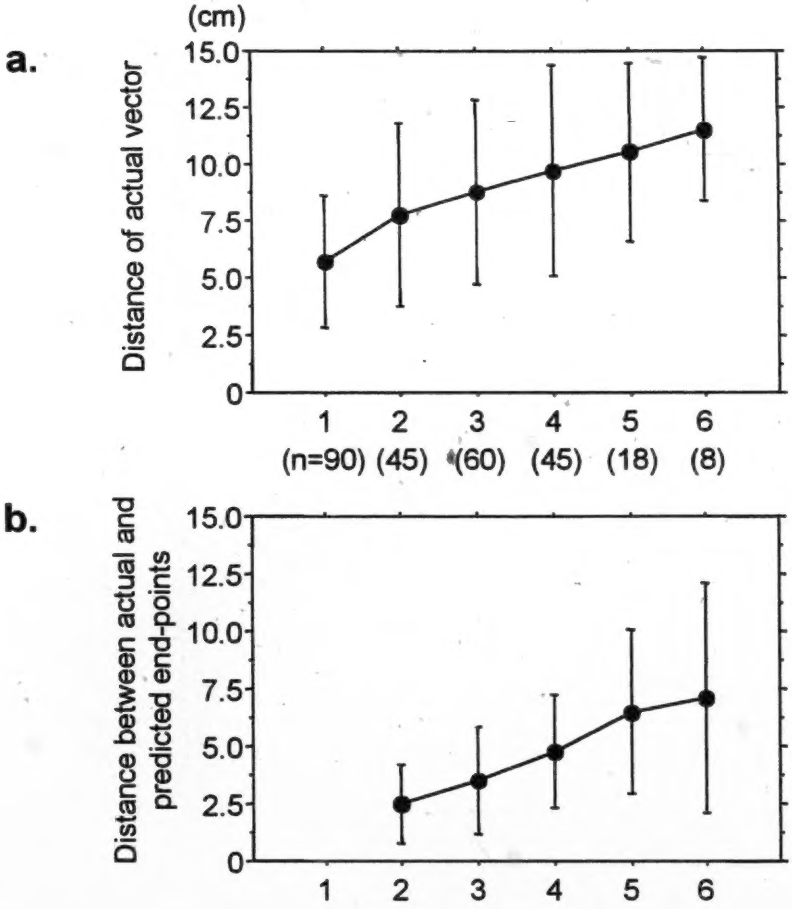

Figure 6-3. a. The actual distance moved increased with an increase in the number of sites stimulated (one-factor ANOVA, $p<0.01$). **b.** The absolute distance between actual and predicted end-points also increased with an increase in the number of sites stimulated (one-factor ANOVA, $p<0.01$). The number of trials (n) is shown and represents complete data of nerve stimulation containing 57 combined and 30 individual trials from 3 cats.

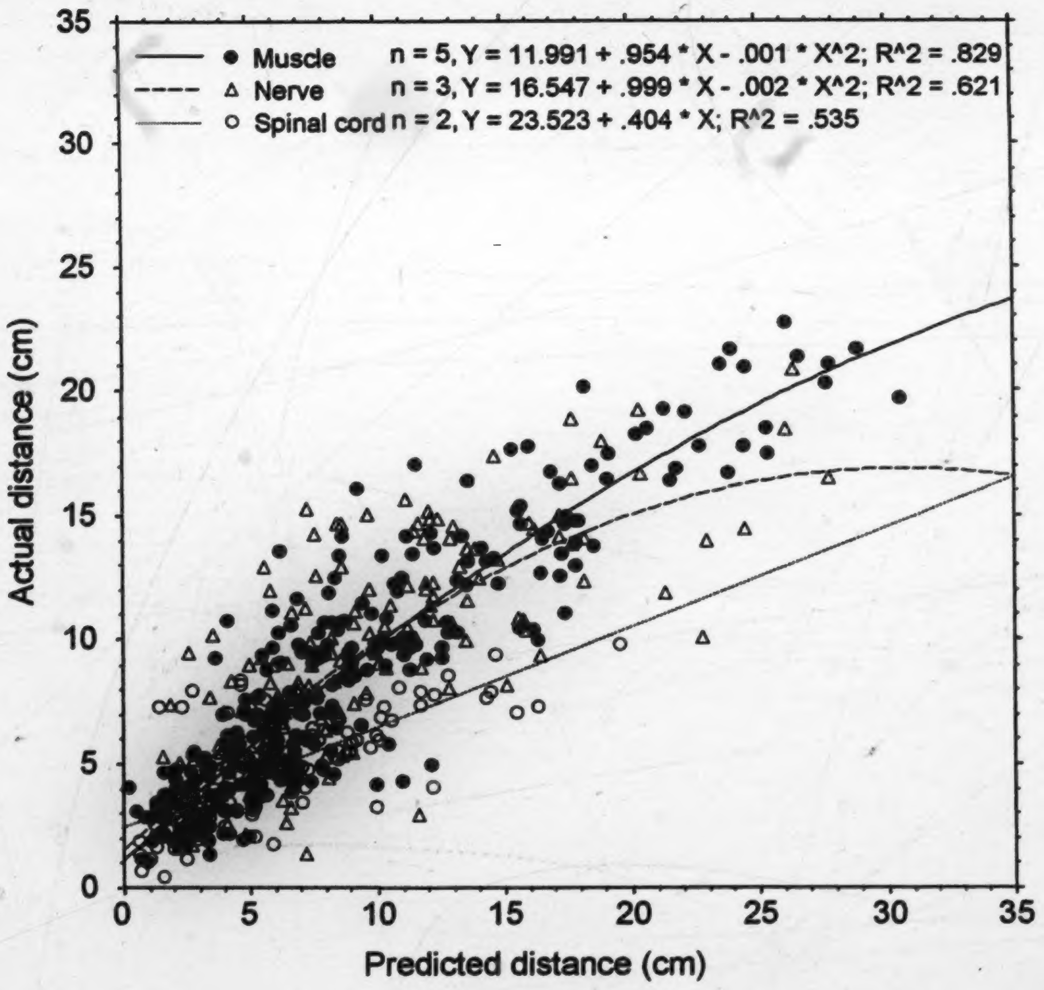

Figure 6-4a. Predicted versus actual distances for intramuscular, nerve and intraspinal stimulation and their regression equations.

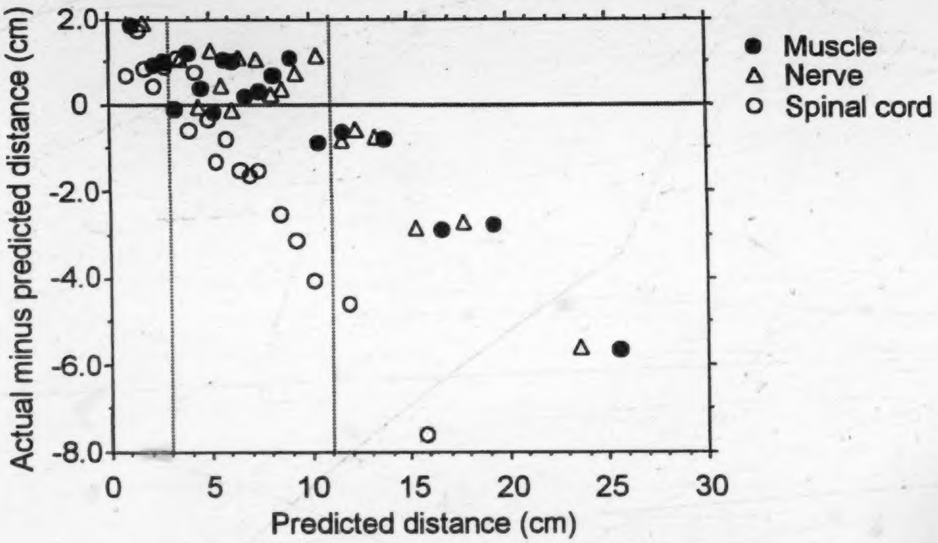

Figure 6-4b. Predicted versus actual distances. Here points with a similar predicted distance have been grouped and the differences of the actual distance from the prediction are plotted as the ordinate.

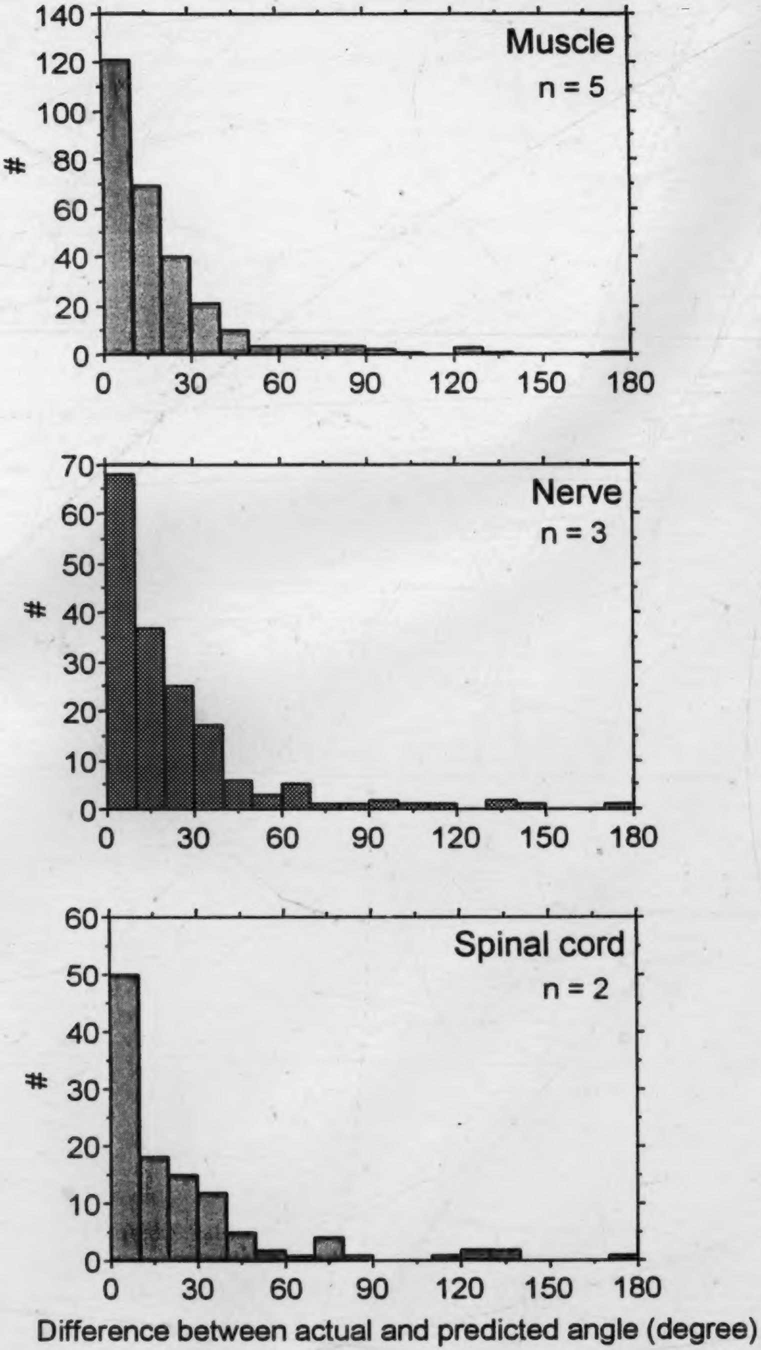

Figure 6-5. Histograms of absolute angle differences between the actual and the corresponding predicted vectors for intramuscular, nerve and intraspinal stimulation.

Equilibrium point

Figure 6-6 demonstrates typical examples of individual intramuscular stimulation at front, neutral and back positions. The equilibrium point index (EPI) (see **METHODS**) calculated for stimulation of individual muscles is shown in **Figure 6-7a**. A value of 0 would represent complete convergence whereas a value >10 represents a divergence. The average EPI from two experiments was 7.8 ± 2.1. BF and SM had the lowest EPIs and showed good convergence. LG and VL, which had EPIs very close to 10, showed no real convergence. SA and TA, with intermediate EPIs, had a weak convergence.

Figure 6-7b compares actual and predicted EPI for combined stimulation of more than one muscle. On average the actual EPI (4.5 ± 2.5) was significantly lower than the predicted EPI (5.5 ± 2.5) (p <0.01, paired t-test) and both were lower than the average EPI for stimulation of individual muscles (p <0.001). **Figure 6-8** shows some examples of actual and predicted vectors with intramuscular stimulation and their end-points elicited at front, neutral and back positions (same animal as in **Figure 6-6**). In some examples (#=3) the actual and predicted movements agree well, whereas in others there is a large difference (#=2, 6). Actual vectors appeared to converge more as the number of stimulation sites became larger from 2 to 6. Indeed statistically, a one-factor ANOVA revealed that the EPI became gradually smaller as the number of stimulation sites increased (p<0.001) (**Figure 6-9**). Conversely, the predicted EPI was rather larger with stimulation of more sites (p<0.05; one-factor ANOVA).

The decrease in the actual EPI may be related to the number of involved joints rather than the number of stimulated muscles. For example, when LG and TA are simultaneously stimulated, only the ankle joint is actively displaced in a major way by stimulation. When TA and SA are simultaneously stimulated, the number of involved joints is two because ankle and hip joints are actively displaced during stimulation. In order to test the effect of the number of involved joints on the actual and predicted EPI, a one-factor ANOVA was performed. As the number of involved joints increased, the actual EPI decreased (p <0.01; one-factor ANOVA), but the predicted EPI did not (**Figure 6-10**). Another possibility is that the EPI is related to whether antagonist groups are stimulated which could stabilize a joint near equilibrium (Bizzi et al. 1982). To test this point, we selected cases where two sites were simultaneously stimulated and divided them into two

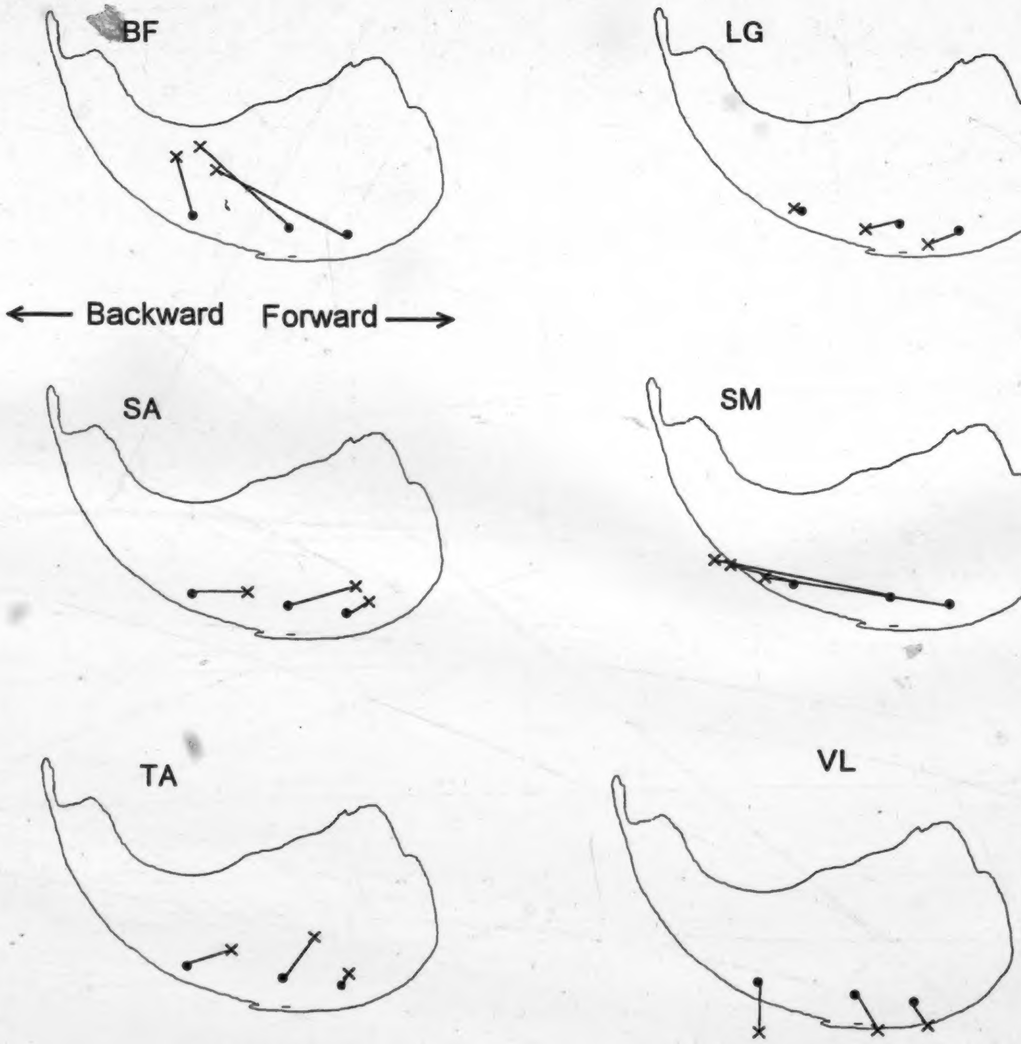
BF
LG
Backward
Forward
SA
SM
TA
VL

Figure 6-6. Examples of individual vectors at front, neutral and back positions from one animal. The chain line represents passive range of motion of the paw.

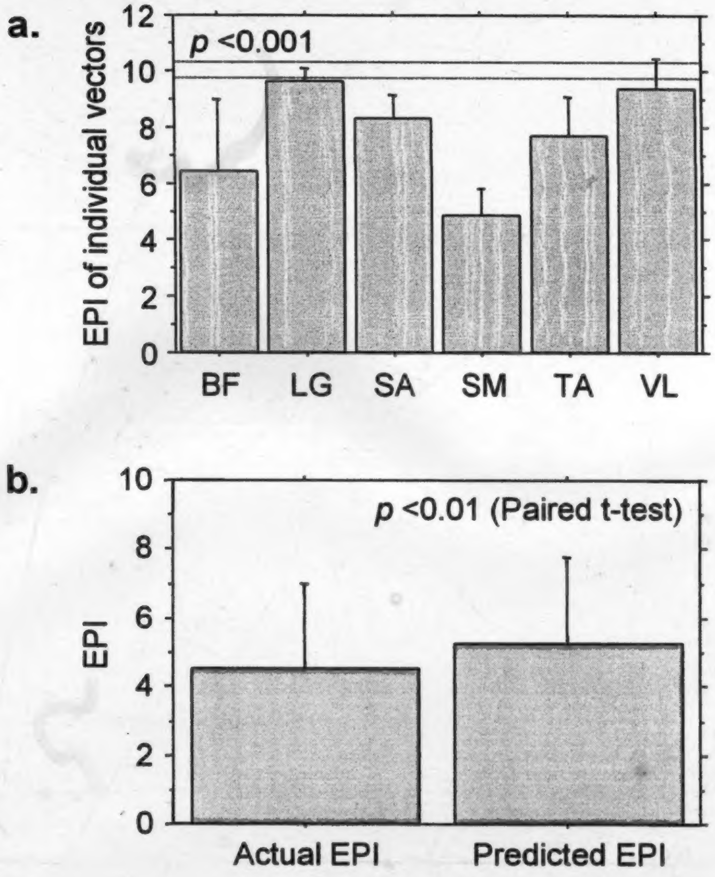

Figure 6-7a. Equilibrium point index (EPI) of individual vectors (see also **METHODS**). Each muscle includes ten data from two animals. Dotted lines (at 9.7 and 10.3 of EPI) represent the averaged length (cm) between front, neutral and back rest positions of the respective animals. Therefore, if vectors from neutral and back rest positions have the same length and angle, the EPI should be 10. If the EPI is zero, the three end-points converge perfectly to an equilibrium point. Thus, a low EPI indicates that the movements converge and a high EPI indicates that the movements diverge. For example, BF and SM, which both had a low EPI, strongly converge (see **Figure 6-6**). **Figure 6-7b.** Actual and predicted EPI calculated based on vectors elicited by stimulus combinations. The average, actual EPI was significantly lower than the predicted EPI ($p < 0.01$, paired t-test).

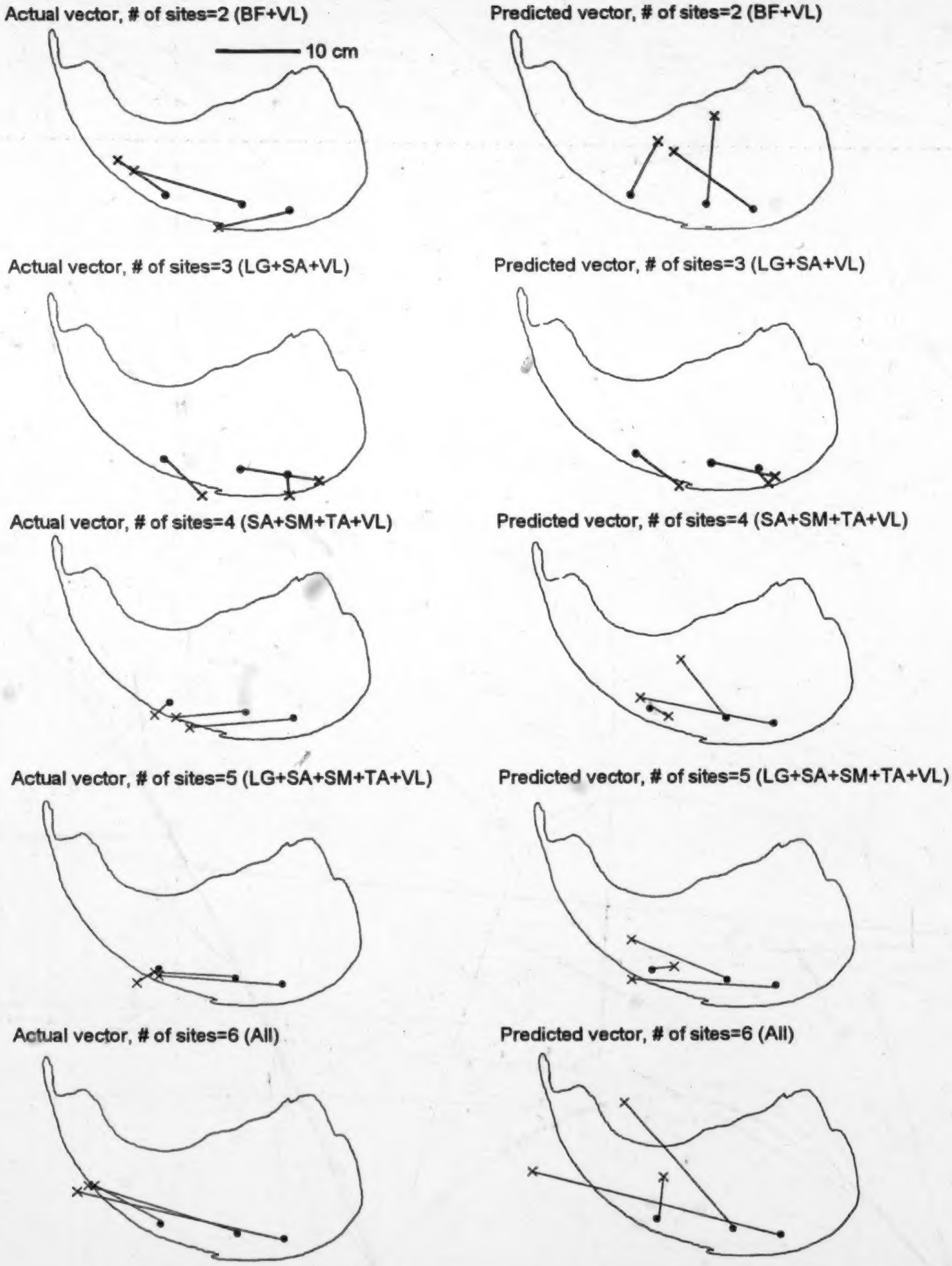
Actual vector, # of sites=2 (BF+VL)

Predicted vector, # of sites=2 (BF+VL)

Actual vector, # of sites=3 (LG+SA+VL)

Predicted vector, # of sites=3 (LG+SA+VL)

Actual vector, # of sites=4 (SA+SM+TA+VL)

Predicted vector, # of sites=4 (SA+SM+TA+VL)

Actual vector, # of sites=5 (LG+SA+SM+TA+VL)

Predicted vector, # of sites=5 (LG+SA+SM+TA+VL)

Actual vector, # of sites=6 (All)

Predicted vector, # of sites=6 (All)

Figure 6-8. Some examples of vectors elicited by intramuscular stimulation of muscles at back, neutral and front positions. The left illustrations represent actual vectors and their end-points whereas the right illustrations represent predicted vectors and their end-points. The uppermost illustration represents an example of combined stimulation of two muscle sites whereas the lowermost illustration represents combined stimulation at six sites.

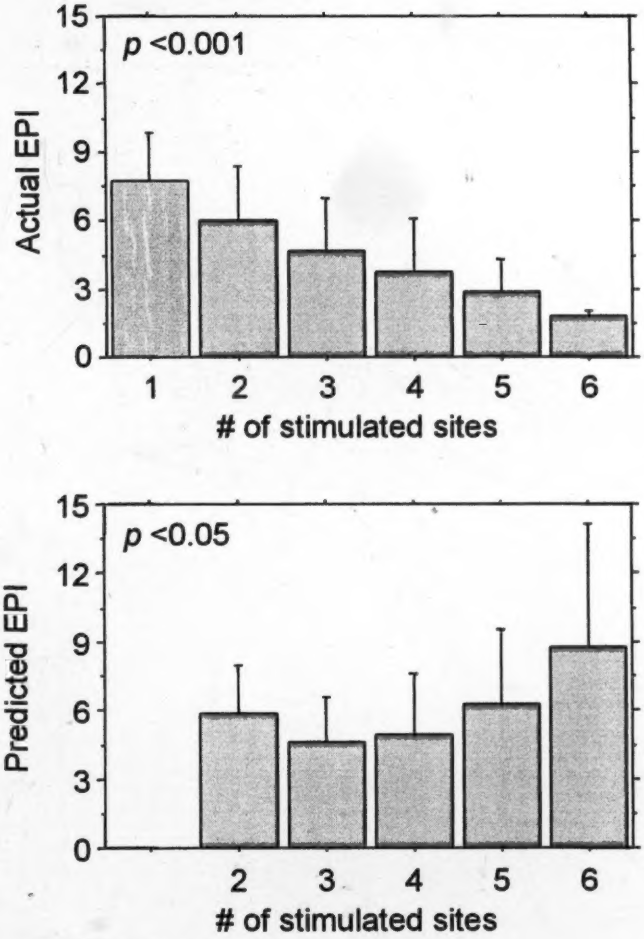

Figure 6-9. a. Actual EPI as a function of the number of stimulated sites. **b.** Predicted EPI as a function of the number of stimulated sites. All the data from two animals are included (60, 30, 40, 30, 12 and 2 trials for 1,2,3,4,5,6 stimulated sites respectively).

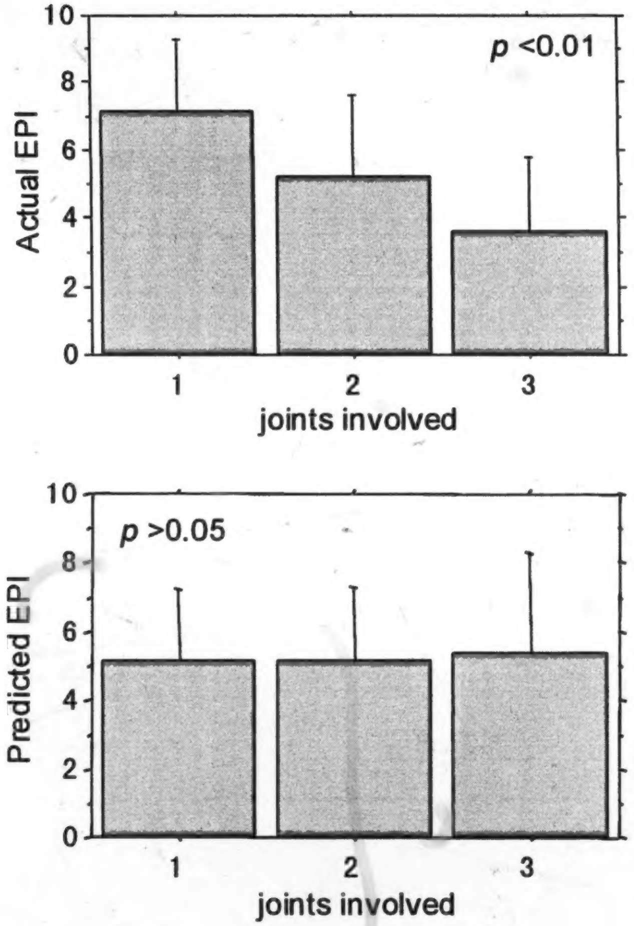

Figure 6-10. a. EPI of actual vectors as a function of the number of joints involved when muscles were stimulated. **b.** EPI of predicted vectors according to the number of joints involved. One, two and three joints included 6, 54 and 54 cases in **a** and **b**.

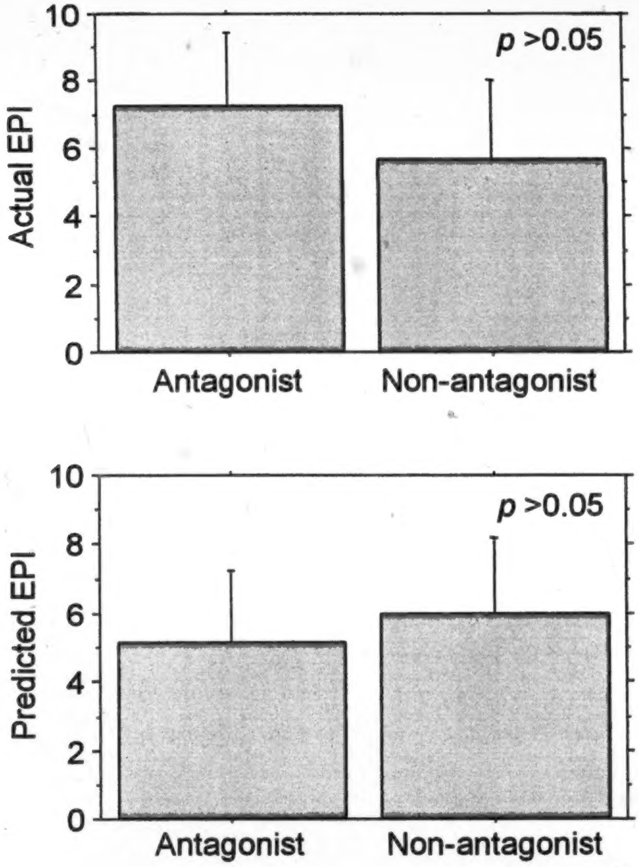

Figure 6-11. a. EPI of actual vectors when combine stimulation of two sites was delivered to antagonistic (n=6) and non-antagonistic muscles (n=24). **b.** EPI of predicted vectors for antagonistic (n=6) and non-antagonistic muscles (n=24). There were no statistical differences in EPI in both actual and predicted vectors between antagonist and non-antagonist muscles. However, in simultaneous stimulation of antagonistic muscles, the actual EPI was bigger than the corresponding predicted EPI ($p < 0.05$, paired t-test).

groups: a group where antagonistic muscles were stimulated (e.g. LG and TA and a second group where non-antagonistic muscle were simulated (e.g. TA and SA). However, no significant differences were seen in the actual EPI for the two groups and the actual EPI tended to be larger for antagonist stimulation, contrary to prediction (**Figure 6-11**). Finally, to test how individual muscles affected the EPI, we calculated the EPI separately according to the involvement of each muscle. The actual EPI was significantly smaller when SM was involved ($p<0.001$), but the predicted EPI was not affected by the involvement of any single muscle.

DISCUSSION

In this paper we addressed a very basic biomechanical question: whether multi-joint movement consists of the simple vectorial summation of each single-joint movement? Clear deviations were seen from linear summation. These could arise from inter-joint torques and the fact that the bones and ligaments limit the range of motion of the limb. We also addressed the question of whether peripherally elicited movements at different positions converge toward an equilibrium point? Interestingly, the answer was almost always yes in our experiments, especially when more muscles participated in a movement. Furthermore, involvement of particular muscles was also important to predict convergence. These results clearly suggest that intrinsic neuromuscular properties by themselves can independently contribute to restrict and determine a movement trajectory and its end-point, independently of the CNS. We therefore stress that the equilibrium-point hypothesis is strongly rooted in the biomechanics of musculoskeletal systems and in particular in their spring-like properties as originally suggested by Feldman and Bizzi (Bizzi et al. 1982; Feldman. 1966). To the extent that the periphery can already form trajectories to an equilibrium point, this simplifies the job of the CNS. It may also circumvent controversial issues based on movement-related CNS hypotheses (cf. (Feldman et al. 1998; Georgopoulos. 1995; Gottlieb. 1998; Kawato. 1999; Loeb et al. 1996; Mussa-Ivaldi and Bizzi. 2000; Wolpert and Ghahramani. 2000)).

Intrinsic peripheral properties contributing to a preferred direction and an equilibrium point

The contractile mechanisms producing spring-like properties of muscle depend on a number of factors: the interaction between actin and myosin filaments, the series elastic elements in the tendons, the actin-myosin cross-bridges themselves and the parallel elastic element of the muscle fibers and the surrounding connective tissue. Few biomechanists or neurophysiologists doubt that spring-like properties of muscles are of significant importance in forming a trajectory and maintaining a stable posture (Nichols et al. 1999). A more fundamental question, however, has been how far this system by itself suffices to generate movements and equilibrium points. The intramuscular and nerve stimulation in this experiment under anesthesia enabled us to directly observe neuromuscular characteristics on movement. The CNS and spinal reflexes were not involved, since no reflex EMG signals were observed during nerve stimulation under anesthesia (not shown). Thus, by separating mechanical effects of the peripheral neuromuscular system from the effects of the CNS, we found a number of characteristics of movement that would not have been predicted if muscles merely generated force.

First, stimulating major nerves or muscles individually produces movements in 6 distinct directions. Combining the stimulation of these nerves or muscles produces movements that are not uniformly distributed. There was a preponderance of backward movements (**Figure 6-2**). As mentioned in the **RESULTS**, the most likely reason is the relative strengths of different muscle groups, since it is seen to some extent in both the actual and the predicted movements. By adjusting the strength of each stimulus a more uniform distribution could presumably be generated. However, to the extent that spinal or supraspinal centers can activate the major muscle groups individually, six or more principal directions would be expected. If these centers activate combinations of these muscle groups a smaller number might result. In short, the presence of a few preferred directions is almost inevitable when groups of muscles are being activated, as has been found experimentally (Bizzi et al. 1991; Giszter et al. 1993).

Second, the actual distances often did not agree with the predictions from linear summation (**Figure 6-4**). When the predicted distance from stimulating several muscles was small (<3 cm), the actual distances were rather larger than predicted (**Figure 6-4b**).

This may be again due to the nonlinear elastic nature of musculoskeletal tissue (e.g. the stiffness of a muscle contracting at one joint will affect the movement produced when activating another joint). Thus, the distance between the actual and predicted end-points got larger as more muscles were activated (**Figure 6-3b**). Nonetheless, in the middle range of predicted magnitude (3~11cm), actual and predicted magnitudes had a fairly linear relationship for intramuscular and nerve stimulation. For larger distances (>11 cm) the actual vectors were smaller than predicted. These smaller actual amplitudes are explainable at least in part by movements approaching the limits of the physiological range of motion (**Figure 6-2a and 6-8**).

Third, in addition, the angles of the predicted movements often varied by at least 30° from the actual vectors (**Figure 6-5**). This occurred during stimulation of muscles, nerves and the spinal cord, suggesting that it arose from peripheral mechanisms. This nonlinear summation of stimulation from multiple sites is therefore distinct from the change in direction with increased intensity of intraspinal stimulation or spinal state that I will describe in Chapter 7. That change in direction appeared to be due to spinal mechanisms.

Fourth, actual movements did not necessarily follow individual vectorial summation but rather converged to an equilibrium point as more muscles are involved in generating movement (**Figure 6-3b, 6-8** and **6-9**). As the number of activated muscles increased, actual end-points appeared to converge to an equilibrium point (**Figure 6-9a**) while the predicted end-points did not (**Figure 6-9b**). This evidence strongly supports the idea that neuromuscular properties by themselves possess the ability to specify an equilibrium point without complex calculations of the CNS. In other words, activating the peripheral nervous system (PNS) can guide a movement to a final end-point, even if both reflex and voluntary muscle activities of the CNS are not available (cf. (Polit and Bizzi. 1978)).

Analyzing our results in detail, several points emerged concerning the equilibrium point issue. Bizzi et al. suggested a hypothesis that the movement to an equilibrium point is determined by an interaction of agonist and antagonist muscles at a joint (Bizzi et al. 1982). This hypothesis is attractive because it suggests the possibility that the trajectory of a simple movement is determined by the inherent inertial and viscoelastic properties of the limb and muscles around a joint. However, our analysis revealed that the number of joints activated during movement is a significant factor in determining an equilibrium point, whereas co-activation of agonist and antagonist at one joint is not (**Figure 6-10** and **6-11**). Actual end-points became less convergent than the corresponding predicted EPI during co-activation of a joint alone (**Figure 6-11**). Accordingly, the increase of stiffness at all joints must be an important strategy in order to stabilize the joints at specific angles and thus maintain limb stability (McIntyre et al. 1996). In more gradual movements, where stiffness does not change rapidly, interaction between agonist and antagonist muscles might be an important control strategy.

Relation to spinal organization

Bizzi and his colleagues have carried out some elegant experiments in spinal frog and showed how spinal interneuronal areas can influence the motor output (Bizzi et al. 1991; Giszter et al. 1993). They found that intraspinal microstimulation produces isometric force fields that converge to a limited number (3-5) of equilibrium points. This was interpreted as evidence for the existence of 3 to 5 'movement primitives' hard-wired in the spinal cord. Later work suggested that simultaneous microstimulation at any two sites produced a new force field that follows a principle of vectorial summation (Mussa-Ivaldi et al. 1994). Our results can not be directly compared to theirs, since their experiments were all done under isometric conditions. However, to be useful, the linear summation should also apply to movements against a variety of loads. We will particularly discuss two issues in this section: the mechanisms of preferred directions and the existence of hard wiring of spinal cord circuits.

We found that intraspinal microstimulation produced movements that were similar to the intramuscular and nerve stimulation, plus flexion and extension synergies (cf. **Figure 5-2e** in Chapter 5). So we raised the possibility that the biomechanical actions of the limb muscles set limitations on the movements that can be generated through central commands. Preferred movement vectors would then reflect biomechanical groupings. Further evidence in the current experiment that peripheral stimulation of several sites elicited end-points that appeared to converge to a limited number of preferred directions convinces us of the above possibility.

In the spinal frog, if the stimulating electrode was moved into the ventral horn so that motoneurons were stimulated directly, then the force fields were divergent or parallel rather than converging. Bizzi et al. therefore concluded that the input to the motoneurons from the intermediate zone imposes a structure on the pattern of motoneuronal activation that is consistent with the form of the equilibrium points. The current experiment revealed that simultaneous activation of numerous muscles in the workspace produced convergent movements toward an equilibrium point. Activation of some single muscles (BF and SA) also produced movements that converged toward an equilibrium point (**Figures 6-6** and **6-7a**), but others produced movements that were parallel or somewhat divergent. Our results suggest that whether a movement converges or diverges depends on a number of factors: the number of activated muscles, the number of joints involved and the sorts of activated muscles. The results in spinal frog that interneuronally- and motoneuronally-elicited movements converged and diverged respectively could simply reflect one of the factors; e.g. the number of activated muscles, rather than 'primitives', since spinal interneurons are remarkably convergent in their output projection. Thus, the microstimulation of interneuronal and motoneuronal areas is likely to activate more and fewer muscles respectively.

Control of the limb at a higher level

There has been long-standing controversy over whether 'muscle activity' or 'direction' is encoded in the primary motor cortex (Evarts. 1966; Fetz and Cheney. 1980; Georgopoulos et al. 1982; Kakei et al. 1999; Scott and Kalaska. 1995; Shen and Alexander. 1997). It has been shown that a fairly small number of motor cortex cells displayed movement related activity that was target-dependent but independent of the pattern of muscle activity or direction of joint movement (Shen and Alexander. 1997). An interpretation of these findings is that motor cortex cells are involved in multiple stages of sequentially computing parameters such as position of the target, trajectory, joint kinematics and muscle activation (Alexander and Crutcher. 1990; Maynard et al. 1999). Different strategies of motor cortex may be used for different types of reaching movements (cf. movements with a similar hand path but a different arm posture (Scott and Kalaska. 1995; Scott and Kalaska. 1997)). Our results do not touch on these ideas directly, but to the extent that directions that are relatively convergent are already available from activating single or multiple muscles in the periphery, this simplifies the job of the motor cortex considerably. Further work is needed to determine to what extent additional computation is needed at the cortical level to provide the normal repertoire of movements that animals require in their daily life.

REFERENCES:

1. Alexander GE, and Crutcher MD. Preparation for movement: neural representations of intended direction in three motor areas of the monkey. *J Neurophysiol* 64: 133-150., 1990.

2. Aoyagi Y, Mushahwar VK, Stein RB, and Prochazka A. Are movement primitives determined by spinal cord circuitry or biomechanics? *Society for Neuroscience 30th Annual Meeting*, New Orleans, La. Society for Neuroscience, 2000, p. 696.

3. Aoyagi Y, Mushahwar VK, Stein RB, and Prochazka A. Comparing movements elicited by electrical stimulation of muscles, nerves, spinal cord and spinal roots in anesthetized and decerebrate cats. *J Neurophysiol*:, submitted.

4. Bernstein NA. The problem of interrelations between coordination and localization (in Russian). *Arch Biol Sci* 38: 1-35, 1935.

5. Bizzi E, Accornero N, Chapple W, and Hogan N. Arm trajectory formation in monkeys. *Exp Brain Res* 46: 139-143, 1982.

6. Bizzi E, Accornero N, Chapple W, and Hogan N. Posture control and trajectory formation during arm movement. *J Neurosci* 4: 2738-2744., 1984.

7. Bizzi E, Mussa-Ivaldi FA, and Giszter S. Computations underlying the execution of movement: a biological perspective. *Science* 253: 287-291, 1991.

8. Bizzi E, Tresch MC, Saltiel P, and d'Avella A. New perspectives on spinal motor systems. *Nat Rev Neurosci* 1: 101-108., 2000.

9. Chapin JK, and Moxon KA. *Neural Prostheses for Restoration of Sensory and Motor Function*. Boca Raton: CRC Press, 2000.

10. Crouch JE. *Text-atlas of cat anatomy*. Philadelphia: Lea & Febiger, 1969.

11. d'Avella A, and Bizzi E. Low dimensionality of supraspinally induced force fields. *Proc Natl Acad Sci U S A* 95: 7711-7714, 1998.

12. Evarts EV. Pyramidal tract activity associated with a conditioned hand movement in the monkey. *J Neurophysiol* 29: 1011-1027., 1966.

13. Feldman AG. Functional tuning of the nervous system with control of movement or maintenance of a steady posture. II. Controllable parameters of the muscle. *Biophysics* 11: 565-578, 1966.

14. Feldman AG, Ostry DJ, Levin MF, Gribble PL, and Mitnitski AB. Recent tests of the equilibrium-point hypothesis (lambda model). *Motor Control* 2: 189-205., 1998.

15. Fetz EE, and Cheney PD. Postspike facilitation of forelimb muscle activity by primate corticomotoneuronal cells. *J Neurophysiol* 44: 751-772, 1980.

16. Georgopoulos AP, Kalaska JF, Caminiti R, and Massey JT. On the relations between the

direction of two-dimensional arm movements and cell discharge in primate motor cortex. *J Neurosci* 2: 1527-1537., 1982.

17. Georgopoulos AP. Current issues in directional motor control. *Trends Neurosci* 18: 506-510., 1995.

18. Giszter SF, Mussa-Ivaldi FA, and Bizzi E. Convergent force fields organized in the frog's spinal cord. *J Neurosci* 13: 467-491, 1993.

19. Gottlieb GL. Rejecting the equilibrium-point hypothesis. *Motor Control* 2: 10-12., 1998.

20. Kakei S, Hoffman DS, and Strick PL. Muscle and movement representations in the primary motor cortex. *Science* 285: 2136-2139., 1999.

21. Kawato M, Furukawa K, and Suzuki R. A hierarchical neural-network model for control and learning of voluntary movement. *Biol Cybern* 57: 169-185, 1987.

22. Kawato M. Internal models for motor control and trajectory planning. *Curr Opin Neurobiol* 9: 718-727., 1999.

23. Loeb GE, Brown IE, and Scott SH. Directional motor control. *Trends Neurosci* 19: 137-138., 1996.

24. Loeb GE. Learning from the spinal cord. *J Physiol* 533: 111-117., 2001.

25. Macpherson JM. Strategies that simplify the control of quadrupedal stance. I. Forces at the ground. *J Neurophysiol* 60: 204-217, 1988.

26. Maynard EM, Hatsopoulos NG, Ojakangas CL, Acuna BD, Sanes JN, Normann RA, and Donoghue JP. Neuronal interactions improve cortical population coding of movement direction. *J Neurosci* 19: 8083-8093., 1999.

27. McIntyre J, Mussa-Ivaldi FA, and Bizzi E. The control of stable postures in the multijoint arm. *Exp Brain Res* 110: 248-264, 1996.

28. Mussa-Ivaldi FA. Do neurons in the motor cortex encode movement direction? An alternative hypothesis. *Neurosci Lett* 91: 106-111., 1988.

29. Mussa-Ivaldi FA, Giszter SF, and Bizzi E. Linear combinations of primitives in vertebrate motor control. *Proc Natl Acad Sci U S A* 91: 7534-7538, 1994.

30. Mussa-Ivaldi FA, and Bizzi E. Motor learning through the combination of primitives. *Philos Trans R Soc Lond B Biol Sci* 355: 1755-1769., 2000.

31. Nichols TR, Lin DC, and Huyghues-Despointes CM. The role of musculoskeletal mechanics in motor coordination. *Prog Brain Res* 123: 369-378, 1999.

32. Polit A, and Bizzi E. Processes controlling arm movements in monkeys. *Science* 201: 1235-1237., 1978.

33. Saltiel P, Tresch MC, and Bizzi E. Spinal cord modular organization and rhythm generation: an

NMDA iontophoretic study in the frog. *J Neurophysiol* 80: 2323-2339, 1998.

34. Scott SH, and Kalaska JF. Changes in motor cortex activity during reaching movements with similar hand paths but different arm postures. *J Neurophysiol* 73: 2563-2567., 1995.

35. Scott SH, and Kalaska JF. Reaching movements with similar hand paths but different arm orientations. I. Activity of individual cells in motor cortex. *J Neurophysiol* 77: 826-852., 1997.

36. Shen L, and Alexander GE. Preferential representation of instructed target location versus limb trajectory in dorsal premotor area. *J Neurophysiol* 77: 1195-1212., 1997.

37. Shen L, and Alexander GE. Neural correlates of a spatial sensory-to-motor transformation in primary motor cortex. *J Neurophysiol* 77: 1171-1194., 1997.

38. Tresch MC, and Kiehn O. Motor coordination without action potentials in the mammalian spinal cord. *Nat Neurosci* 3: 593-599., 2000.

39. Wolpert DM, and Ghahramani Z. Computational principles of movement neuroscience. *Nat Neurosci* 3 Suppl: 1212-1217., 2000.

CHAPTER 7

MOVEMENTS GENERATED BY INTRASPINAL MICROSTIMULATION IN THE INTERMEDIATE GRAY MATTER OF THE ANESTHETIZED, DECEREBRATE AND SPINAL CAT[*]

INTODUCTION

The intermediate regions of the gray matter in the lumbosacral spinal cord in mammals are thought to contain the basic neuronal elements for movement construction (Orlovsky et al., 1999). Using a multitude of methods in anatomical staining and electrophysiological recordings, neurons within this region, especially lamina VII, have been confirmed to be activated during rhythmic motor behaviors such as stepping or scratching. For example, using voltage and calcium-sensitive dyes, neurons in lamina VII throughout the lumbosacral enlargement were heavily stained during fictive locomotion in cats (Carr et al., 1995; Huang et al., 2000) and fictive scratching in turtles (Orlovsky et al., 1999). Furthermore, recording of spinal field potentials during fictive locomotion induced by electrical stimulation of the mesencephalic locomotor region (MLR) of the brainstem demonstrated that the intermediate regions of the cord contained the largest field potentials with the shortest onset latencies. This suggested that these regions receive direct descending inputs associated with the initiation and modulation of locomotion (Noga et al., 1995). Electrophysiological recordings obtained from single cells in the intermediate gray matter during fictive locomotion induced either pharmacologically (using monoaminergic agonists and/or excitatory amino acids) or by electrical stimulation of the MLR resulted in the characterization of various classes of interneurons active during different phases of the step cycle (Duysens and Pearson, 1980; Jankowska, 1992; Pearson et al., 1992; McCrea et al., 1995; Perreault et al., 1999; Gosgnach et al., 2000; Quevedo et al., 2000; Lam, 2001).

---

[*] A version of this chapter will be submitted *to J Neurosci* by the authors of Aoyagi. Y, Mushahwar. VK, Stein. RB, Prochazka, A. Contribution to paper: participated in all experiments and partially contributed to data analysis and editing of manuscript.

Finally, damage of the intermediate regions often resulted in the interruption of fictive locomotion (Deliagina et al., 1983; Kjaerulff and Kiehn, 1996; Cowley and Schmidt, 1997; Orlovsky et al., 1999) further emphasizing the importance of these regions for construction of limb movements.

While the majority of studies investigating the intermediate regions of the lumbosacral spinal cord focused on the use of anatomical markers and electrophysiological recordings, very few attempted to electrically stimulate these regions and characterize the resulting limb responses. In fact, only three laboratories associated with Bizzi (Bizzi et al., 2000), Giszter (Giszter et al., 2000), and Grill (Lemay and Grill, 1999; Grill, 2000) and coworkers performed detailed mapping of the intermediate gray matter regions using intraspinal microstimulation (ISMS). The experiments were primarily conducted in frogs, and to a lesser degree in rats and cats. Results from these studies led to the formulation of the "movement primitives" hypothesis which suggested that the intermediate gray matter contains specialized circuitry for movement construction, or "movement building blocks" (Kargo and Giszter, 2000). These building blocks are *limited* in number (4-5 in the frog) and the activation of each produces a distinct isometric force pattern in the limb in two and three dimensional space (Giszter et al., 1993). They are also suggested to be *autonomous* in the spinal cord with descending input activating them in combinations resulting in force patterns that represent the full repertoire of limb movements, covering the limb's active work space (Giszter et al., 1993; Bizzi et al., 2000; Lemay et al., 2001).

To date, all movement primitive studies were conducted in decapitated frogs (Giszter et al., 1993; d'Avella and Bizzi, 1998; Saltiel et al., 1998), chronically spinalized rats (Tresch and Bizzi, 1999) or anesthetized cats (Lemay and Grill, 1999; Grill, 2000). The isometric force patterns representing these movement primitives resulted from muscle contractions about the hip and knee in frogs and rats (i.e., multi-axial force transducer attached to the limb above the ankle), and knee and ankle in cats (i.e., femur fixed in place and force transducer attached to the foot) (Giszter et al., 1993; Lemay and Grill, 1999). However, to further ascertain the presence of the hypothesized movement primitives and to unravel the level of independence of these neuronal structures from descending input, it is necessary, in our opinion, to characterize the responses evoked by ISMS of the intermediate gray matter while allowing the limb to move widely in space and under conditions of intact and interrupted descending drive.

The goal of this study was to characterize hindlimb responses evoked by ISMS of the intermediate regions of the lumbosacral spinal cord under conditions of anesthesia, acute decerebration and acute low-thoracic spinalization in the same animal. Our study resulted in two main conclusions: 1) under anesthesia, limb responses evoked by ISMS of the intermediate gray matter can be predicted based on the distribution of lumbosacral motoneuron pools in Rexed lamina IX; and 2) altering the descending input through acute decerebration and spinalization leads to a dramatic change in the trajectory of ISMS-induced limb movements. These conclusions suggest that movement building blocks in the spinal cord are most probably composed from anatomically identified and localized motoneuronal zones. Multi-joint synergistic movements result from widespread activation of motoneuronal pools along the lines of inherent flexor and extensor reflexes. Finally, the basic elements of movement construction in the intermediate laminae of the spinal cord seem to be strongly dependent on descending input, with flexor reflexes becoming dominant after acute interruptions of descending drive.

METHODS

General overview

Results from 5 adult cats (3 – 4 kg) were used in the study. All experimental procedures were conducted in compliance with protocols approved by the Laboratory Animals Welfare Committee at the University of Alberta. All animals were initially anesthetized using halothane inhalation and movements of the right hindlimb generated by intramuscular, epineural or intraspinal/root stimulation were recorded. To determine the effect of descending input on the hypothesized neuronal elements of movement composition located within the intermediate regions of the spinal cord, the cats were subsequently decerebrated at the intercollicular level and then completely spinalized at the level of the twelfth thoracic vertebra. All stimulation paradigms and biomechanical measurements were repeated after each level of lesioning.

Hindlimb kinematic and EMG responses elicited by ISMS in 3 cats under conditions of anesthesia, decerebration and spinalization are presented in this report. For purposes of comparison, we also present the kinematic responses evoked by intramuscular stimulation of the main hip, knee and ankle flexor and extensor muscles (4 animals under anesthesia) and epineural stimulation of nerve branches innervating the main flexor or extensor muscle groups (2 animals under anesthesia). We also present the EMG responses evoked by dorsal and ventral root stimulation conducted in one cat under decerebration.

Detailed surgical procedure, experimental protocol, and data acquisition mostly overlap with Chapters 5 and 6. Thus, the methods described next will be partial repetitions of Chapters 5 and 6.

Surgical procedure and electrode implantation

Inhalation anesthesia was induced with halothane (2-3% in carbogen mixture, 1500 ml/min). A tracheotomy was performed and a tracheal tube was used to allow for the maintenance of anesthesia. A jugular vein was cannulated to allow for the periodic administration of fluids, and the carotid arteries were ligated. A cannula, attached to a pressure transducer, was inserted in the proximal end of one of the carotid arteries to obtain continuous measurements of blood pressure. Dextran (5%, i.v.) was administered as needed to maintain pressure above 80 mmHg.

Cuff or epineural patch electrodes (each containing 2 wires for bipolar stimulation spaced ~7 mm apart) were implanted around nerve branches innervating the main hip, knee and ankle flexor or extensor muscle groups (see Chapter 5 and Hamm et al., 1985). A laminectomy was then performed to expose spinal cord segments L4-S2 and the cat was placed in a standard stereotaxic frame using iliac crest pins, vertebral clamps and ear bars, leaving all limbs pendent. A U-shaped foot piece was placed midway along the metatarsals of the right foot and held in place with plastic wire ties without impeding the movements of the paw. The foot piece was in turn attached to a rod-spring assembly that allowed the limb to be positioned in a mid-stance posture and to move in a uniform stiffness field in the saggital plane, i.e., the restoring forces were the same in all directions of limb movement (Figure 7-1). The rod-spring assembly resulted in ~1 cm off-saggital deviation for movements ≥ 15 cm from the origin.

To record limb kinematics, 6D electromagnetic motion sensors (Skill Technologies Inc., Arizona, USA) were fixed to the hip joint, distal femur, distal fibula and metatarsals. The hip joint sensor was sutured to the skin while the metatarsal sensor was

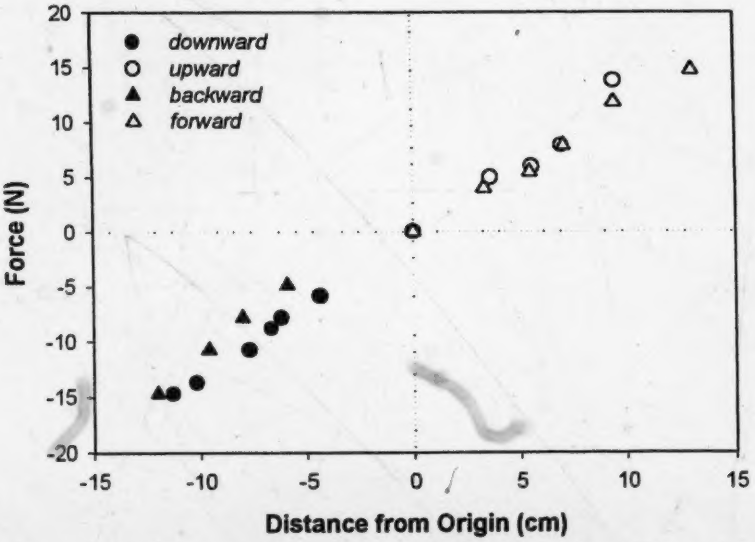

Figure 7-1. Force-displacement curve characterizing the uniformity of the saggital stiffness field through which the limb moved. Restoring forces for movements in the upward, downward, forward and backward directions were similar.

attached to the foot piece using double-sided sticky tape. The femoral and fibular sensors were fixed in place via sutures drilled through the respective bones (Mushahwar et al., 2002). Bipolar intramuscular stimulation and recording of electromyographic (EMG) activity were achieved by implanting pairs of 9-strand stainless steel wires (AS 632 Cooner Wire, insulated with Teflon except for 3-5 mm at one end) into the main hip, knee and ankle flexor and extensor muscles of the right hindlimb [sartorius anterior (SA), iliopsoas (IP), semimembranosus anterior (SM), biceps femoris posterior (BF), vastus lateralis (VL), tibialis anterior (TA) and lateral gastrocnemius (LG)]. The wires were inserted percutaneously to the muscles of interest and fixed to the surface of the skin with the application of small amounts of cyanoacrylate glue (Mushahwar et al., 2002).

ISMS of the intermediate gray matter was conducted using techniques previously published by Mushahwar, Collins and Prochazka (Mushahwar et al., 2000). Briefly, 17 – 19 microwires (stainless steel, 30 μm diameter, insulated except for 30-70 μm at the tip, 10-30 kΩ impedance), spaced 2 mm apart, were individually inserted in the right side of the spinal cord, 0.5-2 mm from the midline and to depths ranging between 2.5-3.5 mm from the epidural dorsal surface. The microwires spanned the L4-S1 extent of the cord and the chosen laterality and ventrality allowed for the tips to be placed within the intermediate laminae. All microwires were fixed in place by placing a small drop of cyanoacrylate at the point of entry of each wire through the dura mater (Mushahwar et al., 2000). This maintained the microwires securely in place throughout the duration of the experiments. The reference electrode was made of 9-strand stainless steel wire (AS 632 Cooner) insulated with Teflon except for a 5-cm exposure at one end and was placed over the longissimus dorsi muscle.

Experimental protocol and data acquisition

Stimulation

For intramuscular and epineural stimulation, trains of bipolar monophasic pulses (300 μs, 50 pulses/s) 0.8 s in duration, were delivered through the implanted electrodes at amplitudes ranging from 0.2 – 4.0 mA and 2 – 350 μA, respectively. ISMS through each microwire was composed of trains of monopolar monophasic pulses (300 μs, 50 pulses/s) 0.8 s in duration, and ranging in amplitude from 2 – 350 μA. A pulse repetition rate of 50/s was used in all trials in order to evoke tetanically fused muscle contractions.

In one cat, the L4 – S1 dorsal and ventral roots were stimulated, following decerebration, using bipolar hook electrodes. Dorsal roots were cut distally and their proximal portions were sequentially mounted into the electrodes for stimulation. Ventral roots were then sequentially stimulated. Stimuli consisted of 0.8 s trains of bipolar monophasic pulses varying in amplitude between 2 and 350 μA. In this cat, *no* ISMS trials were conducted.

Records of limb responses to intramuscular, epineural and intraspinal stimulation were initially obtained under anesthesia. For each stimulation site, stimulus threshold was first determined (stimulus amplitude producing the first visible limb movement). Subsequently, stimuli were delivered in predetermined increments of stimulus amplitude relative to threshold until either maximum limb movement was produced (i.e., further increments in stimulus amplitude did not produce increases in movement amplitude or changes in movement direction) or stimulus amplitude of several times threshold was reached. Cats were then decerebrated at the intercollicular level and anesthesia was terminated. Once decerebrate rigidity developed and spinal reflexes recovered (usually after a maximum duration of 60 min post decerebration), the stimulation protocol for ISMS through each microwire were repeated and the resulting limb movements were documented. Finally, the cats were spinalized at T12 and again limb movements evoked by ISMS were repeated after the recovery of spinal reflexes.

Recording limb kinematics and EMG activity

Limb Kinematics: Stimulus-evoked movements of the right hindlimb were documented by recording the input from the four electromagnetic motion sensors. The 3D location of each sensor was digitized at a rate of 30 samples/s. Kinematic recording was initiated 5-10 s prior to stimulus delivery in each trial and terminated around 10 s following the end of stimulus delivery. A digital trigger marking the beginning and end of stimulation was recorded.

EMG Activity: In addition to limb kinematics, EMG activity was recorded through the bipolar intramuscular electrodes placed in the main flexor and extensor muscles of the hip, knee and ankle. EMG activity was preamplified (x100), band-pass filtered (30 – 1000 Hz) and digitized at a rate of 4000 samples/s.

Data Analysis

All data analysis was conducted using custom-written MATLAB programs (The Mathworks Inc., Natick, Massachusetts, USA).

Calculation of end-point movement vectors

Limb movements evoked by intramuscular, epineural and intraspinal stimulation were represented by end-point movement vectors. For each stimulation trial, the recordings from the 4 motion sensors and the measured lengths of hindlimb segments were used to determine the initial and final positions of the limb and the trajectories of joint motion during stimulation (see Figure 5-2b in Chapter 5). A two-dimensional end-point movement vector was then calculated for each trial based on the initial and final positions of the mid-metatarsal motion sensor.

Analysis of EMG activity and calculation of EMG vectors

a) EMG activity:

Several pieces of information were extracted from the EMG activity evoked in 7 hindlimb muscles after each stimulus train. These included: EMG onset latency, duration of EMG activity, latencies of first and second EMG peaks, EMG amplitude, temporal jitter and amplitude jitter in EMG activity, and a summary of the number of muscles (out of those sampled) activated during each experimental state.

Measurement of onset latency of EMG activity was detailed in a previous publication (Prochazka et al., 2002). Briefly, EMG responses to each stimulus pulse in a train were full-wave rectified, aligned based on stimulus trigger, overlayed, and an average EMG trace was calculated. A 5-ms period of EMG activity immediately preceding the stimulus trigger was used as baseline and the point after stimulus trigger at which the average EMG trace traversed the baseline level + **n***standard deviation (S.D.) of baseline was assigned as the onset latency. The value of **n** varied between 3.0 and 3.5. To determine the duration of EMG activity evoked per trial in each muscle, the time of offset of EMG activity was first obtained (point at which the average EMG activity fell and remained below baseline level + **n***S.D.) and the absolute difference between onset and offset latencies was calculated. Latencies of first and second EMG peaks were determined on a pulse-by-pulse basis. That is, for each muscle, the non-rectified EMG response to each pulse in a stimulus train was used and the times at which the maximum and minimum peaks occurred were determined relative to stimulus trigger. The latencies of first and second EMG peaks were then averaged for each trial and the standard deviation and coefficient of variation were calculated. The coefficient of variation of the latency of the first EMG peak was used to describe the temporal jitter in EMG activity between experimental states. EMG amplitude was also determined on a pulse-by-pulse basis. The rectified EMG response per pulse in a stimulus train was averaged, starting 1.5 ms after stimulus trigger (to bypass any stimulus artifacts) and ending 20 ms after the trigger. The resulting EMG amplitudes were then averaged and the standard deviation and coefficient of variation were calculated. The coefficient of variation was used to describe the jitter in the amplitude of the EMG signals between experimental states.

b) EMG vectors:

Given the magnitude of EMG records acquired per experiment, a method was devised to reduce the representation of EMG activity from the 7 sampled muscles per trial to a single vector (e.g., Figure 7-3c). This was accomplished by converting the evoked response in each muscle to a subvector composed of a magnitude and direction and subsequently summing the 7 individual subvectors to produce a resultant EMG vector. The magnitude of each subvector was based on the amplitude of EMG activity in a given muscle while the direction was based on the angle of the end-point movement vector produced by supra-maximal intramuscular stimulation of the same muscle. The EMG amplitude was calculated as follows. For a given trial, the EMG responses evoked by each pulse in the stimulus train were aligned, overlayed and averaged. The ensuing mean EMG trace was then averaged over the period spanning 1.5 ms to 20 ms after the stimulus trigger, resulting in a single value of EMG amplitude per muscle.

The general directions of EMG and movement vectors closely corresponded to each other in nearly 80% of the trials. However, in this study, the resultant EMG vectors were only used to facilitate the representation of the EMG data and should not be thought of as reliable predictors of end-point movement vectors for several reasons. First, EMG activity was recorded from only 7 hindlimb muscles; thus, the resultant EMG vectors may have inadvertently excluded the contribution of a multitude of other muscles activated by the stimulus. The end-point movement vectors, on the other hand, represented the net action of all activated muscles. Second, the EMG amplitudes were not normalized and the absolute amplitude values per muscle were used instead. This was due to the lack of a consistent normalization value (e.g., EMG activity evoked by maximal epineural stimulation) in all experiments. The use of absolute amplitude values may result in a systematic bias in the representation of some muscles due to, for instance, a less than optimal placement of intramuscular electrodes. Third, the EMG subvectors were linearly summed to produce the resultant EMG vectors. This ignores the biomechanical articulation of the sampled muscles and their viscoelastic properties, both of which lead to a non-linear summation of individual movement vectors.

Localization of intraspinal microwire tips

At the end of each experiment, the cat were deeply anesthetized with an intravenous injection of sodium pentobarbital (25 mg/kg) and subsequently perfused through the heart using a 3.7% formaldehyde solution. The stimulated region of the spinal cord was then removed with the microwires in place and stored in the same fixative. One to four weeks later, the spinal cord was sectioned and the locations of the implanted microwires were determined and marked on anatomical cross-sections of the lumbosacral spinal cord obtained from Vanderhorst and Holstege (Vanderhorst and Holstege, 1997). The locations of microwire tips were also marked on a three-dimensional model of the cat lumbosacral cord (Yakovenko et al., 2002).

RESULTS

Contribution of peripheral elements to movement construction

Elucidating the contribution of the intermediate regions of the spinal cord to movement construction necessitates the characterization of the type of movements that can be generated by the periphery, taking into consideration the biomechanical role of limb structure, articulation and innervation. To determine the peripheral guidelines of movement construction we directly activated the main hip, knee and ankle flexor and extensor muscles either through intramuscular stimulation or epineural stimulation of the nerve branches innervating these muscle groups. The result was the generation of 6 distinct movements of the hindlimb in the saggital plane, combinations of which would produce movements covering the full workspace of the limb. End-point movement vectors evoked by intramuscular stimulation of the main hip, knee and ankle flexor and extensor muscles in one cat under anesthesia are shown in Figure 7-2. Figure 7-2a outlines the limb positions immediately prior to and at the end of stimulus delivery (with maximal stimulus amplitude of 3 to 4x threshold) as well as the resulting end-point movement vectors. Mean ± S.D. of maximal stimulus amplitude for all muscles in this example was 1.49 ± 1.42 mA (range: 0.55 to 4.00 mA). Figure 7-2b illustrates all end-point vectors obtained by trains of stimuli with amplitudes ranging between 1.2 to 4x threshold in the same cat. End-point movement vectors evoked by intramuscular stimulation were similar between cats. Mean ± SD of vector direction and magnitude evoked by stimulating SA, IP, SM, BF, VL, TA and

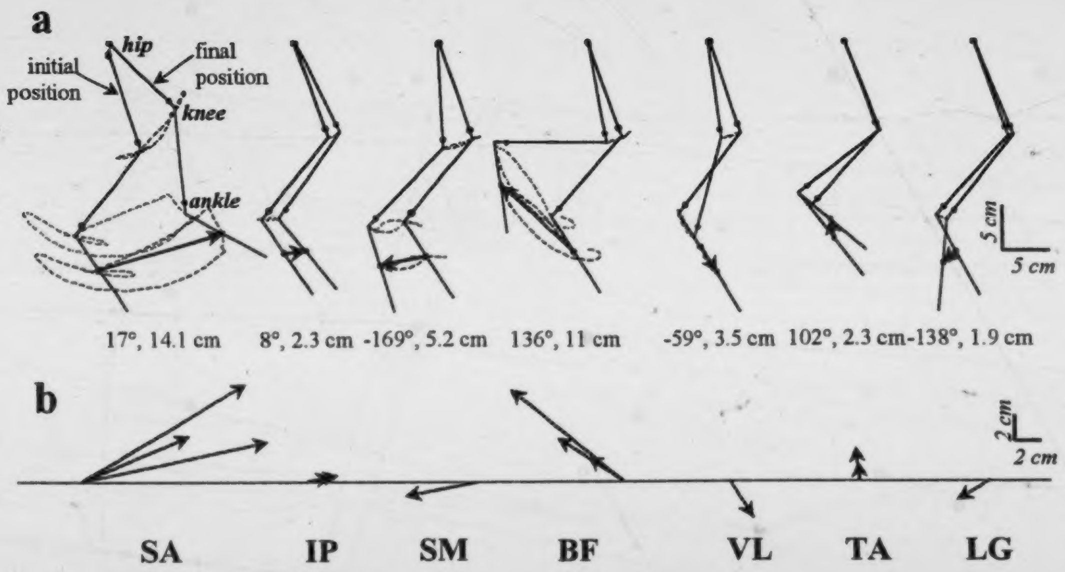

Figure 7-2. End-point movement vectors generated by intramuscular stimulation of the main hip, knee and ankle flexor and extensor muscles in one cat under anesthesia. **a.** Limb positions prior to and at the end of intramuscular stimulation of SA, IP, SM, BF, VL, TA and LG. All movements were evoked by stimulating with maximal pulse amplitude of 3 to 4x threshold. **b.** End-point movement vectors generated by intramuscular stimulation of the same muscles in **a** at varying stimulus amplitudes, ranging from 1.2 to 4x threshold.

LG in 4 cats were 15.4 ± 7.3° and 8.3 ± 4.4 cm, 7.2 ± 2.2° and 2.5 ± 0.9 cm, 177.0 ± 3.6° and 6.8 ± 6.0 cm, 139.9 ± 5.1° and 6.5 ± 3.6 cm, -73.0 ± 10.8° and 4.5 ± 1.6 cm, 88.0 ± 8.3° and 3.3 ± 1.8 cm, -158.8 ± 7.5° and 3.1 ± 0.6 cm, respectively.

Figure 7-3a shows the end-point movement vectors elicited by epineural stimulation of nerve branches innervating the main hip, knee and ankle flexor and extensor muscles in another cat under anesthesia. Stimulus amplitudes varied between 1.2 to 4x threshold (threshold mean ± SD = 64 ± 38 μA). Vectors elicited by stimulating hip flexor (HF), hip extensor (HE), knee flexor (KF), knee extensor (KE), ankle flexor (AF) and ankle extensor (AE) nerve branches were similar between cats. Mean ± S.D. of vector direction and magnitude evoked by stimulation of HF, HE, KF, KE, AF and AE nerve branches in 2 cats were 29.5 ± 4.5° and 11.0 ± 4.4 cm, 175.1 ± 7.4° and 9.5 ± 4.7 cm, 135.9 ± 3.8° and

14.5 ± 2.6 cm, -34.3 ± 7.9° and 5.7 ± 1.2 cm, 87.7 ± 2.1° and 6.9 ± 2.5 cm, -155.0° ± 24.0 and 3.8 ± 1.4 cm, respectively.

Figure 7-3b shows the resultant EMG vectors obtained by epineural stimulation of each of the nerves of interest (solid lines) at various stimulus amplitudes. The dashed lines show the angle of the end-point movement vectors evoked by supramaximal intramuscular stimulation (> 4x threshold) of each muscle and used in calculating the resultant EMG vector. In this cat, angles of EMG subvectors for SA, IP, SM, BF, VL, TA and LG were 31°, 12°, 176°, 141°, -29°, 95° and -139°, respectively.

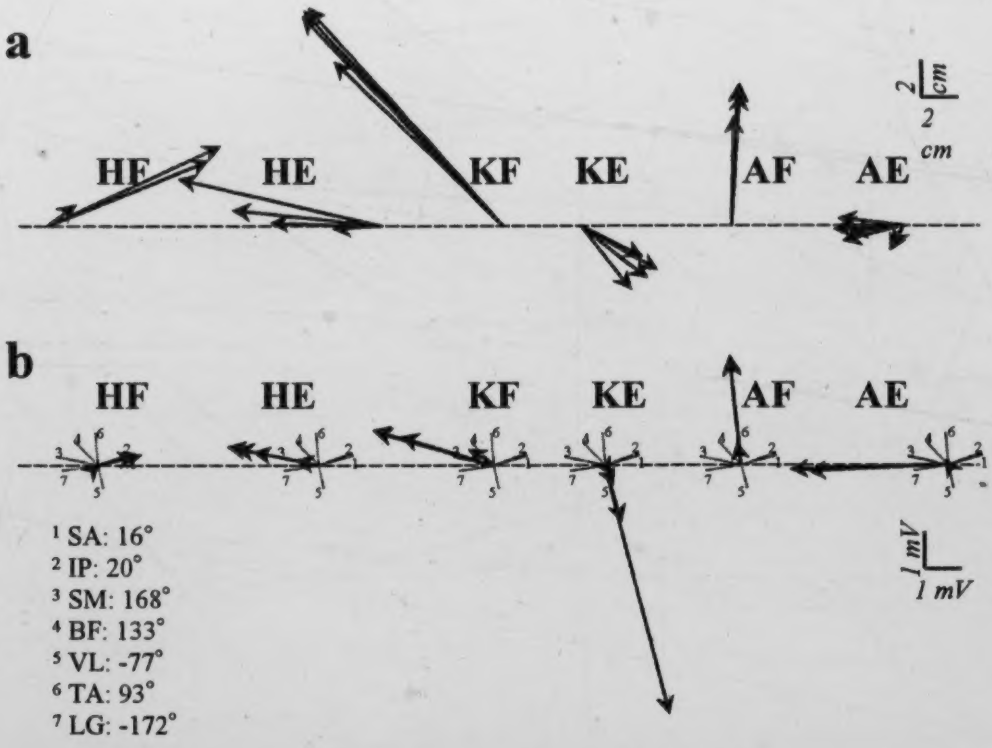

Figure 7-3. End-point movement vectors evoked by epineural stimulation of nerves innervating the main hip, knee and ankle flexor and extensor muscles and the resultant EMG vectors in one cat under anesthesia. **a.** End-point movement vectors generated by stimulus trains of varying amplitudes, ranging from 1.2 to 4x threshold. **b.** The resultant EMG vectors obtained by summing the 7 subvectors produced by the stimulation of each nerve. The multiple arrows represent the vectors produced during nerve stimulation at varying stimulus amplitudes (same amplitudes as in **a**).

Characterization of the role of intermediate neuronal elements in movement construction

Figure 7-4 illustrates the tip locations of intraspinal microwires in 3 cats. The locations were transposed on serial horizontal cross-sections in Figure 7-4a, each representing ~3mm of tissue and spanning the lumbosacral portion of the spinal cord. The anatomical cross-sections were digitized from Vanderhorst and Holstege (Vanderhorst and Holstege, 1997) and the location of segmental labels (L5-S1) corresponds to the beginning of each spinal cord segment. The microwire tips targeted the intermediate laminae of the gray matter (filled black circles). The same tip locations are shown in a three-dimensional model of the spinal cord in Figure 7-4b (Yakovenko et al., 2002). The model is composed of serial cross-sections of the lumbosacral spinal cord, each ~1mm thick, and the arrows from Figure 7-4a point to the corresponding cross-section in Figure 7-4b. Each colorful dot represents a motoneuron and the location of the muscle labels corresponds to the location of the center of mass of their respective motoneuronal pool (Yakovenko et al., 2002). The inset (right) provides a horizontal view of the lumbosacral cord (looking through the central canal) with the microwire tips in place. The "cloud" of colorful dots represents the motoneuronal pools. Note that the vast majority of the filled black circles are located dorsal and medial to the motoneuronal pools.

End-point movement vectors and resultant EMG vectors evoked by ISMS of the intermediate gray matter in one cat under anesthesia are shown in Figure 7-5. The locations of microwire tips are transposed on the 3D model in Figure 7-5a and a 2D horizontal projection of these locations is shown in Figure 7-5b. Figure 7-5c shows all the end-point movement vectors elicited by trains of ISMS with pulse amplitudes ranging from 1.2 to 4x threshold and Figure 7-5d shows the resultant EMG vectors. Mean ± S.D. of ISMS threshold in this cat was 91 ± 52 μA. Limb movements evoked by pulse amplitudes >4x threshold or those eliciting movement vectors with magnitudes < 1 cm are not shown; thus the missing end-point and EMG vectors for some microwire tip locations in the figure. Three important observations can be noted from the end-point movement vectors elicited by ISMS of the intermediate lumbosacral cord under anesthesia. First, some limb movements, similar to those obtained by direct stimulation of the periphery can be identified with ISMS. For example, end-point vectors evoked by ISMS through microwires 4 and 5 resemble HF, microwire 8 KE, microwire 9 AF, microwire 15 HE,

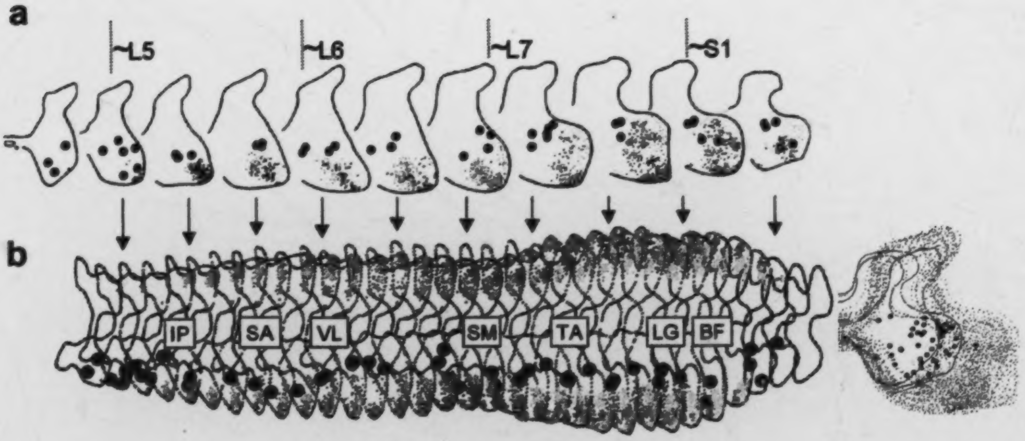

Figure 7-4. Locations of intraspinal microwire tips from 3 cats. **a.** Tip locations transposed on anatomical cross-sections of the lumbosacral spinal cord obtained from Vanderhorst and Holstege (Vanderhorst and Holstege, 1997). The filled back circles represent all the intermediate spinal locations stimulated. The small colorful dots represent the motoneuronal pools at the corresponding cross-sectional level. Each cross section represents ~3 mm of spinal cord tissue and the segmental labels (L5-S1) are positioned approximately at the beginning of each corresponding spinal cord segment. **b.** Microwire tip locations transposed on a 3D model of the lumbosacral spinal cord (Yakovenko et al., 2002). Each cross-section represents ~1 mm of tissue and the arrows from **a** point to the corresponding cross-sectional level in **b**. The location of the muscle labels (IP, SA, VL, SM, TA, LG and BF) represents the location of the center of mass of their respective motoneuron pools (Yakovenko et al., 2002). Inset: 2D projection of the location of microwire tips in the horizontal plane, looking through the central canal. The "cloud" of colorful dots represents the motoneuronal pools. Note that the vast majority of the intermediate microwire tip locations were dorsal and medial to the motoneuronal pools.

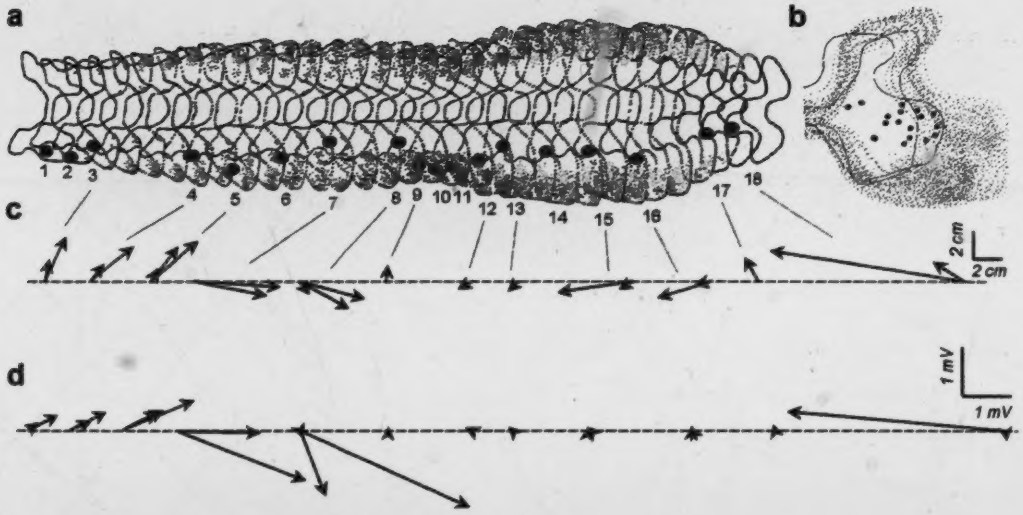

Figure 7-5. End-point movement vectors evoked by ISMS of the *intermediate gray matter* and resultant EMG vectors in one cat under anesthesia. **a.** Locations of microwire tips throughout the lumbosacral spinal cord, transposed on a 3D model. **b.** View of the microwire tips in the horizontal plane. Note that the majority of microwire tip locations were dorsal and medial to the motoneuronal pools. **c.** Movement vectors evoked by stimulating through each of the microwires individually and at varying levels of stimulus amplitude, ranging from 1.2 to 4x threshold. **d.** Resultant EMG vectors corresponding to ISMS through each microwire individually and at varying stimulus amplitudes.

microwire 16 AE and microwire 18 KF. ISMS through the remaining microwires produced end-point vectors resembling combinations of the 6 distinct vectors; e.g., end-point vector evoked by ISMS through microwire 7 may be the result of a combined activation of HF and KE. Second, directions of the end-point vectors evoked by ISMS of intermediate laminae under anesthesia can be predicted from the anatomical distribution of the motoneuronal pools within the stimulated segmental level. For example, the distribution of microwire tips through which ISMS evoked end-point vectors resembling HF, KE, HE, AF, AE and HF approximately corresponds to the distribution of motoneuron pools innervating IP, SA, VL, SM, TA, LG and BF, respectively. Third, evoked movement vectors may also be the result of the activation of neuronal elements within the inherent flexor or extensor reflexes in the spinal cord. For example, the end-point vector evoked by ISMS through microwire 3 may be the result of a combined activation of HF and AF (through interneuronal connections) or the result of activating elements of a flexor reflex. In addition to the coordinated flexor responses, ISMS through some microwires generated powerful extensor synergies (not shown in the example in Figure 7-5).

End-point vectors evoked by ISMS of the intermediate laminae were similar in all animals tested (n = 3). Mean ± S.D. of threshold and maximal ISMS amplitudes used in all animals under anesthesia were 96 ± 50 μA and 258 ± 121 μA, respectively. In all animals, end-point vector directions elicited by ISMS varied somewhat with changes in stimulus amplitude (e.g., Figure 7-5c). The maximal difference in vector direction (i.e., the maximal deviation for each electrode) and the corresponding change in vector magnitude as a function of stimulus amplitude were quantified for all end-point vectors with magnitudes $\geq$1 cm. Mean ± S.D. and median change in vector angle were 27.1 ± 28.2° and 18°, respectively. The corresponding changes in vector magnitude were 3.3 ± 2.7 cm and 2.5 cm. Stimulation through 60% of the microwires resulted in angle changes < 20°, while 3% resulted in changes > 100°.

Effect of descending input on spinal elements of movement construction

To determine the level of autonomy of the hypothesized neuronal elements of movement construction in the intermediate laminae of the spinal cord from descending input, the state of descending drive was altered through acute decerebration and subsequently through acute low-thoracic spinalization. Once decerebration was completed at the intercollicular level and the effect of anesthesia vanished (i.e., decerebrate rigidity was visible and spinal reflexes recovered), ISMS through the same intraspinal microwires was repeated and the evoked end-point vectors and resultant EMG vectors were determined. The same steps were then repeated after spinalization following the recovery of spinal reflexes (end of spinal shock). Figure 7-6 shows the end-point movement and resultant EMG vectors evoked by ISMS of the intermediate laminae under the three experimental states in one animal (same animal in Figure 7-5). Figure 7-6a displays again the location of the microwire tips along the lumbosacral spinal cord. Figure 7-6b shows all the end-point vectors evoked by stimulating with pulse amplitudes of 1.2 to 4x threshold under anesthesia, decerebration and spinalization and Figure 7-6c shows the corresponding resultant EMG vectors. The most striking observation in this example is the dramatic change in the direction of end-point movement vectors resulting from the alteration of descending drive. In 2 animals (including the example in Figure 7-6) almost all extensor movement vectors were lost following acute decerebration and spinalization. This suggested that the observed changes in vector direction with altered descending input could reflect a shift in the excitability of neuronal elements in the intermediate laminae, bringing to light those elements most susceptible to anesthesia. However, the dominant presence of flexor reflexes following acute spinalization may also be the result of flexor release (Sherrington, 1910). Mean ± S.D. of threshold and maximal stimulus amplitudes used for ISMS of the intermediate laminae in 3 cats were 28 ± 27 μA and 87 ± 99 μA under decerebration and 59 ± 26 μA and 195 ± 95 μA under spinalization. Stimulus amplitudes used under decerebration and spinalization were significantly lower ($p < 0.05$) than those used under anesthesia.

In general, the end-point movement vectors elicited by ISMS of the intermediate laminae after acute decerebration or spinalization could be subdivided into 3 classes of flexor reflex movements and 1-2 classes of extensor movements. The directions of the flexor classes could be loosely characterized as upward (center ~90°), upward forward (center ~60°) and upward-backward (center ~120°). The orientation of the flexor reflex movements was dependent on the site of stimulation in the spinal cord. For example, upward-forward movements were elicited from rostral regions of the lumbosacral cord containing hip flexor motoneurons while upward-backard movements were elicited by stimulating caudal regions of the cord containing knee flexor motoneurons. Upward forward movements were elicited from regions containing ankle flexor motoneurons (central regions of the lumbosacral cord). Thus, the orientation of flexor movements could be predicted from the anatomical distribution of motoneurons innervating flexor muscles in the hindlimb. The extensor movements were infrequently evoked by ISMS of the intermediate regions after acute decerebration and spinalization. When present, extensor movements were centered around -60° and -120°, reflecting the anatomical distribution of extensor motoneurons.

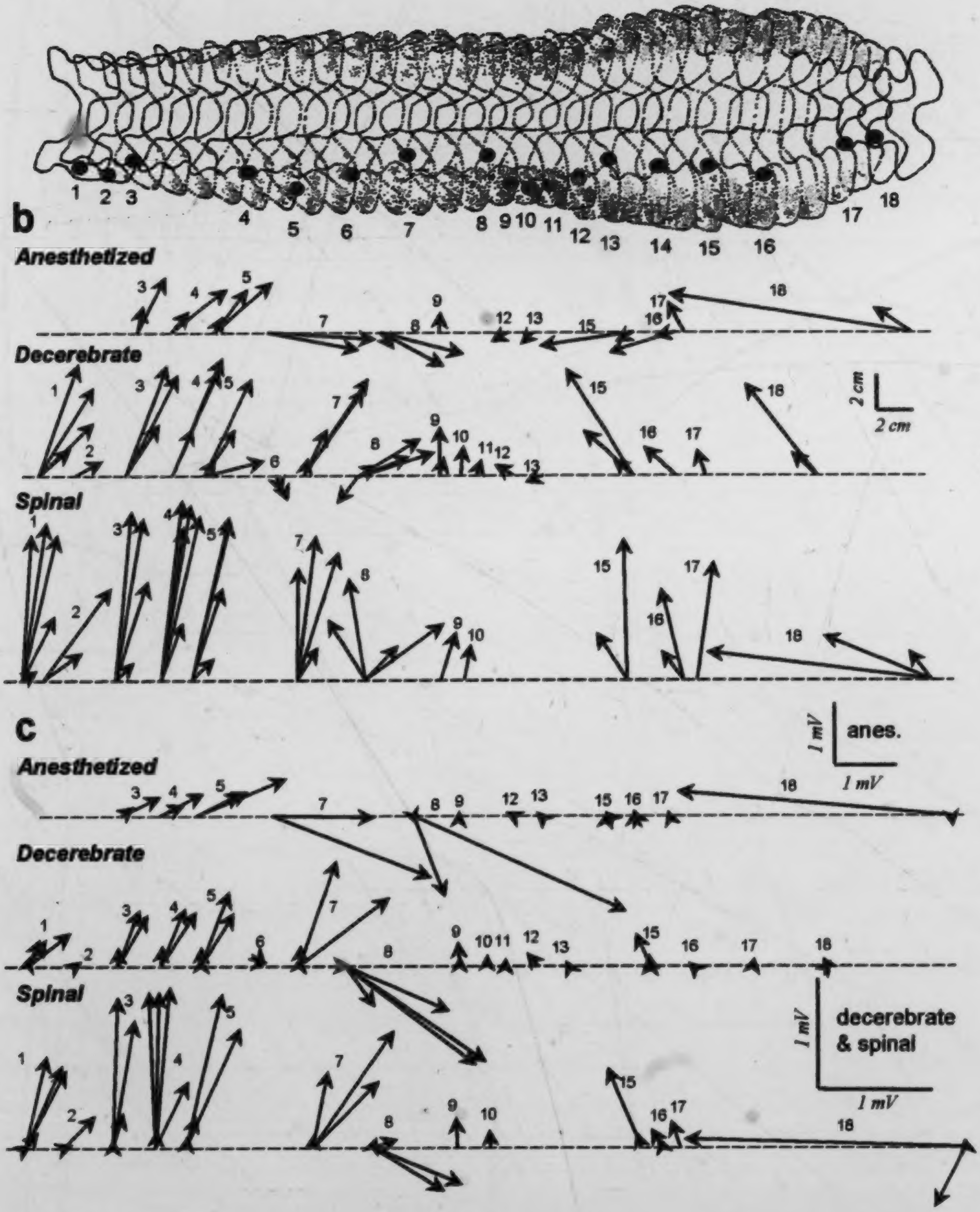

Figure 7-6. End-point movement vectors evoked by ISMS of the *intermediate spinal cord* under conditions of anesthesia, decerebration and low-thoracic spinalization in one cat. **a.** Locations of intraspinal microwire tips throughout the lumbosacral spinal cord. **b.** End-point movement vectors evoked by ISMS through each microwire individually, at varying stimulus amplitudes (1.2 – 4x threshold), and under three different states of descending input. **c.** Resultant EMG vectors corresponding to the same ISMS stimuli in **b**.

Similar to the end-point movement vectors evoked by ISMS under anesthesia, the direction of vectors elicited under decerebration and spinalization covaried with stimulus amplitude in all animals. Under decerebration, the mean ± S.D. and median of change in vector angle was 24.2 ± 28.7° and 13° and the corresponding change in vector magnitude was 4.5 ± 2.9 cm and 5.1 cm. Stimulation through 70% of the microwires resulted in angle changes < 20°, while 3% resulted in changes > 100°. Under spinalization, vector changes as a function of stimulus strength were 35.5 ± 29.7° and 32°, 4.0 ± 3.0 cm and 3.2 cm. Stimulation through 40% of the microwires resulted in angle changes < 20°, while 10% resulted in changes > 100°. To ensure the stability of the decerebrate and spinal states, thus the validity of the ISMS evoked responses, records obtained early after decerebration or spinalization (~60 min post) were repeated at a later time (2-3 hours post) and compared in 3 cats. The range, between cats, of average changes in end-point vector directions and amplitudes early and late after decerebration and spinalization were 5.5 ± 4.3° to 9.0 ± 4.7° and 0.8 ± 0.6 to 5.4 ± 2.3 cm, and 5.7 ± 2.1° to 9.4 ± 7.1° and 0.6 ± 0.4 to 1.5 ± 0.5 cm, respectively. Given these relatively small changes in vector direction and magnitude, the decerebrate and spinal states were judged to be stable in all cats tested.

Figure 7-7a shows an example of the EMG activity evoked by ISMS through a single microwire under the three experimental states, with pulse amplitude of 2.5x threshold. Figure 7-7b displays the positions of the limb immediately prior to and at the end of stimulus delivery, the trajectories of joint movements during stimulation and the end-point movement vectors. There was a significant change in the evoked EMG signals between states as well as in the trajectory of hindlimb movement. Under conditions of acute decerebration and spinalization, flexor muscles were most dominantly activated by ISMS of the intermediate laminae. This often resulted in diminishing the extensor movements evoked under anesthesia. Note that the end-point movement vector resulting from eliciting a flexor reflex is similar to that evoked by direct stimulation of TA or AF nerve. This is a result of the lack of uniqueness of the end-point movement vectors used in this study.

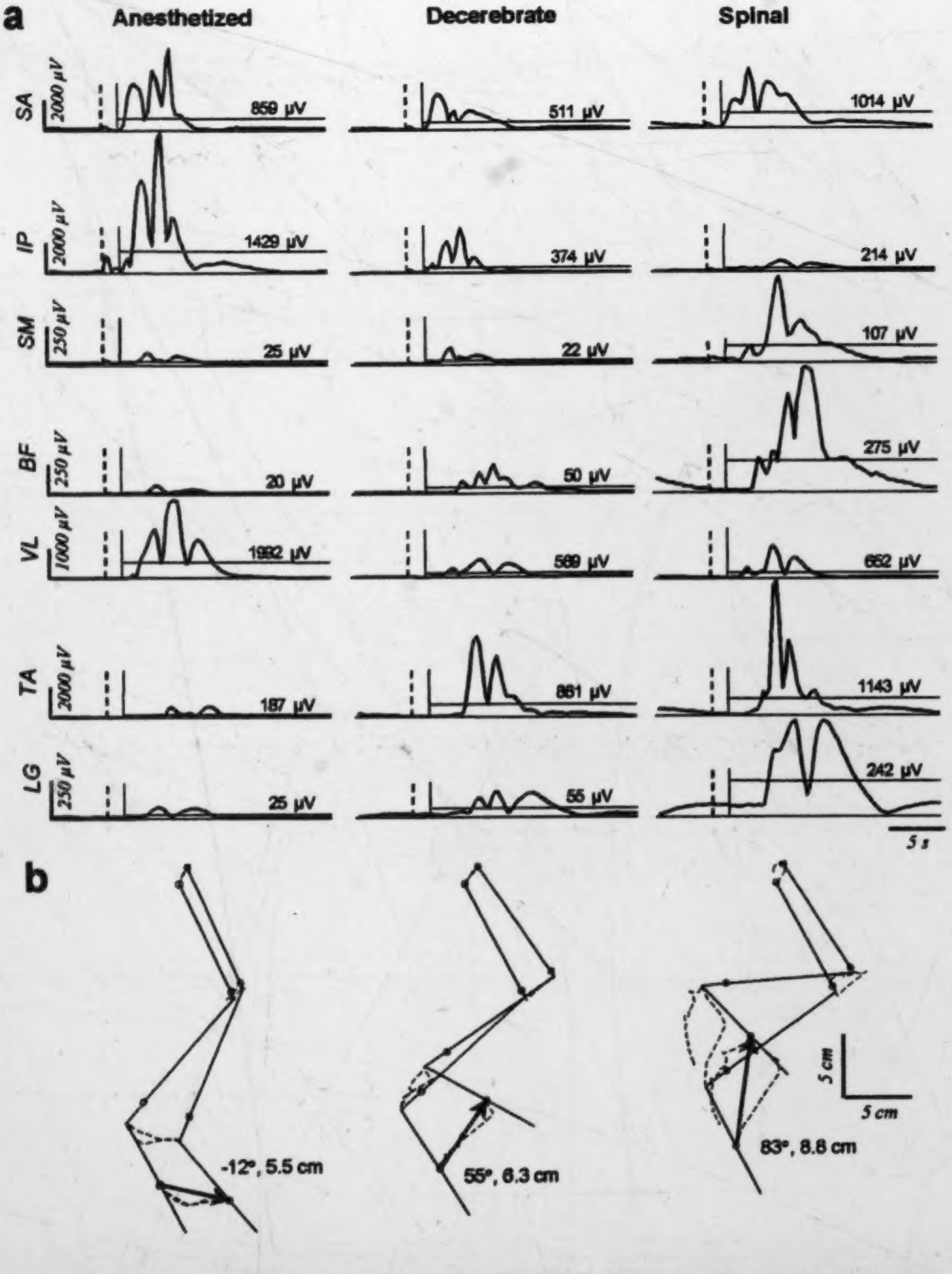

Figure 7-7. Example of changes in movement composition between experimental states. **a.** EMG activity recorded from 7 hindlimb muscles during ISMS through one intraspinal microwire at 2.5x threshold, under anesthesia, decerebration and spinalization in the same cat shown in Figure 6. **b.** Positions of the right hindlimb immediately before and at the end of stimulus delivery. Shown also are the trajectories of joint movements during stimulation. Note the significant change in movement trajectory between experimental states.

Summary of evoked responses under conditions of intact and interrupted descending drive

Figure 7-8 summarizes the changes in the direction of end-point movement vectors between states in 3 cats with ISMS in intermediate and ventral locations. The absolute difference in vector direction was calculated for trials in the same animal in which stimulus amplitudes (relative to threshold) between experimental states could be matched. All vectors with magnitudes <1 cm were excluded. Figure 7-8a shows the distribution of end-point vector directions for each of the experimental states. The vector directions under anesthesia were not statistically different from uniform distribution ($p > 0.05$, Kolmogorov-Smirnoff test). The distributions under decerebration and spinalization were significantly different from uniform ($p < 0.001$) and from the distribution under anesthesia ($p < 0.01$) but were not significantly different from each other. In particular, the distributions obtained under decerebration and spinalization lacked vectors with negative (extension) directions. Figure 7-8b shows the distribution of change in vector directions between states, further emphasizing the shift towards flexor dominance under decerebration and spinalization. The absolute change in vector directions and magnitudes were 43.3 ± 32.7° (median 36°) and 2.8 ± 3.2 cm (median 1.8 cm) between the anesthetized and decerebrate states, 53.0 ± 51.5° (median 27°) and 3.3 ± 2.8 cm (median 2.8 cm) between the decerebrate and the spinal states and 70.3 ± 53.8° (median 55.5°) and 2.6 ± 2.2 cm (median 2.1 cm) between the anesthetized and spinal states. In other words, in the transition from the anesthetized to the decerebrate states, there was, on average, a 43° in vector angles, mostly towards a more flexed direction. The transition from decerebrate and spinal states also resulted in large changes in end-point vector angles (on average 53°); however, the changes were in random directions.

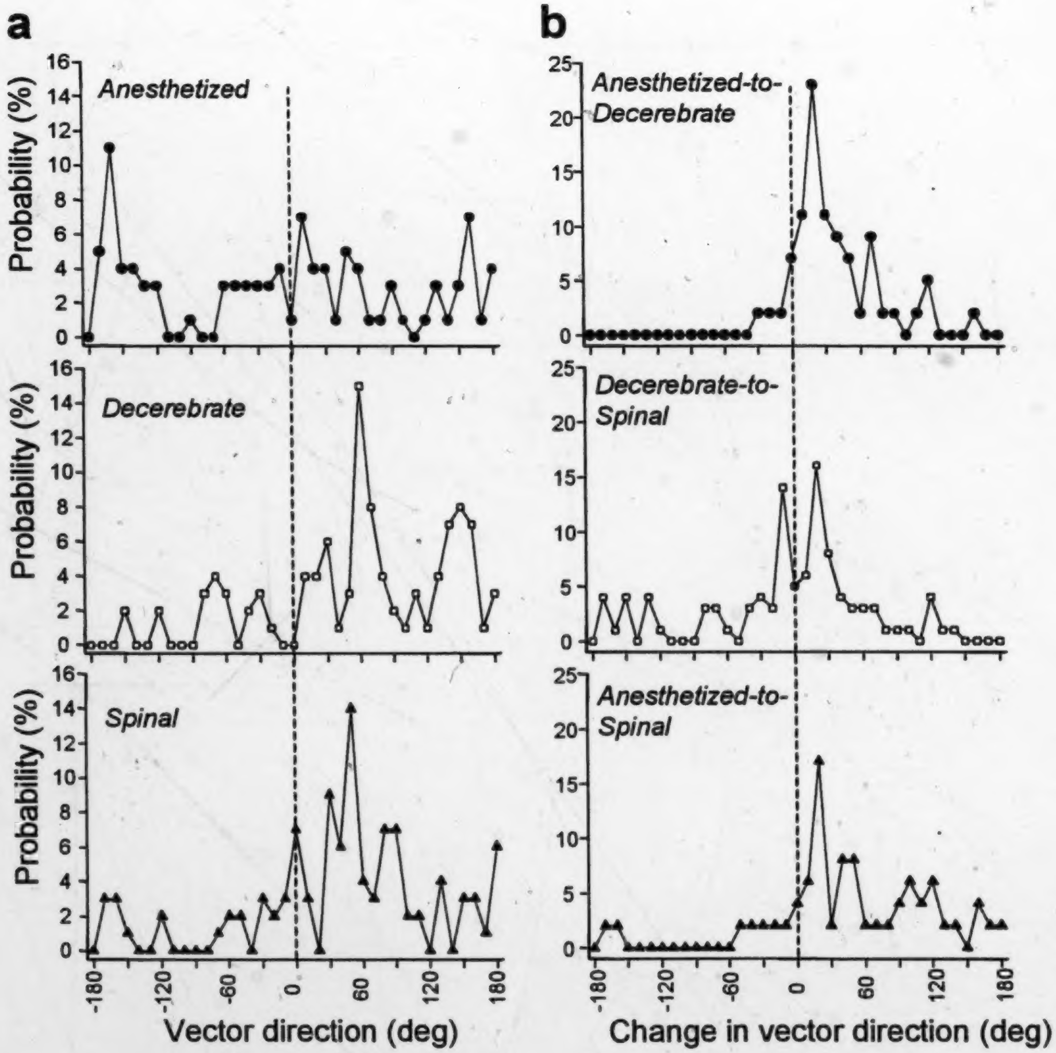

Figure 7-8. Summary of changes in direction of end-point movement vectors between experimental states in all animals. **a.** Distribution of vector directions evoked by ISMS of the intermediate laminae in 3 animals under anesthesia, decerebration and spinalization.

DISCUSSION

The goal of this study was to investigate the nature of neuronal elements within the intermediate laminae of the lumbosacral cord involved in movement construction. We were specifically interested in the hypothesized movement primitives or autonomous movement building blocks thought to reside within these regions of the spinal cord (Giszter et al., 1993; Mussa-Ivaldi et al., 1994; Bizzi et al., 1995; Saltiel et al., 1998; Bizzi et al., 2000; Kargo and Giszter, 2000). In contrast to previous movement primitive studies, the activated hindlimb in the present study was allowed to move freely within a uniform stiffness field in the saggital plane (Figure 7-1). Furthermore, the state of descending input in each experiment was altered systematically to determine the extent of dependence of movement primitives on descending drive.

Two main findings can be extracted from the results of this study. First, intermediate neuronal elements involved in movement construction are organized according to anatomical landmarks in the spinal cord. End-point movement vectors and EMG activity evoked under anesthesia by ISMS in the intermediate laminae corresponded to the anatomical distribution of motoneuronal pools in the lumbosacral spinal cord (Figure 7-5). ISMS through some microwires also generated coordinated flexor (e.g., microwire 3, Figure 7-5c) or extensor synergies. Therefore, we propose that the neuronal networks encompassing the movement building blocks in the intermediate laminae may be composed of local interneuronal circuits involving segmental motoneurons as well as components of inherent spinal reflexes. Alternatively, the end-point movement vectors and EMG activity evoked by ISMS of the intermediate laminae under anesthesia could be a result of direct motoneuronal activation due to stimulus spread, with the contribution of interneuronal connections kept to a minimum as an artifact of anesthesia. In fact, the radius of stimulus spread in the gray matter could be as large as 0.5 and 1.0 mm for pulse amplitudes of 100 and 400 μA, respectively (Mushahwar and Horch, 1997). However, the majority of microwire tips in the intermediate laminae were located more than 1 mm away from the motoneuronal pools (Figure 7-4). Furthermore, 70% of the maximal stimulus amplitudes used in all trials under anesthesia were ≤ 260 μA, resulting in stimulus spread < 0.8 mm.

Second, the basic neuronal elements of movement construction in the intermediate laminae are strongly dependent on descending drive and the excitable state of the spinal cord. There was a significant shift in end-point movement direction towards flexion after decerebration and spinalization. This result questions the suggested autonomous nature of movement primitive circuitry in the intermediate regions of the spinal cord. It also questions the suggested notion that movement primitives form the output elements of the locomotor central pattern generator in mammals (Bizzi, 2000).

The dramatic changes in end-point vectors are most probably due to two factors: the masking of interneuronal networks in the intermediate laminae by anesthesia and the release of flexor reflexes after acute decerebration and spinalization (Sherrington, 1910). They also suggest that testing of the spinal neuronal elements involved in movement construction may best be tested under conditions of chronic spinalization. However, the findings from this study argue to some extent with the results obtained by ISMS of the intermediate laminae in chronically spinalized rats (Tresch and Bizzi, 1999). Different experimental approaches were used (the use of end-point movement vectors instead of isometric force fields to characterize the responses evoked by ISMS of the intermediate laminae and conducting the experiments after acute rather than chronic lesions of the central nervous system). Nonetheless, as in the rat studies, flexor movements were the most frequently evoked responses.

The predominance of flexor movements evoked by ISMS of the intermediate laminae under conditions of decerebration and spinalization disagrees with the suggested notion that basic and unique building blocks of movement construction reside entirely in these regions. Given the importance of extensor activation for maintaining anti-gravity posture in mammals, it is difficult to justify the sparse representation of extensor building blocks in the intermediate laminae of the cat. It would therefore seem more appropriate to conclude that elements of movement construction are distributed throughout the intermediate and ventral laminae of the spinal cord. They include interneurons of inherent spinal reflexes (e.g., interneurons within the flexor reflex afferent pathways), premotoneurons and motoneurons. The specificity of their action appears to be determined by the anatomical distribution of the motoneuronal pools in the spinal cord.

REFERENCES:

1. Bizzi E, Giszter SF, Loeb E, Mussa-Ivaldi FA, Saltiel P (1995) Modular organization of motor behavior in the frog's spinal cord. *Trends Neurosci* 18:442-446.
2. Bizzi E, Tresch MC, Saltiel P, d'Avella A (2000) New perspectives on spinal motor systems. *Nat Rev Neurosci* 1:101-108.
3. Carr PA, Huang A, Noga BR, Jordan LM (1995) Cytochemical characteristics of cat spinal neurons activated during fictive locomotion. *Brain Res Bull* 37:213-218.
4. Cowley KC, Schmidt BJ (1997) Regional distribution of the locomotor pattern-generating network in the neonatal rat spinal cord. *J Neurophysiol* 77:247-259.
5. d'Avella A, Bizzi E (1998) Low dimensionality of supraspinally induced force fields. *roc Natl Acad Sci U S A* 95:7711-7714.
6. Deliagina TG, Orlovsky GN, Pavlova GA (1983) The capacity for generation of rhythmic oscillations is distributed in the lumbosacral spinal cord of the cat. *Exp Brain Res* 53:81-90.
7. Duysens J, Pearson KG (1980) Inhibition of flexor burst generation by loading ankle extensor muscles in walking cats. *Brain Res* 187:321-332.
8. Giszter SF, Grill WM, Lemay MA, Mushahwar VK, Prochazka A (2000) Intraspinal Microstimulation: Techniques, Perspectives and Prospects for FES. In: Neural Prostheses for Restoration of Sensory and Motor Function (Chapin JK, Moxon KA, eds), pp 101-138. London: CRC Press.
9. Giszter SF, Mussa-Ivaldi FA, Bizzi E (1993) Convergent force fields organized in the frog's spinal cord. *J Neurosci* 13:467-491.
10. Gosgnach S, Quevedo J, Fedirchuk B, McCrea DA (2000) Depression of group Ia monosynaptic EPSPs in cat hindlimb motoneurones during fictive locomotion. *J Physiol (Lond)* 526:639-652.
11. Grill WM (2000) Electrical activation of spinal neural circuits: application to motor-system neural prostheses. *Neuromodulation* 3:97-106.
12. Hamm TM, Koehler W, Stuart DG, Vanden Noven S (1985) Partitioning of monosynaptic Ia excitatory post-synaptic potentials in the motor nucleus of the cat semimembranosus muscle. *J Physiol (Lond)* 369:379-398.
13. Huang A, Noga BR, Carr PA, Fedirchuk B, Jordan LM (2000) Spinal cholinergic

neurons activated during locomotion: localization and electrophysiological characterization. *J Neurophysiol* 83:3537-3547.

14. Jankowska E (1992) Interneuronal relay in spinal pathways from proprioceptors. *Prog Neurobiol* 38:335-378.

15. Kargo WJ, Giszter SF (2000) Rapid correction of aimed movements by summation of force-field primitives. *J Neurosci* 20:409-426.

16. Kjaerulff O, Kiehn O (1996) Distribution of networks generating and coordinating locomotor activity in the neonatal rat spinal cord in vitro: a lesion study. *J Neurosci* 16:5777-5794.

17. Lam TPKG (2001) Proprioceptive modulation of hip flexor activity during the swing phase of locomotion in decerebrate cats. *J Neurophysiol* 86:1321-1332.

18. Lemay MA, Galagan JE, Hoga N, Bizzi E (2001) Modulation and vectorial summation of the spinalized frog's hindlimb endpoint force produced by intraspinal electrical stimulation of the cord. *IEEE Trans Neural Syst Rehabil Eng* 9:12-23.

19. Lemay MA, Grill WM (1999) Spinal force fields in the cat spinal cord. In: *29th Annual Meeting of the Society for Neuroscience*, p 1396. Miami Beach, Florida.

20. McCrea DA, Shefchyk SJ, Stephens MJ, Pearson KG (1995) Disynaptic group I excitation of synergist ankle extensor motoneurones during fictive locomotion in the cat. *J Physiol (Lond)* 487:527-539.

21. Mushahwar VK, Collins DF, Prochazka A (2000) Spinal cord microstimulation generates functional limb movements in chronically implanted cats. *Exp Neurol* 163:422-429.

22. Mushahwar VK, Gillard DM, Gauthier MJA, Prochazka A (in press) Spinal cord microstimulation generates locomotor-like and feedback-controlled movements. *IEEE Trans Neural Syst Rehabil Eng.*

23. Mushahwar VK, Horch KW (1997) Proposed specifications for a lumbar spinal cord electrode array for control of lower extremities in paraplegia. *IEEE Trans Rehabil Eng* 15:237-243.

24. Mussa-Ivaldi FA, Giszter SF, Bizzi E (1994) Linear combinations of primitives in vertebrate motor control. *Proc Natl Acad Sci U S A* 91:7534-7538.

25. Noga BR, Fortier PA, Kriellaars DJ, Dai X, Detillieux GR, Jordan LM (1995) Field

potential mapping of neurons in the lumbar spinal cord activated following stimulation of the mesencephalic locomotor region. *J Neurosci* 15:2203-2217.

26. Orlovsky GN, Deliagina TG, Grillner S (1999) Neuronal Control of Locomotion. New York: Oxford University Press, Inc.

27. Pearson KG, Ramirez JM, Jiang W (1992) Entrainment of the locomotor rhythm by group Ib afferents from ankle extensor muscles in spinal cats. *Exp Brain Res* 90:557-566.

28. Perreault MC, Shefchyk SJ, Jimenez I, McCrea DA (1999) Depression of muscle and cutaneous afferent-evoked monosynaptic field potentials during fictive locomotion in the cat. *J Physiol (Lond)* 521:691-703.

29. Prochazka A, Mushahwar VK, Yakovenko S (2002) Activation and coordination of spinal motoneuron pools after spinal cord injury. *Prog Neurobiol*.

30. Quevedo J, Fedirchuk B, Gosgnach S, McCrea DA (2000) Group I disynaptic excitation of cat hindlimb flexor and bifunctional motoneurones during fictive locomotion. *J Physiol (Lond)* 525:549-564.

31. Saltiel P, Tresch MC, Bizzi E (1998) Spinal cord modular organization and rhythm generation: an NMDA iontophoretic study in the frog. *J Neurophysiol* 80:2323-2339.

32. Sherrington CS (1910) Flexion-reflex of the limb, crossed extension-reflex, and reflex stepping and standing. *J Physiol (Lond)* 40:28-121.

33. Tresch MC, Bizzi E (1999) Responses to spinal microstimulation in the chronically spinalized rat and their relationship to spinal systems activated by low threshold cutaneous stimulation. *Exp Brain Res* 129:401-416.

34. Vanderhorst VGJM, Holstege G (1997) Organization of lumbosacral motoneuronal cell groups innervating hindlimb, pelvic floor, and axial muscles in the cat. *J Comp Neurol* 382:46-76.

35. Yakovenko S, Mushahwar V, VanderHorst V, Holstege G, Prochazka A (2002) Saptiotemporal activation of lumbosacral motoneurons in the locomotor step cycle. *J Neurophysiol* 87:1542-53.

CHAPTER 8

DIFFERENTIAL DISTRIBUTION OF THE INTERNEURONS IN THE NEURAL NETWORKS FOR WALKING IN THE MUDPUPPY (*Necturus Maculatus*) SPINAL CORD*

INTRODUCTION

Locomotion can be generated by neuronal networks in the spinal cord (Székely et al. 1969; Delcomyn 1980; Grillner 1981, 1985; Pearson 1993). Descending and sensory inputs play an important role in modulating the activities of the spinal neuronal networks so as to provide an adaptive capacity of locomotor patterns to a changing external environment (Jordan 1991; Armstrong 1988; Pearson 1993, 1995). The work on the lamprey (Grillner 1985; Grillner et al.1991; Grillner and Matsushima 1991) and tadpole (Roberts et al. 1995, 1998) have opened the way to an understanding at the cellular level of the circuitry responsible for generating and coordinating the bending motion of the trunk required for swimming. An essential feature of the characterized segmental circuitry is a pair of half centres that are mutually inhibitory and contribute to burst generation.

Progress has also been made to localize the networks for mammalian walking, a more complex motor task that involves coordinated limb movement about multiple joints in different limbs (e.g., Deliagina et al. 1983; Cazalets et al. 1995; Bracci et al. 1996; Kjaerulff and Kiehn 1996). However, the complexity of mammalian spinal cord makes it difficult experimentally to investigate the neuronal organization of the circuitry for walking. We have studied *in vitro* a simpler, amphibian preparation from the mudpuppy (Wheatley and Stein 1992, Wheatley et al. 1992) and demonstrated distinct flexor and extensor centres in the spinal cord for elbow movements that could generate rhythmic motor output independent of each other (Cheng et al. 1998). In this study, we further

---

* A version of this chapter will be published in *Exp Brain Res* by the authors of Cheng J, Jovanovic K, Aoyagi Y, Bennett, DJ, Han Y, Stein RB. Contribution to paper: participated in 25% of experiments and contributed

attempted to identify interneurons within these centres, to classify them in phases of the step cycle and to explore the connectivity between the interneurons and motoneurons. The previous study by Wheatley et al. (1994) only recorded cells spanning the C3 segment. In light of the finding of distinct flexor and extensor centers (Cheng et al. 1998), we studied cells extending from several mm rostral to the C2 root to several mm caudal to the C3 root. This region should contain both the flexor and extensor centers and allow us to determine the distribution patterns of the four types of rhythmic cells. Parts of this work have been reported in abstract form (Cheng and Stein 1998).

METHODS

Fifty-seven adult mudpuppies (22-28 cm in length) were used for the experiments. The *in vitro* mudpuppy walking preparation has been described previously (Wheatley and Stein 1992; Wheatley et al. 1992; Cheng et al. 1998). Briefly, the preparation contains a part of the spinal cord, the brachial nerves and a forelimb. Following a dorsal laminectomy under anaesthesia [3-aminobenzoic acid ethyl ester (Sigma, St. Louis, MO. 1-2 g/l], the first five segments of the spinal cord were isolated from the rest of the body with the right forelimb attached by the brachial nerves. The paraspinal muscles were removed for stable recording from interneurons. A segment border is defined as midway between two adjacent spinal dorsal roots.

Rhythmic walking-like motion of the leg (0.3 – 1.5 Hz; details in Wheatley et al., 1992) was induced by bath application of N-methyl-D-aspartate (NMDA, 20-120 μM, Sigma, St. Louis, MO) with 5-20 μM D-serine and monitored by electromyography (EMG) of the elbow flexor (*Brachialis*) and extensor (*Anconeus*) muscles. Pairs of fine teflon-insulated silver wires (75 μm in diameter, Medwire, Leico Industries Inc., New York, NY) were inserted into the muscles for EMG recording. The preparation was placed dorsal side up in a recording chamber superfused at a rate of 2-5 ml/min with continuously oxygenated Ringer's solution (NaCl 115 mM; KCl 2 mM; $CaCl_2$ 2 mM, $MgCl_2$ 1.8 mM, Hepes 5 mM, glucose 1 g/l, pH 7.35). The recording chamber consisted of two communicating subdivisions, one for the spinal cord and the other for the limb. The cord was stabilized by pinning down the vertebral column to the base of the recording chamber

---

to data analysis and editing of manuscript.

which contained Sylgard® resin (Dow Corning). The proximal end of the forelimb was also fixed to this base by the procoracoid cartilage. Recordings of interneurons were made during rhythmic walking-like movement of the limb.

Recording cells

Intracellular and extracellular recordings were made through the dorsal surface of the spinal cord starting approximately one hour after the dissection of the preparation. The recording microelectrodes (54~130 MΩ resistance when filled with 2M potassium acetate) were made from filament-containing glass capillaries (borosilicate, o.d.= 1.5, mm i.d.=0.85 mm, AM Systems Inc. Everrett, WA, USA, or Clarke Electromedical, Redding, UK) with a puller (P-87, Sutter Instrument, CA, USA, or Narishige, Japan).

Cells were recorded along a rostro-caudal line about 300 μm from the midline of the spinal cord where there are no motoneurons in this animal (Cheng et al. 1998). The pia of the dorsal surface of the C2 and C3 segments was removed for better penetration of the recording microelectrode, with a pair of fine forceps under a dissection microscope (Leica, Switzerland). A fine micro-manipulator (Soma Scientific Instruments Inc., Irvine, CA), which supported the holder for the electrode, was secured to a 3-dimensional coarse manipulator (Soma Scientific Instruments Inc., Irvine, CA). The tips of the electrodes were lowered by the use of the 3-D manipulator to the dorsal surface at an angle of 70 ° from the longitudinal plane of the cord into the gray matter (~200 to 500 μm deep). The fine manipulator was then used to lower the microelectrode into the cord until spikes were recorded from single cells. The depth of penetration of the electrode was not corrected for the angle, which remained approximately constant. Intracellular or extracellular potentials were amplified (Axoprobe 1A), digitized (Digidata 1200A), and stored (Axoscope 7, Axon Instruments Inc., CA) in a computer for later analysis. EMGs were simultaneously recorded from the elbow flexor and extensor muscles along with the neuronal activity.

Stimulation of the ventral roots

To test whether the recorded cells could be antidromically activated, the ventral roots were stimulated with constant cathodic currents (Master 8, A.M.P.I., Jerusalem, Israel) through a stimulus isolation unit (Neuro Log NL800, Digitimer Ltd., Walwyn

Garden City, U.K.). Single pulses (0.5 ms pulse duration) or trains of 6 pulses at 40 Hz were used to stimulate the ventral roots (C2-C4) innervating the forelimb. The stimulus intensity was up to 2 times motor threshold (10 to 20 μA). An intrafascicular electrode was employed in these experiments because it produced smaller stimulus artifacts, did not require external support from micromanipulators, and allowed for stimulation of multiple sites (Yoshida et al. 2000). Briefly, the electrodes were constructed from a 25 cm length of Teflon insulated 90% Pt 10% Ir wires (#7750, AM Systems, Carlsborg, WA). The diameter of the wire was 25 μm bare and 60-75 μm with insulation. A 250 to 500 μm segment of insulation was removed along the length of the wire, 3 cm from the end, by edgewise contact to a glowing Pt Ir filament foil. This bared segment becomes the stimulation site and is referred to as the active site of the electrode which is platinized by electrodeposition of finely divided platinum black. The impedance of the active site measured in normal (0.9%) saline at 1 kHz was between 50-400 KΩ.

The electrodes were threaded through the spinal roots by means of an electrosharpened tungsten needle (15 mm long, 50 μm in diameter) attached to the end of the platinized electrode lead. The electrodes were implanted nearly perpendicular to the axis of the spinal roots and parallel to the longitudinal axis of the spinal cord so as not to obstruct access of the recording microelectrode to the spinal cord. Care was taken to keep the active sites of the electrodes within the body of the spinal root to minimize current shunting. A distantly placed intrafascicular electrode, with exposed area of up to 5 mm, was used as an indifferent electrode for stimulation.

Analysis

The phase relationship between the activity of the recorded cells and the activation of the elbow flexor and extensor muscles was quantified in several ways using specially written programs in Matlab (Math Works, Inc., Natick MA). First, the rectified flexor and extensor EMGs were averaged with respect to the time of the spikes in each interneuron. This *spike-triggered averaging* has been described in previous papers (Wheatley et al., 1994). Essentially, a large EMG modulation in the spike-triggered average means good phasic localization of the cell's bursting in a cycle. The timing of the peaks in the EMG, relative to the spikes, is used to determine the phase of the spikes. For example, in Figure

8-1B the time between two successive peaks (i.e., the step cycle) is 1.6 s. The peak in spike rate occurs 0.1 s before the flexor peak, which represents a phase difference of -23 °. The whole cycle is divided into 4 quadrants. If, as in Figure 8-1, the spikes occurred on average within ± 45° of the peak in flexor EMG, the unit was classified as a flexor (F) interneuron. If they occurred within ± 45° of the peak in extensor EMG, it was classed as an extensor (E) interneuron. The quadrants in between were referred to as transition regions and the units were classed as either flexor to extensor (F→E) or extensor to flexor (E→F) transition interneurons.

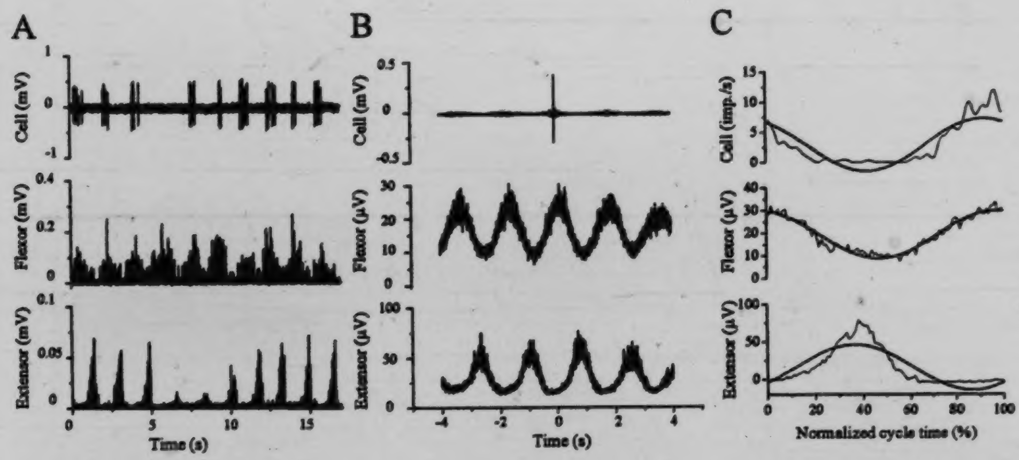

Figure 8-1. Extracellular recording of an interneuron at 1 mm caudal to the C2 dorsal root, together with the rectified flexor and extensor EMG (A). The spike-triggered average suggests that this cell is a flexor interneuron (B). A similar result was obtained by selecting the flexor bursts and computing a normalized cycle histogram (C). The histograms were fitted with sine curves and cells, such as this one, which fitted curves peaked within 45° of the flexor EMG were classed as flexor interneurons. Those that peaked within 45° of the extensor EMG were classed as extensor interneurons. Cells with peaks between these regions were classed as transition interneurons. See further details in the Methods section.

The spike-triggered averaging was also done on a brief time scale (tens of milliseconds, instead of seconds). Short latency, spike-triggered responses were examined to identify interneurons that make monosynaptic connections with the flexor or extensor motoneurons (e.g., Figure 8-6).

Finally, *normalized cycle histograms* were analysed, particularly for cells whose bursting was less rhythmic. Periods of relatively regular, walking-like activity were selected and the onset of each burst was marked in the flexor or extensor EMG (depending on which was more vigorous and well-defined). Typically, 50-100 cycles were selected and each cycle was normalized in duration. Then, the EMGs were averaged over the normalized cycle and a cycle histogram of the neural data was computed (Figure 8-1C). The traces could be digitally smoothed without introducing phase delays. The average EMGs and the cycle histogram were fitted with sine waves of the form:

$$y = a + b \sin \theta + c \cos \theta$$

For the cycle histogram the parameter a gives the mean rate in imp./s, the modulation is given by $m = \sqrt{}(b^2+c^2)$ and the phase by $\tan^{-1}(b/c)$. In Figure 8-1C, $a = 2.9$ imp./s, $m = 4.4$ imp./s and the peak of the fitted curve occurred at a phase of 331°. The phase of the spikes was again compared to that of the EMG and the cycle was divided in four parts as described above. In the example shown, the curve fitted to the flexor EMG had a peak at a phase of 350°, so the unit would again be classified as a flexor interneuron. This method was considered more accurate than the spike-triggered average, because the cycles could be carefully selected and normalized. Where there was a discrepancy between the two methods, the classification was made based on the cycle histogram method. Although the activity was often not completely sinusoidal, this method of fitting was also considered preferable because it depended on activity throughout the cycle, rather than merely at the peak.

The variance accounted for (VAF) by the linear, least mean squares fitting procedure gave a useful measure of how rhythmically the cell was modulated during the walking cycle. Cells were only classified when the VAF was greater than 30%. This corresponds to a linear correlation coefficient of 0.55. The choice of this criterion level was rather arbitrary, but a value of 50% (a correlation coefficient of 0.71) gave very similar results, although fewer cells met the higher criterion. The relative depth of the modulation in % was given by 100 *m/a*. Cells such as that in Figure 8-1 which had a burst followed by a prolonged pause typically had a computed modulation greater than 100%. Cells that fired throughout the cycle had a modulation < 100%.

RESULTS

A total of 328 cells were recorded during walking-like movement of the limb induced by bath application of NMDA (20 to 120 μM). 240 of the cells were recorded intracellularly and 88 cells were recorded extracellularly. The same information on the timing of cell firing could be obtained from either intracellular or extracellular recordings and no significant differences were observed between the spike rates and modulation of the two groups. We therefore accepted all cells for which the recordings were sufficiently stable that we could do the full analysis described in the Methods. 289 cells met this criterion and formed the basis for later analysis. Figure 8-2 shows the distribution of the recorded cells in the C2 and C3 segments of the spinal cord at a resolution of 1 mm. The number of cells recorded peaked in the rostral and caudal parts of the C2 segment. Cells were recorded in the medial part of the spinal cord, not exceeding 300 μm from the midline of the spinal cord, where there are no motoneurons (Cheng et al. 1998). Many of the cells (n=58) recorded in this region were tested with stimulation of the ventral roots and none of them were activated antidromically. The lack of spike-triggered, short latency (less than 6 ms) responses in the flexor or extensor muscle about the elbow joint further confirmed that these cells were interneurons (further described later).

Phasic classification of the cells

To classify the cells a criterion was used based on the variance accounted for (VAF) by fitting the cycle histogram with a sine wave (see Methods). 116 of the 289 cells (40%) satisfied the criterion that 30% or more of the variance was accounted for by the sinusoidal fit (Figure 8-3D). Very similar results were obtained with a criterion of 50%, except that the number of cells was reduced to 77 out of 289 (27%). Cells that did not meet the criteria could fire tonically or sporadically or with another rhythm, such as respiration, and were presumably involved in other activities of the brachial spinal cord. Rhythmic and non-rhythmic cells were compared, as shown in Figure 8-3. The rhythmic and non-rhythmic cells were similarly distributed along the spinal cord (Figure 8-3A). The firing rates of the non-rhythmic and rhythmic cells were also similar (Figure 8-3B, 6.6 ± 0.6, compared to 6.4 ± 0.4 imp./s; mean ± S.E.). As expected, the modulation was quite different for the two groups (Figure 8-3C). All the cells showing more than 100% modulation and nearly all with modulation more than 50% belonged to the rhythmic group. The mean values for the modulation of the non-rhythmic and rhythmic groups were 16 ± 2, compared to 55 ± 3 %.

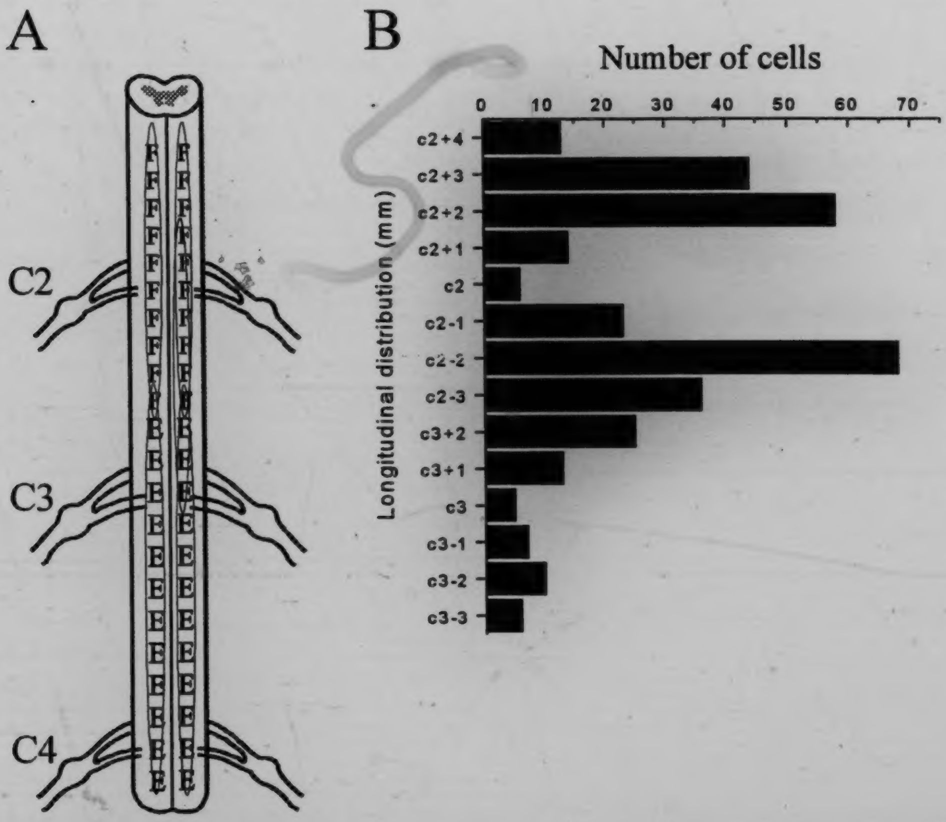

Figure 8-2. Longitudinal distribution of cells recorded in the C2 and C3 segments. The number of cells is plotted against the longitudinal axis of the spinal cord at a resolution of 1 mm. C2-4 denotes 4 mm rostral to the C2 dorsal root; C2+3 denotes 3 mm caudal to the C2 dorsal root, etc. C2+3 = C3-3. The distribution of the cells relative to the flexor (F) and extensor (E) motoneurons of the elbow joint is shown schematically.

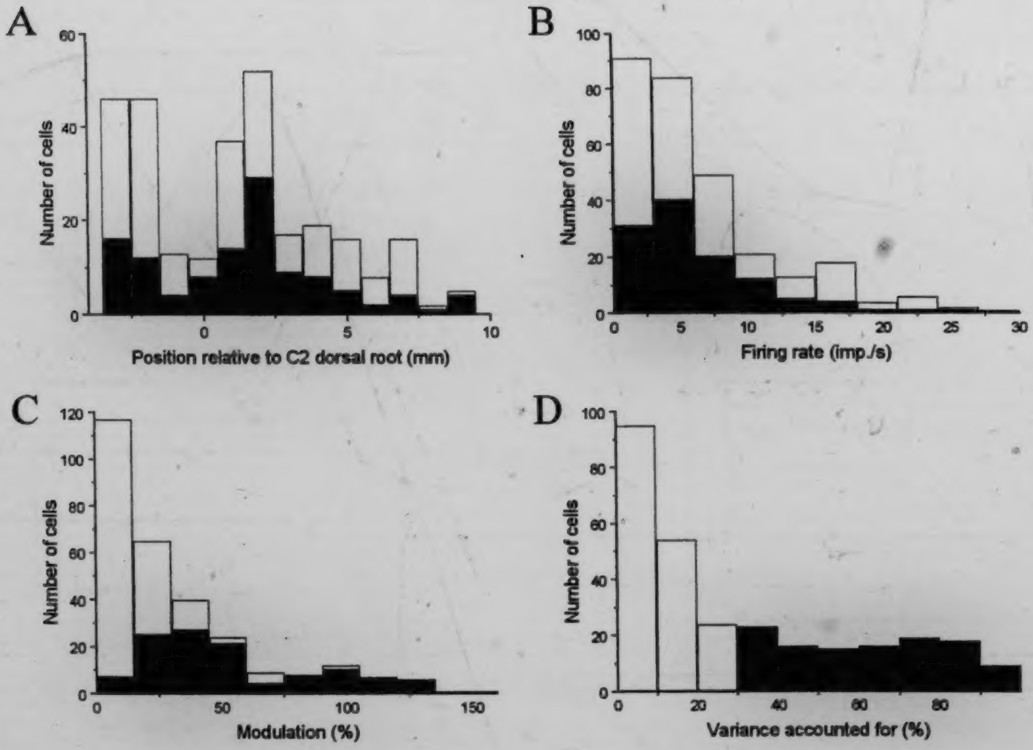

Figure 8-3. A) Rhythmic (black) and non-rhythmic (white) cells were distributed in a similar way along the spinal cord. The entry point of the C2 dorsal roots is taken as 0 mm. B) The mean firing rates of the two groups of neurons were also similarly distributed. C) The rhythmic cells had a much higher depth of modulation with the walking rhythm, as would be expected. D) The criterion for selecting a cell as rhythmic was that at least 30% of the variance in the average discharge over the step cycle was accounted for by fitting a sine wave to the cycle histogram.

The rhythmically active cells that met a VAF criterion of either 30 or 50% were further classified into four groups (F, F→E, E and E→ F), based on the timing of their discharges in a step cycle (see Methods). In approximately 30% of the preparations cells could not be classified because the flexor and extensor EMG were not sufficiently out of phase (>90°) to make this classification meaningful, even though flexion and extension movements of the limb were robust. Of the 75 cells that could be classified reliably (Figure 8-4A), over 41% were flexor (F) interneurons, 13% were flexor to extensor interneurons (F→E), 15% were extensor (E) interneurons and nearly 30% were extensor to flexor (E→ F) interneurons.

An example of a flexor interneuron recorded extracellularly in the presence of NMDA (40 µM) was shown in Figure 8-1. This cell was located in the gray matter, 200 µm from the midline of the cord, 300 µm below the dorsal surface, and 2 mm rostral to the C2 dorsal root. This cell did not have a short-latency response in the flexor or extensor EMG, so it was not considered to be a last-order interneuron (see later section on *Connectivity of the rhythmic cells*). Figure 8-5 shows an example of a transitional cell. This cell was located in the caudal part of the C2 segment, about 300 µm lateral to the midline of the cord, and at a depth of 460 µm from the dorsal surface. It did not respond to stimulation of the C2 and C3 ventral root at an intensity of 2 times motor threshold. The spikes tended to occur on the rising phase of rhythmic membrane depolarization and occurred 68° in advance of the flexor EMG on average (Figure 8-5A). This cell was therefore classified as an E→F interneuron. Application of depolarizing current (0.1-0.2 nA) inactivated the action potentials, but the rhythmic depolarizations of the membrane potential continued at the walking frequency (Figure 8-5B). The rhythmic depolarizations were typical of recordings from some interneurons (n=12). The amplitude of the depolarizations ranged from 2 to12 mV and the shapes were similar to that seen in motoneurons (locomotor drive potential). Since the rhythm continued unchanged whether this cell generated spikes or not and whether it was depolarized or not, it was presumably not part of the rhythm generator. Other cells showed rhythms that depended on the depolarization of the cell, but more detailed studies of such cells are needed to determine if they form part of the rhythm generator.

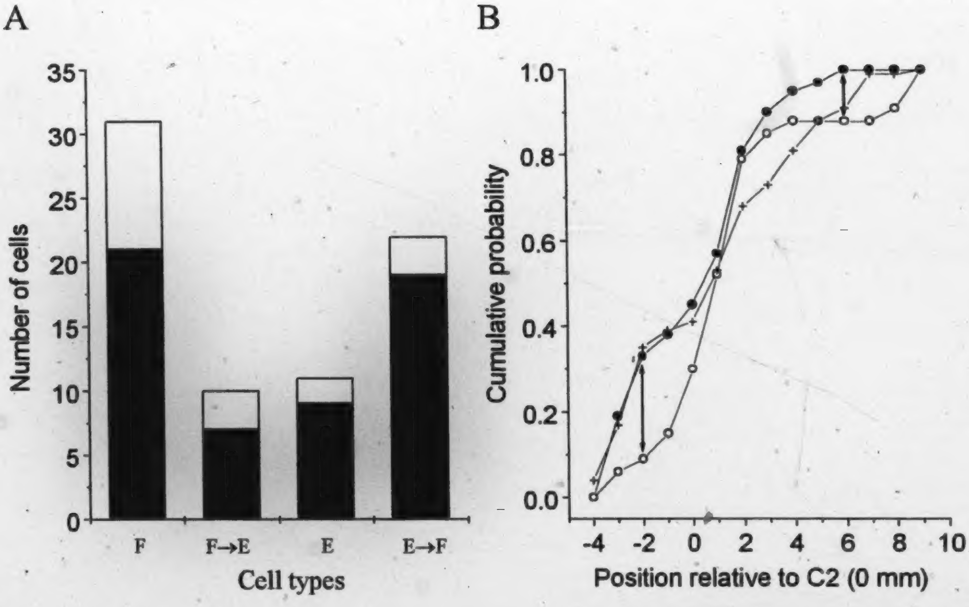

Figure 8-4. A) The cells were classified into the four categories when a criterion of 50% (dark) or 30% (all) was used for the variance accounted for (VAF) in the cycle histogram. B) The F (black) and F→E (black) interneurons were distributed similarly along the cord. The E (white) and E→F interneurons (white) were also similarly distributed and were significantly more caudal.

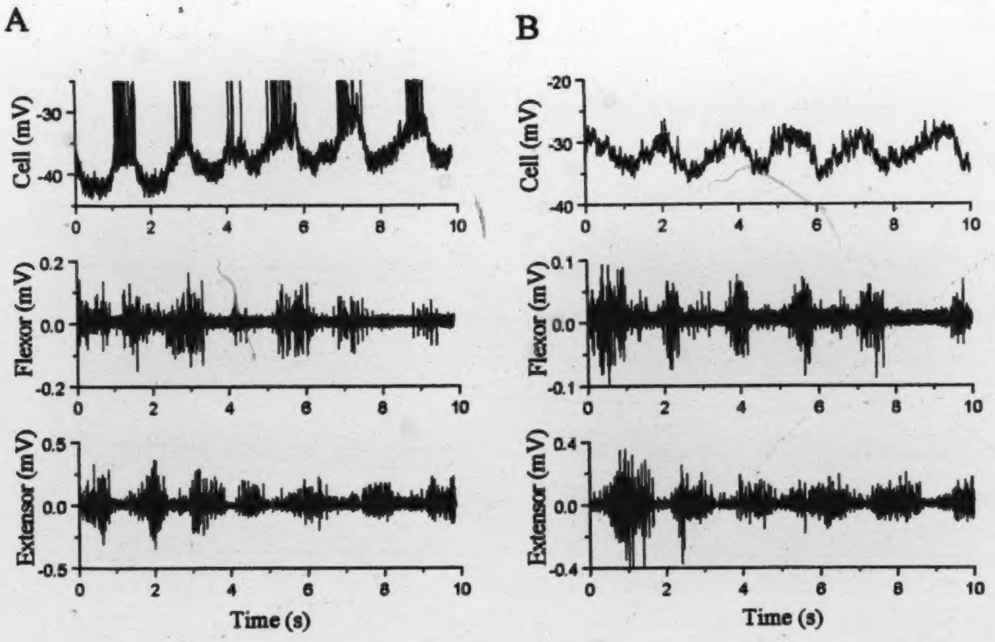

Figure 8-5. A) Rhythmic discharges on top of membrane voltage undulations. This cell was located 2 mm caudal to the C2 dorsal root, 300 µm from the midline, and 460 µm from the dorsal surface. It fired rhythmically (spikes are truncated) somewhat in advance of the flexor EMG and did not trigger short latency responses in either flexor or extensor EMGs (not shown). B) Inactivation of the spikes by depolarizing current injection (0.1-0.2 nA) eliminated the action potentials while the pattern of membrane potential oscillations did not change its temporal relationship to the flexor activation.

Longitudinal distribution of the recorded cells in the spinal cord

Rhythmic and non-rhythmic cells were distributed in much the same manner along the spinal cord as shown in Figure 8-3A. Using the C2 dorsal root as a zero reference point non-rhythmic cells and rhythmic cells were found at similar average positions (0.9 ± 0.3, compared to 1.4 ± 0.2 mm). All the cells were recorded from the C2 and C3 segments. The distance between the C2 and C3 dorsal root was approximately 6 mm and the differences between the animals used were insignificant (less than 0.5 mm). Figure 8-4B shows the longitudinal distribution of the classified cells along the cord. The F (dark) and F→E (white) interneurons have been grouped together in Figure 8-4B because they were distributed longitudinally along the spinal cord in a similar way (no significant differences in position). The E (dark) and E→F interneurons (white) were also grouped together for the same reason in Figure 8-4C. Over 33% of the flexor-related neurons were located at more than 2 mm rostral to the C2 dorsal root, whereas less than 9% of the extensor-related neurons were found at that level. Also, no flexor-related neurons were located at levels caudal to C3 dorsal root (a position of 6). The extensor-related neurons were located significantly more caudally on average than the flexor-related neurons ($p<0.05$).

Connectivity of the rhythmic cells

Analysis was performed on 224 cells recorded to explore the connectivity of these cells to the motoneurons of the flexor and extensor muscles. Spike-triggered, short-latency responses in these muscles suggest direct connection of the recorded cells to the motoneurons (last-order interneurons). Figure 8-6 shows an example of spike-triggered short latency excitation of the extensor muscle. This cell, localized in the rostral part of the C3 segment and classified as an extensor interneuron, triggered an excitation of the extensor muscle at an estimated latency of 7-8 ms (Figure 8-6A). The time for an action potential of the motoneurons to evoke muscle activation was measured to be about 6 ms at room temperature (20-22 °C). This is the latency from stimulating the C3 ventral root to the onset of the extensor muscle activation (Figure 8-6B). The latency from this cell to the motoneuron was likely 1-2 ms (7 to 8 minus 6 ms) and could be monosynaptic. This cell is therefore considered to be a last-order extensor interneuron. Overall, 40 out of 224 cells showed spike-triggered short latency responses; 23 triggered flexor responses and 17 triggered extensor activities. All but one of the responses was excitatory. Three cells showed triggered responses with latencies shorter than 6 ms and were considered to be cells that were co-activated with or activated after motoneurons. Twelve of the cells with short latency responses > 6 ms were among the 75 neurons whose phase could be classified. Of the six cells that excited flexors at short latency, 5 had their peak activity in the F phase. The six cells that excited extensors at short latency had peak activities in various phases, but the numbers are too small to draw any definite conclusions.

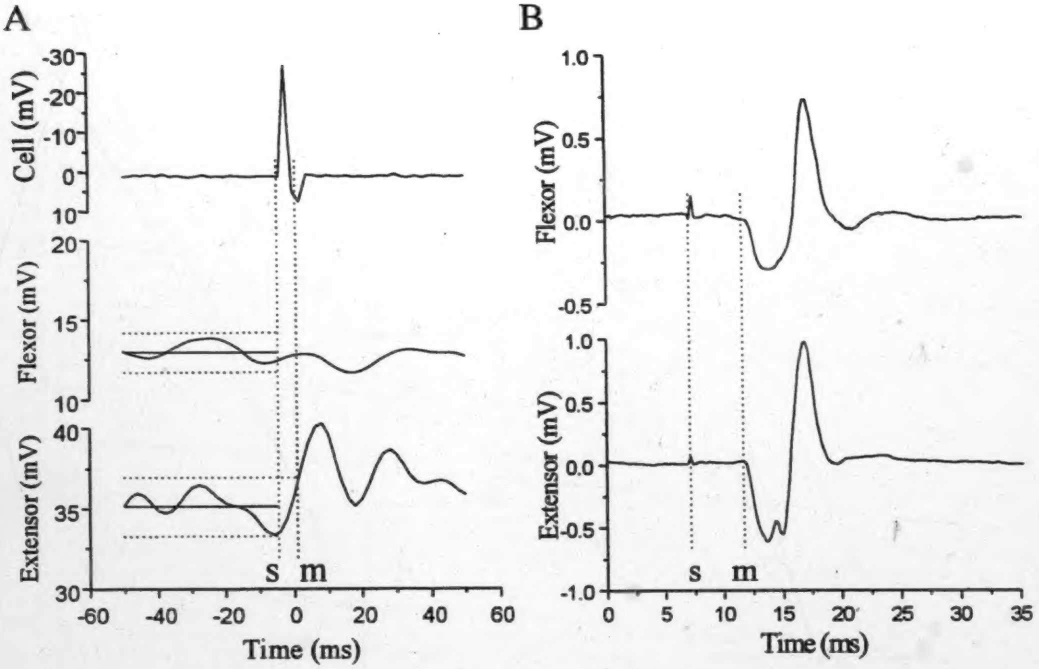

Figure 8-6. Spike-triggered, short latency excitation of the extensor muscle. A) This cell resided 2 mm rostral to the C3 dorsal root, 300 μm from the midline, 230 μm from the dorsal surface and triggered an excitation of the extensor muscle. The latency from the onset of the spike (s) to the onset of the muscle activation (m) was estimated to be 7-8 ms. The horizontal dotted lines denote 2 standard deviations around the mean of the average responses and the latency was chosen as the point where the values first exceeded this range. B) Latency of motoneuron excitation to activation of the extensor. Stimulation (0.5 ms square wave, 1.2 times motor threshold) of the C3 dorsal root induced responses (m) in the flexor and extensor muscles of the elbow joint with a latency of 6 ms. The latency from the firing of the cell to activation of the extensor motoneurons was estimated to be 1-2 ms (7-8 ms minus 6 ms), suggesting monosynaptic connections.

DISCUSSION

In this study we recorded interneurons in the neural networks for walking in the C2 and C3 segments during walking-like movement, classified them into four groups in a step cycle, and mapped their longitudinal distribution along the spinal cord. Rhythmic cells had similar firing rates to those of the non-rhythmic cells. Some of the cells were likely last-order interneurons. The interneurons were identified by a combination of criteria. We targeted cells located in the medial region of the gray matter (not exceeding 300 μm from the midline) where there are no motoneurons in this animal. The interneuronal nature of the recorded cells was confirmed by the lack of antidromic responses to ventral root stimulation, and the lack of spike-triggered, short-latency (less than 6 ms) responses in the flexor or extensor muscle about the elbow joint.

About 40% of the cells recorded in the C2 and C3 segments were related to walking in that their firing rate varied rhythmically with the walking-like motion and the activation of the flexor and extensor muscles of the forelimbs. In some preparations the flexor and extensor patterns were nearly synchronous, so the phase of the cells could not be determined. Of the 75 cells that could be classified reliably, over 40% were flexor interneurons, 13% were flexor to extensor interneurons, 15% were extensor interneurons and nearly 30% were extensor to flexor interneurons, based on the timing of their discharges in a step cycle. Comparison of these data with those of Wheatley et al. (1994) reveals important features of longitudinal distribution of phase-specific cells along the spinal cord. The percentage of transition interneurons (32/75 or 43%) is somewhat smaller than that reported by Wheatley et al. (34/50 or 68%), but the difference between these percentages is not statistically significant with these sample sizes. Combining the two samples, the percentage of transition interneurons appears to be close to half (53%).

The most common interneurons recorded here were flexor neurons (31/75, or 41%), whereas they were the least common (6/50, or 12%) in Wheatley's sample. However, we concentrated in this study on the C2 region (Figure 8-2), whereas Wheatley's sample was from a "segment of spinal cord spanning segment C3 (shaded area in Fig. 1"; Wheatley et al., 1994). This region contains more extensor interneurons than flexor interneurons in both samples. In fact, the results provide an interneuronal substrate for the flexor and extensor centers we reported earlier (Cheng et al. 1998). Many flexor-related interneurons were recorded rostral to the C2 dorsal root and none were recorded at the level of the C3 dorsal root or more caudally (Figure 8-4). This is in agreement with the observation that a 4 mm region of the cord rostral to the C2 ventral root (inclusive) in isolation generated rhythmic flexor bursts without extensor bursts. Some flexor interneurons in this region may have generated the flexor rhythm. On the other hand, a 5 mm long region caudal to the C3 ventral root (inclusive) in isolation generated rhythmic extensor bursts without flexor bursts. Finally, an 8 mm long segment of cord spanning the C3 ventral roots in isolation generated rhythmic alternating flexor-extensor bursts and walking-like motion of the forelimb about the elbow, reflecting the presence of both flexor and extensor interneurons in this region. The differential distribution of flexor and extensor interneurons is consistent with the distribution of the respective flexor and extensor motoneurons (Cheng et al. 1998) and may therefore constitute the basis for independent, but overlapping flexor and extensor centers. The observation of distinct flexor and extensor centers may reflect a common principle that is applicable to the mammalian locomotor networks. In the neonatal rat, the rhythmic activity of the large majority of the interneurons (7/9) recorded in L2 segment were in phase with the locomotor-like output from L2 ventral root that is primarily flexor related (Cheng and Magnuson 2001). These observations also collectively provide experimental support for the concept of functional subunits, called unit burst generators (Grillner 1981) or modules (Jordan 1991) for locomotion.

The distribution of the transition interneurons is of interest. Although the numbers are not enough to be conclusive, the F→E interneurons were distributed similarly to the F interneurons (Figure 8-4B) and the E→F interneurons were distributed similarly to the E interneurons (Fig 8-4C). Perhaps, activation of the flexor interneurons in turn activates F→E cells that send axons to the extensor region. Conversely, excitation of the extensor interneurons could activate E→F cells that in turn activate the flexor interneurons. The switch between flexion and extension is presumably dependent upon the intrinsic membrane properties of the cells as well as the integration of input from the transition interneurons, the sensory pathways from the moving limbs, and the descending pathways of the supraspinal centers. Thus, activation of transition cells may be responsible for supplying delayed excitation of the antagonist "half centre" (Gelfand et al. 1988; Grillner and Matsushima, 1991). By doing so, the transitional cells have replaced the need for what

Brown (1911, 1914) termed "fatigue" of the half centers. This picture of information flow appears to be consistent with the experiments that demonstrated or suggested both excitatory and inhibitory inputs from sensory pathways (Conway et al. 1987; Cheng et al. 1998), the flexor and extensor centres (Cheng et al. 1998), and supraspinal centres (Jordan 1991).

This study describes the pattern of interneuronal activity but provides only limited information on the connectivity within the walking circuitry. The activity of a proportion of interneurons (40/224; 18%) was cross-correlated with short latency responses in the flexor or extensor muscles about the elbow joint (Figure 8-6). Further evidence is needed to confirm that they are last-order interneurons (Puskar and Antal 1997). More precise measurements could have been made if the ventral roots were also recorded or if larger numbers of spikes were recorded (thousands, rather than hundreds). It would also be of interest in future studies to see if the EMG increases at a short latency when these cells are stimulated intracellularly or if paired recordings are possible from interneurons and motoneurons. However, clearly the vast majority of cells (> 80%) were less directly related to the motoneurons. They could have no connections, polysynaptic connections or monosynaptic connections that were too weak to detect with the number of spikes recorded. Recordings from the ventral horn, rather than the intermediate region of the grey matter would be desirable to study last-order interneurons.

At least four basic models have been proposed over the last century for the neural circuitry of locomotion, namely the half-centre model (Brown 1911, 1914; Lundberg 1981), the ring model (Székely 1965), the "unit burst generator" model (Grillner 1981), and the pacemaker model (DeLong 1978, Grillner and Matsushima 1991). Interneurons that could be involved in generating walking have been identified in the cat (e.g., Orlovsky and Feldman 1972), rabbit (Viala et al. 1991), rat (e.g., Hochman et al. 1994; Kiehn et al. 1996), and chick (O'Donovan et al. 1992). Oscillatory properties of the cell membranes of interneurons as well as motoneurons have been reported in the rat (e.g., Hochman et al., 1994; Hochman and Schmidt 1998; Kiehn et al. 1996) and in the turtle (Guertin and Hounsgaard 1998). However, their relation to the generation of walking remains speculative. Tests of these hypotheses rely heavily on recording from identified interneurons in the cord during walking movements. The spinal cord-forelimb preparation from the mudpuppy is an excellent system in which to address these important questions (Wheatley and Stein 1992). It may therefore hold promise to understand the circuitry for walking and to determine the mechanisms whereby descending and sensory input interact with the spinal circuitry to control walking.

REFERENCES:

1. Armstrong DM (1988) The supraspinal control of mammalian locomotion. Journal of Physiology 405:1-37.
2. Bracci E, Ballerini L, Nistri A (1996) Localization of rhythmogenic networks responsible for spontaneous bursts induced by strychnine and bicuculline in the rat isolated spinal cord. Journal of Neuroscience 16:7063-7076.
3. Brown TG (1911) The intrinsic factors in the act of progression in the mammal. Proceedings of the Royal Society of London Series B Biological Sciences 84:308-319.
4. Brown TG (1914) On the nature of the fundamental activity of the nervous centres: together with an analysis of the conditioning of rhythmic activity in progression, and a theory of the evolution of function in the nervous system. Journal of Physiology 48:18-46.
5. Cazalets JR, Borde M, Clarac F (1995) Localization and organization of the central pattern generator for hindlimb locomotion in newborn rat. Journal of Neuroscience 15:4943-4951.
6. Cheng J, Stein RB, Jovanovic K, Yoshida K, Bennett DJ, Han Y (1998) Identification, localization, and modulation of neural networks for walking in the mudpuppy (Necturus maculatus) spinal cord. Journal of Neuroscience 18:4295-4304.
7. Cheng J, Stein RB (1998) Spinal interneurons that generate walking rhythm in the mudpuppy. Society for Neuroscience Abstracts 24: 1169.
8. Cheng J, Magnuson DSK (2001) Ventrolateral funiculus activation of interneurons that are associated with locomotion in the neonatal rat. Submitted
9. Chub N, O'Donovan MJ (1998) Blockade and recovery of spontaneous rhythmic activity after application of neurotransmitter antagonists to spinal networks of the chick embryo. Journal of Neuroscience 18:294-306.
10. Conway BA, Hultborn H, Kiehn O (1987) Proprioceptive input resets central locomotor rhythm in the spinal cat. Experimental Brain Research 68:643-656.
11. Delcomyn F (1980) Neural basis of rhythmic behavior in animals. Science 210:492-498.

12. Deliagina TG, Orlovsky GN, Pavlova GA (1983) The capacity for generation of rhythmic oscillation is distributed in the lumbosacral spinal cord of the cat. Experimental Brain Research 53:81-90.

13. DeLong MR (1978) Possible involvement of central pacemakers in clinical disorders of movement. Federation Proceedings 37:2171-2175.

14. Douglas JR, Noga BR, Dai X, Jordan LM (1993) The effects of intrathecal administration of excitatory amino acid agonists and antagonists on the initiation of locomotion in the adult cat. Journal of Neuroscience 13:990-1000.

15. Gelfand IM, Orlovsky GN, Shik ML (1988) Locomotion and scratching in tetrapods. In: *Neural Control of Rhythmic Movements in Vertebrates,* ed. Cohen, A. H., Rossignol, S. & Grillner, S., pp. 167-199. Wiley, New York.

16. Grillner S (1981) Control of locomotion in bipeds, tetrapods, and fish. In: *Handbook of Physiology, Sec 2, The nervous system,* ed. Brookhardt, J. M. & Mountcastle, V. B., pp. 1179-1236. American Physiological Society, Bethesda, MD.

17. Grillner S (1985) Neurobiological bases of rhythmic motor acts in vertebrates. Science 228:143-149.

18. Grillner S, Wallén P, Brodin L (1991) Neural network generating locomotor behavior in lamprey: circuitry, transmitters, membrane properties and simulation. Annual Review of Neuroscience 14:169-199.

19. Grillner S, Matsushima T (1991) The neural network underlying locomotion in lamprey-synaptic and cellular mechanisms. Neuron. 7:1-15.

20. Guertin PA, Hounsgaard J (1998) Chemical and electrical stimulation induce rhythmic motor activity in an in vitro preparation of the spinal cord from adult turtles. Neuroscience Letters 245:5-8.

21. Hochman S, Jordan LM, MacDonald JF (1994) *N*-methyl-D-aspartate receptor-mediated voltage oscillations in neurons surrounding the central canal in slices of rat spinal cord. Journal of Neurophysiology 72:565-577.

22. Hochman S, Schmidt BJ (1998) Whole cell recordings of lumbar motoneurons during locomotor-like activity in the in vitro neonatal rat spinal cord. Journal of Neurophysiology 79:743-752.

23. Jordan LM (1991) Brainstem and spinal cord mechanisms for the initiation of locomotion. In *Neurobiological Basis of Human Locomotion,* ed. Shimamura, M., Grillner, S. & Edgerton, V. R., pp. 3-20. Japan Scientific Societies Press, Tokyo.

24. Kiehn O, Johnson BR, Raastad M (1996) Plateau potentials in mammalian spinal interneurons during transmitter-induced locomotor activity. Neuroscience 75:263-273.

25. Kjaerulff O, Kiehn O (1996) Distribution of networks generating and coordinating locomotor activity in the neonatal rat spinal cord *in vitro*: A lesion study. Journal of Neuroscience 16:5777-5794.

26. Lundberg A (1981) Half-centres revisited. In *Regulatory Functions of the CNS. Principles of Motion and Organization. Advances in Physiological Sciences. Vol. 1*, ed. Szentagothai, J., Palkovits, M. & Hamori, J., pp. 155-167. Pergamon Press, Budpest.

27. MacLean JN, Schmidt BJ, Hochman S (1997) NMDA receptor activation triggers voltage oscillations, plateau potentials and bursting in neonatal rat lumbar motoneurons in vitro. European Journal of Neuroscience 9:2702-2711.

28. O'Donovan M, Sernagor E, Sholomenko G, Ho S, Antal M, Yee W (1992) Development of spinal motor networks in the chick embryo. Journal of Experimental Zoology 261:261-273.

29. Orlovsky GN, Feldman AG (1972) Classification of lumbosacral neurons by their discharge pattern during evoked locomotion. Neurophysiology 4:311-317.

30. Pearson KG (1993) Common principles of motor control in vertebrates and invertebrates. Annual Review of Neuroscience 16:265-297.

31. Pearson KG (1995) Proprioceptive regulation of locomotion. Current Opinion in Neurobiology 5:786-791.

32. Puskar Z, Antal M (1997) Localization of last-order premotor interneurons in the lumbar spinal cord of rats. Journal of Comparative Neurology 389:377-389.

33. Roberts A, Tunstall MJ, Wolf E (1995) Properties of networks controlling locomotion and significance of voltage dependency of NMDA channels: simulation study of rhythmic generations sustained by positive feedback. Journal of Neurophysiology 73:485-495.

34. Roberts A, Soffe SR, Wolf ES, Yoshida M, Zhao FY (1998) Central circuits controlling locomotion in young frog tadpoles. Annals of the New York Academy of Sciences 860:19-34.

35. Székely G (1965) Logical network for controlling limb movements in urodela. Acta Physiologica Academiae Scientiarum Hungaricae 27:285-289.

36. Székely G, Czéh G, Vörös G (1969) The activity pattern of limb muscles in freely moving normal and deafferented newts. Experimental Brain Research 9:53-62.

37. Viala D, Viala G, Jordan L (1991) Interneurons of the lumbar cord related to spontaneous locomotor activity in the rabbit. I. Rhythmically active interneurons. Experimental Brain Research 84:177-186.

38. Wheatley M, Jovanovic K, Stein RB, Lawson V (1994) The activity of interneurons during locomotion in the *in vitro* Necturus spinal cord. Journal of Neurophysiology 71:2025-2032.

39. Wheatley M, Stein RB (1992) An *in vitro* preparation of the mudpuppy for simultaneous intracellular and electromyographic recording during locomotion. Journal of Neuroscience Methods 42:129-137.

40. Wheatley M, Edamura M, Stein RB (1992) A comparison of intact and *in vitro* locomotion in an adult amphibian. Experimental Brain Research 88:609-614.

41. Yoshida K, Jovanovic K, Stein RB (2000) Intrafascicular electrodes for stimulation and recording from mudpuppy spinal roots. Journal of Neuroscience Methods. 96:47-55.

CHAPTER 9

GENERAL DISCUSSION

This thesis had two main objectives: (1) to pursue the sensorimotor control principles underlying natural and artificial movement, especially focusing on spinal cord organization, biomechanics of multiarticulated limb, and sensorimotor regulation by the first order sensory neurons, and (2) to establish basic characteristics of a penetrating microelectrode array including stimulation, recording and biocompatibility in peripheral nerve and DRG for testing feasibility in neuroprostheses. Since most of the particular issues were discussed in detail in each chapter, this section summarizes the main findings of this thesis and integrates particular issues into a framework encompassing movement science and clinical application.

SPINAL CORD ORGANIZATION FOR MOTOR OUTPUT

Intraspinal microstimulation produced movements to all directions as did intramuscular and nerve stimulation. However, we found in intraspinal microstimulation that the evoked patterns often changed markedly depending on stimulus intensity and the states (anesthetized, decerebrate, and spinal states). In peripheral nerve or intramuscular stimulation the evoked patterns were fairly constant irrespective of stimulus intensity and the states. So a possibility was raised that the biomechanical actions of the limb muscles set limits on the movements that can be generated through central commands. This idea is also supported by our results and the recent experiment by Grill and Lemay in the cat (Grill and Lemay 2001). They found that the electrically-induced end-point vector (***movement***) did not necessarily follow individual vectorial summation. In Chapter 6, movements elicited by simultaneous stimulation of multiple sites did not follow the linear summation of the vectors produced by stimulating individual sites, but tended to converge to an equilibrium point. These findings indicate that intrinsic peripheral properties inter-joint torques, neuromuscular spring-like properties, bones and ligaments etc. can contribute to restrict and determine a movement trajectory and its end-point, independently of the CNS.

In the spinal frog, if the stimulating electrode was moved from intermediate zone into the ventral horn, then the force fields were divergent or parallel rather than converging (Giszter et al. 1993). Bizzi and his colleagues therefore concluded that the input to the motoneurons from the intermediate zone imposes a structure on the pattern of motoneuronal activation that is consistent with the form of the equilibrium points. However, this may simply mean that spinal interneurons generate activity in multiple muscles and thus account for the convergence in their output projection. Our experiment revealed that simultaneous activation of numerous muscles produced convergent movements toward an equilibrium point in the workspace whereas activation of most single muscles produced movements that were parallel or divergent. These results suggest that whether a movement converges or diverges may simply depend on the number of activated muscles rather than the existence of 'primitives'.

Taking these considerations together, it is reasonable to conclude that 'primitives' producing constant evoked patterns do not exist in the spinal cord, at least in a simple form that can be distinguished by stimulation in the cat. However, it can not plausibly be argued that the spinal cord does contain some functional localization. It must be stressed that microstimulation of the rostral interneuronal area of the lumber enlargement often produced flexion responses whereas microstimulation on caudal area produced extension responses. Indeed, a conclusion drawn from Chapter 8 was that interneurons activated during flexor phase tended to be located more rostrally whereas those fired during extensor phase tended to be located more caudally although these regional distributions were not completely distinct but significantly overlapped. The nature of the distributed network supports the hypothesis that the CPG can be subdivided into unit burst generators controlling limb movements (Beato and Nistri. 1999; Cheng et al. 1998; Kiehn and Kjaerulff. 1998; Rossignol. 1996; Stein. 1997).

With regard to the localization in the transverse plane, at the moment it is not possible to make a clear statement, although there seems to exist some transversely distributed CPG network (for review (Kiehn and Kjaerulff. 1998)). In *in vitro* studies focusing on CPG networks in the transverse plane, in addition to conventional extracellular recording technique researchers have applied more recently developed technique such as intracellular tight-seal whole cell recordings, activity-dependent labeling, calcium imaging. All of these techniques may have their own problems of interpretation, which is perhaps one reason why there a less clear picture of transverse localization. Lemay and Grill reported in the cat that intraspinal stimulation at superficial depths (≈800μm) produced mostly flexor withdrawal responses, whereas responses at intermediate depths (≈1500μm) were varied (Chapin and Moxon. 2000; Lemay and Grill. 1999). The evidences that ventral root stimulation produced primarily extension responses while dorsal root stimulation produced flexion responses (Chapter 5) are not contradictory to the existence of ventrodorsal localization.

In summary, we could not verify the evidence for the existence of 4 or 5 clear 'movement primitives' hard-wired in the cat spinal cord. However, it cannot reasonably assumed that there exists functional localization in intermediate gray zone. It contains at least some rostrocaudal and ventrodorsal localization (but not complete modules) that may produce coordinated synergies. Clearly, more systematic mapping of the intermediate gray zone in different animals is needed to clarify the exact transverse as well as longitudinal functional anatomy. Penetrating microelectrode array such as the UEA that are regularly spaced on 400 μm centers should be an excellent candidate for that purpose.

FES TO RESTORE MOTOR FUNCTION

Motor prostheses have been developed to restore functional movement and partially overcome the paralysis of spinal cord injury by electrical stimulation (Kralj and Bajd 1989; Stein et al. 1992; Chapin and Moxon 2000). Although some clinical applications of electrical stimulation have been successful (Kralj et al. 1988; Peckham and Creasey 1992; Dai et al. 1996; Wieler et al. 1999), the electrical restoration of whole limb movements remains problematic (Prochazka 1993; Field-Fote 2000). As was discussed in Chapter 5, stimulation of muscle, nerve and spinal cord and, spinal roots has particular advantages and disadvantages. No perfectly ideal stimulation method appears to exist, at least as compared under acute anesthetized, decerebrate, and spinal states in the cat, but the results of the present study should help in deciding the best site for a given clinical application as far as the acute data were concerned. Chronic studies in decerebrate and spinal states will be needed to substantiate the acute results.

Stimulation hardware containing external stimulator and percutaneous electrodes caused infrequent but serious problems such as wire breakage and skin infection. It is likely that efficacious FES systems will require complete implantation and activation of large numbers of motor units. A high-density neural interface such as the UEA, which was shown to selectively stimulate each muscle group in chronic animals in the Chapter 4, seems a promising stimulating device while the design of miniaturized implantable stimulators is being developed. Loeb and his colleagues have recently developed a new class of wireless, injectable microelectronic modules, called BIONs that receive power and exchange data by radio frequency (RF) magnetic coupling to an externally worn coil (Chapin and Moxon 2000). The BION neuromuscular stimulators, now being used in clinical trials to prevent disuse atrophy and shoulder subluxation seems also promising.

In the rest of this section, some important clinical FES issues linked with this thesis will be discussed. I will discuss the effective way of stimulating selective muscle groups after central motor paralysis. I will then argue what control strategies may be available to increase biomechanical stability in FES and what limitations the multi-segmental limb biomechanics place on FES by making a comparison of natural and artificial movement. Finally, I will comprehensively consider the near future perspectives on restoration of functional limb movement.

Stimulation of selective muscle groups

Biarticular muscles enhance interjoint coordination and provide some mechanical coupling effects between joints in natural movement. Conversely, the 'nonselective' function of biarticular muscle could be a drawback in generating selective single joint movement. However, contrary to the common view of biarticular function, it was demonstrated in Chapter 5 that biarticular muscles can be stimulated selectively for each joint through electrical stimulation of motor nerve branches. This finding is consistent with recent evidence suggests that movements can be generated quite effectively at one joint in such biarticular, but compartmentalised muscles (Herrmann and Flanders 1998). This finding provides the future possibility that implantation of a small number (~6) of electrodes in peripheral nerve innervating flexor and extensor of ankle, knee, and hip joints might generate functional rhythmic movements.

Branner, Stein, and Normann implanted a variant (the Utah Slanted Electrode

Array) into the sciatic nerve of the cat (Branner and Normann 2000; Branner et al. 2001) and showed this electrode permitted more selective stimulation with more graded recruitment of individual muscles than was achieved by conventional cuff electrodes. This suggests another possibility of stimulating selective muscle groups through peripheral nerve. Chapter 4 focused its attention on the long-term stimulation properties of the microelectrode array in cat sciatic nerve and showed that muscle groups stimulated by individual electrodes changed very little over the life of the implant. This fact supports the possibility that these devices may provide an effective neural interface for various motor neuroprosthetic applications.

Closed loop control

As discussed in General Introduction, a fascinating method for closed loop control in FES would be to use the natural sensors which are already present within the body. In Chapter 3, we have shown using extracellular recording of DRG cells that only a few (~3) afferent units can predict well the limb trajectory and joint angles in anesthetized cats. In deed, Prochazka has shown that spinal Ia and tendon organ Ib response properties have been investigated in detail and represented using equations (Prochazka 1999). Thus, the multielectrode arrays, if the long-term stability and recording ability is established, may be an accurate sensor to be applied in a feedback-controlled motor neuroprosthesis. We failed to establish long-term recording ability of first-order sensory neuron in peripheral nerve (Chapter 4); the amplitudes of the recorded sensory units decreased day by day and the units disappeared within one week after implantation. DRG, receiving from a variety of receptors in peripheral nerve fibers and having the advantage of containing large somata (40–70 μm) (Willis and Coggeshall 1991), allowed much better recording ability as the acute experiments were concerned. The long-term recording ability is now being established in this laboratory.

Sensors being developed for the BION system, in which one implant is commanded to emit an RF signal whose strength (and hence distance) is detected by a second BION implant, seems a sophisticated alternative for feedback controlled neural prosthesis (Loeb et al. 2001).

Problems associated with rhythmic movement such as locomotion

In terms of lower limb control of FES, the early clinical attempts involved electrical stimulation of the ankle dorsiflexors in hemiplegia in order to obtain foot clearance during the swing phase of gait (Dai et al. 1996; Liberson et al. 1961) and stimulation of the quadriceps in paraplegia to maintain standing position (Kralj et al. 1980). For the last 20 years' extensive research has been developed toward paraplegic gait through the aid of FES (Stein et al. 1992; Chapin and Moxon 2000; Kralj et al. 1988). Despite the extensive work, currently no FES system for gait adequately meets all the requirements for daily use.

Despite advances of biomechanical technology, numerous problems with rhythmic movement control of multi-joint movement must be overcome before wide usage of the FES system for gait. Several models have been proposed for gait control in FES (Gerritsen et al. 1998; Bobet 1998; Popovic et al. 1999; Sweeney et al. 2000). Gerritsen et al. found using their forward models that force-length-velocity properties of muscles contribute substantially to intersegmental stability of the musculoskeletal system, but they stressed that unsupported sustained simulated gait would require a highly complex feedback control system. Such a high degree of complexity would severely compromise the feasibility of practical applications in FES-assisted paraplegic locomotion. This merely highlights again the remarkable performance of the CNS that is involved in the control of locomotion. In that sense in spinal cord injury, inaccessibility to higher centers including the mesencephalic locomotor region and cerebellar locomotor region (Mori et al. 1999) that have abundant plastic and adaptive abilities may be an irreparable, fundamental loss for stabilizing the locomotion. Making the most of residual function of CPG (Calancie et al. 1994; Barbeau et al. 1999; Dimitrijevic et al. 1998) below the spinal cord lesions, for example, by locomotor training, use of afferent fiber stimulation or neuropharmacology, stimulation of CPG region, or some combination of these strategies might enhance locomotor function in the future. For individuals with complete paraplegia, however, hybrid methods combined with gait aids such as arm support (e.g. cane, crutch, walker) and orthoses (e.g. a reciprocating gait orthosis (Nene and Patrick 1990)) would be a realistic near future goal to use FES system for community ambulation.

Concluding remarks: the future

The countless normal physiological events that continuously occur with even the simplest motor task are clearly still far more complex than what can be currently accomplished by FES, even with the most sophisticated technology with computer controlled multichannel stimulators and closed loop sensory feedback. One may feel this rather disappointing, considering that numerous researchers have been involved in the FES research since the Liberson's first practical introduction (Liberson et al. 1961). Although significant progress has been made in the last few decades in clinical and basic investigation, the researchers are still standing at a primitive stage. In this thesis, we have shown a few new ideas indicating possible neuroprosthesis application. In compliance with patients' wishes, however, simple, soluble clinical problems (e.g. foot drop stimulation, grasping) should be approached to offer a decent payoff in a reasonable time, rather than orienting exclusively on the most difficult issues such as locomotion after complete spinal cord injury.

REFERENCES:

1. Grill WM and Lemay MA. Control of movement by inraspinal stimulation in the cat. *31th annual meeting of Society for Neuroscience*, San Diego, CA, 2001, p. 935.934.

2. Kralj AR and Bajd T. *Functional electrical stimulation: standing and walking after spinal cord injury*. Boca Raton, Fla.: CRC Press, 1989.

3. Stein RB, Peckham PH and Popovic D. *Neural prostheses: replacing motor function after disease or disability*. New York: Oxford University Press, 1992.

4. Chapin JK and Moxon KA. *Neural Prostheses for Restoration of Sensory and Motor Function*. Boca Raton: CRC Press, 2000.

5. Kralj A, Bajd T and Turk R. Enhancement of gait restoration in spinal injured patients by functional electrical stimulation. *Clin Orthop*: 34-43, 1988.

6. Peckham PH and Creasey GH. Neural prostheses: clinical applications of functional electrical stimulation in spinal cord injury. *Paraplegia* 30: 96-101, 1992.

7. Dai R, Stein RB, Andrews BJ, James KB and Wieler M. Application of tilt sensors in functional electrical stimulation. *IEEE Trans Rehabil Eng* 4: 63-72, 1996.

8. Wieler M, Stein RB, Ladouceur M, Whittaker M, Smith AW, Naaman S, Barbeau H, Bugaresti J and Aimone E. Multicenter evaluation of electrical stimulation systems for walking. *Arch Phys Med Rehabil* 80: 495-500, 1999.

9. Prochazka A. Comparison of Natural and artificial control of movement. *IEEE Trans Rehabil Eng* 1: 7-17, 1993.

10. Field-Fote EC. Spinal cord control of movement: implications for locomotor rehabilitation following spinal cord injury. *Phys Ther* 80: 477-484, 2000.

11. Herrmann U and Flanders M. Directional tuning of single motor units. *J Neurosci* 18: 8402-8416, 1998.

12. Branner A and Normann RA. A multielectrode array for intrafascicular recording and stimulation in sciatic nerve of cats. *Brain Res Bull* 51: 293-306, 2000.

13. Branner A, Stein RB and Normann RA. Selective stimulation of cat sciatic nerve using an array of varying-length microelectrodes. *J Neurophysiol* 85: 1585-1594, 2001.

14. Prochazka A. Quantifying proprioception. *Prog Brain Res* 123: 133-142, 1999.

15. Willis WD and Coggeshall RE. Dorsal root ganglion cells and their process. In: *Sensory mechanisms of the spinal cord* (2nd ed.). New York: Plenum Press, 1991, p. 47-78.

16. Loeb GE, Richmond FJ, Brown IE, Lan N, Davoodi R, Fornwalt HC and Troyk PR. Bionic systems for reanimation of paralyzed limbs. *31th annual meeting of Society for Neuroscience*, San Diego, CA, 2001, p. 832.817.

17. Liberson WT, Holmquest HJ, Scott D and Dow M. Functional electrotherapy: stimulation of the peroneal nerve synchronized with the swing phase of the gait of hemiplegic patients. *Arch Phys Med Rehabil* 42: 101-105, 1961.

18. Kralj A, Bajd T and Turk R. Electrical stimulation providing functional use of paraplegic patient muscles. *Med Prog Technol* 7: 3-9, 1980.

19. Gerritsen KG, van den Bogert AJ, Hulliger M and Zernicke RF. Intrinsic muscle properties facilitate locomotor control - a computer simulation study. *Motor Control* 2: 206-220., 1998.

20. Bobet J. Can muscle models improve FES-assisted walking after spinal cord injury? *J Electromyogr Kinesiol* 8: 125-132, 1998.

21. Popovic D, Stein RB, Oguztoreli N, Lebiedowska M and Jonic S. Optimal control of walking with functional electrical stimulation: a computer simulation study. *IEEE Trans Rehabil Eng* 7: 69-79, 1999.

22. Sweeney PC, Lyons GM and Veltink PH. Finite state control of functional electrical stimulation for the rehabilitation of gait. *Med Biol Eng Comput* 38: 121-126, 2000.

23. Mori S, Matsui T, Kuze B, Asanome M, Nakajima K and Matsuyama K. Stimulation of a restricted region in the midline cerebellar white matter evokes coordinated quadrupedal locomotion in the decerebrate cat. *J Neurophysiol* 82: 290-300, 1999.

24. Calancie B, Needham-Shropshire B, Jacobs P, Willer K, Zych G and Green BA. Involuntary stepping after chronic spinal cord injury. Evidence for a central rhythm generator for locomotion in man. *Brain* 117: 1143-1159, 1994.

25. Barbeau H, McCrea DA, O'Donovan MJ, Rossignol S, Grill WM and Lemay MA. Tapping into spinal circuits to restore motor function. *Brain Res Brain Res Rev* 30: 27-51, 1999.

26. Dimitrijevic MR, Gerasimenko Y and Pinter MM. Evidence for a spinal central pattern generator in humans. *Ann N Y Acad Sci* 860: 360-376, 1998.

27. Nene AV and Patrick JH. Energy cost of paraplegic locomotion using the ParaWalker--electrical stimulation "hybrid" orthosis. *Arch Phys Med Rehabil* 71: 116-120,

1990.